Precision Phenomenology in Higgs-Strahlung with Fully-Differential Cross Sections at Next-to-Next-to-Leading Order

Von der Fakultät für Mathematik, Informatik und Naturwissenschaften der RWTH Aachen University zur Erlangung des akademischen Grades eines Doktors der Naturwissenschaften genehmigte Dissertation

vorgelegt von
Lukas Simon
aus
Prüm

Berichter: Univ.-Prof. Dr. rer. nat. Robert V. Harlander
Univ.-Prof. Dr. rer. nat. Michał Czakon

Tag der mündlichen Prüfung: 17. November 2023

Diese Dissertation ist auf den Internetseiten der Universitätsbibliothek verfügbar.

Zusammenfassung

In dieser Arbeit präsentieren wir den Monte Carlo Event Generator `history`, welcher auf die Berechnung vollständig differenzieller Wirkungsquerschnitte von Farb-Singulett-Zuständen bis zur nächst-nächst-führenden Ordnung in der Störungstheorie der Quantenchromodynamik ausgelegt ist. Diese Präzision wird erreicht durch die Anwendung des Nested Soft-Collinear Subrtraktionsschemas, eine lokale Methode zur Subtraktion infraroter Divergenzen, welche während der Phasenraumintegration auftreten. Wir resümieren die grundlegenden Konzepte dieses Schemas und präsentieren die für eine Implementierung essenziellen Komponenten. Dies umfasst insbesondere die expliziten Ausdrücke aller Subtraktionsfunktionen, die für die Produktion eines farblosen Endzustandes, der auf führender Ordnung durch die Kollision eines Quark-Antiquark Paares ausgelöst wird, benötigt werden. Des Weiteren erläutern wir die Phasenraumparametrisierung, welche ursprünglich zur Konstruktion von `STRIPPER` entworfen wurde. Schließlich erhalten wir ein flexibles Programm, welches eine schnelle und nummerisch stabile Berechnung von Korrekturen höherer Ordnung ermöglicht.

Das Programm `history` besteht aus einer prozessunabhängigen Implementierung des Subtraktionsschemas, welche mit prozessspezifischen Streuamplituden kombiniert werden muss. Die hier vorgestellte Version ermöglicht eine phänomenologische Anwendung für die gemeinsame Produktion eines Higgs-Bosons mit einem schwachen Eichboson in hadronischen Kollisionen. Der Fokus liegt dabei auf dem Drell-Yan-artigen Produktionsmechanismus, $pp \to V^* \to VH$, wobei V entweder ein W-Boson oder ein Z-Boson sein kann. Darüber hinaus ist aber auch der schleifeninduzierte Gluonfusionprozess, welcher nur zur ZH Produktion beiträgt, auf der Ordnung α_s^2 implementiert. Wirkungsquerschnitte können sowohl für das Standardmodell als auch für alternative Modelle berechnet werden. Teil des Programms sind das Zwei-Higgs-Dublett-Modell und das B–L Modell.

Schlussendlich validieren wir die Implementierung durch einen Vergleich mit etablierten Standardmodellergebnissen und präsentieren neue differentielle Wirkungsquerschnitte unter Einbeziehung der Effekte Neuer Physik, um das Potenzial von `history` aufzuzeigen.

Abstract

In this thesis, we present the novel Monte Carlo Event Generator `history` which is designed to predict fully-differential cross sections for color-singlet final states at next-to-next-to-leading order accuracy in perturbative quantum chromodynamics. This precision level is achieved through the application of the Nested Soft-Collinear Subtraction scheme, a fully local method to subtract infrared divergences that arise during phase-space integrations. We review the concepts behind this scheme and present the essential components which are crucial for a practical implementation. This includes a collection of the explicit expressions for all subtraction functions that are substantial for arbitrary color-singlet-production processes initiated by a quark-antiquark pair at leading order. Furthermore, we outline the adopted phase-space parametrization, that originally has been introduced in the `STRIPPER` framework. In conclusion, we obtain a flexible program that enables fast and numerically stable evaluations of higher-order corrections. The code of `history` contains a process-independent implementation of the subtraction scheme that has to be combined with process-specific matrix elements. The current version provides a phenomenological application to Higgs boson production in association with a weak gauge boson in hadron collisions. Thereby, the focus lies on the Drell-Yan-like production mechanism, $pp \to V^* \to VH$, where V represents either a W or a Z boson, but also the loop-induced gluon-fusion process, which exclusively contributes to ZH production, is included at $\mathcal{O}(\alpha_s^2)$. Cross-section predictions can be made within the Standard Model and in theories beyond the Standard Model. Particularly, the Two-Higgs-Doublet Model and the B–L Model are accessible.

Finally, we validate the correctness of the software with cross-checks against established results within the Standard Model and illustrate first physical applications that are affected by New Physics scenarios to demonstrate the potential of `history` as a versatile tool for fully-differential cross-section computations with high precision.

Contents

1 Introduction

Since its development in the 1960s, the Standard Model of particle physics (SM) [1–12] has captured the interest of experimental and theoretical particle physicists alike. It elegantly describes all known elementary particles and their interactions through the fundamental strong, weak, and electromagnetic forces. A pivotal milestone of the SM was the empirical confirmation of the existence of the massive weak gauge bosons, the W and Z bosons, which had been predicted beforehand [13–16]. Furthermore, the SM postulated the top quark and the τ neutrino prior these particles were measured for the first time [17–19]. Finally, the crowning achievement arrived with the observation of the Higgs boson by the ATLAS [20] and CMS [21] experiments at CERN's Large Hadron Collider (LHC) in 2012, leading to the complete discovery of the SM's particle content. To this day, the SM predicts a wide range of experiments with remarkable accuracy, making it the most successful model we have in particle physics.
Nevertheless, despite the numerous successes, it leaves open questions and ambiguities. For instance, the SM unifies the strong, weak, and electromagnetic forces, but attempts to incorporate gravity as the fourth fundamental force fail as they contradict Einsteins well-proven theory of general relativity. Another unsolved riddle in the context of the SM is the appearance of Dark Matter. In the ΛCDM model, the most common cosmological Big Bang model, precise measurements reveal that roughly 26.6 % of the universe's energy density constitutes out of this unknown type of matter, whereas ordinary SM matter contributes to just 4.9 % [22]. The remaining 68.5 % are referred to as Dark Energy whose nature is even more hypothetical than that of Dark Matter. The next phenomenon the SM cannot describe, is the specific role the neutrinos take in it. Due to the absence of left-handed neutrinos and right-handed antineutrinos, the SM predicts them to be massless. In contradiction, the discovery of neutrino oscillations [23–25] proves that their masses cannot be zero, even though the masses are tiny compared those of the other SM particles [26], giving a hint that the mechanism behind differs from the Higgs mechanism. Moreover, within the SM the matter-antimatter asymmetry in the universe cannot be understood entirely. The measured complex $\mathcal{CP}$-violating phases in the Cabibbo-Kobayashi-Maskawa (CKM) quark-mixing matrix [27] as well as in the Pontecorvo–Maki–Nakagawa–Sakata (PMNS) neutrino-mixing matrix [28] give rise to this asymmetry, but their contributions are by far too small to explain all the observed baryogenesis. Additionally, beyond inexplicable experimental observations, the SM comes with miracles like the hierarchy problem that leads theorists dissatisfied due to large discrepancies between the fundamental value of some physical parameters in the Lagrangian and their effective value appearing in experiments. This is just a collection of a few shortcomings and many other questions are still unsolved, motivating to extend the SM in order to eliminate these issues.
A modern approach for uncovering the origin of Beyond Standard Model (BSM) physics is the accurate empirical study of the SM itself, driven by the aspiration to detect devi-

ations from the model's forecasts. With more and more precise experimental methods and percent-level measurements it becomes more and more relevant that theoretical calculations reach the same level of accuracy. Unfortunately, leading order (LO) and even next-to-leading order (NLO) calculations in perturbative quantum field theory (QFT) do not deliver the necessary precision. New tools have to be developed and refined for next-to-next-to-leading order (NNLO) precision level in the strong coupling parameter α_s. Nowadays, the NNLO revolution is in full swing and much progress has been made in the recent years to archive the goal of fully-automatized NNLO predictions, but still further challenges have to be mastered before completion. On the one side, algorithms for dealing with infrared (IR) singularities are successfully applied to many different $2 \to 2$ and a few $2 \to 3$ processes with double-real corrections, which is becoming the new standard [29–40]. On the other side, also significant improvements on the computation of multi-loop scattering amplitudes is made by the progress in understanding the structure of Feynman integrals [41–46].

In this thesis, we want to apply some of these state-of-the-art techniques and pay attention to Higgs boson production in association with a massive SM gauge boson, commonly known as Higgs-Strahlung, at NNLO accuracy. From a phenomenological point of view, this is one of the most exciting processes to study in modern collider experiments. Latest, since the first observation in proton-proton collisions, $pp \to VH$ with $V \in \{W^{\pm}, Z\}$, in 2018 by the ATLAS [47, 48] and CMS [49, 50] detectors, Higgs-Strahlung is in the focus of interest of many experimentalists as well as theorists.

Higgs-Strahlung not only allows us to investigate the properties of the 2012 discovered Higgs boson in depth and compare them to theoretical SM predictions, it is also sensitive to a wide variety of promising New Physics scenarios in different BSM extension.

For theoretical studies it is convenient to split the Higgs-Strahlung process in different subprocesses, such as the Drell-Yan-like subprocess, $pp \to V^* \to VH$, where a virtual vector boson is produced which radiates off a Higgs boson, or the loop-induced gluon-fusion subprocess, $gg \to ZH$.

The NLO quantum chromodynamics (QCD) effects of the Drell-Yan-like contributions were investigated in Refs. [51–53] and the exact NNLO QCD corrections to the fully-inclusive cross section are known from Ref. [54] since almost 20 years. The total NNLO cross section is implemented in the public code `vh@nnlo` [55] on the basis of the tool `ZWPROD` [56] which was designed for computing the $\mathcal{O}(\alpha_s^2)$ corrections of the original Drell-Yan process. Fully-exclusive NNLO results for WH and ZH production including various decay channels of the Higgs and the gauge bosons were presented in Refs. [57–66]. While the effects of the fixed-order computations play a major role in predicting the Higgs-Strahlung cross section, it had been shown that the effects of soft-gluon resummation are very small, leading to the conclusion that the perturbative series converges well [67]. Moreover, $\mathcal{O}(\alpha_s^3)$ corrections for VH in association with a hard jet were calculated in Refs. [68, 69] and, recently, as one of the first next-to-next-to-next-to leading order ($\mathrm{N^3LO}$) QCD computations, results for the fully-inclusive Drell-Yan-like Higgs-Strahlung were provided in Ref. [70]. Besides QCD effects also NLO electroweak (EW) corrections to the inclusive [71] and exclusive cross section [72, 73] were investigated. On top, fixed-order NLO and NNLO Higgs-Strahlung calculations were combined with parton-shower effects [74–82].

A second important subprocess is the gluon-induced contribution, $gg \to ZH$. Due to charge conservation only ZH final states can be created in this process, which is already in its lowest order appearance mediated by a bottom-quark or a top-quark loop. This production mode is suppressed with respect to the Drell-Yan-like process by a factor

α_s^2, but this suppression is partly compensated by the high gluon luminosity at high collision energies and partly by the large top Yukawa coupling. Moreover, its relevance lies in the high sensitivity of possible BSM effects in this channel.
The leading contributions of the gluon-induced process at $\mathcal{O}(\alpha_s^2)$ were presented in Refs. [54, 83–85]. The computation of the $\mathcal{O}(\alpha_s^3)$ contributions is very complicated because of the appearance of two-loop integrals with three different massive particles. The K-factor in the heavy-top limit was calculated in Ref. [86] and is used for cross section predictions in a second release of the program `vh@nnlo` [87]. Top mass effects were taken into account as expansion in $1/m_t$ combined with Padé approximants in Ref. [88] and also other approaches for computing the gluon-induced Higgs-Strahlung in different kinematic regions with finite mass effects are applied successfully, namely a small transverse-momentum expansion [89] and, complementarily, a high-energy expansion [90]. The approximations of these mass effects in Refs. [91–93] as well as the semi-analytic approach to incorporate them in Ref. [94] instead are valid over the complete phase space. Finally, the numerical result in Ref. [95] is computed with full top-mass dependence and does not rely on approximations, but it is computational extremely expensive and an analytic calculation is still desirable. In addition to the fixed-order calculations, a study of soft-gluon resummation effects has shown that they are necessary to reduce the scale uncertainty of the $gg \to ZH$ contribution significantly [96].
The Drell-Yan-like subprocess and the gluon-fusion channel are the most discussed contributions in the context of associated Higgs production, nevertheless, in the SM two more subprocesses appear, namely VH production in top-mediated processes where the Higgs boson couples to a virtual top loop and ZH production through an initial state bottom-antibottom pair. The former were studied in Ref. [97], revealing that these contributions are small. At LHC energies they give typically rise to corrections of the order of 1 % to the total cross section. The latter subprocess, $b\bar{b} \to ZH$, refers only to contribution with a direct Higgs-to-bottom Yukawa coupling, since contributions with a bottom-to-gauge boson coupling are included in the Drell-Yan-like terms. The LO QCD effects are implemented in `vh@nnlo` [87] assuming the bottom quark to be massless, but keeping its Yukawa coupling non-zero. Due to the small value of the bottom Yukawa coupling the impact of these effects is negligible in the SM, their contribution to the total cross section is at the permille level.
As mentioned before, Higgs-Strahlung is of great importance for unraveling the physics of the Higgs boson in the SM, but is also of interest in the hunt for New Physics. Therefore, associated Higgs production is studied taking into account different possible BSM effects. Potential New Physics effects on boosted Higgs regimes for the gluon-induced channel were first disussed in Refs. [98–100]. The phenomenological implications in the Two-Higgs-Doublet Model (2HDM) [76, 87, 99] and in the Minimal Supersymmetric Standard Model (MSSM) [87, 101–109] are in the focus of research as well as models with vector-like quarks [87]. Additionally, model-independent studies of anomalous couplings with higher-dimensional operators in Effective Field Theorys (EFTs) such as the Standard Model Effective Field Theory (SMEFT) [110–112] obtain more and more attention [87, 113, 114].
All studies of BSM scenarios in Higgs-Strahlung give rise to the desire for an experimental analysis of the gluon-induced subprocess. However, such a measurement comes with significant challenges since the Drell-Yan-like Higgs-Strahlung, which is typically less sensitive to those New Physics effects, occurs as an irreducible background. One of the primary goals of this thesis is the development of a framework that aims to predict observables that access the gluon channel, inspired by the Refs. [99, 115]. To

accomplish this, precise predictions of the fully-differential Higgs-Strahlung cross sections are essential. For this purpose, we have created a novel tool based on the Nested Soft-Collinear Subtraction scheme [38, 116–118], enabling the calculation of the Drell-Yan-like process for arbitrary kinematic observables at NNLO QCD accuracy. Moreover, fully-differential cross sections for the $\mathcal{O}(\alpha_s^2)$ contributions of the gluon-induced component can be obtained with our code. This program with the name `history` (**Hi**ggs-**St**rahlung The**ory**)[1] is designed in the spirit of `vh@nnlo` and `SusHi` [119, 120] with the aim to compute cross sections for associated Higgs production in a wide variety of phenomenological relevant models. In the presented version, predictions can be made within the SM, the 2HDM, and the Baryon Number minus Lepton Number Model (B–L Model). Nevertheless, this framework is highly flexible and can be extended to other theories and processes in the future, enhancing its potential for broader phenomenological applications.

Organization of the Thesis

In this thesis, we discuss the details of the implementation of the Nested Soft-Collinear Subtraction scheme as done in `history`, but we also provide an insight into the phenomenology of the Higgs-Strahlung process with a main focus on the Drell-Yan-like mechanism. The organization is as follows:

Chapter 1 In the introduction we highlighted the relevance of the Higgs-Strahlung process, which is used for precision measurements of SM parameters on the one hand, but whose gluon-induced channel is potentially sensitive to BSM physics on the other hand. In this regard, we reviewed the numerous phenomenological studies in the literature that pointed to the need for high-precision calculations.

Chapter 2 The second chapter introduces the notation for cross sections that is used throughout this work. Moreover, the Higgs-Strahlung mechanism is described in the context of the SM and its modifications in the 2HDM as well as the B–L Model are outlined. In a final section, the R^{VH} double ratio is explained, an observable that makes New Physics effects in the gluon-induced subprocess experimentally accessible.

Chapter 3 The third chapter addresses the challenges that arise in higher-order calculations of fully-differential cross sections. To solve the issues that come up due to IR divergences, the ideas behind slicing methods and subtraction schemes are described.

Chapter 4 A detailed NLO computation for color-singlet production, such as the Higgs-Strahlung process, in the Frixione-Kunszt-Signer (FKS) formalism is presented in the fourth chapter. The FKS subtraction scheme forms the basis of the NNLO Nested Soft-Collinear Subtraction scheme. Useful notations are introduced and the subtraction formalism is outlined in depth, including the full list of subtraction functions, the explicit computation of the related counterterms, and a proof of analytic pole cancellation.

[1] Special thanks go to Stefan Liebler for coming up with this brilliant name.

Chapter 5 The fifth chapter is the heart piece of this thesis and describes the Nested Soft-Collinear Subtraction scheme. After introducing the formalism itself, the focus is on providing a complete list of ingredients that are necessary for the implementation of this scheme instead of recomputing the counterterms or reproving analytic pole cancellation. Thus, all subtraction functions are systematically presented and the finite remainder for the fully-differential color-singlet-production cross section, which can be computed numerically in $d = 4$ dimensions, is shown.

Chapter 6 In the sixth chapter the phase-space parametrization that is used in our Monte Carlo (MC) Event Generator is explained. This parametrization is adopted from the `STRIPPER` framework [34, 35, 121, 122]. Additionally, more details of our implementation and links to external codes are described.

Chapter 7 The seventh chapter contains some results that are obtained with our novel tool. The validity of our implementation is cross-checked against `vh@nnlo` and, exemplarily, Higgs rapidity distributions in the SM are shown. Moreover, an invariant mass spectrum for the B–L Model model is produced and the R^{VH} double ratio for a simple model with a modified top-to-Higgs Yukawa coupling is computed for the first time as a Higgs rapidity distribution.

Chapter 8 A conclusion is given in the eighth chapter and an outlook for exploiting the potential of the `history` framework in the future is outlined.

Appendices In Appendix A, the relevant Feynman rules for the computation of Higgs-Strahlung amplitudes are provided in the SM, the 2HDM, and the B–L Model.
Appendix B summarizes the ultraviolet (UV) renormalization of the strong coupling constant with the conventions used in this thesis and lists the UV- and IR-renormalized finite remainders for the purely virtual corrections of the Drell-Yan-like Higgs-Strahlung process that appear up to NNLO.
The full set of splitting functions that we use is given Appendix C.
Quantities that are related to soft singularities are presented in Appendix D.
Finally, Appendix E provides a complete list of IR limits and subtraction functions for all partonic channels of Drell-Yan-like Higgs-Strahlung that are needed up to NNLO in QCD.

2
Higgs-Strahlung

Contents

In this chapter, we want to introduce the process for associated Higgs production with a weak gauge boson, $pp \to VH$, where V can be either a charged $W^{\pm}$ boson or a neutral Z boson. This process is commonly know as Higgs-Strahlung. In section 2.1, we provide the general definition of cross sections that we use throughout the thesis. Next, in section 2.2, we describe the occurrence of Higgs-Strahlung in the SM. Furthermore, we explore the modifications of this process in two universal BSM theories, namely the 2HDM and the B–L Model, which are also in the focus of our study. Finally, in section 2.3, we present a promising observable that is sensitive to potential New Physics effects that might show up in Higgs-Strahlung. The creation of a framework for investigating this observable in future studies serves as one of the primary motivation behind the project of this thesis.

2.1. Cross Sections

Accelerator experiments play a crucial role for our understanding of the fundamental laws of nature and the universe. In particular, in high-energy collisions of subatomic particles, we can investigate the properties and interactions of matter. The basic quantity that is measured in such experiments is an event rate which is a number of interesting events N that are counted in a time interval $\mathrm{d}t$. The event rate is given as the product of the accelerator's luminosity $\mathcal{L}$ and the process-specific cross section σ,

$$\frac{\mathrm{d}N}{\mathrm{d}t} = \mathcal{L} \cdot \sigma. \tag{2.1}$$

While the luminosity characterizes the particle accelerator and determines the collision rate depending on its attributes like beam current, beam size and crossing frequency, the cross sections is a universal quantity, independent of the accelerator's properties, and can be interpreted as the probability for a specific type of scattering in a single collision. The latter can be computed from theoretical models and thus builds a link to experimental observations.

Although cross sections in QCD cannot be calculated from first principle nowadays, the factorization theorem allows for the separation of short-distance and long-distance effects from each other at collision energies Q that are much higher than the fundamental QCD scale $\Lambda_{\mathrm{QCD}} \sim 200\,\mathrm{MeV}$ [123]. In this case the cross section can be factorized into the non-perturbative long-distance parton distribution functions (PDFs) and the short-distance partonic cross section which can be calculated in perturbative QCD. For a collision of the hadrons A and B which produce a final state X we can write[1]

$$\sigma_{AB\to X} = \sum_{i,j} \int_0^1 \mathrm{d}\tau \, \frac{\mathrm{d}\mathcal{L}_{AB}^{ij}(\tau, \mu_\mathrm{F})}{\mathrm{d}\tau} \, \hat{\sigma}_{ij\to X}(\tau, \mu_\mathrm{R}, \mu_\mathrm{F}) + \mathcal{O}\left(\left(\frac{\Lambda_{\mathrm{QCD}}}{Q}\right)^p\right), \tag{2.2}$$

where the sums i and j run over all partons that can be found inside hadron A and B, respectively. The parton luminosity function $\mathcal{L}_{AB}^{ij}$ is defined as a convolution integral,

$$\frac{\mathrm{d}\mathcal{L}_{AB}^{ij}(\tau, \mu_\mathrm{F})}{\mathrm{d}\tau} = \int_0^1 \mathrm{d}\xi_1 \mathrm{d}\xi_2 \, f_{i/A}(\xi_1, \mu_\mathrm{F}) f_{j/B}(\xi_2, \mu_\mathrm{F}) \, \delta(\xi_1 \xi_2 - \tau), \tag{2.3}$$

where the functions $f_{i/A}(\xi, \mu_\mathrm{F})$ are the PDFs which describe the probability to find a parton i inside a hadron A that carries the momentum fraction ξ of the original hadron momentum.
The partonic cross section for producing a final state X in a collision of the partons i and j can be computed perturbatively as an expansion in the coupling constant of the strong force, denoted as α_s,

$$\hat{\sigma}_{ij\to X} = \hat{\sigma}_{ij\to X}^{\mathrm{LO}} + \hat{\sigma}_{ij\to X}^{\mathrm{NLO}} + \hat{\sigma}_{ij\to X}^{\mathrm{NNLO}} + \mathcal{O}\left(\alpha_s^3\right), \tag{2.4}$$

where we refer to $\hat{\sigma}_{ij\to X}^{\mathrm{LO}}$, $\hat{\sigma}_{ij\to X}^{\mathrm{NLO}}$, and $\hat{\sigma}_{ij\to X}^{\mathrm{NNLO}}$ as LO, NLO, and NNLO contribution, respectively. Moreover, we omitted the explicit dependence of $\hat{\sigma}_{ij\to X}$ on the variable τ, as well as on the factorization scale μ_F and the renormalization scale μ_R.
The factorization scale represents the energy scale at which the short-distance effects are separated from the long-distance effects and is connected to IR phenomena. In contrast, the renormalization scale specifies the energy scale at which the UV divergences that appear in perturbative calculations are removed [124].
The partonic cross section can be computed according to

$$\mathrm{d}\hat{\sigma}_{ij\to X} = \frac{1}{2\hat{s}} \, \mathrm{d}\Pi_X^{(4)} \left|\mathcal{M}_{ij\to X}(p_i, p_j \,|\, \{p_X\})\right|^2. \tag{2.5}$$

The first factor on the right-hand side is the Lorentz invariant Møller flux which depends on the partonic center-of-mass energy[2] $\sqrt{\hat{s}}$, the Lorentz-invariant four-dimensional final-state phase-space element is denoted by $\mathrm{d}\Pi_X^{(4)}$, and $\mathcal{M}_{ij\to X}(p_i, p_j \,|\, \{p_X\})$ is the scattering matrix element for the process under consideration, which is also invariant under Lorentz transformations. All these quantities depend on the momenta of the particles that are involved in the process, which are p_i and p_j for the incoming parton i and j, respectively, and $\{p_X\}$ is a set of momenta for the final-state particles X.
In order to obtain the total, unpolarized inclusive cross section, the phase-space integration has to be carried out, and initial states have to be averaged over their spin and

[1] In the following we will omit the term for the power corrections. The related exponent p is a process dependent number, but always larger than one ensuring that they are small when $Q \gg \Lambda_{\mathrm{QCD}}$.
[2] In particular, it holds $Q = \sqrt{\hat{s}}$.

color states, which is represented by a bar on top of the squared matrix element in the following,

$$\hat{\sigma}_{ij\to X} = \frac{1}{2\hat{s}} \int \mathrm{d}\Pi_X^{(4)} \overline{\left|\mathcal{M}_{ij\to X}(p_i, p_j \mid \{p_X\})\right|^2}. \tag{2.6}$$

To test theoretical models in scattering experiments, preserving the kinematic information of the final-state particles, as encoded in the differential cross sections of Eq. (2.5), is desirable. While total cross sections are integrated over the full phase space, differential cross sections provide a more detailed picture of the underlying physical mechanisms. However, computing differential cross sections introduces some additional challenges in regulating the divergences that typically arise during the phase-space integration. For retaining the kinematic information, the utilization of special techniques is required. This techniques will be further explored and discussed in chapter 3.

2.2. Associated Higgs Production

Associated production of a Higgs boson with a massive vector boson, or short Higgs-Strahlung, is one of the main Higgs production mechanisms in the SM. Despite the low production rate which predicts that roughly 5 % of the Higgs bosons are created via this mechanism, it has huge experimental relevance: The additional tag of the vector boson allows for a good background separation and, thus, gives a clean signal.
Higgs-Strahlung played a central role in the groundbreaking discovery of the Higgs decaying into a pair of bottom quarks. This observation was made in 2018 by the ATLAS [48] and CMS [50] experiments, marking a significant milestone achieved through tremendous experimental efforts.
According to Eq. (2.2) we can write the cross section in proton-proton collisions as

$$\mathrm{d}\sigma_{pp\to VH+X} = \sum_{i,j} \int_0^1 \mathrm{d}\tau \, \frac{\mathrm{d}\mathcal{L}_{pp}^{ij}(\tau, \mu_\mathrm{F})}{\mathrm{d}\tau} \, \mathrm{d}\hat{\sigma}_{ij\to VH+X}(\tau, \mu_\mathrm{R}, \mu_\mathrm{F}) \,, \tag{2.7}$$

where V can be either massive SM weak gauge boson, $V \in \{W^\pm, Z\}$, and X can be any finial-state parton which is allowed by quantum-number conservation.

2.2.1. In the Standard Model of Particle Physics

Many different contributions give rise to the associated Higgs boson-production cross section in the SM. The most important mechanisms at proton-proton colliders such as the LHC are

$$\mathrm{d}\sigma_{pp\to VH+X} = \mathrm{d}\sigma_\mathrm{DY} + \delta_{VZ} \, \mathrm{d}\sigma_{gg}, \tag{2.8}$$

where $\mathrm{d}\sigma_\mathrm{DY}$ is the dominant production mechanism, the so-called Drell-Yan-like contribution. In case for ZH final states, denoted by the Kronecker symbol δ_{VZ}, we consider one more partonic production channel which is initiated by a gluon pair, $\mathrm{d}\sigma_{gg}$.
However, it is important to note that Eq. (2.8) is not comprehensive and requires expansion to incorporate additional channels, which are beyond the scope of our discussion. Further information regarding these effects mediated by the top quark can be found in Ref. [97]. These effects result in minor corrections of approximately 1 % to the total cross section at LHC energies, but for our specific purpose, they can be safely disregarded. Moreover, ZH can be produced in a bottom-quark annihilation process,

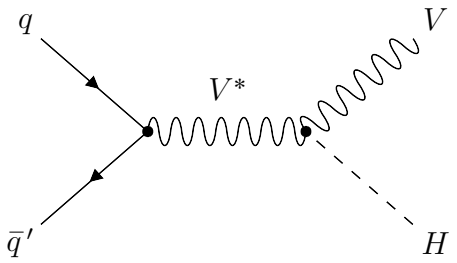

Figure 2.1.: The LO Feynman diagram for Drell-Yan-like Higgs-Strahlung. The vector boson can be either massive SM gauge boson, so that $V \in \{W^{\pm}, Z\}$. All Feynman diagrams in this thesis are generated with `FeynGame` [126].

where both final-state particle couple to bottom quarks originating from the colliding hadrons. As the direct coupling of the Higgs boson to the bottom quark is proportional to the small bottom mass, this contribution gives rise to less than 0.1 % in the SM, allowing us to neglect these sub-leading effects in the following.

Drell-Yan-Like Higgs-Strahlung

The only Feynman diagram of associated Higgs production at LO is shown in Figure 2.1. A quark and an antiquark annihilate into a virtual vector boson from which a Higgs boson is radiated off, $q\bar{q}' \to V^* \to VH$. Since this contribution is dominating the total cross section, associated Higgs production with a vector boson is commonly know as Higgs-Strahlung.

This mechanism exists for vector bosons V that can either be charged $W^{\pm}$ bosons or neutral Z bosons. The particular process $q\bar{q}' \to V^* \to VH$ is very similar to the Drell-Yan process $q\bar{q} \to \gamma^*/Z \to \ell\ell$ from a QCD perspective. In the Drell-Yan process $\ell\ell$ represents a lepton-antilepton pair, and the mediator can be a virtual photon γ^* or an on-shell Z boson [125]. Hence, we will refer to it as the Drell-Yan-like contribution. A main goal of this thesis is the numerical computation of the fully-differential cross section for Drell-Yan-like Higgs-Strahlung at NNLO QCD precision. Since the final state is colorless and is not affected by the strong force we can factorize the Drell-Yan-like cross section into the production of the (virtual) vector boson and its subsequent decay into the final-state VH system,

$$\mathrm{d}\sigma_{\mathrm{DY}} = \sum_{i,j} \int \mathrm{d}\tau \, \mathrm{d}q^2 \, \frac{\mathrm{d}\mathcal{L}^{ij}_{pp}(\tau, \mu_{\mathrm{F}})}{\mathrm{d}\tau} \, \mathrm{d}\hat{\sigma}_{ij \to V^* + X}(\tau, \mu_{\mathrm{R}}, \mu_{\mathrm{F}}) \, \frac{\mathrm{d}\Gamma_{V^* \to VH}(q^2)}{\mathrm{d}q^2}. \tag{2.9}$$

Here, $\mathrm{d}\hat{\sigma}_{ij \to V^* + X}$ is the cross section section for the production of the virtual vector boson V^* with mass $\sqrt{q^2}$ together with an arbitrary number of final-state partons X. Moreover, the differential decay function is known, *e.g.* see Refs. [51, 54], and reads

$$\frac{\mathrm{d}\Gamma_{V^* \to VH}(q^2)}{\mathrm{d}q^2} = \frac{G_{\mathrm{F}} M_V^4}{2\sqrt{2}\pi^2} \frac{\sqrt{\lambda(M_V^2, M_H^2, q^2)\,/q^4}}{\left(q^2 - M_V^2\right)^2} \left(1 + \frac{\lambda(M_V^2, M_H^2, q^2)}{12\, q^2 M_V^2}\right). \tag{2.10}$$

Fermi's coupling constant, denoted as G_{F}, was originally introduced in the theory of beta decay [127]. The Källén function, also known as triangle function, depends on the on-shell vector boson mass M_V, the Higgs boson mass M_H, and the virtuality of the decaying vector boson q. It has the form

$$\lambda(x, y, z) = x^2 + y^2 + z^2 - 2xy - 2xz - 2yz. \tag{2.11}$$

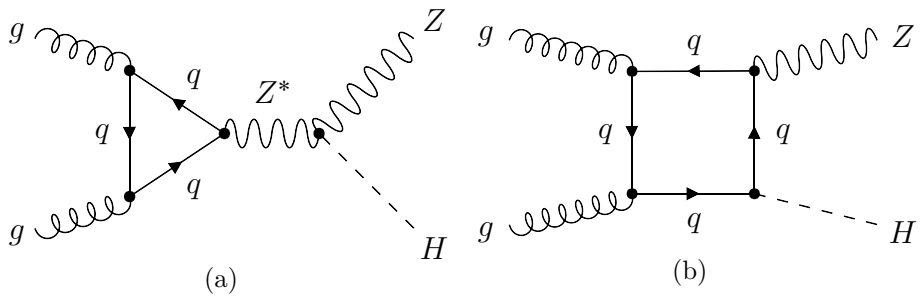

Figure 2.2.: Feynman diagrams for gluon-initiated Higgs-Strahlung.

Gluon-Initiated Higgs-Strahlung

At $\mathcal{O}(\alpha_s^2)$, new loop-induced modes emerge, initiating ZH production through a gluon pair. Their Feynman diagrams are shown in Figure 2.2. The triangle contributions in Figure 2.2(a) exhibit a similarity to the Drell-Yan-like diagrams, where the Higgs boson is radiated off the vector boson. However, these triangles only involve heavy third-generation quarks. This restriction arises from Furry's theorem, which prohibits contributions with vectorial couplings of the Z boson therein. Moreover, terms with axial couplings cancel each other for contributions with up-type and down-type quarks if they have the same mass, as is the case for the mass-degenerated quark doublets of the first two generations. Furthermore, the box diagrams in Figure 2.2(b) contain a direct Yukawa coupling that connects the Higgs to the closed quark loop. Given that the Yukawa coupling becomes zero for massless particles, only bottom and top quarks yield a non-zero contribution, bearing in mind that we keep a non-vanishing Yukawa coupling for the bottom quark.
The cross section can be written as

$$\mathrm{d}\sigma_{gg} = \int_0^1 \mathrm{d}\tau \, \frac{\mathrm{d}\mathcal{L}_{pp}^{gg}(\tau, \mu_\mathrm{F})}{\mathrm{d}\tau} \, \mathrm{d}\hat{\sigma}_{gg\to ZH+X}(\tau, \mu_\mathrm{R}, \mu_\mathrm{F}) \,. \tag{2.12}$$

2.2.2. In the Two-Higgs-Doublet Model

One of the simplest extensions of the SM is obtained by the introduction of a second scalar doublet in the Higgs sector. This so-called Two-Higgs-Doublet Model (2HDM) [128–136] has the potential to tackle some deficiencies of the SM and is the basis of a wide variety of BSM theories. For example, the inert Two-Higgs-Doublet Model (i2HDM) [137, 138] provides a minimal Dark Matter model or the MSSM [108, 139, 140], whose Higgs sector is a specific type of a 2HDM, solves the Hierarchy problem in a very natural way.
The introduction of a second scalar doublet in the Higgs sector modifies the phenomenological predictions of the Higgs-Strahlung process significantly [99]. In particular, this model predicts the existence of five Higgs bosons, whereof two are electrically charged, $H^\pm$, while the other three are neutral, conventionally indicated by h, H, and A. Since we can produce with the Higgs-Strahlung mechanism the final states Vh, VH, and VA, for our analysis only the neutral Higgs bosons are relevant. Thereby, we assume to have a $\mathcal{CP}$-conserving 2HDM, implying that the bosons h and H are $\mathcal{CP}$-even scalars while A is a $\mathcal{CP}$-odd pseudoscalar. The necessary set of Feynman rules is summarized in Appendix A.

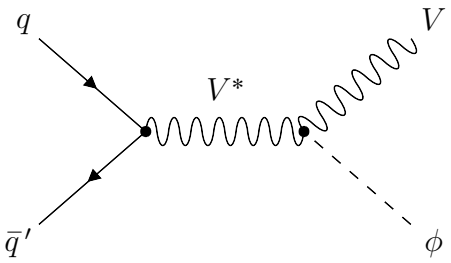

Figure 2.3.: The LO Feynman diagram for Drell-Yan-like Higgs-Strahlung of a $\mathcal{CP}$-even boson in the 2HDM, $\phi \in \{h, H\}$. The vector boson can be either massive gauge boson, $V \in \{W^{\pm}, Z\}$.

In the 2HDM these three Higgs bosons can couple to the weak gauge bosons with the coupling of the SM multiplied by a factor g^{ϕ}_{VV} for the $VV\phi$ vertices with $\phi \in \{h, H\}$ or by g^{A}_{VV} for the VVA vertex. Specifically, the factors are

$$g^{h}_{VV} = \sin(\beta - \alpha), \quad g^{H}_{VV} = \cos(\beta - \alpha), \quad g^{A}_{VV} = 0. \tag{2.13}$$

Here, α is a mixing angle describing the rotation of the $\mathcal{CP}$-even Higgs bosons from the isospin basis into mass eigenstates and $\tan(\beta)$ is the ratio of the vacuum-expectation values of the two Higgs doublets. From Eq. (2.13) it can be deduced that the coupling of the $\mathcal{CP}$-odd Higgs to the massive gauge bosons vanishes. Consequently, in analogy to the Drell-Yan-like production mechanism of the SM, in the 2HDM only the two scalar Higgs bosons can be produced via the same mechanism, as illustrated in Figure 2.3. The cross sections for these processes can thereby be obtained by a replacement of the Higgs-gauge couplings in accordance to the modifications just described, which is equivalent to a rescaling of the SM cross sections by a square of the factor g^{h}_{VV} for Vh production and g^{H}_{VV} for VH production.
The changes of the Higgs-gauge coupling have also to be taken into account in the triangle diagrams of the gluon-initiated process for Zh and ZH production depicted in Figure 2.4(a), again resulting in a global rescaling factor. In contrast, the modifications that are necessary to calculate the box diagrams in the 2HDM come from the direct coupling of the Higgs bosons to the quarks which differ from the SM Yuakwa couplings. In particular, the exact form of these coupling parameters depends on the realization of the $\mathbb{Z}_2$ symmetry which is imposed by the Paschos-Glashow-Weinberg theorem [141, 142]. This additional symmetry ensures that each fermion type can couple to only one of the Higgs doublets in order to avoid flavor-changing neutral currents at tree-level since they were never observed in nature so far. Considering that we have two Higgs doublets and three different types of fermions that obtain their mass through the Higgs mechanism, four different 2HDMs can be distinguished in the Yukawa sector that all respect the Paschos-Glashow-Weinberg theorem, see Table 2.1. However, in all four types of the 2HDM the Yukawa couplings of the scalar Higgs bosons h and H are the same as in the SM multiplied with a scaling factor g^{h}_{f} and g^{H}_{f}, respectively, which are given in Table A.1 in Appendix A. The pseudoscalar instead, has a new coupling including the fifth Dirac gamma matrix which has no correspondence in the SM. Beyond the specific details where more information is provided in Appendix A, via the box diagrams all three kinds of neutral Higgs bosons can be produced, *cf.* Figure 2.4(b). Additionally, due to tri-linear couplings that allow the vertices ZAh and ZAH, new interactions with a Higgs boson as s-channel mediator are possible in the 2HDM as shown in Figure 2.4(c-d). Finally, it is worth to mention that the Yukawa

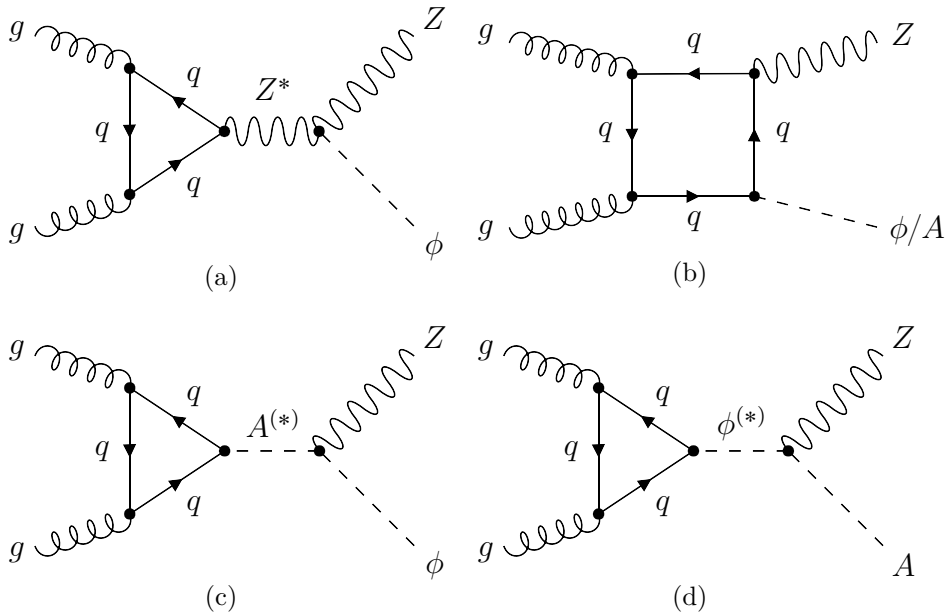

Figure 2.4.: Feynman diagrams for gluon-initiated Higgs-Strahlung production in the 2HDM. The $\mathcal{CP}$-even Higgs boson ϕ is either h or H.

couplings for the first two fermion generations can be neglected since these couplings are proportional to the quark masses. Moreover we can argue again that triangle diagrams with a coupling to the Z bosons cancel each other for quarks from mass-degenerated doublets. Similarly to the SM case, only bottom and top quarks can appear in the loops of the gluon-induced process.
In conclusion, the 2HDM offers a similar signature for its $\mathcal{CP}$-even Higgs bosons as predicted for the SM Higgs boson in the Drell-Yan-like channel. The only difference are the global rescaling factors due to the modified couplings. If for example $\sin(\beta - \alpha)$ in Eq. (2.13) is close to one, the h boson of the 2HDM would be hard to distinguish from a SM Higgs. The gluon-fusion process has higher sensitivity to the implications from effects beyond the SM. Because of the different impact of the 2HDM on the triangle and the box diagrams as well as the new contributions with s-channel Higgs bosons, the partonic cross section for $gg \to Zh$ or $gg \to ZH$ cannot be obtained by a rescaling of the related SM cross section. Moreover, these effects can show up to be smaller or higher in particular kinematic regions, leading to different shapes of differential cross sections [115]. Furthermore, in the gluon-induced channel a Z boson can be produced in association with a pseudoscalar Higgs boson, $gg \to ZA$, a process that has no analog in the SM.

2.2.3. In the B–L Model

Another popular extension of the SM that paves the way for a wide class of BSM theories, but, nevertheless, is characterized by a simple structure is the Baryon Number minus Lepton Number Model (B–L Model) [143–146]. This model adds a local $\mathbf{U(1)}_{B-L}$ symmetry to the SM and manifests the global B–L symmetry that accidentally is preserved by the SM. In order to take care of the anomalies that are introduced by the new symmetry, one additional fermion singlet is introduced for each fermion generation. Finally, the B–L symmetry can be broken by a complex scalar singlet. As

Table 2.1.: Types of the 2HDM which are allowed by the Paschos-Glashow-Weinberg theorem. The table shows to which Higgs doublet (Φ_1 or Φ_2) the right-handed up-type quarks (u^i_{R}), right-handed down-type quarks (d^i_{R}), and right-handed leptons (e^i_{R}) couple. The superscript i represents the fermion generation.

	u^i_{R}	d^i_{R}	e^i_{R}
Type I	Φ_2	Φ_2	Φ_2
Type II	Φ_2	Φ_1	Φ_1
Lepton-specific	Φ_2	Φ_2	Φ_1
Flipped	Φ_2	Φ_1	Φ_2

a consequence, the model contains a second neutral Higgs boson, where we identify the SM-like Higgs as h and the new one as H, but also a second massive and neutral gauge boson that we name Z'. Moreover, the see-saw mechanism is naturally incorporated into this model, so that the newly introduced fermions can be interpreted as heavy right-handed neutrinos, explaining the origin of SM neutrino masses.
In summary, the B–L Model is a triple-minimal extension of the SM by adding a new symmetry group whose charge Y_{B-L} is given as the difference of the baryon number B and the lepton number L with no distinction between generations, introducing a minimal set of new fermions, and introducing a new scalar singlet.
In the context of the Higgs-Strahlung process, we can have either a Wh, WH, Zh or ZH final state. Studies of the phenomenology in electron-positron collisions have been made in Refs. [147–149], while our focus lies on hadron collisions which have been investigated at LO in Ref. [150]. Similar to the 2HDM, the Drell-Yan like production mechanism for Wh and WH as shown in Figure 2.5(a) is affected by a global rescaling of Higgs-gauge coupling, so that the vertices WWh and WWH correspond to the SM vertex that couples its Higgs boson to a pair of W bosons multiplied with

$$g^h_{WW} = \cos(\alpha), \qquad g^H_{WW} = \sin(\alpha), \tag{2.14}$$

respectively. Here, α is the mixing angle that rotates the two Higgs bosons from their isospin eigenstates into mass eigenstates[3]. Consequently, the cross sections for these processes can be obtained by a rescaling of the related SM cross section. In addition to the changes of the Higgs-gauge coupling with the factors

$$g^h_{ZZ} = \cos(\alpha), \qquad g^H_{ZZ} = \sin(\alpha), \tag{2.15}$$

the production modes for Zh and ZH are also modified by a new contribution where the Z' boson can occur as mediator particle in the Drell-Yan-like process which decays via the vertices $ZZ'h$ or $ZZ'H$ into a Higgs-Strahlung final state, *cf.* Figure 2.5(b).
The cross section for associated Higgs production for either of the two Higgs bosons can be written as

$$\mathrm{d}\sigma_{\mathrm{DY}} = \sum_{i,j} \int \mathrm{d}\tau \, \frac{\mathrm{d}\mathcal{L}^{ij}_{pp}(\tau, \mu_{\mathrm{F}})}{\mathrm{d}\tau} \, \mathrm{d}\hat{\sigma}^{\mathrm{DY}}_{ij\to Z\phi+X}(\tau, \mu_{\mathrm{R}}, \mu_{\mathrm{F}}) \,, \tag{2.16}$$

[3]Conventionally, the angles α of the 2HDM and the B–L Model are different by a phase of $\pi/2$. Nevertheless, they describe in both models the same physics.

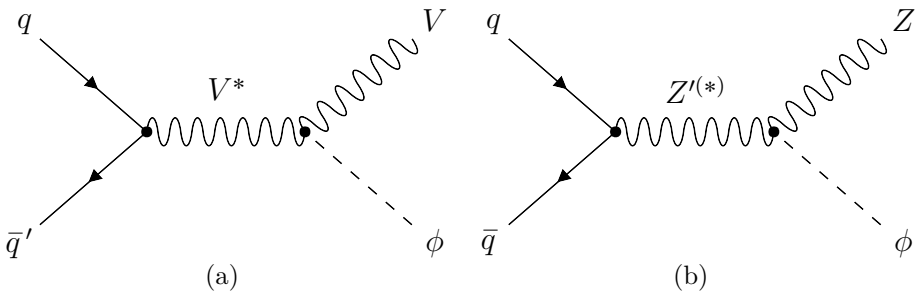

Figure 2.5.: LO Feynman diagrams for Drell-Yan-like Higgs-Strahlung with $\phi \in \{h, H\}$ and $V \in \{W^{\pm}, Z\}$ in the B–L Model.

where $\phi \in \{h, H\}$. The partonic cross section can be split in three processes

$$\begin{aligned} \mathrm{d}\hat{\sigma}^{\mathrm{DY}}_{ij\to Z\phi+X}(\tau,\mu_{\mathrm{R}},\mu_{\mathrm{F}}) = &\int \mathrm{d}q^2\, \mathrm{d}\hat{\sigma}_{ij\to Z^*+X}(\tau,\mu_{\mathrm{R}},\mu_{\mathrm{F}})\, \frac{\mathrm{d}\Gamma_{Z^*\to Z\phi}(q^2)}{\mathrm{d}q^2} \\ &+ \int \mathrm{d}q^2\, \mathrm{d}\hat{\sigma}_{ij\to Z'^{(*)}+X}(\tau,\mu_{\mathrm{R}},\mu_{\mathrm{F}})\, \frac{\mathrm{d}\Gamma_{Z'^{(*)}\to Z\phi}(q^2)}{\mathrm{d}q^2} \\ &+ \int \mathrm{d}q^2\, \mathrm{d}\hat{\sigma}_{ij\to Z^*/Z'^{(*)}+X}(\tau,\mu_{\mathrm{R}},\mu_{\mathrm{F}})\, \frac{\mathrm{d}\Gamma_{Z^*/Z'^{(*)}\to Z\phi}(q^2)}{\mathrm{d}q^2}, \end{aligned} \tag{2.17}$$

that all factorize into the production of a color singlet and a subsequent decay into the desired final state. The first term on the right-hand side of Eq. (2.17) describes the production of a virtual Z^* boson with the virtual mass $\sqrt{q^2}$ and its decay,

$$\frac{\mathrm{d}\Gamma_{Z^*\to Zh}(q^2)}{\mathrm{d}q^2} = \frac{G_{\mathrm{F}} M_Z^4}{2\sqrt{2}\pi^2} \frac{\sqrt{\lambda(M_Z^2, M_h^2, q^2)/q^4}}{\left(q^2 - M_Z^2\right)^2 + M_Z^2\Gamma_Z^2} \left(1 + \frac{\lambda(M_Z^2, M_h^2, q^2)}{12\, q^2 M_Z^2}\right) \cos^2(\alpha), \tag{2.18}$$

$$\frac{\mathrm{d}\Gamma_{Z^*\to ZH}(q^2)}{\mathrm{d}q^2} = \frac{G_{\mathrm{F}} M_Z^4}{2\sqrt{2}\pi^2} \frac{\sqrt{\lambda(M_Z^2, M_H^2, q^2)/q^4}}{\left(q^2 - M_Z^2\right)^2 + M_Z^2\Gamma_Z^2} \left(1 + \frac{\lambda(M_Z^2, M_H^2, q^2)}{12\, q^2 M_Z^2}\right) \sin^2(\alpha). \tag{2.19}$$

This contribution is the analog to the SM contribution, but we introduce the dependence on the Z boson's decay width, Γ_Z, that originates from the replacement of ordinary propagators with Breit-Wigner propagators. The production cross section for the virtual Z^* boson, $\mathrm{d}\hat{\sigma}_{ij\to Z^*+X}$, is unchanged with respect to the SM. In the same manner, the second term of Eq. (2.17) is factorized into the production of a Z' boson with a squared momentum q^2 and its decay into a Z and a Higgs. The Z' can be either a virtual particle or an on-shell particle if its mass is higher than the threshold energy that is necessary to produce the final state, which is the reason for the introduction of Breit-Wigner propagators. The Breit-Wigner propagator ensures a finite value for the decay functions, even for a propagating on-shell Z' boson,

$$\begin{aligned} \frac{\mathrm{d}\Gamma_{Z'^{(*)}\to Zh}(q^2)}{\mathrm{d}q^2} = &\frac{G_{\mathrm{F}} M_Z^4}{2\sqrt{2}\pi^2} \frac{\sqrt{\lambda(M_Z^2, M_h^2, q^2)/q^4}}{\left(q^2 - M_{Z'}^2\right)^2 + M_{Z'}^2\Gamma_{Z'}^2} \left(1 + \frac{\lambda(M_Z^2, M_h^2, q^2)}{12\, q^2 M_Z^2}\right) \\ &\times \left[\frac{v g_1'}{M_Z} \cos(\alpha)\right]^2, \end{aligned} \tag{2.20}$$

$$\begin{aligned} \frac{\mathrm{d}\Gamma_{Z'^{(*)}\to ZH}(q^2)}{\mathrm{d}q^2} = &\frac{G_{\mathrm{F}} M_Z^4}{2\sqrt{2}\pi^2} \frac{\sqrt{\lambda(M_Z^2, M_H^2, q^2)/q^4}}{\left(q^2 - M_{Z'}^2\right)^2 + M_{Z'}^2\Gamma_{Z'}^2} \left(1 + \frac{\lambda(M_Z^2, M_H^2, q^2)}{12\, q^2 M_Z^2}\right) \\ &\times \left[\frac{v g_1'}{M_Z} \sin(\alpha)\right]^2. \end{aligned} \tag{2.21}$$

The decay functions have a very similar structure to the decay functions of the Z boson, which is to be expected considering the similarity of the Z and Z' bosons, but they depend on the mass and the decay width of the new boson, $M_{Z'}$ and $\Gamma_{Z'}$, respectively. In both equations, the last term in square brackets stems form the coupling of Z' to Z and the Higgs boson. Therein, the coupling constant g'_1 of the $\mathbf{U}(\mathbf{1})_{B-L}$ symmetry group as well as the SM vacuum expectation value v appear. Moreover, it is notable that the production cross section of the Z' boson cross section, $\mathrm{d}\hat{\sigma}_{ij\to Z'(*)+X}$, is, up to different values of the coupling constants, the same as for the production of a virtual Z^* and, thus, they are linked by a global scaling factor. The details can be found in Appendix A.
This behavior is used in the third term of Eq. (2.17) that describes the Higgs-Strahlung production due to the interference of the diagrams with a Z and a Z' mediator. The fact that the interactions of both neutral gauge bosons with other particles only differ by the strength of the couplings, but not by any other property, allows for performing a factorization as we made it before. The production of the color singlet, $\mathrm{d}\hat{\sigma}_{ij\to Z*/Z'(*)+X}$, has the same functional dependence on the kinematic parameters as for producing a Z or a Z' boson[4], the difference are the appearing couplings that take one time the value for a $q\bar{q}Z$ coupling and the other time for a $q\bar{q}Z'$ coupling in the squared matrix elements. The resulting decay functions of the interference term then take the shapes

$$\begin{aligned}\frac{\mathrm{d}\Gamma_{Z*/Z'(*)\to Zh}(q^2)}{\mathrm{d}q^2} &= \frac{G_\mathrm{F} M_Z^4}{\sqrt{2}\pi^2} \frac{(q^2-M_Z^2)(q^2-M_{Z'}^2)+M_Z M_{Z'}\Gamma_Z\Gamma_{Z'}}{\left[(q^2-M_Z^2)^2+M_Z^2\Gamma_Z^2\right]\left[(q^2-M_{Z'}^2)^2+M_{Z'}^2\Gamma_{Z'}^2\right]} \\ &\quad\times\sqrt{\lambda(M_Z^2,M_h^2,q^2)/q^4}\left(1+\frac{\lambda(M_Z^2,M_h^2,q^2)}{12\,q^2M_Z^2}\right) \\ &\quad\times\left[\frac{vg'_1}{M_Z}\cos(\alpha)\right]\cos(\alpha),\end{aligned} \tag{2.22}$$

$$\begin{aligned}\frac{\mathrm{d}\Gamma_{Z*/Z'(*)\to ZH}(q^2)}{\mathrm{d}q^2} &= \frac{G_\mathrm{F} M_Z^4}{\sqrt{2}\pi^2} \frac{(q^2-M_Z^2)(q^2-M_{Z'}^2)+M_Z M_{Z'}\Gamma_Z\Gamma_{Z'}}{\left[(q^2-M_Z^2)^2+M_Z^2\Gamma_Z^2\right]\left[(q^2-M_{Z'}^2)^2+M_{Z'}^2\Gamma_{Z'}^2\right]} \\ &\quad\times\sqrt{\lambda(M_Z^2,M_H^2,q^2)/q^4}\left(1+\frac{\lambda(M_Z^2,M_H^2,q^2)}{12\,q^2M_Z^2}\right) \\ &\quad\times\left[\frac{vg'_1}{M_Z}\sin(\alpha)\right]\sin(\alpha).\end{aligned} \tag{2.23}$$

The effects of the B–L Model, however, do not just show up in the Drell-Yan-like Higgs-Strahlung production, they also have relevance for the phenomenology of the gluon-induced process. The triangle diagrams in Figure 2.6(a) are impacted by the same modifications as the Drell-Yan-like mode, so, their contribution is affected by the changes of the coupling constants at the Higgs-gauge vertices but additionally by the presence of the new Z' mediator. Besides the triangle contributions, the box diagrams can give rise to Zh as well as ZH production, *cf.* Figure 2.6(b), where the Yukawa couplings for the interactions $q\bar{q}h$ and $q\bar{q}H$ obtain rescaling factors in comparison to their SM pendant that read

$$g_q^h = \cos(\alpha), \qquad g_q^H = \sin(\alpha), \tag{2.24}$$

[4]Note that both bosons are produced with the (virtual) momentum square q^2, so that their different physical masses do not impact the computation.

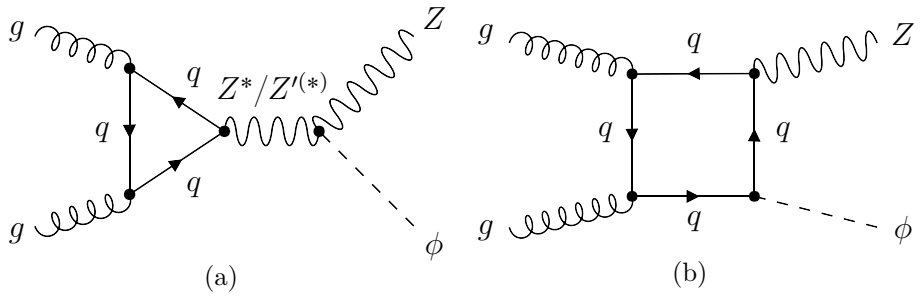

Figure 2.6.: Feynman diagrams for gluon-initiated Higgs-Strahlung in the B–L Model. The Higgs boson ϕ can be either h or H.

respectively. With the same arguments as in the SM and the 2HDM we can conclude that only bottom and top quarks give rise to the loop-induced cross sections.
While the 2HDM has not changed the kinematical dependence of the Drell-Yan-like process for final states with a charged W boson and a neutral Z boson comparing it with the SM predictions, the situation is different when comparing the SM and the B–L Model. In the former case, the cross sections of both models are simply related by a global factor, but, in the second scenario, only the Higgs-Strahlung cross sections with a W boson in the final state can be recovered due to such a global rescaling. If, instead, a Z appears to be in the final state, the kinematic dependence is changed because of the presence of a new Z' that gives rise to new contributions and interference effects. Furthermore, the gluon-induced process obtains non-trivial modifications to its kinematic distributions in the B–L Model making this mode sensitive to possible BSM signatures in experimental measurements.

2.3. R^{VH} Double Ratio

As pointed out in the last section, the Higgs-Strahlung reaction might be sensitive to New Physics effects that are not covered by the SM. Depending on the BSM scenario, these effects can show up by keeping the the symmetry of the Drell-Yan-like contributions between the Higgs production in association W or with a Z boson or the new effects can have different impact on both production modes. As example for the former scenario, where symmetry effects are kept, we have seen the 2HDM where the ratio of Drell-Yan-like WH and ZH production is unchanged with respect to the SM. The B–L Model instead changes this ratio as more New Physics effects influence the ZH creation as the WH production. However, experimental constrains hint for a good agreement of the Higgs-Strahlung cross sections with SM predictions. Since the Drell-Yan-like contribution is the dominant one, we can deduce that large impact of New Physics on them is very unlikely, at least at energies that are accessible in the range of the LHC. Still, New Physics effects can have high impact on the subleading non-Drell-Yan-like contributions, manly driven by the gluon-induced process, that are suppressed with respect to the Drell-Yan-like production and to which measurements are not sensitive yet. In particular, we have seen that the gluon-initiated component reveals interesting features potentially leading to characteristic, model-dependent structures in kinematical distributions of cross sections. For instance, it is well-known that triangle and box diagrams interfere destructively in the SM, but if the top-quark Yukawa coupling would be smaller than predicted by the SM the impact of the box diagrams with a top-quark

loop becomes small and the destructive effects above the top-pair production threshold would be smaller resulting in a larger $gg \to ZH$ cross section.
In order to use the gluon-fusion mode for ZH production as a probe of BSM theories, it needs to be separated from the Drell-Yan-like production mode that appears as an irreducible experimental background. Therefore, Ref. [115] has extended the idea that originally has been suggested in Ref. [99] and it has been shown that the symmetry of the WH and ZH Drell-Yan-like components[5] can be exploited to define the R^{VH} double ratio

$$R^{ZH}(x) = \frac{R^{VH}(x)}{R^{VH}_{\mathrm{DY}}(x)} \tag{2.25}$$

which serves a suitable observable that is sensitive to the non-Drell-Yan-like Higgs-Strahlung contributions. The numerator of this double ratio is a ratio of differential cross sections for a specific kinematic variable x of the ZH and WH process,

$$R^{VH}(x) = \frac{\mathrm{d}\sigma_{pp\to ZH+X}/\mathrm{d}x}{\mathrm{d}\sigma_{pp\to WH+X}/\mathrm{d}x}. \tag{2.26}$$

This quantity can be measured in an experiment such as ATLAS or CMS. The numerator of Eq. (2.26) contains events from Drell-Yan-like and non-Drell-Yan-like Higgs-Strahlung, while the WH process in the denominator does only receive contributions from the Drell-Yan-like mechanism. The second ratio in the denominator of Eq. (2.25) is the ratio of the Drell-Yan-like production modes,

$$R^{VH}(x) = \frac{\mathrm{d}\sigma^{\mathrm{DY}}_{pp\to ZH+X}/\mathrm{d}x}{\mathrm{d}\sigma^{\mathrm{DY}}_{pp\to WH+X}/\mathrm{d}x}. \tag{2.27}$$

This ratio requires input from theoretical predictions as its direct measurement is not possible.
If the double ratio in Eq. (2.25) would be computed in a pure theory calculation, the WH terms would cancel each other and we would find

$$\begin{aligned} R^{ZH}(x) &= \frac{R^{VH}(x)}{R^{VH}_{\mathrm{DY}}(x)} \\ &= \frac{\mathrm{d}\sigma_{pp\to ZH+X}/\mathrm{d}x}{\mathrm{d}\sigma^{\mathrm{DY}}_{pp\to ZH+X}/\mathrm{d}x} \\ &= 1 + \frac{\mathrm{d}\sigma^{\mathrm{non-DY}}_{pp\to ZH+X}/\mathrm{d}x}{\mathrm{d}\sigma^{\mathrm{DY}}_{pp\to ZH+X}/\mathrm{d}x}, \end{aligned} \tag{2.28}$$

where the second term in the third line unravels why this double ratio is sensitive to the physics of the non-Drell-Yan-like contributions, $\mathrm{d}\sigma^{\mathrm{non-DY}}_{pp\to ZH+X}$.
The advantage of using the double ratio instead of directly comparing the experimental measurement of the ZH cross section with the theoretical prediction of the Drell-Yan-like component, as appearing in the second line of Eq. (2.28), lies in the cancellation of systematic uncertainties in the experimental as well as in the theoretical inputs. Measuring the ratio in an experiment, it is expected that systematic uncertainties, as for example uncertainties due to the beam luminosity, are significantly reduced. Addi-

[5] To be precise, some diagrams of the above mentioned subprocess that is mediated by top quarks do also contribute to what we call Drell-Yan-like contributions in the context of the double ratio. However, their effects are negligible and are not considered here. Taking them into account would not break the symmetry.

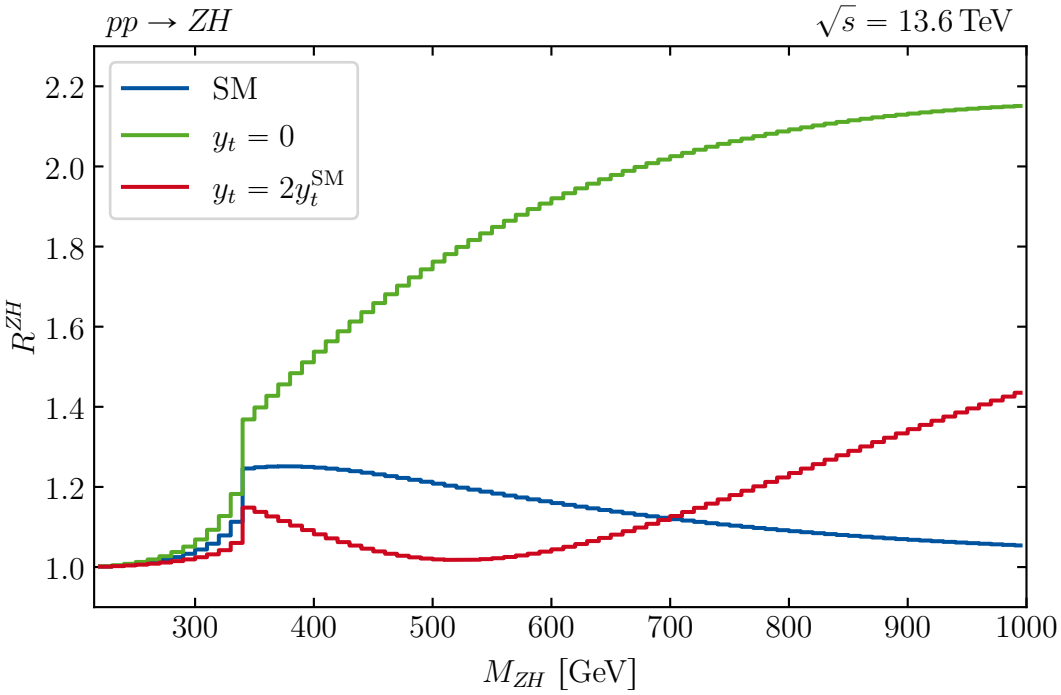

Figure 2.7.: Invariant mass spectrum of the double ratio $R^{ZH} \equiv R^{ZH}(M_{ZH})$. The blue line shows the SM prediction, the green line represents a modified SM without a top-quark Yukawa coupling, and the red line a model with a top-quark Yukawa coupling that is the double of the SM value. This plot is produced with `vh@nnlo` and a recreation of a plot in Ref. [115], tuned to the input parameters we will use for our later studies. In particular, we use the `PDF4LHC21_40` PDF set [151] and set the factorization as well as the renormalization scale dynamically to the invariant mass of the Higgs-vector boson system, $\mu_{\text{F}} = \mu_{\text{R}} = M_{ZH}$.

tionally, the Drell-Yan ratio in the denominator can be predicted with high accuracy. Systematic uncertainties, for example errors introduced due to fixed order computations, are strongly correlated between WH and ZH production in this mode and cancel, at least partly, each other.

An example for this double ratio, predicted by a theory computation, is shown in Figure 2.7. The ratio is computed as spectrum of the invariant mass of the final-state ZH system, M_{ZH}. Moreover, the ratios for two New Physics scenarios are compared to the SM (blue line). Both models are variations of the SM where only the top-quark Yukawa coupling is modified. In a modification where the top-quark and the Higgs boson do not couple directly (green line) we observe the behavior that we have mentioned previously. Due to the absence of the Yukawa coupling, top quarks cannot appear in the box diagrams, only bottom quarks can be present therein. This means that the negative interference effects of those box diagrams with top-quark loops and triangle diagrams are not reducing the cross section anymore. This missing interference effects become particularly visible in the kinematic region where the contribution of these box diagrams is most important in the SM, namely above the threshold for having on-shell top quarks in the box, so for M_{ZH} bigger than twice the top mass. Indeed, above roughly 350 GeV the double ratio for the model without a Higgs-to-top coupling is much larger

than the SM prediction. Since the Drell-Yan-like contributions in both models are the same, these changes can clearly be deduced to originate from the non-Drell-Yan-like component, *cf.* Eq. (2.28). In contrast, the model with an increased Yukawa coupling (red line) is expected to show more destructive interference effects. Specifically, above the top-pair threshold a reduction of the corresponding double ratio can be seen. However, the double ratio of the model with the enhanced Yukawa coupling becomes larger than the SM double ratio for M_{ZH} bigger than approximately 700 GeV. This effect is driven by the increased contribution from the squared amplitudes of the box diagrams.

3

Infrared Divergences

Contents

Prior we discuss the computation of the fully-differential Higgs-Strahlung cross section at NNLO precision, it is crucial to obtain a comprehensive overview of the challenges inherent in such calculations. One of the most difficult tasks addresses the occurrence of IR singularities that show up all over in the evaluation of phase-space integrals. In this chapter, we want to elucidate the origin of these singularities and outline the general strategies that are used to regulate them.

3.1. Kinoshita–Lee–Nauenberg Theorem

According to Eq. (2.4) we can write a differential cross section with initial-state partons i and j as

$$\mathrm{d}\hat{\sigma}_{ij} = \mathrm{d}\hat{\sigma}_{ij}^{\mathrm{LO}} + \mathrm{d}\hat{\sigma}_{ij}^{\mathrm{NLO}} + \mathrm{d}\hat{\sigma}_{ij}^{\mathrm{NNLO}} + \mathcal{O}\left(\alpha_s^3\right). \tag{3.1}$$

The LO cross section can be computed from the corresponding diagrams and we will not have to face any issues with divergences in our calculations. In the final state we will just have the particles that we aim to produce in the scattering process. As this part of the cross section corresponds to its Born approximation we will call the LO cross section also the Born cross section, $\mathrm{d}\sigma_{ij}^{\mathrm{B}}$,

$$\mathrm{d}\hat{\sigma}_{ij}^{\mathrm{LO}} = \mathrm{d}\hat{\sigma}_{ij}^{\mathrm{B}}. \tag{3.2}$$

The phase space of the particles that appear in the Born approximation will be referred to as Born phase space from now on.
At NLO, however, the situation becomes more complicated. The cross section will just be finite if we take into account Feynman diagrams with virtual corrections, $\mathrm{d}\hat{\sigma}_{ij}^{\mathrm{V}}$, as well as real-emission contributions, $\mathrm{d}\hat{\sigma}_{ij}^{\mathrm{R}}$, which means that we will have additional massless partons in the final state on top to the particles from the Born process,

$$\mathrm{d}\hat{\sigma}_{ij}^{\mathrm{NLO}} = \mathrm{d}\hat{\sigma}_{ij}^{\mathrm{R}} + \mathrm{d}\hat{\sigma}_{ij}^{\mathrm{V}} + \mathrm{d}\hat{\sigma}_{ij}^{\mathrm{C_{NLO}}}. \tag{3.3}$$

The collinear counterterm $\mathrm{d}\hat{\sigma}_{ij}^{\mathrm{C_{NLO}}}$ has its origin in the separation of the short- and long-distance effects during mass factorization. This term shifts the collinear divergences of

the bare PDFs into the partonic cross section, resulting in finite PDFs. Each of the three contributions of Eq. (3.3) is individually divergent and contains IR singularities. However, the Kinoshita–Lee–Nauenberg (KLN) theorem has proven that their sum is finite, as it is associated with a physical observable [152–154].
The IR divergences in virtual contributions are manifest at the level of scattering matrix elements. In dimensional regularization with $d = 4 - 2\epsilon$ dimensions they appear in the loop integrations as explicit poles in terms of the regulator ϵ.
The same holds for the collinear counterterm that stems from mass factorization where all singularities are expressed as $1/\epsilon^k$ poles.
In real contributions the singularities only become manifest after the integration over the phase space of the emitted partons. This can be seen in the following way: If we consider a general process where a massless incoming parton i with momentum p_i emits a massless final state parton f with momentum p_f we can schematically write the squared matrix element as

$$|\mathcal{M}|^2 = \left| \quad \right|^2 \sim \frac{1}{(p_i - p_f)^2} = \frac{1}{E_i E_f \,(1 - \cos\theta_{fi})}, \tag{3.4}$$

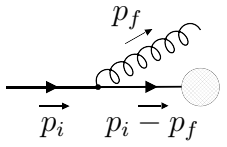

where E_i and E_f are the energies of the incoming and outgoing parton, respectively, and θ_{fi} is the angle between them. The gray hatched dot in the Feynman diagram can represent any hard scattering process. To obtain the cross section we have to integrate over the phase space of all final state particles, including the real emitted parton,

$$\hat{\sigma} \sim \int \overline{|\mathcal{M}|^2}\, \mathrm{d}\Pi_f^{(4)} \sim \int_0^{E_{\max}} \mathrm{d}E_f \int_{-1}^{1} \mathrm{d}\cos\theta_{fi} \frac{1}{E_i E_f \,(1 - \cos\theta_{fi})} \to \infty \begin{cases} \text{if } E_f \to 0, \\ \text{if } \theta_{fi} \to 0. \end{cases} \tag{3.5}$$

The phase-space integral is determined by integrating over all possible energies of the final-state parton, ranging from zero to a maximum energy $E_{\max}$, which is constrained by the energy conservation of the entire process. Additionally, an integration over all possible emission angles θ_{fi} is performed. It is important to notice that the cross section exhibits divergences in two different phase-space regions. The first divergence arises when the final-state parton becomes soft, meaning it has zero energy. These kind of divergencies are called soft singularities. The second type of divergences appears when the angle between the emitted parton and the emitter parton approaches zero, known as collinear singularities. If both scenarios show up simultaneously, we encounter soft-collinear singularities.
Since we are interested in computing fully-differential cross sections, it is necessary to extract the implicit IR singularities of the real contributions without explicitly performing an analytic phase-space integration where these divergences can be regulated. Commonly, two different techniques are used to archive this goal. The first technique is based on so-called phase-space slicing methods, which will be explained in section 3.2. These methods provide a systematic approach to isolate and handle the IR singularities in the calculations. The second technique uses IR subtraction schemes to provide a specific strategy for removing divergences. The concept behind subtraction schemes will be described in section 3.3.
Before we move on to the technical details of the slicing methods and the subtraction schemes, we would like to briefly remark on the NNLO cross section,

$$\mathrm{d}\hat{\sigma}_{ij}^{\mathrm{NNLO}} = \mathrm{d}\hat{\sigma}_{ij}^{\mathrm{RR}} + \mathrm{d}\hat{\sigma}_{ij}^{\mathrm{RV}} + \hat{\sigma}_{ij}^{\mathrm{VV}} + \mathrm{d}\hat{\sigma}_{ij}^{\mathrm{C_{NNLO}}}. \tag{3.6}$$

All singularities of the double-real emission $\mathrm{d}\hat{\sigma}_{ij}^{\mathrm{RR}}$ are encoded in the phase space of the two emitted partons. Due to overlapping singularities in this case, complex techniques have to be introduced to extract them. The real-virtual contributions $\mathrm{d}\hat{\sigma}_{ij}^{\mathrm{RV}}$ contain both, non-explicit phase-space singularities as well as manifest poles from loop integrals. In contrast, all poles are manifest in the double-virtual contributions $\hat{\sigma}_{ij}^{\mathrm{VV}}$ and the collinear counterterm $\mathrm{d}\hat{\sigma}_{ij}^{\mathrm{C_{NNLO}}}$.

3.2. Phase-Space Slicing

To obtain a meaningful differential cross section it is essential to introduce an infrared-safe measurement function to define an infrared-safe observable [155]. Such an observable is important to ensure that the appearance of unresolved partons does not lead to unphysical configurations. With unresolved parton we mean a real emitted parton that is aligned in such a way to its parent parton that they cannot be resolved as independent particles in an experimental signature. This is the case in the soft as well as collinear limit. In the soft limit, the emitted parton has no energy, thus, a detector is unable to measure its presence, leading to a signature where the parent parton appears indistinguishable from a scenario where no additional particle was emitted. Likewise, in the collinear case, both partons reach the detector simultaneously and occupy the same spatial position. This results in a signal that is impossible to distinguish from a signal the parent parton would generate without any emission. According to Eq. (2.6) the NLO cross section can be written as

$$2\hat{s}\cdot\hat{\sigma}^{\mathrm{NLO}} = \lim_{d\to 4}\left(\int \overline{|\mathcal{M}|^2}F_J\,\mathrm{d}\Pi_{\mathrm{B}}^{(4)} + \int \overline{|\mathcal{M}_J|^2}F_J\,\mathrm{d}\Pi_{\mathrm{B+1}}^{(d)}\right), \tag{3.7}$$

where the measurement function F_J defines the infrared-safe observable[1]. The matrix elements $\mathcal{M}$ contain only particles of the Born cross section in the final state, and are integrated over the Born phase space $\mathrm{d}\Pi_{\mathrm{B}}^{(4)}$. On the other hand, the matrix elements $\mathcal{M}_J$ include the processes with real radiation and, therefore, have to be integrated over one additional final-state particle, $\mathrm{d}\Pi_{\mathrm{B+1}}^{(d)}$. The second phase-space integration is explicitly carried out in $d = 4-2\epsilon$ dimensions since the contribution is divergent. Only after summing up the two terms in Eq. (3.7) the limit $d \to 4$ can be taken safely.
The phase-space slicing method [156–159] allows us to manifest all singularities of the phase-space integration, enabling us to perform both integrals in $d = 4$ dimensions. Assuming that the integration over the IR-sensitive observable goes from 0 to 1 and the integral diverges at the lower boundary, we can place a cut δ on the phase space and slice it up into a hard region and a soft-collinear region,

$$\begin{aligned} 2\hat{s}\cdot\hat{\sigma}^{\mathrm{NLO}} &= \lim_{d\to 4}\left(\int_0^{\delta} \overline{|\mathcal{M}|^2}F_J\,\mathrm{d}\Pi_{\mathrm{B}}^{(4)} + \int_0^{\delta} \overline{|\mathcal{M}_J|^2}F_J\,\mathrm{d}\Pi_{\mathrm{B+1}}^{(d)} + \int_{\delta}^{1} \overline{|\mathcal{M}_J|^2}F_J\,\mathrm{d}\Pi_{\mathrm{B+1}}^{(d)}\right) \\ &= \lim_{d\to 4}\left(\int_0^{\delta}\left[\overline{|\mathcal{M}|^2}F_J\,\mathrm{d}\Pi_{\mathrm{B}}^{(4)} + \overline{|\mathcal{M}_J|^2}F_J\,\mathrm{d}\Pi_{\mathrm{B+1}}^{(d)}\right]\right) + \int_{\delta}^{1} \overline{|\mathcal{M}_J|^2}F_J\,\mathrm{d}\Pi_{\mathrm{B+1}}^{(4)}. \end{aligned} \tag{3.8}$$

[1]The function F_J depends on all external momenta, including possible real-emitted partons. However, in any IR limit the measurement function with the unresolved parton has to reduce to the measurement function that only depends on the parent parton's momentum without emission. More details can be found in Ref. [155].

In the first line we have also placed the cut on the integral $\mathrm{d}\Pi_{\mathrm{B}}^{(4)}$, but since this cut just acts on the phase space of the real-emitted particle it appears to be trivial. This allows us to combine the two pieces which contain IR poles in the soft-collinear region that goes from 0 to δ in the second line. In this way, we can easily carry out the integration in the hard region that goes from δ to 1 in $d = 4$ dimensions as this region is, by construction, free of poles.
If the cut-off parameter is chosen to be small enough, the integrand in the square brackets can be approximated in the soft-collinear limit. In this approximation, the IR phase-space poles will show up explicitly and cancel analytically against the singularities that appear already as manifest poles in $|\mathcal{M}|^2$, which have their origin in the virtual loops and collinear counterterm. Hence, the integral in the soft-collinear region can be performed in $d = 4$ dimensions,

$$\begin{aligned} 2\hat{s}\cdot\hat{\sigma}^{\mathrm{NLO}} &= \lim_{d\to 4}\left(\int_0^\delta \left[\overline{|\mathcal{M}|^2}F_J\,\mathrm{d}\Pi_{\mathrm{B}}^{(4)} + \overline{|\mathcal{M}_J|^2}F_J\,\mathrm{d}\Pi_{\mathrm{B+1}}^{(d)}\right]\right) + \int_\delta^1 \overline{|\mathcal{M}_J|^2}F_J\,\mathrm{d}\Pi_{\mathrm{B+1}}^{(4)} \\ &= \int_0^\delta \left[\overline{|\mathcal{M}|^2}F_J\,\mathrm{d}\Pi_{\mathrm{B}}^{(4)} + \overline{|\mathcal{M}_J|^2}F_J\,\mathrm{d}\Pi_{\mathrm{B+1}}^{(4)}\right]_{\mathrm{s.c.}} + \int_\delta^1 \overline{|\mathcal{M}_J|^2}F_J\,\mathrm{d}\Pi_{\mathrm{B+1}}^{(4)} + \mathcal{O}(\delta). \end{aligned} \tag{3.9}$$

The index s.c. symbolizes that this integrand is taken in a soft-collinear approximation which introduces also power corrections proportional to the cut-off parameter δ.
In a similar manner, the phase-space slicing can be applied to NNLO processes without requiring any conceptual modifications. The analogous expression to Eq. (3.7) takes the form

$$2\hat{s}\cdot\hat{\sigma}^{\mathrm{NNLO}} = \lim_{d\to 4}\left(\int \overline{|\mathcal{M}|^2}F_J\,\mathrm{d}\Pi_{\mathrm{B}}^{(4)} + \int \overline{|\mathcal{M}_J|^2}F_J\,\mathrm{d}\Pi_{\mathrm{B+1}}^{(d)} + \int \overline{|\mathcal{M}_{2J}|^2}F_J\,\mathrm{d}\Pi_{\mathrm{B+2}}^{(d)}\right), \tag{3.10}$$

where the matrix element $\mathcal{M}_{2J}$ includes the contributions with double-real radiation and the d-dimensional phase space $\mathrm{d}\Pi_{\mathrm{B+2}}^{(d)}$ contains the particles of the Born process plus two additional partons. The slicing method can now be constructed along the lines as described for the NLO cross section.
The application of phase-space slicing to compute exclusive cross sections comes with many advantages. One of the main features is that the methods are conceptually simpler than subtraction schemes. This makes them easier to handle and implement in MC phase-space generators, so that phenomenological results can be obtained with a reasonable amount of work. In addition, concepts do not change when going to higher orders in perturbation theory, which allows us to significantly benefit from the amount of experience collected at NLO computations when going the step towards NNLO. Even first processes have been computed fully differentially at $\mathrm{N^3LO}$ in this way [160–162].
Despite their advantages, these methods are accompanied by certain drawbacks. Slicing methods, in particular, suffer from non-locality, meaning that they are not well-defined point-by-point in phase space and matrix elements are not finite everywhere. Thus, large numerical cancellations in intermediate steps are unavoidable which can introduce numerical instabilities and tremendous computational effort. Although increasing the cut-off parameter δ can partially stabilize the numerical issues, it also gives rise to larger power corrections. Hence, finding a suitable balance for the cut-off parameter is a challenging task.
Anyhow, slicing methods are applied successfully to a wide variety of QCD processes at NLO as well as NNLO. Depending on the choice of the infrared-safe observable that splits the phase space different slicing methods can be created. The first NNLO slicing

method is known as q_{T} slicing [29] which is based on counterterms that are constructed by transverse momentum resummation [163, 164] and is used in the public available code `MATRIX` [165]. Another famous strategy is N-jettiness slicing [30, 166, 167] which uses the N-jettiness event shape variable [168] to split the phase space and is implemented in the public tools `MCFM` [169] as well as `MATRIX` [165].

3.3. Infrared Subtraction Schemes

Another commonly used approach to compute fully-differential IR-safe cross sections is to employ IR subtraction schemes. These schemes require a suitable subtraction function, denoted by $\mathcal{S}$, which must reproduce the squared matrix element $|\mathcal{M}_J|^2$ in all limits with unresolved partons. To construct the subtraction functions, one needs to identify a parameter, denoted by x, that is sensitive to the leading IR singularities of $\mathcal{M}_J$ for the observable defined by F_J. Assuming that these limits are obtained when x approaches zero, the subtraction function can be computed as

$$\mathcal{S} = \lim_{x\to 0} \overline{|\mathcal{M}_J|^2} F_J. \tag{3.11}$$

The limit is not uniquely defined, but for $\mathcal{S}$ to be useful, the subtraction function must be analytically integrable in the unresolved phase-space region without approximations. In that case, the IR-safe expression for the cross section, given by Eq. (3.7), can be rewritten as a sum of three integrals,

$$2\hat{s}\cdot\hat{\sigma}^{\mathrm{NLO}} = \lim_{d\to 4}\left(\int \overline{|\mathcal{M}|^2} F_J \,\mathrm{d}\Pi_{\mathrm{B}}^{(4)} + \int \left[\overline{|\mathcal{M}_J|^2} F_J - \mathcal{S}\right]\mathrm{d}\Pi_{\mathrm{B+1}}^{(d)} + \int \mathcal{S}\,\mathrm{d}\Pi_{\mathrm{B+1}}^{(d)}\right). \tag{3.12}$$

The first integral involves $|\mathcal{M}|^2 F_J$ and is taken over the Born phase space. The second integral involves the difference between $|\mathcal{M}_J|^2 F_J$ and $\mathcal{S}$, and is taken over the phase space including real radiation in d dimensions. This difference does not contain any IR singularities, since the subtraction function $\mathcal{S}$ has been constructed to cancel them. Therefore, the second integral can be performed exactly in $d = 4$ dimensions. Finally, the third integral adds the subtraction function back again and is also taken over the phase space with real radiation in d dimensions. This integral reintroduces the singularities that were subtracted in the second integral. However, since the subtraction function can be integrated analytically over the phase space of unresolved particles, the singularities become manifest and can be safely canceled against those in $|\mathcal{M}|^2$, allowing one to take the limit $d \to 4$ everywhere. In the following we will refer to the subtraction term that we add back and integrate over the phase space of the real emitted parton as integrated counterterm. After pole cancellation, all terms in Eq. (3.12) are finite, and hence the phase space can be integrated numerically.

Subtraction schemes offer the main advantage that they can be constructed fully local, where subtracted matrix elements remain finite point-by-point in the phase space. Another key benefit is that they do not rely on an unphysical cut-off parameter that requires tuning and introduces power corrections. In combination with analytic pole cancellation, this leads to numerically stable results, minimizing the extent of numerical cancellations observed in slicing methods. As consequence, the computational resources required for precise predictions is reduced. At NLO, previous experiences have demonstrated that subtraction schemes usually outperform phase-space slicing with regard to accuracy and speed [170–172]. Therefore, it is desirable to apply such schemes also in higher-order calculations.

However, constructing subtraction schemes is very challenging. The search for suitable subtraction functions demands extensive effort and must be carried out order-by-order, as a general method for this purpose is not known yet. A further challenge is the analytic integration of the counterterms over the unresolved phase space, which often leads to intricate integrals and can only be solved using complex and sophisticated mathematical techniques. But once this groundwork is done, subtraction schemes prove to be highly effective. So, we have made the decision to utilize one of these schemes for computing the Higgs-Strahlung process at NNLO precision.
For NNLO processes many different schemes have been developed. The first general NNLO subtractions schemes were the so-called Antenna Subtraction [31, 66, 68, 69, 173–214], Sector Decomposition [32, 33], and Sector-Improved Residue Subtraction [34, 35, 121, 122]. Antenna Subtraction is used in the `NNLOjet` framework and Sector-Improved Residue Subtraction in the `STRIPPER` (SecToR Improved Phase sPacE for real Radiation) library which are both private tools. A `Python` implementation of Sector Decomposition is available under the name `pySecDec` [215]. More special subtraction schemes are the CoLoRFulNNLO (Completely Local subtRactions for Fully differential NNLO) Subtraction [36, 216–229] and the Projection-to-Born method [37]. The former scheme is only fully worked out for colorless initial-state particles, but it allows for an arbitrary number of final-state partons. The latter is specifically applicable to processes with colorless final states, but it posses the unique feature of being valid at N^3LO for them. The first computation of such a process was conducted in Ref. [230]. Additionally, in recent years, a new wave of general NNLO subtraction schemes has emerged. They are known as Geometric IR Subtraction [39], Local Analytic Sector Subtraction [40], and Nested Soft-Collinear Subtraction [38, 116–118]. An overview discussing some of these state-of-the-art schemes, as well as slicing methods, can be found in Ref. [231].
Adapted to our purpose, we decided to implement the Nested Soft-Collinear Subtraction scheme. As a modification of the `STRIPPER` scheme it unifies the generality of this approach, which has proven to be successfully applicable to a wide variety of complex and phenomenologically relevant processes [232–237], with a physically intuitive as well as modern perspective on NNLO subtraction. Notably, an implementation of this scheme has already contributed to a deeper understanding of color-singlet production and Higgs-Strahlung in the SM [62–65, 238–242] as well as scenarios beyond [114, 243, 244].

4

Frixione-Kunszt-Signer Subtraction

Contents

The NNLO Nested Soft-Collinear Subtraction scheme builds upon the idea of the NLO Frixione-Kunszt-Signer (FKS) Subtraction method [245, 246] and extends the same strategy to NNLO calculations. The FKS scheme, along with the Catani-Seymour (CS) Dipole Subtraction [247, 248] method, has become the standard tool for NLO computations. Both schemes are fully automatized and widely used in various applications.
Since the Nested Soft-Collinear Subtraction scheme coincides with the FKS Subtraction at NLO, we present an outline of this method and compute the NLO corrections for Higgs-Strahlung. We aim to become familiar with the notation that we will utilize in the subsequent NNLO computation.

4.1. Color-Singlet Production at Next-to-Leading Order

In this chapter, we apply the FKS formalism to the production of a general color singlet in proton-proton collisions, $pp \to V + X$. The arbitrary color singlet V corresponds to the Born process of interest and should not be confused with the notation for a vector boson used in chapter 2. The final state X represents the partons from real radiation corrections.
For the Drell-Yan-like Higgs-Strahlung production the color singlet V can be identified as the virtual vector boson according to Eq. (2.9). For the gluon-induced Higgs-Strahlung contribution in Eq. (2.12), factorization into vector boson production and a subsequent decay is not possible. Therefore, the color singlet V consists of two particles and corresponds to the ZH pair. Since our primary focus lies on the Drell-Yan-like contributions, we concentrate on the processes that are initiated by a quark-antiquark pair at LO.

Quark-Antiquark Channel

The LO Feynman diagram showing color-singlet production in quark-antiquark annihilation is depicted in Figure 4.1. In agreement with Eq. (3.2), the cross section for the

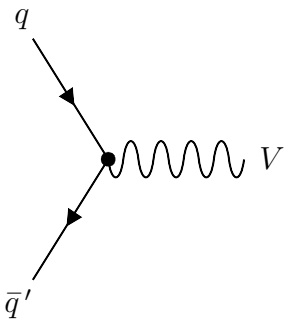

Figure 4.1.: LO Feynman diagram for color-singlet production in quark-antiquark annihilation.

process $q(p_1)\bar{q}'(p_2) \to V(p_3)$, where the momenta of the involved particles are indicated within the parentheses, can be represented as

$$2\hat{s} \cdot \mathrm{d}\hat{\sigma}^{\mathrm{B}}_{f_a f_b} = F_{\mathrm{LM}}(1_{f_a}, 2_{f_b}), \tag{4.1}$$

with f_a and f_b being massless quarks according to the notation in Table 4.1. The indices a and b are non-zero integers within the range of $-n_f$ to n_f, where n_f is the number of light quarks in the theory under investigation. The handy notation,

$$F_{\mathrm{LM}}(1_{f_a}, 2_{f_b}) = \mathcal{N}\, \mathrm{d}\Pi^{(d)}_{\mathrm{B}}\, |\mathcal{M}^{(0)}_{f_a f_b \to V}(p_1, p_2, p_3)|^2 F_J(p_1, p_2, p_3), \tag{4.2}$$

is introduced to have a compact expression for the cross section. The index L on the function F_{LM}, represents the Lorentz-invariant Born phase-space element that can be written as[1]

$$\mathrm{d}\Pi^{(d)}_{\mathrm{B}} = \frac{\mathrm{d}^{d-1}p_3}{(2\pi)^{d-1}2E_3}\,(2\pi)^d\,\delta^{(d)}(p_1 + p_2 - p_3). \tag{4.3}$$

The index M comes from the UV-renormalized[2] squared matrix element $|\mathcal{M}^{(0)}_{f_a f_b \to V}|^2$ of the tree-level process at LO, according to the expansion of the amplitude in terms of the strong coupling constant α_s,

$$\mathcal{M}(p_1, p_2, p_3) = \mathcal{M}^{(0)}(p_1, p_2, p_3) + \mathcal{M}^{(1)}(p_1, p_2, p_3) + \mathcal{O}(\alpha_s^2). \tag{4.4}$$

The IR-safe observable in Eq. (4.2) is defined by the jet function F_J that depends on the process kinematics, and $\mathcal{N}$ is a symmetry factor. As arguments for F_{LM} we give just the numbers 1_{f_a} and 2_{f_b} which stand for the two colored initial-state (anti)quarks with momentum p_1 and p_2, respectively. The momentum of the color singlet follows trivially from momentum conservation and it is not necessary to specify it explicitly.
At NLO, virtual and real corrections, which are shown in Figure 4.2, give rise to IR divergences[3]. We split the cross section into three parts as in Eq. (3.3) and consider each term separately. The term with virtual corrections can be written as

$$2\hat{s} \cdot \mathrm{d}\hat{\sigma}^{\mathrm{V}}_{f_a f_b} = F_{\mathrm{LV}}(1_{f_a}, 2_{f_b}), \tag{4.5}$$

[1] If the color singlet is a cluster made out of multiple particles, all particles have to be taken into account. For n final-state particles with momenta k_i, $i \in \{1, \ldots, n\}$, the phase-space element reads

$$\mathrm{d}\Pi^{(d)}_{\mathrm{B}} = \prod_{i=1}^{n} \frac{\mathrm{d}^{d-1}k_i}{(2\pi)^{d-1}2E_i}\,(2\pi)^d\,\delta^{(d)}\left(p_1 + p_2 - \sum_{i=1}^{n} k_i\right).$$

[2] All quantities are assumed to be UV renormalized in the $\overline{\mathrm{MS}}$ scheme. For color-singlet production this only requires UV renormalization of the strong coupling constant (*cf.* Appendix B).

[3] In physical gauges only real-radiation diagrams where partons are emitted from external legs can lead to IR singularities.

Table 4.1.: Quark numerbering scheme.

a	1	2	3	4	5	6
f_a	d	u	s	c	b	t
f_{-a}	$\overline{d}$	$\overline{u}$	$\overline{s}$	$\overline{c}$	$\overline{b}$	$\overline{t}$

with the abbreviation

$$F_{\mathrm{LV}}(1_{f_a}, 2_{f_b}) = \mathcal{N}\,\mathrm{d}\Pi_{\mathrm{B}}^{(d)}\,2\,\mathfrak{Re}\Big\{\mathcal{M}^{(1)}_{f_a f_b\to V}(p_1,p_2,p_3)\mathcal{M}^{*(0)}_{f_a f_b\to V}(p_1,p_2,p_3)\Big\}\,F_J(p_1,p_2,p_3), \tag{4.6}$$

where the index V indicates that we have to consider the interference of the one-loop amplitudes $\mathcal{M}^{(1)}_{f_a f_b\to V}$ with the tree-level diagrams $\mathcal{M}^{(0)}_{f_a f_b\to V}$. The index L indicates the same Lorentz-invariant phase-space element as defined in Eq. (4.3).
Next, we write the real corrections, $q(p_1)\overline{q}\,'(p_2) \to V(p_3) + g(p_4)$, as

$$\begin{aligned} 2\hat{s}\cdot\mathrm{d}\hat{\sigma}^{\mathrm{R}}_{f_a f_b} &= \int[\mathrm{d}p_4]\,F_{\mathrm{LM}}(1_{f_a}, 2_{f_b}\,|\,4_g) \\ &= \big\langle F_{\mathrm{LM}}(1_{f_a}, 2_{f_b}\,|\,4_g)\big\rangle, \end{aligned} \tag{4.7}$$

with the function

$$F_{\mathrm{LM}}(1_{f_a}, 2_{f_b}\,|\,4_g) = \mathcal{N}\,\mathrm{d}\Pi_{\mathrm{B}}^{(d)}\,|\mathcal{M}^{(0)}_{f_a f_b\to V+g}(p_1,p_2,p_3,p_4)|^2 F_J(p_1,p_2,p_3,p_4). \tag{4.8}$$

It is important to note that the Born phase space includes the momentum-conserving δ-distribution for the entire process and is different from Eq. (4.3),

$$\mathrm{d}\Pi_{\mathrm{B}}^{(d)} = \frac{\mathrm{d}^{d-1}p_3}{(2\pi)^{d-1}2E_3}\,(2\pi)^d\,\delta^{(d)}(p_1+p_2-p_3-p_4). \tag{4.9}$$

Although these two phase spaces are different, it should be highlight that we use the same symbol for convenience. However, this usage of the same symbol should not create confusion in the specific context. The Lorentz-invariant squared matrix element $|\mathcal{M}^{(0)}_{f_a f_b\to V+g}|^2$ contains all tree-level processes with real radiation. As a new argument the function F_{LM} has the number 4_g, which represents the gluon with momentum p_4. This argument is separated from the other arguments by a vertical bar, indicating that this particle arises from real-emission corrections. In Eq. (4.7) the integration over the real-radiation phase space is treated explicitly, and we use

$$[\mathrm{d}p_i] = \frac{\mathrm{d}^{d-1}p_i}{(2\pi)^{d-1}2E_i}\,\Theta(E_{\max}-E_i)\,, \tag{4.10}$$

with the Heaviside step function Θ constraining the energy of the final-state parton to an arbitrary dimensional value $E_{\max}$, which has to be equal to or larger than the maximum energy the parton can have due to momentum conservation. The final result will not depend on the choice of $E_{\max}$. In the second line of Eq. (4.7), we employ a shorthand notation to represent the integration over real emission. Instead of explicitly writing the integral over the phase space, we enclose the expression to be integrated

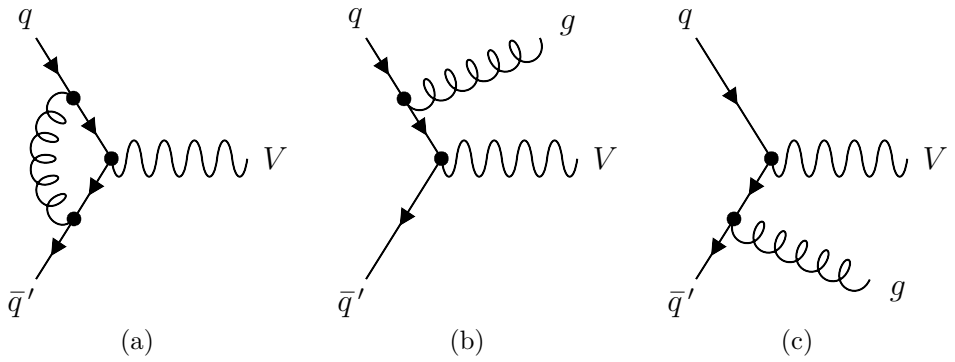

Figure 4.2.: NLO Feynman diagrams for color-singlet production in quark-antiquark annihilation with virtual corrections (a) and real emission from the initial-state quark (b) or antiquark (c).

within angled brackets[4], $\langle \cdot\cdot \rangle$. If the expression inside the angled brackets does not depend on the kinematics of real-radiated partons, the brackets can be understood as a trivial operation without any effect.
The last ingredient we need for computing Eq. (3.3) is the term coming from the collinear renormalization of the PDFs. Its result is well-known and was calculated in Ref. [123]. In our notation we write this contribution as[5]

$$\begin{aligned} 2\hat{s}\cdot \mathrm{d}\hat{\sigma}^{\mathrm{C_{NLO}}}_{f_a f_b} &= \frac{\alpha_s(\mu_\mathrm{R})}{2\pi} 2\hat{s}\cdot \left[\Gamma_1 \otimes \mathrm{d}\hat{\sigma}^{\mathrm{LO}}_{f_a f_b} + \mathrm{d}\hat{\sigma}^{\mathrm{LO}}_{f_a f_b} \otimes \Gamma_1\right] \\ &= \frac{\alpha_s(\mu_\mathrm{R})}{2\pi} \frac{1}{\epsilon} \int_0^1 \mathrm{d}z\, \hat{P}^{(0)}_{qq}(z) \left\langle \frac{F_{\mathrm{LM}}(z\cdot 1_{f_a}, 2_{f_b}) + F_{\mathrm{LM}}(1_{f_a}, z\cdot 2_{f_b})}{z} \right\rangle, \end{aligned} \tag{4.11}$$

where we convolute the LO cross section with the renormalization constant Γ_1 which is given by

$$\Gamma_1(z) = \frac{\hat{P}^{(0)}_{qq}(z)}{\epsilon}. \tag{4.12}$$

The convolution symbol itself is defined as

$$(f \otimes g)(z) = \int_0^1 \mathrm{d}x\, \mathrm{d}y f(x) g(y) \delta(z - xy). \tag{4.13}$$

In the second line of Eq. (4.11), the arguments $z\cdot 1_{f_a}$ or $z\cdot 2_{f_b}$ of the function F_{LM} tell us that momentum p_1 or p_2, respectively, has to be multiplied by the factor z inside the function F_{LM}. Here, the UV-renormalized strong coupling constant is evaluated at the renormalization scale μ_R in the $\overline{\mathrm{MS}}$ scheme as explicitly indicated by the functional dependence of α_s.

[4]This integration has always to be understood in the same frame as the one that is predetermined by the choice of the subtraction terms. We will compute our subtraction terms and the related counterterms in the center-of-mass frame of the colliding partons which will break the Lorentz invariance of the formalism.

[5]When the convolution symbol is positioned to the left of $\mathrm{d}\hat{\sigma}_{ij}$, it indicates that the convolution operates on the momentum of the incoming parton i. Conversely, when the convolution symbol is on the right, it signifies that the convolution operates on the momentum of the incoming parton j.

Finally, the residue of the collinear renormalization is given by the LO Altarelli-Parisi splitting function [249] for an (anti)quark decaying into an (anti)quark,

$$\hat{P}^{(0)}_{qq}(z) = \hat{P}^{(0)}_{qq,\mathrm{R}}(z) + \hat{P}^{(0)}_{qq,\delta}\,\delta(1-z) \tag{4.14}$$

with the regular part

$$\hat{P}^{(0)}_{qq,\mathrm{R}}(z) = C_{\mathrm{F}}\big(2\,\mathcal{D}_0 - (1+z)\big) \tag{4.15}$$

and the term proportional to the δ-distribution

$$\hat{P}^{(0)}_{qq,\delta} = \gamma_q = \frac{3}{2}C_{\mathrm{F}}, \tag{4.16}$$

where $C_{\mathrm{F}} = (N_c^2-1)/(2N_c)$ is the quadratic Casimir operator of the $\mathbf{SU(3)}$ color symmetry group in the fundamental representation with $N_c = 3$ colors and γ_q denotes the anomalous dimension of the quark.
The plus-distribution in Eq. (4.15),

$$\mathcal{D}_n(z) = \left[\frac{\ln^n(1-z)}{1-z}\right]_+, \tag{4.17}$$

acts on a bump function $G(z)$ that is smooth and compactly supported in the integration domain $z \in [0,1)$ as

$$\int_0^1 \mathrm{d}z\,\mathcal{D}_n(z)G(z) = \int_0^1 \mathrm{d}z\left[\frac{\ln^n(1-z)}{1-z}\right]\big(G(z)-G(1)\big) \tag{4.18}$$

and is by construction free of divergences in the limit $z \to 1$.
In Eq. (4.11), the singularities are presented as Laurent series in the dimensional regulator ϵ. On the other hand, the IR poles arising from the virtual corrections in Eq. (4.5) are implicitly encoded within the one-loop matrix element. The detailed investigation of their structure is carried out in section 4.4. However, our first task is to determine the subtraction terms for the contributions with real radiation in Eq. (4.7) in order to manifest the phase-space singularities following the strategy of section 3.3. This part is discussed in section 4.2. Subsequently, in section 4.3, we extract the IR poles in terms of ϵ poles by integrating analytically over the real-radiation phase space.

4.2. Infrared Limits and Subtraction Terms

At NLO, there exist two types of IR singularities. Soft singularities that arise when the energy of the emitted parton becomes small, and collinear divergences that occur when the emitted particle becomes collinear with the emitter particle. In order to compute the required subtraction functions to handle these singular limits, the FKS scheme utilizes two types of operators.
The first operator, denoted as $\mathcal{S}_i$, isolates the leading divergences as the energy E_i of the particle with momentum p_i approaches zero. Specifically,

$$\mathcal{S}_i A = \lim_{E_i \to 0} A, \tag{4.19}$$

where A represents a general function.

The second operator, $\mathcal{C}_{ji}$, is used for extracting the leading collinear divergence when partons i and j become collinear to each other,

$$\mathcal{C}_{ji}A = \lim_{\eta_{ij}\to 0} A. \tag{4.20}$$

The parameter η_{ij} is defined as

$$\eta_{ij} = \frac{1-\cos\theta_{ij}}{2}, \tag{4.21}$$

where θ_{ij} is the angle between the two particles in Euclidean space.
The contribution $q\overline{q}' \to V + g$ can exhibit three IR divergences in three phase-space regions. Firstly, the phase-space integral diverges when the gluon becomes soft. To remove this singularity, we construct a subtraction term using the operator $\mathcal{S}_4$. By combining Eq. (4.7) with Eq. (3.12), we can write the cross section as

$$2\hat{s}\cdot \mathrm{d}\hat{\sigma}^{\mathrm{R}}_{f_a f_b} = \langle (1-\mathcal{S}_4)\, F_{\mathrm{LM}}(1_{f_a}, 2_{f_b} \,|\, 4_g)\rangle + \langle \mathcal{S}_4 F_{\mathrm{LM}}(1_{f_a}, 2_{f_b} \,|\, 4_g)\rangle\,. \tag{4.22}$$

The soft operator acts on the squared matrix element as well as on the momentum-conserving δ-distribution in the Born phase-space element of the function F_{LM}. This is known as Eikonal approximation, given by

$$\mathcal{S}_4 F_{\mathrm{LM}}(1_{f_a}, 2_{f_b} \,|\, 4_g) = 2\, C_{\mathrm{F}}\, g^2_{s,\epsilon} \frac{(p_1\cdot p_2)}{(p_1\cdot p_4)(p_2\cdot p_4)} F_{\mathrm{LM}}(1_{f_a}, 2_{f_b}), \tag{4.23}$$

with the strong QCD coupling $g^2_{s,\epsilon} = 4\pi\alpha_s(\mu_{\mathrm{R}})\mu^{2\epsilon}_{\mathrm{F}} S^{-1}_{\epsilon}$ where $S_\epsilon = (4\pi)^\epsilon e^{-\epsilon\gamma_{\mathrm{E}}}$ in the $\overline{\mathrm{MS}}$ scheme and γ_{E} is the Euler–Mascheroni constant, *cf.* Eq. (B.6). The scalar products read

$$(p_i\cdot p_j) = 2E_iE_j\eta_{ij}. \tag{4.24}$$

The first term on the right-hand side of Eq. (4.22) is free of soft divergences, they are all included in the second summand. To make the poles in this counterterm apparent, we have to integrate Eq. (4.23) over the unresolved phase space of the gluon. However, even though if the singular structure of the counterterm can be calculated analytically, the first term still diverges in the collinear phase-space regions.
Hence, we need to regulate the two possible collinear IR limits that arise when the real-emitted gluon becomes collinear to one of the initial-state quarks. To obtain the related subtraction functions we use operators $\mathcal{C}_{41}$ and $\mathcal{C}_{42}$. Upon regulating these divergences, Eq. (4.22) becomes

$$\begin{aligned} 2\hat{s}\cdot \mathrm{d}\hat{\sigma}^{\mathrm{R}}_{f_a f_b} &= \langle (1-\mathcal{C}_{41}-\mathcal{C}_{42})\,(1-\mathcal{S}_4)\, F_{\mathrm{LM}}(1_{f_a}, 2_{f_b} \,|\, 4_g)\rangle + \langle \mathcal{S}_4 F_{\mathrm{LM}}(1_{f_a}, 2_{f_b} \,|\, 4_g)\rangle \\ &\quad + \langle (\mathcal{C}_{41}+\mathcal{C}_{42})\,(1-\mathcal{S}_4)\, F_{\mathrm{LM}}(1_{f_a}, 2_{f_b} \,|\, 4_g)\rangle \\ &= \left\langle \hat{\mathcal{O}}_{\mathrm{NLO}} F_{\mathrm{LM}}(1_{f_a}, 2_{f_b} \,|\, 4_g)\right\rangle + \langle (\mathcal{C}_{41}+\mathcal{C}_{42})\, F_{\mathrm{LM}}(1_{f_a}, 2_{f_b} \,|\, 4_g)\rangle \\ &\quad + \langle (1-\mathcal{C}_{41}-\mathcal{C}_{42})\, \mathcal{S}_4 F_{\mathrm{LM}}(1_{f_a}, 2_{f_b} \,|\, 4_g)\rangle\,, \end{aligned} \tag{4.25}$$

where we obtain the NLO subtraction operator

$$\hat{\mathcal{O}}_{\mathrm{NLO}} = (1-\mathcal{C}_{41}-\mathcal{C}_{42})\,(1-\mathcal{S}_4)\,. \tag{4.26}$$

The limit where the final-state gluon becomes collinear to the initial-state quark f_a reads

$$\mathcal{C}_{41} F_{\mathrm{LM}}(1_{f_a}, 2_{f_b} \,|\, 4_g) = g_{s,\epsilon}^2 \frac{1}{(p_1 \cdot p_4)} P_{qq}^{(0)}(z;\epsilon) \frac{F_{\mathrm{LM}}(z \cdot 1_{f_a}, 2_{f_b})}{z} \quad \text{with} \quad z = \frac{E_1 - E_4}{E_1}, \tag{4.27}$$

and similar for the final-state gluon becoming collinear to the initial-state quark f_b,

$$\mathcal{C}_{42} F_{\mathrm{LM}}(1_{f_a}, 2_{f_b} \,|\, 4_g) = g_{s,\epsilon}^2 \frac{1}{(p_2 \cdot p_4)} P_{qq}^{(0)}(z;\epsilon) \frac{F_{\mathrm{LM}}(1_{f_a}, z \cdot 2_{f_b})}{z} \quad \text{with} \quad z = \frac{E_2 - E_4}{E_2}, \tag{4.28}$$

where the splitting function is given by

$$P_{qq}^{(0)}(z;\epsilon) = C_{\mathrm{F}} \left(\frac{1+z^2}{1-z} - \epsilon\,(1-z) \right). \tag{4.29}$$

When both soft and collinear singularities are regulated, it leads to overlapping soft-collinear limits when the soft operator and one of the collinear projectors are applied simultaneously. To extract the appropriate projections, we apply the corresponding collinear operator to Eq. (4.23), resulting in

$$\mathcal{C}_{41}\mathcal{S}_4 F_{\mathrm{LM}}(1_{f_a}, 2_{f_b} \,|\, 4_g) = 2\, C_{\mathrm{F}}\, g_{s,\epsilon}^2 \frac{(p_1 \cdot p_2)}{(p_1 \cdot p_4)\{p_2 \cdot p_4\}_{4\|1}} F_{\mathrm{LM}}(1_{f_a}, 2_{f_b}) \tag{4.30}$$

for $\vec{p}_4 \,\|\, \vec{p}_1$ and, analogously, for the case $\vec{p}_4 \,\|\, \vec{p}_2$ we find

$$\mathcal{C}_{42}\mathcal{S}_4 F_{\mathrm{LM}}(1_{f_a}, 2_{f_b} \,|\, 4_g) = 2\, C_{\mathrm{F}}\, g_{s,\epsilon}^2 \frac{(p_1 \cdot p_2)}{\{p_1 \cdot p_4\}_{4\|2}(p_2 \cdot p_4)} F_{\mathrm{LM}}(1_{f_a}, 2_{f_b}), \tag{4.31}$$

where we make use of the short notation

$$\{p_i \cdot p_j\}_{j\|k} = \lim_{\theta_{ij} \to \theta_{ik}} (p_i \cdot p_j) = 2 E_i E_j \eta_{ik}. \tag{4.32}$$

The $\hat{\mathcal{O}}_{\mathrm{NLO}}$ term on the right-hand side of Eq. (4.25) is free of singularities and can be integrated (numerically) in four dimensions. All divergencies are contained in the counterterms, which we will discuss in the next section.
Before, we want to note that for the special case of a head-to-head collision, where $\theta_{12} = \pi$, or equivalently $\eta_{12} = 1$, the terms with soft and soft-collinear projectors simplify,

$$\begin{aligned}
&(1 - \mathcal{C}_{41} - \mathcal{C}_{42})\, \mathcal{S}_4 F_{\mathrm{LM}}(1_{f_a}, 2_{f_b} \,|\, 4_g) \\
&= 2\, C_{\mathrm{F}}\, g_{s,\epsilon}^2 \left(\frac{(p_1 \cdot p_2)}{(p_1 \cdot p_4)(p_2 \cdot p_4)} - \frac{(p_1 \cdot p_2)}{(p_1 \cdot p_4)\{p_2 \cdot p_4\}_{4\|1}} - \frac{(p_1 \cdot p_2)}{\{p_1 \cdot p_4\}_{4\|2}(p_2 \cdot p_4)} \right) F_{\mathrm{LM}}(1_{f_a}, 2_{f_b}) \\
&= C_{\mathrm{F}} \frac{g_{s,\epsilon}^2}{E_4^2} \left(\frac{1 - \eta_{14} - \eta_{24}}{\eta_{14}\eta_{24}} \right) F_{\mathrm{LM}}(1_{f_a}, 2_{f_b}) \\
&= C_{\mathrm{F}} \frac{g_{s,\epsilon}^2}{E_4^2} \left(\frac{1 - \eta_{14} - (1 - \eta_{14})}{\eta_{14}\eta_{24}} \right) F_{\mathrm{LM}}(1_{f_a}, 2_{f_b}) \\
&= 0.
\end{aligned} \tag{4.33}$$

In the second last step we used the relation $\eta_{24} = 1 - \eta_{14}$, which follows immediately from Eq. (4.21) for $\theta_{24} = \theta_{12} + \theta_{14} = \pi + \theta_{14}$. As a consequence it is sufficient to regulate only the collinear singularities for NLO color-singlet production,

$$2\hat{s} \cdot \mathrm{d}\hat{\sigma}^{\mathrm{R}}_{f_a f_b} = \Big\langle \hat{\mathcal{O}}_{\mathrm{NLO}} F_{\mathrm{LM}}(1_{f_a}, 2_{f_b} \,|\, 4_g) \Big\rangle + \big\langle (\mathcal{C}_{41} + \mathcal{C}_{42})\, F_{\mathrm{LM}}(1_{f_a}, 2_{f_b} \,|\, 4_g) \big\rangle, \tag{4.34}$$

with

$$\hat{\mathcal{O}}_{\mathrm{NLO}} F_{\mathrm{LM}}(1_{f_a}, 2_{f_b} \,|\, 4_g) = (1 - \mathcal{C}_{41} - \mathcal{C}_{42})\, F_{\mathrm{LM}}(1_{f_a}, 2_{f_b} \,|\, 4_g). \tag{4.35}$$

4.3. Integrated Counterterms

We proceed with the integration of the counterterms without making assumptions about the hard process. As we integrate over the unresolved phase-space regions, the singularities will appear as explicit poles in the dimensional regulator ϵ, but at the same time we keep all information about the kinematics of the Born process.

Soft Counterterms

Even though soft singularities do not need to be regulated explicitly in our NLO computation, we want to stay for the moment in a more general context and begin by integrating the counterterm of the soft subtraction function in Eq. (4.23) over the gluon phase space,

$$\begin{aligned}
\big\langle \mathcal{S}_4 F_{\mathrm{LM}}(1_{f_a}, 2_{f_b} \,|\, 4_g) \big\rangle &= \int [\mathrm{d}p_4]\, 2\, C_{\mathrm{F}}\, g_{s,\epsilon}^2 \frac{(p_1 \cdot p_2)}{(p_1 \cdot p_4)(p_2 \cdot p_4)} \big\langle F_{\mathrm{LM}}(1_{f_a}, 2_{f_b}) \big\rangle \\
&= C_{\mathrm{F}}\, g_{s,\epsilon}^2 \int \frac{\mathrm{d}^{d-1} p_4}{(2\pi)^{d-1} 2E_4} \Theta\left(E_{\max} - E_4\right) \frac{\eta_{12}}{E_4^2 \eta_{14} \eta_{24}} \big\langle F_{\mathrm{LM}}(1_{f_a}, 2_{f_b}) \big\rangle \\
&= C_{\mathrm{F}}\, g_{s,\epsilon}^2 \int_0^{E_{\max}} \frac{\mathrm{d}E_4}{E_4^{1+2\epsilon}} \int \frac{\mathrm{d}\Omega_4^{(d-1)}}{2(2\pi)^{d-1}} \frac{\eta_{12}}{\eta_{14}\eta_{24}} \big\langle F_{\mathrm{LM}}(1_{f_a}, 2_{f_b}) \big\rangle.
\end{aligned} \tag{4.36}$$

Since the gluon decouples from the function F_{LM}, we are left with two process-independent integrals. The integral over the gluon energy yields

$$\int_0^{E_{\max}} \frac{\mathrm{d}E_4}{E_4^{1+2\epsilon}} = -\frac{1}{2\epsilon} E_{\max}^{-2\epsilon}, \tag{4.37}$$

while the solid angle integral is a special case of known results from Refs. [250, 251],

$$\int \frac{\mathrm{d}\Omega_4^{(d-1)}}{2(2\pi)^{d-1}} \frac{\eta_{12}}{\eta_{14}\eta_{24}} = -\frac{2^{2-2\epsilon}}{\epsilon} \left[\frac{1}{8\pi^2} \frac{(4\pi)^\epsilon}{\Gamma(1-\epsilon)}\right] \eta_{12}^{-\epsilon} K(\eta_{12}; \epsilon). \tag{4.38}$$

The function K is given by

$$K(\eta_{ij}; \epsilon) = \left[\frac{\Gamma^2(1-\epsilon)}{\Gamma(1-2\epsilon)}\right] \eta_{ij}^{1+\epsilon}\, {}_2F_1(1, 1; 1-\epsilon; 1-\eta_{ij}), \tag{4.39}$$

where ${}_2F_1$ denotes the Gaussian hypergeometric function and Γ the Euler gamma function.

In summary, we get the integrated soft counterterm

$$\big\langle \mathcal{S}_4 F_{\mathrm{LM}}(1_{f_a}, 2_{f_b} \,|\, 4_g)\big\rangle = 2\, C_{\mathrm{F}}\, [\alpha_{s,\epsilon}] \frac{(2E_{\max})^{-2\epsilon}}{\epsilon^2} \eta_{12}^{-\epsilon} K(\eta_{12};\epsilon) \big\langle F_{\mathrm{LM}}(1_{f_a}, 2_{f_b})\big\rangle, \tag{4.40}$$

with the replacement

$$[\alpha_{s,\epsilon}] = \left[\frac{g_{s,\epsilon}^2}{8\pi^2} \frac{(4\pi)^\epsilon}{\Gamma(1-\epsilon)}\right]. \tag{4.41}$$

Soft-Collinear Counterterms

In order to obtain the integrated soft-collinear counterterms, we follow a procedure similar to that used for the soft counterterm. Starting from Eq. (4.30) we get

$$\begin{aligned}
\big\langle \mathcal{C}_{41}\mathcal{S}_4 F_{\mathrm{LM}}(1_{f_a}, 2_{f_b} \,|\, 4_g)\big\rangle &= \int [\mathrm{d}p_4]\, 2\, C_{\mathrm{F}}\, g_{s,\epsilon}^2 \frac{(p_1\cdot p_2)}{(p_1\cdot p_4)\{p_2\cdot p_4\}_{4\|1}} \big\langle F_{\mathrm{LM}}(1_{f_a}, 2_{f_b})\big\rangle \\
&= C_{\mathrm{F}}\, g_{s,\epsilon}^2 \int \frac{\mathrm{d}^{d-1}p_4}{(2\pi)^{d-1} 2E_4} \Theta\left(E_{\max} - E_4\right) \frac{1}{E_4^2 \eta_{14}} \big\langle F_{\mathrm{LM}}(1_{f_a}, 2_{f_b})\big\rangle \\
&= C_{\mathrm{F}}\, g_{s,\epsilon}^2 \int_0^{E_{\max}} \frac{\mathrm{d}E_4}{E_4^{1+2\epsilon}} \int \frac{\mathrm{d}\Omega_4^{(d-1)}}{2(2\pi)^{d-1}} \frac{1}{\eta_{14}} \big\langle F_{\mathrm{LM}}(1_{f_a}, 2_{f_b})\big\rangle \\
&= C_{\mathrm{F}}\, [\alpha_{s,\epsilon}] \frac{(2E_{\max})^{-2\epsilon}}{\epsilon^2} \left[\frac{\Gamma^2(1-\epsilon)}{\Gamma(1-2\epsilon)}\right] \big\langle F_{\mathrm{LM}}(1_{f_a}, 2_{f_b})\big\rangle,
\end{aligned} \tag{4.42}$$

where we used the solution of the energy integral in Eq. (4.37) and the the angular integration is carried out straightforwardly, resulting in

$$\int \frac{\mathrm{d}\Omega_4^{(d-1)}}{2(2\pi)^{d-1}} \frac{1}{\eta_{14}} = -\frac{2^{1-2\epsilon}}{\epsilon} \left[\frac{1}{8\pi^2} \frac{(4\pi)^\epsilon}{\Gamma(1-\epsilon)}\right] \left[\frac{\Gamma^2(1-\epsilon)}{\Gamma(1-2\epsilon)}\right]. \tag{4.43}$$

The result for $\mathcal{C}_{42}\mathcal{S}_4$ can be obtained by the replacement of momentum p_1 against p_2 and conversely,

$$\big\langle \mathcal{C}_{42}\mathcal{S}_4 F_{\mathrm{LM}}(1_{f_a}, 2_{f_b} \,|\, 4_g)\big\rangle = C_{\mathrm{F}}\, [\alpha_{s,\epsilon}] \frac{(2E_{\max})^{-2\epsilon}}{\epsilon^2} \left[\frac{\Gamma^2(1-\epsilon)}{\Gamma(1-2\epsilon)}\right] \big\langle F_{\mathrm{LM}}(1_{f_a}, 2_{f_b})\big\rangle. \tag{4.44}$$

Collinear Counterterms

Lastly, we are interested in the integrated counterterms for the collinear subtraction functions. In this case, we encounter a final-state parton that only partially decouples in the collinear limit. This is in contrast to the soft and soft-collinear factorization theorems, where we observed complete decoupling of the gluon. This distinction arises due to the dependence of F_{LM} on the energy of the parton, which is implicitly encoded in the variable z in Eq. (4.27) and Eq. (4.28).

However, it is possible to extract all the singularities analytically. By integrating equation Eq. (4.27), we obtain the expression

$$\begin{aligned}
\big\langle \mathcal{C}_{41} F_{\mathrm{LM}}(1_{f_a}, 2_{f_b} \,|\, 4_g)\big\rangle &= \int [\mathrm{d}p_4]\, g_{s,\epsilon}^2 \frac{1}{(p_1\cdot p_4)} P_{qq}^{(0)}(z;\epsilon) \left\langle \frac{F_{\mathrm{LM}}(z\cdot 1_{f_a}, 2_{f_b})}{z} \right\rangle \\
&= g_{s,\epsilon}^2 \int \frac{\mathrm{d}^{d-1}p_4}{(2\pi)^{d-1} 2E_4} \Theta\left(E_{\max} - E_4\right) \frac{1}{2E_1 E_4 \eta_{14}} P_{qq}^{(0)}(z;\epsilon) \\
&\quad \times \left\langle \frac{F_{\mathrm{LM}}(z\cdot 1_{f_a}, 2_{f_b})}{z} \right\rangle
\end{aligned}$$

$$
\begin{aligned}
&= g_{s,\epsilon}^2 \int_0^{E_{\max}} \frac{\mathrm{d}E_4}{E_4^{2\epsilon}} \int \frac{\mathrm{d}\Omega_4^{(d-1)}}{2(2\pi)^{d-1}} \frac{1}{\eta_{14}} \frac{1}{2E_1} P_{qq}^{(0)}(z;\epsilon) \\
&\quad \times \left\langle \frac{F_{\mathrm{LM}}(z \cdot 1_{f_a}, 2_{f_b})}{z} \right\rangle .
\end{aligned} \tag{4.45}
$$

Since z is free of an angular dependence, the solid angle integral is identical to the one solved in Eq. (4.43). Moreover, we want to substitute the energy integration with an integration over the collinear parameter z,

$$
z = \frac{E_1 - E_4}{E_1} \quad \text{and} \quad \mathrm{d}z = \frac{\mathrm{d}E_4}{E_1}, \tag{4.46}
$$

with the boundaries $z \in \{z_{\min}, 1\}$ and $z_{\min} = (E_1 - E_{\max})/E_1$.
Combining all these findings, we get

$$
\begin{aligned}
\left\langle \mathcal{C}_{41} F_{\mathrm{LM}}(1_{f_a}, 2_{f_b} \,|\, 4_g) \right\rangle &= -\frac{1}{\epsilon} [\alpha_{s,\epsilon}] \left[\frac{\Gamma^2(1-\epsilon)}{\Gamma(1-2\epsilon)} \right] (2E_1)^{-2\epsilon} \int_{z_{\min}}^1 \frac{\mathrm{d}z}{(1-z)^{2\epsilon}} P_{qq}^{(0)}(z;\epsilon) \\
&\quad \times \left\langle \frac{F_{\mathrm{LM}}(z \cdot 1_{f_a}, 2_{f_b})}{z} \right\rangle \\
&= -\frac{1}{\epsilon} [\alpha_{s,\epsilon}] \left[\frac{\Gamma^2(1-\epsilon)}{\Gamma(1-2\epsilon)} \right] (2E_1)^{-2\epsilon} \int_{z_{\min}}^1 \mathrm{d}z \left[\frac{2C_{\mathrm{F}}}{(1-z)^{1+2\epsilon}} \right. \\
&\quad \left. + (1-z)^{-2\epsilon} P_{qq}^{\mathrm{reg}}(z;\epsilon) \right] \left\langle \frac{F_{\mathrm{LM}}(z \cdot 1_{f_a}, 2_{f_b})}{z} \right\rangle ,
\end{aligned} \tag{4.47}
$$

where we decomposed the splitting function into a part that diverges in the soft limit $z \to 1$, and a regular term, P^{reg}, according to

$$
P_{qq}^{(0)}(z;\epsilon) = \frac{2C_{\mathrm{F}}}{1-z} + P_{qq}^{\mathrm{reg}}(z;\epsilon) \quad \text{with} \quad P_{qq}^{\mathrm{reg}}(z;\epsilon) = -C_{\mathrm{F}}[(1+z) + \epsilon(1-z)]. \tag{4.48}
$$

We previously defined $E_{\max}$ as an arbitrary quantity and stated that its value must be greater than or equal to the maximum energy the final state parton can have due to momentum conservation. As a result, $z_{\min} \leqslant 0$ can be set without any loss of generality. If $z < 0$, the process described by the F_{LM} function is forbidden by the energy-conservation law, which is contained in the δ-distribution of the Born phase-space element. This allows us to fix $z_{\min} = 0$.
We can now extract the soft singularity of the z integration in Eq. (4.47). Focusing on the first term in the square bracket inside the integral, we have an object like

$$
\begin{aligned}
\int_0^1 \mathrm{d}z \frac{2C_{\mathrm{F}}}{(1-z)^{1+2\epsilon}} G(z) &= \int_0^1 \mathrm{d}z \frac{2C_{\mathrm{F}}}{(1-z)^{1+2\epsilon}} G(1) + \int_0^1 \mathrm{d}z \frac{2C_{\mathrm{F}}}{(1-z)^{1+2\epsilon}} \big(G(z) - G(1)\big) \\
&= -\frac{C_{\mathrm{F}}}{\epsilon} G(1) + \int_0^1 \mathrm{d}z \frac{2C_{\mathrm{F}}}{(1-z)^{1+2\epsilon}} \big(G(z) - G(1)\big),
\end{aligned} \tag{4.49}
$$

where $G(z)$ is a smooth and compactly supported function of z in the integration domain $z \in [0, 1)$. This is a requirement that the function in our integrand fulfills. The second term on the right-hand side is by construction free of singularities and, thus, we can perform the expansion $\epsilon \to 0$ before we carrying out the integration,

$$
\frac{G(z) - G(1)}{(1-z)^{1+2\epsilon}} = \left[\sum_{n=0}^{\infty} \frac{(-1)^n (2\epsilon)^n}{n!} \mathcal{D}_n(z) \right] G(z), \tag{4.50}
$$

where $\mathcal{D}_n(z)$ is the plus-distribution given in Eq. (4.17).
If we perform the expansion in ϵ also for the term with the regular splitting function in Eq. (4.47), we find

$$\begin{aligned}\left\langle \mathcal{C}_{41} F_{\mathrm{LM}}(1_{f_a}, 2_{f_b} \,|\, 4_g) \right\rangle = -\frac{1}{\epsilon}[\alpha_{s,\epsilon}] \left[\frac{\Gamma^2(1-\epsilon)}{\Gamma(1-2\epsilon)}\right] (2E_1)^{-2\epsilon} \left[-\left(\frac{C_\mathrm{F}}{\epsilon} + \gamma_q\right) \left\langle F_{\mathrm{LM}}(1_{f_a}, 2_{f_b}) \right\rangle \right. \\ \left. + \int_0^1 \mathrm{d}z\, \mathcal{P}_{qq}(z;\epsilon) \left\langle \frac{F_{\mathrm{LM}}(z\cdot 1_{f_a}, 2_{f_b})}{z} \right\rangle \right],\end{aligned} \tag{4.51}$$

with a generalized version of the splitting function in Eq. (4.14),

$$\mathcal{P}_{qq}(z;\epsilon) = \hat{P}_{qq}^{(0)}(z) - \epsilon\, \mathcal{P}'_{qq}(z) + \mathcal{O}\left(\epsilon^2\right) \tag{4.52}$$

with its $\mathcal{O}(\epsilon)$ related part

$$\mathcal{P}'_{qq}(z) = C_\mathrm{F}\big(4\,\mathcal{D}_1(z) - 2(1+z)\ln(1-z) + (1-z)\big). \tag{4.53}$$

By replacing the index 1 against 2 and vice versa we obtain the result for collinear gluon emission from the second incoming parton,

$$\begin{aligned}\left\langle \mathcal{C}_{42} F_{\mathrm{LM}}(1_{f_a}, 2_{f_b} \,|\, 4_g) \right\rangle = -\frac{1}{\epsilon}[\alpha_{s,\epsilon}] \left[\frac{\Gamma^2(1-\epsilon)}{\Gamma(1-2\epsilon)}\right] (2E_2)^{-2\epsilon} \left[-\left(\frac{C_\mathrm{F}}{\epsilon} + \gamma_q\right) \left\langle F_{\mathrm{LM}}(1_{f_a}, 2_{f_b}) \right\rangle \right. \\ \left. + \int_0^1 \mathrm{d}z\, \mathcal{P}_{qq}(z;\epsilon) \left\langle \frac{F_{\mathrm{LM}}(1_{f_a}, z\cdot 2_{f_b})}{z} \right\rangle \right].\end{aligned} \tag{4.54}$$

We have now all subtraction functions and their integrated counter parts so that we can go on with the full expansion in ϵ and the investigation of the virtual corrections.

Fully-Regulated Cross Section

By making use of the definition

$$[\alpha_{s,\epsilon}] = \frac{\alpha_s(\mu_\mathrm{R})}{2\pi} \frac{\mu_\mathrm{F}^{2\epsilon}}{S_\epsilon} \frac{(4\pi)^\epsilon}{\Gamma(1-\epsilon)} \big(1 + \mathcal{O}(\alpha_s)\big), \tag{4.55}$$

by combining Eq. (4.41) with Eq. (B.6) of Appendix B, *cf.* Eq. (B.7), we expand in terms of the dimensional regulator while neglecting $\mathcal{O}(\epsilon)$ contributions. In particular, the series for the Gaussian hypergeometric function is obtained by the use of the `Mathematica` [252] package `HypExp` [253, 254]. The soft counterterm in Eq. (4.40) becomes

$$\begin{aligned}\left\langle \mathcal{S}_4 F_{\mathrm{LM}}(1_{f_a}, 2_{f_b} \,|\, 4_g) \right\rangle = 2\, C_\mathrm{F}\, \frac{\alpha_s(\mu_\mathrm{R})}{2\pi} \left(\frac{\mu_\mathrm{F}}{2E_{\max}}\right)^{2\epsilon} \left[\frac{1}{\epsilon^2} - \frac{1}{\epsilon}\ln(\eta_{12}) \right. \\ \left. + \left(-\frac{\pi^2}{4} + \frac{1}{2}\ln^2(\eta_{12}) + \mathrm{Li}_2(1-\eta_{12})\right)\right] \left\langle F_{\mathrm{LM}}(1_{f_a}, 2_{f_b}) \right\rangle \\ + \mathcal{O}\left(\alpha_s^2; \epsilon\right),\end{aligned} \tag{4.56}$$

the soft-collinear counterterms according to Eq. (4.42) and Eq. (4.44) read

$$\begin{aligned}\left\langle \mathcal{C}_{41}\mathcal{S}_4 F_{\mathrm{LM}}(1_{f_a}, 2_{f_b} \,|\, 4_g) \right\rangle = C_\mathrm{F}\, \frac{\alpha_s(\mu_\mathrm{R})}{2\pi} \left(\frac{\mu_\mathrm{F}}{2E_{\max}}\right)^{2\epsilon} \left(\frac{1}{\epsilon^2} - \frac{\pi^2}{4}\right) \left\langle F_{\mathrm{LM}}(1_{f_a}, 2_{f_b}) \right\rangle \\ + \mathcal{O}\left(\alpha_s^2; \epsilon\right),\end{aligned} \tag{4.57}$$

$$\left\langle \mathcal{C}_{42}\mathcal{S}_4 F_{\mathrm{LM}}(1_{f_a}, 2_{f_b} \,|\, 4_g)\right\rangle = C_{\mathrm{F}}\,\frac{\alpha_s(\mu_{\mathrm{R}})}{2\pi}\left(\frac{\mu_{\mathrm{F}}}{2E_{\max}}\right)^{2\epsilon}\left(\frac{1}{\epsilon^2}-\frac{\pi^2}{4}\right)\left\langle F_{\mathrm{LM}}(1_{f_a}, 2_{f_b})\right\rangle + \mathcal{O}\left(\alpha_s^2;\epsilon\right), \tag{4.58}$$

and the collinear counterterms of Eq. (4.51) and Eq. (4.54) are

$$\left\langle \mathcal{C}_{41} F_{\mathrm{LM}}(1_{f_a}, 2_{f_b} \,|\, 4_g)\right\rangle = \frac{\alpha_s(\mu_{\mathrm{R}})}{2\pi}\left(\frac{\mu_{\mathrm{F}}}{2E_1}\right)^{2\epsilon}\left[\left(\frac{C_{\mathrm{F}}}{\epsilon^2}+\frac{\gamma_q}{\epsilon}-\frac{\pi^2}{4}C_{\mathrm{F}}\right)\left\langle F_{\mathrm{LM}}(1_{f_a}, 2_{f_b})\right\rangle - \frac{1}{\epsilon}\int_0^1 \mathrm{d}z\,\mathcal{P}_{qq}(z;\epsilon)\left\langle\frac{F_{\mathrm{LM}}(z\cdot 1_{f_a}, 2_{f_b})}{z}\right\rangle\right] + \mathcal{O}\left(\alpha_s^2;\epsilon\right), \tag{4.59}$$

$$\left\langle \mathcal{C}_{42} F_{\mathrm{LM}}(1_{f_a}, 2_{f_b} \,|\, 4_g)\right\rangle = \frac{\alpha_s(\mu_{\mathrm{R}})}{2\pi}\left(\frac{\mu_{\mathrm{F}}}{2E_2}\right)^{2\epsilon}\left[\left(\frac{C_{\mathrm{F}}}{\epsilon^2}+\frac{\gamma_q}{\epsilon}-\frac{\pi^2}{4}C_{\mathrm{F}}\right)\left\langle F_{\mathrm{LM}}(1_{f_a}, 2_{f_b})\right\rangle - \frac{1}{\epsilon}\int_0^1 \mathrm{d}z\,\mathcal{P}_{qq}(z;\epsilon)\left\langle\frac{F_{\mathrm{LM}}(1_{f_a}, z\cdot 2_{f_b})}{z}\right\rangle\right] + \mathcal{O}\left(\alpha_s^2;\epsilon\right). \tag{4.60}$$

Finally, the expressions simplify significantly in the partonic center-of-mass frame, there we have the relations $2E_1 = 2E_2 = \sqrt{\hat{s}}$ and $\eta_{12} = 1$. Consequently, we obtain the equation

$$\left\langle \mathcal{S}_4 F_{\mathrm{LM}}(1_{f_a}, 2_{f_b} \,|\, 4_g)\right\rangle - \left\langle \mathcal{C}_{41}\mathcal{S}_4 F_{\mathrm{LM}}(1_{f_a}, 2_{f_b} \,|\, 4_g)\right\rangle - \left\langle \mathcal{C}_{42}\mathcal{S}_4 F_{\mathrm{LM}}(1_{f_a}, 2_{f_b} \,|\, 4_g)\right\rangle = 0, \tag{4.61}$$

which is in full agreement with the statement in Eq. (4.33). Therefore, we are again left with only the collinear counterterms, which add up to

$$\begin{aligned}\left\langle \left(\mathcal{C}_{41}+\mathcal{C}_{42}\right) F_{\mathrm{LM}}(1_{f_a}, 2_{f_b} \,|\, 4_g)\right\rangle = \frac{\alpha_s(\mu_{\mathrm{R}})}{2\pi}\left(\frac{\mu_{\mathrm{F}}^2}{\hat{s}}\right)^{\epsilon}\Bigg[&2\left(\frac{C_{\mathrm{F}}}{\epsilon^2}+\frac{\gamma_q}{\epsilon}-\frac{\pi^2}{4}C_{\mathrm{F}}\right)\\ &\times\left\langle F_{\mathrm{LM}}(1_{f_a}, 2_{f_b})\right\rangle - \frac{1}{\epsilon}\int_0^1 \mathrm{d}z\,\mathcal{P}_{qq}(z;\epsilon)\\ &\times\left\langle\frac{F_{\mathrm{LM}}(z\cdot 1_{f_a}, 2_{f_b}) + F_{\mathrm{LM}}(1_{f_a}, z\cdot 2_{f_b})}{z}\right\rangle\Bigg]\\ &+\mathcal{O}\left(\alpha_s^2;\epsilon\right).\end{aligned} \tag{4.62}$$

The cross section for real emission in Eq. (4.34) then becomes

$$\begin{aligned}2\hat{s}\cdot \mathrm{d}\hat{\sigma}^{\mathrm{R}}_{f_a f_b} = \frac{\alpha_s(\mu_{\mathrm{R}})}{2\pi}\left(\frac{\mu_{\mathrm{F}}^2}{\hat{s}}\right)^{\epsilon}\Bigg[&2\left(\frac{C_{\mathrm{F}}}{\epsilon^2}+\frac{\gamma_q}{\epsilon}-\frac{\pi^2}{4}C_{\mathrm{F}}\right)\left\langle F_{\mathrm{LM}}(1_{f_a}, 2_{f_b})\right\rangle\\ &-\frac{1}{\epsilon}\int_0^1 \mathrm{d}z\,\mathcal{P}_{qq}(z;\epsilon)\left\langle\frac{F_{\mathrm{LM}}(z\cdot 1_{f_a}, 2_{f_b}) + F_{\mathrm{LM}}(1_{f_a}, z\cdot 2_{f_b})}{z}\right\rangle\Bigg]\\ &+\left\langle \hat{\mathcal{O}}_{\mathrm{NLO}} F_{\mathrm{LM}}(1_{f_a}, 2_{f_b} \,|\, 4_g)\right\rangle.\end{aligned} \tag{4.63}$$

All IR poles in the cross section are now visible as a Laurent series in ϵ. In the next section, we demonstrate that these poles cancel against the singularities of the virtual corrections and the collinear-renormalization contribution.

4.4. Pole Cancellation

To see how the poles cancel we have to give a closer look to the IR singularities of the virtual corrections. In Ref. [247] it has been shown that IR structure of one-loop amplitudes can be expressed as

$$\mathcal{M}^{(1)}(p_1,p_2,p_3) = [\alpha_{s,\epsilon}]\,\mathcal{I}_1(\epsilon)\mathcal{M}^{(0)}(p_1,p_2,p_3) + \mathcal{M}^{(1),\text{fin}}(p_1,p_2,p_3), \tag{4.64}$$

with the Catani-Seymour insertion operator

$$\mathcal{I}_1(\epsilon) = -e^{i\pi\epsilon}\left(\frac{1}{\hat{s}}\right)^{\epsilon}\left(\frac{C_\text{F}}{\epsilon^2}+\frac{\gamma_q}{\epsilon}\right). \tag{4.65}$$

All IR singularities are contained in the first term of Eq. (4.64) while $\mathcal{M}^{(1),\text{fin}}$ is free of them. In combination with Eq. (4.6) this results in

$$F_\text{LV}(1_{f_a},2_{f_b}) = [\alpha_{s,\epsilon}]\,I_{qq}(\epsilon)F_\text{LM}(1_{f_a},2_{f_b}) + F_\text{LV}^\text{fin}(1_{f_a},2_{f_b}), \tag{4.66}$$

where we use

$$\begin{aligned} I_{qq}(\epsilon) &= 2\,\mathfrak{Re}\{\mathcal{I}_1(\epsilon)\} \\ &= -2\cos(\epsilon\,\pi)\left(\frac{1}{\hat{s}}\right)^{\epsilon}\left(\frac{C_\text{F}}{\epsilon^2}+\frac{\gamma_q}{\epsilon}\right) \end{aligned} \tag{4.67}$$

and the UV- as well as IR-renormalized finite remainder

$$F_\text{LV}^\text{fin}(1_{f_a},2_{f_b}) = \mathcal{N}\,\mathrm{d}\Pi_\text{B}^{(d)}\,2\,\mathfrak{Re}\Big\{\mathcal{M}^{(1),\text{fin}}_{f_af_b\to V}(p_1,p_2,p_3)\mathcal{M}^{*(0)}_{f_af_b\to V}(p_1,p_2,p_3)\Big\}\,F_J(p_1,p_2,p_3). \tag{4.68}$$

Utilizing Eq. (4.55) we find upon ϵ expansion

$$2\hat{s}\cdot\mathrm{d}\hat{\sigma}^\text{V}_{f_af_b} = -2\frac{\alpha_s(\mu_\text{R})}{2\pi}\left(\frac{\mu_\text{F}^2}{\hat{s}}\right)^{\epsilon}\left(\frac{C_\text{F}}{\epsilon^2}+\frac{\gamma_q}{\epsilon}-\frac{7\pi^2}{12}C_\text{F}\right)\big\langle F_\text{LM}(1_{f_a},2_{f_b})\big\rangle + \big\langle F_\text{LV}^\text{fin}(1_{f_a},2_{f_b})\big\rangle, \tag{4.69}$$

as an expansion in terms of the dimensional regulator.
With this at hand, we have all ingredients to compute the NLO cross section for the quark-antiquark channel on basis of Eq. (3.3) as a sum of the real corrections, Eq. (4.63), the virtual corrections, Eq. (4.69), and the collinear-renormalization contribution, Eq. (4.11),

$$\begin{aligned} 2\hat{s}\cdot\mathrm{d}\hat{\sigma}^\text{NLO}_{f_af_b} &= 2\hat{s}\cdot\left(\mathrm{d}\hat{\sigma}^\text{R}_{f_af_b}+\mathrm{d}\hat{\sigma}^\text{V}_{f_af_b}+\mathrm{d}\hat{\sigma}^{\text{C}_\text{NLO}}_{f_af_b}\right) \\ &= \frac{\alpha_s(\mu_\text{R})}{2\pi}\left(\frac{2\pi^2}{3}C_\text{F}\big\langle F_\text{LM}(1_{f_a},2_{f_b})\big\rangle + \int_0^1\mathrm{d}z\left[\mathcal{P}'_{qq}(z)-\hat{P}^{(0)}_{qq}(z)\ln\left(\frac{\mu_\text{F}^2}{\hat{s}}\right)\right]\right. \\ &\quad\left.\times\left\langle\frac{F_\text{LM}(z\cdot 1_{f_a},2_{f_b})+F_\text{LM}(1_{f_a},z\cdot 2_{f_b})}{z}\right\rangle\right) + \big\langle F_\text{LV}^\text{fin}(1_{f_a},2_{f_b})\big\rangle \\ &\quad + \Big\langle\hat{\mathcal{O}}_\text{NLO}F_\text{LM}(1_{f_a},2_{f_b}\,|\,4_g)\Big\rangle. \end{aligned} \tag{4.70}$$

The cross section in Eq. (4.70) is free of all divergences and can be evaluated in four dimensions, which allows us to perform the entire phase-space integration numerically. This gives us all the freedom we need for computing the cross section fully differentially and extracting arbitrary IR-safe observables.

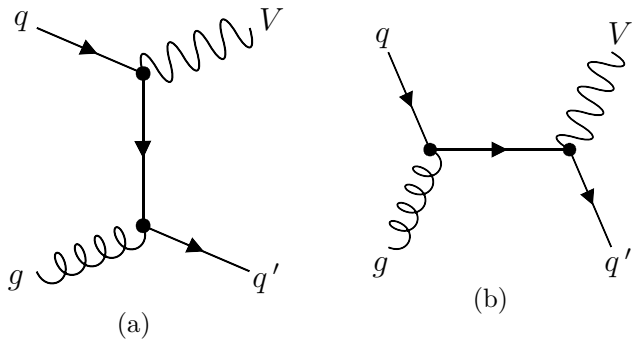

Figure 4.3.: Feynman diagrams for color-singlet production in the quark-gluon channel.

4.5. Fully-Differential Next-to-Leading Order Cross Section

Beside the quark-antiquark channel the quark-gluon channels open at NLO. The diagrams for these processes, $q(p_1)g(p_2) \to V(p_3)+q'(p_4)$ and $g(p_1)q(p_2) \to V(p_3)+q'(p_4)$, are depicted in Figure 4.3 and always include the emission of a real parton, which is a quark in our case. In analogy to Eq. (4.7) we write the cross sections as

$$\begin{aligned} 2\hat{s}\cdot \mathrm{d}\hat{\sigma}^{\mathrm{R}}_{f_a g} &= \sum_{x\in\mathcal{Q}} \int [\mathrm{d}p_4]\, F_{\mathrm{LM}}(1_{f_a}, 2_g \,|\, 4_{f_x}) \\ &= \sum_{x\in\mathcal{Q}} \big\langle F_{\mathrm{LM}}(1_{f_a}, 2_g \,|\, 4_{f_x}) \big\rangle, \\ 2\hat{s}\cdot \mathrm{d}\hat{\sigma}^{\mathrm{R}}_{g f_a} &= \sum_{x\in\mathcal{Q}} \int [\mathrm{d}p_4]\, F_{\mathrm{LM}}(1_g, 2_{f_a} \,|\, 4_{f_x}) \\ &= \sum_{x\in\mathcal{Q}} \big\langle F_{\mathrm{LM}}(1_g, 2_{f_a} \,|\, 4_{f_x}) \big\rangle. \end{aligned} \tag{4.71}$$

The sum runs over the set of light quarks $\mathcal{Q}$ according to the notation in Table 4.1 so that $\mathcal{Q} \in \{-n_f, \ldots, n_f\}\backslash\{0\}$. The F_{LM} functions read

$$\begin{aligned} F_{\mathrm{LM}}(1_{f_a}, 2_g \,|\, 4_{f_x}) &= \mathcal{N}\, \mathrm{d}\Pi^{(d)}_{\mathrm{B}}\, |\mathcal{M}^{(0)}_{f_a g\to V+f_x}(p_1,p_2,p_3,p_4)|^2 F_J(p_1,p_2,p_3,p_4), \\ F_{\mathrm{LM}}(1_g, 2_{f_a} \,|\, 4_{f_x}) &= \mathcal{N}\, \mathrm{d}\Pi^{(d)}_{\mathrm{B}}\, |\mathcal{M}^{(0)}_{g f_a\to V+f_x}(p_1,p_2,p_3,p_4)|^2 F_J(p_1,p_2,p_3,p_4), \end{aligned} \tag{4.72}$$

with the same phase-space elements as defined in Eq. (4.9).
The cross-section contributions arising from the collinear renormalization are

$$\begin{aligned} 2\hat{s}\cdot \mathrm{d}\hat{\sigma}^{\mathrm{C_{NLO}}}_{f_a g} &= \frac{\alpha_s(\mu_{\mathrm{R}})}{2\pi}\frac{1}{\epsilon}\int_0^1 \mathrm{d}z \sum_{x\in\mathcal{Q}} \hat{P}^{(0)}_{qg}(z) \left\langle \frac{F_{\mathrm{LM}}(1_{f_a}, z\cdot 2_{f_x})}{z} \right\rangle, \\ 2\hat{s}\cdot \mathrm{d}\hat{\sigma}^{\mathrm{C_{NLO}}}_{g f_a} &= \frac{\alpha_s(\mu_{\mathrm{R}})}{2\pi}\frac{1}{\epsilon}\int_0^1 \mathrm{d}z \sum_{x\in\mathcal{Q}} \hat{P}^{(0)}_{qg}(z) \left\langle \frac{F_{\mathrm{LM}}(z\cdot 1_{f_x}, 2_{f_a})}{z} \right\rangle, \end{aligned} \tag{4.73}$$

with the LO Altarelli-Parisi splitting function for a gluon decaying into an (anti)quark, given by

$$\hat{P}^{(0)}_{qg}(z) = \hat{P}^{(0)}_{qg,\mathrm{R}}(z) = T_{\mathrm{R}}\left(z^2 + (1-z)^2\right), \tag{4.74}$$

where $T_\mathrm{R} = 1/2$ is known as the index of the $\mathbf{SU(3)}$ color symmetry group in the fundamental representation.
In the production channels $qg \to V + q'$ and $gq \to V + q'$, the cross section is only divergent in the limit when the initial-state gluon and the final-state quark become collinear to each other, so just one operator needs to be taken into account,

$$\begin{aligned} 2\hat{s}\cdot \mathrm{d}\hat{\sigma}^\mathrm{R}_{f_a g} &= \sum_{x\in\mathcal{Q}} \left\langle \hat{\mathcal{O}}_\mathrm{NLO} F_\mathrm{LM}(1_{f_a}, 2_g \,|\, 4_{f_x}) \right\rangle + \sum_{x\in\mathcal{Q}} \left\langle \mathcal{C}_{42} F_\mathrm{LM}(1_{f_a}, 2_g \,|\, 4_{f_x}) \right\rangle, \\ 2\hat{s}\cdot \mathrm{d}\hat{\sigma}^\mathrm{R}_{g f_a} &= \sum_{x\in\mathcal{Q}} \left\langle \hat{\mathcal{O}}_\mathrm{NLO} F_\mathrm{LM}(1_g, 2_{f_a} \,|\, 4_{f_x}) \right\rangle + \sum_{x\in\mathcal{Q}} \left\langle \mathcal{C}_{41} F_\mathrm{LM}(1_g, 2_{f_a} \,|\, 4_{f_x}) \right\rangle \end{aligned} \tag{4.75}$$

with the NLO subtraction operator acting as

$$\begin{aligned} \hat{\mathcal{O}}_\mathrm{NLO} F_\mathrm{LM}(1_{f_a}, 2_g \,|\, 4_{f_x}) &= (1 - \mathcal{C}_{42})\, F_\mathrm{LM}(1_{f_a}, 2_g \,|\, 4_{f_x}), \\ \hat{\mathcal{O}}_\mathrm{NLO} F_\mathrm{LM}(1_g, 2_{f_a} \,|\, 4_{f_x}) &= (1 - \mathcal{C}_{41})\, F_\mathrm{LM}(1_g, 2_{f_a} \,|\, 4_{f_x}), \end{aligned} \tag{4.76}$$

while the collinear operators project out the leading singularities according to

$$\begin{aligned} \mathcal{C}_{41} F_\mathrm{LM}(1_g, 2_{f_a} \,|\, 4_{f_x}) &= g^2_{s,\epsilon} \frac{1}{(p_1\cdot p_4)} P^{(0)}_{qg}(z;\epsilon) \frac{F_\mathrm{LM}(z\cdot 1_{\bar{f}_x}, 2_{f_a})}{z} \quad \text{with} \quad z = \frac{E_1 - E_4}{E_1}, \\ \mathcal{C}_{42} F_\mathrm{LM}(1_{f_a}, 2_g \,|\, 4_{f_x}) &= g^2_{s,\epsilon} \frac{2}{(p_2\cdot p_4)} P^{(0)}_{qg}(z;\epsilon) \frac{F_\mathrm{LM}(1_{f_a}, z\cdot 2_{\bar{f}_x})}{z} \quad \text{with} \quad z = \frac{E_2 - E_4}{E_2}. \end{aligned} \tag{4.77}$$

The new notation $\bar{f}_x$ is used to indicate the antiparticle to f_x and should be understood as $\bar{f}_x = f_{-x}$ following the scheme of Table 4.1. The splitting function for a gluon going into a quark reads

$$P^{(0)}_{qg}(z;\epsilon) = T_\mathrm{R} \left(1 - \frac{2\,z\,(1-z)}{1-\epsilon} \right). \tag{4.78}$$

In full analogy to the calculation in section 4.3, we derive the results for the integrated counterterms, resulting in

$$\begin{aligned} 2\hat{s}\cdot \mathrm{d}\hat{\sigma}^\mathrm{R}_{f_a g} &= \frac{\alpha_s(\mu_\mathrm{R})}{2\pi} \left(\frac{\mu^2_\mathrm{F}}{\hat{s}} \right)^\epsilon \left[-\frac{1}{\epsilon} \int_0^1 \mathrm{d}z \sum_{x\in\mathcal{Q}} \mathcal{P}_{qg}(z;\epsilon) \left\langle \frac{F_\mathrm{LM}(1_{f_a}, z\cdot 2_{f_x})}{z} \right\rangle \right] \\ &\quad + \sum_{x\in\mathcal{Q}} \left\langle \hat{\mathcal{O}}_\mathrm{NLO} F_\mathrm{LM}(1_{f_a}, 2_g \,|\, 4_{f_x}) \right\rangle, \\ 2\hat{s}\cdot \mathrm{d}\hat{\sigma}^\mathrm{R}_{g f_a} &= \frac{\alpha_s(\mu_\mathrm{R})}{2\pi} \left(\frac{\mu^2_\mathrm{F}}{\hat{s}} \right)^\epsilon \left[-\frac{1}{\epsilon} \int_0^1 \mathrm{d}z \sum_{x\in\mathcal{Q}} \mathcal{P}_{qg}(z;\epsilon) \left\langle \frac{F_\mathrm{LM}(z\cdot 1_{f_x}, 2_{f_a})}{z} \right\rangle \right] \\ &\quad + \sum_{x\in\mathcal{Q}} \left\langle \hat{\mathcal{O}}_\mathrm{NLO} F_\mathrm{LM}(1_g, 2_{f_a} \,|\, 4_{f_x}) \right\rangle, \end{aligned} \tag{4.79}$$

where the generalized splitting function in relation to Eq. (4.74) is

$$\mathcal{P}_{qg}(z;\epsilon) = \hat{P}^{(0)}_{qg}(z) - \epsilon\, \mathcal{P}'_{qg}(z) + \mathcal{O}\left(\epsilon^2\right) \tag{4.80}$$

with the $\mathcal{O}(\epsilon)$ term

$$\mathcal{P}'_{qg}(z) = T_\mathrm{R} \left(2\left[z^2 + (1-z)^2 \right] \ln(1-z) + 2\,z\,(1-z) \right). \tag{4.81}$$

In the sum of the collinear-renormalization contribution and the real-emission cross section we observe pole cancellation and obtain results in the quark-gluon channel which are finite in four dimensions,

$$\begin{aligned} 2\hat{s}\cdot \mathrm{d}\hat{\sigma}^{\mathrm{NLO}}_{f_a g} &= 2\hat{s}\cdot\left(\mathrm{d}\hat{\sigma}^{\mathrm{R}}_{f_a g} + \mathrm{d}\hat{\sigma}^{\mathrm{C_{NLO}}}_{f_a g}\right) \\ &= \frac{\alpha_s(\mu_{\mathrm{R}})}{2\pi}\int_0^1 \mathrm{d}z \sum_{x\in\mathcal{Q}}\left[\mathcal{P}'_{qg}(z) - \hat{P}^{(0)}_{qg}(z)\ln\left(\frac{\mu_{\mathrm{F}}^2}{\hat{s}}\right)\right]\left\langle \frac{F_{\mathrm{LM}}(1_{f_a}, z\cdot 2_{f_x})}{z}\right\rangle \\ &\quad + \sum_{x\in\mathcal{Q}}\left\langle \hat{\mathcal{O}}_{\mathrm{NLO}} F_{\mathrm{LM}}(1_{f_a}, 2_g \,|\, 4_{f_x})\right\rangle, \end{aligned} \tag{4.82}$$

for the process $qg \to V + q'$, and

$$\begin{aligned} 2\hat{s}\cdot \mathrm{d}\hat{\sigma}^{\mathrm{NLO}}_{g f_a} &= 2\hat{s}\cdot\left(\mathrm{d}\hat{\sigma}^{\mathrm{R}}_{g f_a} + \mathrm{d}\hat{\sigma}^{\mathrm{C_{NLO}}}_{g f_a}\right) \\ &= \frac{\alpha_s(\mu_{\mathrm{R}})}{2\pi}\int_0^1 \mathrm{d}z \sum_{x\in\mathcal{Q}}\left[\mathcal{P}'_{qg}(z) - \hat{P}^{(0)}_{qg}(z)\ln\left(\frac{\mu_{\mathrm{F}}^2}{\hat{s}}\right)\right]\left\langle \frac{F_{\mathrm{LM}}(z\cdot 1_{f_x}, 2_{f_a})}{z}\right\rangle \\ &\quad + \sum_{x\in\mathcal{Q}}\left\langle \hat{\mathcal{O}}_{\mathrm{NLO}} F_{\mathrm{LM}}(1_g, 2_{f_a} \,|\, 4_{f_x})\right\rangle \end{aligned} \tag{4.83}$$

for the process $gq \to V + q'$.
With the cross sections in Eq. (4.1), Eq. (4.70), Eq. (4.82), and Eq. (4.83) we can compute the hadronic cross section for color-singlet production up to NLO based on Eq. (2.2),

$$\begin{aligned} \mathrm{d}\sigma^{\mathrm{LO}}_{pp} &= \sum_{a\in\mathcal{Q}}\sum_{b\in\mathcal{Q}}\int_0^1 \mathrm{d}\tau\, \frac{\mathrm{d}\mathcal{L}^{f_a f_b}_{pp}(\tau,\mu_{\mathrm{F}})}{\mathrm{d}\tau}\,\mathrm{d}\hat{\sigma}^{\mathrm{B}}_{f_a f_b}(\tau,\mu_{\mathrm{R}},\mu_{\mathrm{F}}) \\ \mathrm{d}\sigma^{\mathrm{NLO}}_{pp} &= \sum_{a\in\mathcal{Q}}\sum_{b\in\mathcal{Q}}\int_0^1 \mathrm{d}\tau\, \frac{\mathrm{d}\mathcal{L}^{f_a f_b}_{pp}(\tau,\mu_{\mathrm{F}})}{\mathrm{d}\tau}\,\mathrm{d}\hat{\sigma}^{\mathrm{NLO}}_{f_a f_b}(\tau,\mu_{\mathrm{R}},\mu_{\mathrm{F}}) \\ &\quad + \sum_{a\in\mathcal{Q}}\int_0^1 \mathrm{d}\tau\, \frac{\mathrm{d}\mathcal{L}^{f_a g}_{pp}(\tau,\mu_{\mathrm{F}})}{\mathrm{d}\tau}\,\mathrm{d}\hat{\sigma}^{\mathrm{NLO}}_{f_a g}(\tau,\mu_{\mathrm{R}},\mu_{\mathrm{F}}) \\ &\quad + \sum_{b\in\mathcal{Q}}\int_0^1 \mathrm{d}\tau\, \frac{\mathrm{d}\mathcal{L}^{g f_b}_{pp}(\tau,\mu_{\mathrm{F}})}{\mathrm{d}\tau}\,\mathrm{d}\hat{\sigma}^{\mathrm{NLO}}_{g f_b}(\tau,\mu_{\mathrm{R}},\mu_{\mathrm{F}}), \end{aligned} \tag{4.84}$$

where the whole phase-space integration can be preformed (numerically) in four dimensions. At each phase-space point, subtracted matrix elements are finite, which is the reason why we call the FKS Subtraction scheme a local subtraction scheme[6].
The natural next step is the calculation of the NNLO cross section. Due to a richer singularity structure the subtraction procedure will become more complex. In particular, we have to deal with two main challenges: Firstly, we need to devise a method to disentangle overlapping singularities, as their simultaneous presence complicates the subtraction process. Secondly, it becomes significantly more demanding to identify suitable subtraction functions whose counterterms can be integrated analytically.

[6]Slicing methods instead are never local since their matrix elements still diverge in the singular limits and these singularities are only tamed by the numerical cut-off.

5

Nested Soft-Collinear Subtraction

Contents

The Nested Soft-Collinear Subtraction scheme provides an effective framework for addressing the challenges in computations of fully-differential NNLO cross sections. It is based on the strategy of Sector-Improved Residue Subtraction, known as `STRIPPER`, but introduces modifications to enhance its efficiency. In particular, the Nested Soft-Collinear Subtraction scheme eliminates a redundant sector that contains correlated soft-collinear singularities. This is achieved by incorporating the concept of color coherence, which was not considered in the original construction of `STRIPPER`. By exploiting these simplifications, the Nested Soft-Collinear Subtraction scheme enables for a systematic separation of soft and collinear singularities in a nested way. Additionally, this approach offers a physically transparent and intuitive picture of the underlying subtraction procedure.
In this chapter, we focus on introducing the Nested-Soft Collinear Subtraction scheme and provide a comprehensive derivation of all subtraction functions necessary for the implementation of color-singlet production. Moreover, we will present the finite remainder that has been obtained in Ref. [116] through analytic pole cancellation. This finite remainder forms the basis of our MC event generator. However, we will not conduct explicit recalculations of the counterterms since their outcomes are already documented in existing literature. Instead, we will refer to these sources at the relevant stage of our discussion.

5.1. Guiding Principles

The goal of the Nested Soft-Collinear Subtraction scheme is the construction of an optimal NNLO subtraction scheme following a set of general guiding principles:

1) The scheme should ensure that cross sections are well-defined at every resolved phase-space point, making it *fully local*.

2) *Efficiency* is crucial for making predictions of relevant physical processes, necessitating the ability to numerically evaluate cross sections due to the arbitrary complexity of phase-space integrals.

3) The subtraction scheme should be generally applicable to any NNLO process, remaining *process independent*.

4) A desirable attribute is a *physically transparent* subtraction scheme where each singularity has a clear physical origin and their cancellations can be interpreted in a physical picture.

5) Poles should cancel *analytically*, independent of the matrix elements. This is a useful criterion to ensure physical transparency as well as process independence, but also to obtain a finite remainder that can be evaluated efficiently.

6) The finite remainder should have a relatively *simple structure* with simple functions for the counterterms that multiply matrix elements with a reduced number for final-state partons. This can be achieved by recombining sectors before integrating the subtraction terms[1].

7) The scheme should offer *flexibility* by allowing freedom in choosing a phase-space mapping.

8) To facilitate ease of use and application to new processes, the scheme should have a *modular* structure with building blocks that can be recombined to calculate specific cross section.

In the upcoming sections and chapters, we will explain the first seven points more thoroughly. Regarding the eighth point, the building blocks can be identified as three fundamental elements. They can be constructed based on the fact that at NNLO no more than two partons simultaneously appear unresolved. Since collinear singularities factorize on external legs and the factorization of non-trivial terms of soft singularities depends on a maximum of two external particles of the Born cross section, each $2 \to n$ QCD process can be decomposed into three types of singular structures. In each structure, two colored initial-state partons, two colored final-state partons, or one colored initial-state parton and one colored final-state parton are involved, while the colors of the other external particles do not impact factorization. Consequently, the three building blocks are constructed by examining exemplary processes where only one singular structure contributes. For initial-state-initial-state singularities, studying color-singlet production, such as the Drell-Yan process and Higgs boson production in the gluon-fusion channel, is convenient. The cross sections of these processes are known analytically [56, 255] and, thus, they are perfectly suited for validating the building block of the Nested Soft-Collinear Subtraction scheme that was constructed in Refs. [38, 116]. The final-state-final-state building block can be assembled by inves-

[1]The meaning of the term "sector" will be explained in section 5.2.

tigating the well-known decay of a color singlet, such as the decay of a Higgs boson into two colored particles [256–258], as done in Ref. [117]. The last building block, concerning initial-state-final-state singularities, can be studied in deep inelastic scattering. The analytic result of its cross section is available and extensively investigated in the literature [259–261]. This component for the Nested Soft-Collinear Subtraction scheme was presented in Refs. [118, 262].

5.2. Color-Singlet Production at Next-to-Next-to-Leading Order

According to Eq. (3.6), at NNLO, we need to compute processes with double-real corrections, real-virtual corrections, and double-virtual corrections. The IR poles of pure virtual contributions are explicitly encoded in the loops of the matrix elements, some IR singularities of the real-virtual contributions are contained manifestly in the matrix elements, and some show up upon phase-space integration. These phase-space singularities can be extracted with the techniques of the NLO FKS Subtractions scheme that we have seen before since only one real parton is emitted. All IR singularities of the double-real emission process show up during phase-space integration, but they have a richer and more complex structure than at NLO and require an NNLO subtraction scheme to make them manifest. As regulating the double-real emission is key in constructing an NNLO subtraction scheme, firstly, we want to pay attention to these contributions.

5.2.1. Double-Real Corrections

Double-real corrections for our study of color-singlet production occur in four different channels, representative Feynman diagrams for the quark-antiquark channel with the emission of a gluon pair, $q(p_1)\bar{q}'(p_2) \to V(p_3) + g(p_4)g(p_5)$, are shown in Figure 5.1. Double-real corrections for the quark-gluon channel, $q(p_1)g(p_2) \to V(p_3) + q'(p_4)g(p_5)$, are depicted in Figure 5.2. The diagrams for the gluon-quark channel can be easily obtained by exchanging the two initial state particles. On top, two new channels open: A quark-quark channel with two incoming quarks, $q_i(p_1)q_j(p_2) \to V(p_3) + q_k(p_4)q_l(p_5)$, where the indices indicate the related quark flavor[2], and a gluon-induced contribution, $g(p_1)g(p_2) \to V(p_3) + q(p_4)\bar{q}'(p_5)$. Exemplary Feynman diagrams of the former production mechanism are given in Figure 5.3(a) and of the latter in Figure 5.3(b). For clarity, we will focus the discussion for regulating IR singularities in case of double-parton emission on the quark-antiquark channel with a real-emitted gluon pair since this channel has the most complex structure. Results for the other channels can be obtained analogously with the strategy that we will present and are shown at the end of this chapter without repeating the regularization procedure in detail.
We adopt the same notation that was used in the NLO calculation,

[2]In the following, we will call the process with two initial-state quarks and two final-state gluons the "quark-antiquark channel" and the channel with two final-state quarks "quark-quark channel", even though the latter process also includes quark-antiquark initial states.

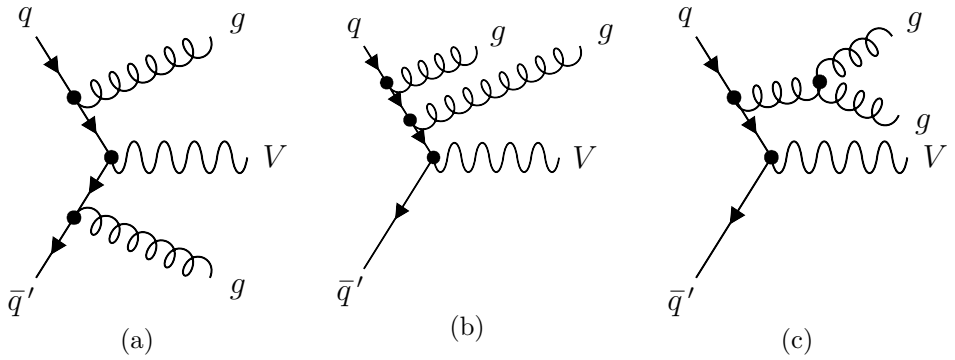

Figure 5.1.: Representative Feynman diagrams for double-real corrections in color-singlet production in the quark-antiquark channel.

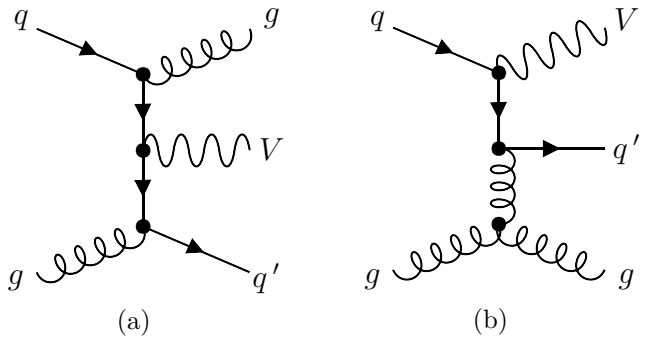

Figure 5.2.: Representative Feynman diagrams for double-real corrections in color-singlet production in the quark-gluon channel.

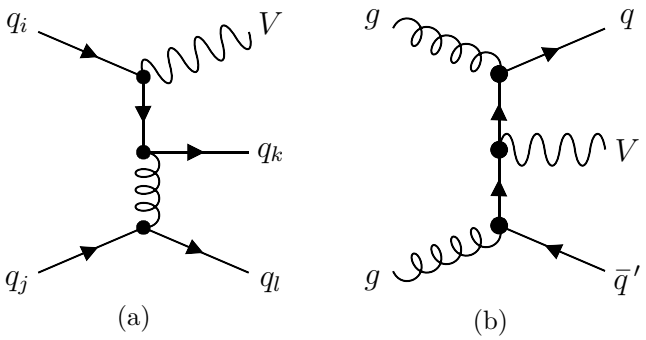

Figure 5.3.: Representative Feynman diagrams for double-real corrections in color-singlet production in the quark-quark channel (a) and the gluon-gluon channel (b).

$$\begin{aligned} 2\hat{s}\cdot \mathrm{d}\hat{\sigma}^{\mathrm{RR}}_{f_a f_b} &= 2\int [\mathrm{d}p_4][\mathrm{d}p_5]\Theta(E_4-E_5)\, F_{\mathrm{LM}}(1_{f_a},2_{f_b}\,|\,4_g,5_g) \\ &= \big\langle F_{\mathrm{LM}}(1_{f_a},2_{f_b}\,|\,4_g,5_g)\big\rangle, \end{aligned} \tag{5.1}$$

with the function

$$F_{\mathrm{LM}}(1_{f_a},2_{f_b}\,|\,4_g,5_g) = \mathcal{N}\,\mathrm{d}\Pi_{\mathrm{B}}^{(d)}\,|\mathcal{M}^{(0)}_{f_a f_b\to V+gg}(p_1,p_2,p_3,p_4,p_5)|^2 F_J(p_1,p_2,p_3,p_4,p_5), \tag{5.2}$$

where the Born phase-space element contains the momentum conserving δ-distribution,

$$\mathrm{d}\Pi_{\mathrm{B}}^{(d)} = \frac{\mathrm{d}^{d-1}p_3}{(2\pi)^{d-1}2E_3}\,(2\pi)^d\,\delta^{(d)}(p_1+p_2-p_3-p_4-p_5), \tag{5.3}$$

and the angled brackets imply the integration over the phase space of both real-emitted gluons. In Eq. (5.1), we introduced an energy ordering, $E_4 \geqslant E_5$, giving an additional factor of two due to the symmetry when permuting the two gluons. This factor will cancel the symmetry factor, $\mathcal{N} = 1/2!$, which appears for having two identical particles in the final state[3].
When integrating over the unresolved phase space of the gluons, various IR divergences spoil the calculation. This includes soft divergences, many collinear divergences, and combinations of them. To regulate the soft singularities, we introduce the operators

$$\begin{aligned} \mathcal{S}_i A &= \lim_{E_i\to 0} A, \\ \boldsymbol{\mathcal{S}} A &= \lim_{E_4,E_5\to 0} A, \quad \text{at fixed ratio} \quad \frac{E_5}{E_4}, \end{aligned} \tag{5.4}$$

where $\mathcal{S}_i$ extracts the leading singularity of a single parton i that becomes soft and is identical to the definition in Eq. (4.19). At the same time, $\boldsymbol{\mathcal{S}}$ is a new projector to extract the leading singularity when both partons become soft simultaneously. For projecting out the collinear limits, we make use of the operators

$$\begin{aligned} \mathcal{C}_{ji} A &= \lim_{\eta_{ij}\to 0} A, \\ \boldsymbol{\mathcal{C}}_i A &= \lim_{\eta_{i4},\eta_{i5}\to 0} A, \quad \text{with non-vanishing ratios} \quad \frac{\eta_{i4}}{\eta_{i5}}, \frac{\eta_{45}}{\eta_{i4}}, \frac{\eta_{45}}{\eta_{i5}}, \end{aligned} \tag{5.5}$$

where $\mathcal{C}_{ji}$, as established in Eq. (4.20), extracts the leading singularities when partons i and j appear to be collinear to each other. The triple-collinear operator $\boldsymbol{\mathcal{C}}_i$ instead describes the leading singular limit when both final-state partons become collinear to the incoming parton i at the same time.

5.2.1.1. Soft Singularities

Even if, in general, single Feynman diagrams contain entangled singularities, *e.g.* singularities that appear when one gluon becomes soft and the other gluon becomes collinear, these entangled singularities drop out for on-shell amplitudes of the whole physical process because of color-coherence properties [263–265]. Consequently, soft and collinear

[3]The main reason for introducing the energy ordering is that it will simplify the discussion for regulating soft divergences in the following. However, the computation can also be done without this. In particular, in the other channels for double-real emission, the energy ordering will not have any advantage and should be omitted.

divergencies can be regulated independently.
It is convenient to start by removing the soft divergencies. In a first step, double-soft parton emissions are regulated. According to the subtraction formalism, the cross section becomes

$$2\hat{s}\cdot \mathrm{d}\hat{\sigma}^{\mathrm{RR}}_{f_a f_b} = \langle (1-\boldsymbol{\mathcal{S}})\, F_{\mathrm{LM}}(1_{f_a}, 2_{f_b} \,|\, 4_g, 5_g)\rangle + \langle \boldsymbol{\mathcal{S}} F_{\mathrm{LM}}(1_{f_a}, 2_{f_b} \,|\, 4_g, 5_g)\rangle\,, \tag{5.6}$$

where the first term is free of double-soft singularities and the second term is the counterterm with manifest IR poles after integration over the unresolved parton phase spaces. Next, the single-soft singularities that are still included in the first summand can be regulated. Due to the energy ordering, the limit $E_4 \to 0$ can only be reached when $E_5 \to 0$. Hence, this divergence only appears as double-soft emission, making it sufficient to remove the singularity for $E_5 \to 0$ as the last soft singularity,

$$\begin{aligned} 2\hat{s}\cdot \mathrm{d}\hat{\sigma}^{\mathrm{RR}}_{f_a f_b} = {} & \langle (1-\boldsymbol{\mathcal{S}})\,(1-\mathcal{S}_5)\, F_{\mathrm{LM}}(1_{f_a}, 2_{f_b} \,|\, 4_g, 5_g)\rangle + \langle \boldsymbol{\mathcal{S}} F_{\mathrm{LM}}(1_{f_a}, 2_{f_b} \,|\, 4_g, 5_g)\rangle \\ & + \langle (1-\boldsymbol{\mathcal{S}})\,\mathcal{S}_5 F_{\mathrm{LM}}(1_{f_a}, 2_{f_b} \,|\, 4_g, 5_g)\rangle\,, \end{aligned} \tag{5.7}$$

so that just collinear singularities are left in the first term. The originating counterterm in the last line of Eq. (5.7) has two pieces. One is obtained by a strongly-ordered limit where first the gluon with momentum p_5 becomes soft and subsequently the gluon with momentum p_4. The related operator, $\boldsymbol{\mathcal{S}}\mathcal{S}_5$, decouples both gluons from the hard process. In the second term, only the operator $\mathcal{S}_5$ is present that decouples one gluon from the hard process. Since one gluon is still part of the hard process, NLO-like IR singularities will remain in the hard matrix element. However, as discussed in the last chapter, they can be treated with the FKS approach for NLO processes.
In subsubsection 5.2.1.4, we will show the action of the soft operators in more detail in order to give proper definitions of the subtraction terms which give rise to counterterms that can be evaluated analytically. Before we come to this, we want to unravel the structure of the collinear singularities and obtain a fully-regulated cross section for double-real emission.

5.2.1.2. Collinear Singularities

Already at NNLO with two real-radiated partons and two partons in the hard process, many different collinear limits lead to divergences. Collinear limits are obtained when one of the incoming partons becomes collinear to a final-state parton, $\vec{p}_1 \parallel \vec{p}_i$ and $\vec{p}_2 \parallel \vec{p}_i$, where $i \in \{4, 5\}$, or when the two final-state partons become collinear to each other, $\vec{p}_4 \parallel \vec{p}_5$. Additionally, triple-collinear limits appear when both final-state partons become collinear to one of the initial-state partons at the same time, $\vec{p}_1 \parallel \vec{p}_4 \parallel \vec{p}_5$ as well as $\vec{p}_2 \parallel \vec{p}_4 \parallel \vec{p}_5$. Moreover, overlaps of these collinear singularities introduce particular challenges.

Phase-Space Partitions

In order to separate these overlaps, the phase space can be split into different partitions where each partition contains only a subset of collinear singularities. The phase-space split can be done by introducing a decomposed one according to

$$1 = w^{41,51} + w^{41,52} + w^{42,52} + w^{42,51}, \tag{5.8}$$

so that the collinear operators act on the partition functions as

$$\mathcal{C}_{4k} w^{4i,5j} = \delta_{ik}, \quad \mathcal{C}_{5k} w^{4i,5j} = \delta_{jk}, \quad \mathcal{C}_{45} w^{4i,5j} = \delta_{ij}, \quad i,j,k \in \{1,2\}. \tag{5.9}$$

If we consider the object

$$F_{\mathrm{LM}}(1_{f_a}, 2_{f_b} \,|\, 4_g, 5_g) = \left(w^{41,51} + w^{41,52} + w^{42,52} + w^{42,51}\right) F_{\mathrm{LM}}(1_{f_a}, 2_{f_b} \,|\, 4_g, 5_g), \tag{5.10}$$

the first term on the right-hand side contains IR divergences in the triple-collinear limit when both final-state partons become collinear to the incoming parton with momentum p_1, when either one of the two final-state partons is emitted collinearly from parton 1, or when both final-state partons are collinear to each other. However, no singularities involving parton 2 appear in this partition. This can be seen from Eq. (5.9) since the extraction of a leading singularity with an operator that contains parton 2 leads to no contribution. The same arguments are valid for the third term, with the difference that the first parton has to be replaced with the second one and vice versa. We refer to the partitions $w^{41,51}$ and $w^{42,52}$ as triple-collinear partitions due to the presence of triple-collinear limits within them. Although these partitions contain only a subset of collinear singularities, there are still overlapping singularities that require further investigation. Before delving into the details, we want to look closer at the second term of Eq. (5.10). Collinear divergences arise when partons 4 and 1, or partons 5 and 2 become collinear to each other while other collinear singularities do not show up by construction, *cf.* Eq. (5.9). Both singularities can occur simultaneously, but there are no overlaps in this particular partition. Similar scenarios are described by the last term, where partons 1 and 2 are interchanged. The two partitions $w^{41,52}$ and $w^{42,51}$, where at most two pairs of partons can be collinear, are called double-collinear partitions.
The choice of partition functions is not unique. In our implementation, we will use a specific set of functions described by

$$\begin{aligned} w^{41,51} &= \eta_{24}\eta_{25}\left(1 + \frac{\eta_{14}}{d_{4521}} + \frac{\eta_{15}}{d_{4512}}\right), \quad w^{41,52} = \frac{\eta_{24}\eta_{15}\eta_{45}}{d_{4512}}, \\ w^{42,52} &= \eta_{14}\eta_{15}\left(1 + \frac{\eta_{24}}{d_{4521}} + \frac{\eta_{25}}{d_{4512}}\right), \quad w^{42,51} = \frac{\eta_{14}\eta_{25}\eta_{45}}{d_{4521}}. \end{aligned} \tag{5.11}$$

Here, we introduce a convenient shorthand notation for the denominators

$$d_{45ij} = \eta_{45} + \eta_{i4} + \eta_{j5}, \tag{5.12}$$

which allows us to express the partition functions succinctly. It is straightforward to demonstrate that these particular functions satisfy the conditions given in Eq. (5.9).

Sector Decomposition

While all singularities in the double-collinear partitions are separated, a further sector decomposition is required in the triple-collinear partitions. A natural parametrization of these sectors was introduced in Ref. [34], where angles are ordered in such a way that in each sector no overlapping singularities appear. For partition $w^{41,51}$ we define four sectors denoted as sector (a), (b), (c), and (d), given by

$$\begin{aligned} 1 &= \Theta\left(\eta_{15} \leqslant \frac{\eta_{14}}{2}\right) + \Theta\left(\frac{\eta_{14}}{2} < \eta_{15} \leqslant \eta_{14}\right) + \Theta\left(\eta_{14} \leqslant \frac{\eta_{15}}{2}\right) + \Theta\left(\frac{\eta_{15}}{2} < \eta_{14} < \eta_{15}\right) \\ &\equiv \Theta_1^{(a)} + \Theta_1^{(b)} + \Theta_1^{(c)} + \Theta_1^{(d)}, \end{aligned} \tag{5.13}$$

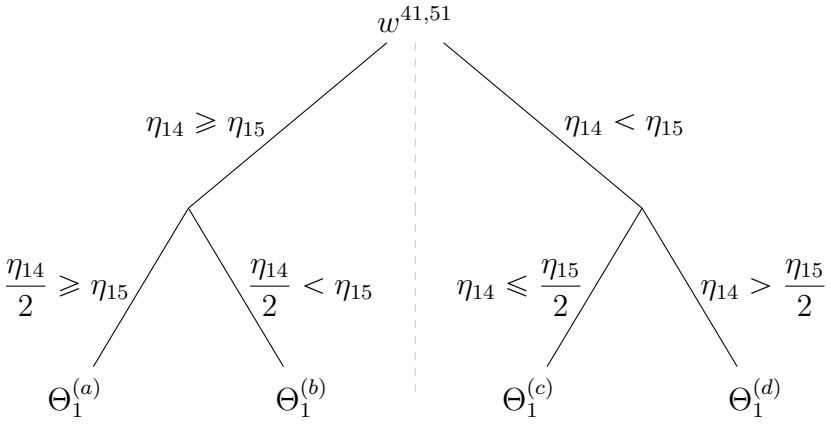

Figure 5.4.: Tree diagram representing a schematic division of partition $w^{41,51}$ into the four sectors (a), (b), (c), and (d) accordingly to the angular ordering.

so that in the first term on the right-hand side of

$$w^{41,51} F_{\mathrm{LM}}(1_{f_a}, 2_{f_b} \,|\, 4_g, 5_g) = w^{41,51} \left(\Theta_1^{(a)} + \Theta_1^{(b)} + \Theta_1^{(c)} + \Theta_1^{(d)}\right) F_{\mathrm{LM}}(1_{f_a}, 2_{f_b} \,|\, 4_g, 5_g) \tag{5.14}$$

collinear singularities are present for the configurations $\vec{p}_1 \parallel \vec{p}_5$ with η_{15} approaching zero and $\vec{p}_1 \parallel \vec{p}_4 \parallel \vec{p}_5$ in the limit of η_{14} going to zero, which automatically includes a vanishing angle η_{15}. This means that parton 4 cannot become collinear to parton 1 without parton 5 also being collinear to parton 1. Moreover, the partons 4 and 5 can only become collinear to each other in the triple-collinear limit, since the angle between parton 1 and 5 is always smaller than the angle between 4 and 5. In contrast, sector (b) contains divergences when both final-state partons become collinear to each other in the scenario where η_{15} tends to η_{14}. Additionally, the triple-collinear limit can be reached for vanishing η_{14} which imposes η_{15} going to zero and vice versa. Just one vanishing angular parameter while the other one stays unequal to zero is not possible, what forbids singularities where only one of the final-state partons becomes collinear to the initial-state parton. Sectors (c) and (d) correspond to the sectors (a) and (b), respectively, with a switched role of the two final-state partons 4 and 5. A schematic overview of the angular ordering in partition $w^{41,51}$ and the separation into the sectors is depicted in Figure 5.4.
In partition $w^{42,52}$, we obtain the sector decomposition by a replacement of the index 1 against 2 everywhere in Eq. (5.13), leading to a similar conclusion with just a limited number of non-overlapping singularities occurring in each sector,

$$\begin{aligned} 1 &= \Theta\Big(\eta_{25} \leqslant \frac{\eta_{24}}{2}\Big) + \Theta\Big(\frac{\eta_{24}}{2} < \eta_{25} \leqslant \eta_{24}\Big) + \Theta\Big(\eta_{24} \leqslant \frac{\eta_{25}}{2}\Big) + \Theta\Big(\frac{\eta_{25}}{2} < \eta_{24} < \eta_{25}\Big) \\ &\equiv \Theta_2^{(a)} + \Theta_2^{(b)} + \Theta_2^{(c)} + \Theta_2^{(d)}. \end{aligned} \tag{5.15}$$

Since only a subset of divergences is present within each partition and sector, in each separate contribution, just a small number of IR projectors is necessary to acquire the relevant subtraction terms, see Table 5.1.

Table 5.1.: Overview of the basic projectors that are necessary to extract the leading IR singularities in (a) the double-collinear partitions and (b) the triple-collinear partitions.

(a)

	Soft Singularities	Angular Singularities
$w^{41,52}$	$\boldsymbol{\mathcal{S}}$, $\mathcal{S}_5$	$\mathcal{C}_{41}$, $\mathcal{C}_{52}$
$w^{42,51}$	$\boldsymbol{\mathcal{S}}$, $\mathcal{S}_5$	$\mathcal{C}_{42}$, $\mathcal{C}_{51}$

(b)

	Soft	Angular Singularities			
	Singularities	$\Theta^{(a)}$	$\Theta^{(b)}$	$\Theta^{(c)}$	$\Theta^{(d)}$
$w^{41,51}$	$\boldsymbol{\mathcal{S}}$, $\mathcal{S}_5$	$\boldsymbol{\mathcal{C}}_1$, $\mathcal{C}_{51}$	$\boldsymbol{\mathcal{C}}_1$, $\mathcal{C}_{45}$	$\boldsymbol{\mathcal{C}}_1$, $\mathcal{C}_{41}$	$\boldsymbol{\mathcal{C}}_1$, $\mathcal{C}_{45}$
$w^{42,52}$	$\boldsymbol{\mathcal{S}}$, $\mathcal{S}_5$	$\boldsymbol{\mathcal{C}}_2$, $\mathcal{C}_{52}$	$\boldsymbol{\mathcal{C}}_2$, $\mathcal{C}_{45}$	$\boldsymbol{\mathcal{C}}_2$, $\mathcal{C}_{42}$	$\boldsymbol{\mathcal{C}}_2$, $\mathcal{C}_{45}$

5.2.1.3. Nested Subtractions

In summary, we are now able to reshape the first term of Eq. (5.7) into the form

$$\begin{aligned}
&\big\langle (1-\boldsymbol{\mathcal{S}})\,(1-\mathcal{S}_5)\,F_{\mathrm{LM}}(1_{f_a},2_{f_b}\,|\,4_g,5_g)\big\rangle \\
&= \Bigg\langle (1-\boldsymbol{\mathcal{S}})\,(1-\mathcal{S}_5)\left[\sum_{(i,j)\in \mathrm{dc}} w^{4i,5j} + \sum_{i\in \mathrm{tc}} w^{4i,5i}\left(\Theta_i^{(a)}+\Theta_i^{(b)}+\Theta_i^{(c)}+\Theta_i^{(d)}\right)\right] \\
&\quad \times F_{\mathrm{LM}}(1_{f_a},2_{f_b}\,|\,4_g,5_g)\Bigg\rangle,
\end{aligned} \tag{5.16}$$

with a sum over the set of double-collinear terms, $\mathrm{dc} = \{(1,2),(2,1)\}$, and the set of the two triple-collinear partitions, $\mathrm{tc} = \{1,2\}$. This gives us the opportunity to regulate collinear divergences partition-by-partition and sector-by-sector, using the same strategy that we applied at NLO in the FKS formalism.

Double-Collinear Partitions

In the double-collinear partition $w^{41,52}$ we regulate the collinear divergences with the operators $\mathcal{C}_{41}$ and $\mathcal{C}_{52}$ in a nested way. The expression becomes

$$\begin{aligned}
&\big\langle (1-\boldsymbol{\mathcal{S}})\,(1-\mathcal{S}_5)\,w^{41,52}F_{\mathrm{LM}}(1_{f_a},2_{f_b}\,|\,4_g,5_g)\big\rangle \\
&= \big\langle (\mathcal{C}_{41}+\mathcal{C}_{52}-\mathcal{C}_{41}\mathcal{C}_{52})\,(1-\boldsymbol{\mathcal{S}})\,(1-\mathcal{S}_5)\,w^{41,52}F_{\mathrm{LM}}(1_{f_a},2_{f_b}\,|\,4_g,5_g)\big\rangle \\
&\quad + \big\langle (1-\mathcal{C}_{41})\,(1-\mathcal{C}_{52})\,(1-\boldsymbol{\mathcal{S}})\,(1-\mathcal{S}_5)\,w^{41,52}F_{\mathrm{LM}}(1_{f_a},2_{f_b}\,|\,4_g,5_g)\big\rangle \\
&= \big\langle (\mathcal{C}_{41}+\mathcal{C}_{52}-\mathcal{C}_{41}\mathcal{C}_{52})\,(1-\boldsymbol{\mathcal{S}})\,(1-\mathcal{S}_5)\,w^{41,52}F_{\mathrm{LM}}(1_{f_a},2_{f_b}\,|\,4_g,5_g)\big\rangle \\
&\quad + \Big\langle \hat{\mathcal{O}}^{(1,2)}_{\mathrm{NNLO}}F_{\mathrm{LM}}(1_{f_a},2_{f_b}\,|\,4_g,5_g)\Big\rangle .
\end{aligned} \tag{5.17}$$

Similarly, the results for the double-collinear partition $w^{42,51}$ can be obtained through replacing the index 1 with 2 and vice versa in the collinear operators. Then, the terms with the NNLO subtraction operator for double-collinear partitions,

$$\hat{\mathcal{O}}^{(i,j)}_{\text{NNLO}} = (1-\mathcal{C}_{4i})\,(1-\mathcal{C}_{5j})\,(1-\boldsymbol{\mathcal{S}})\,(1-\mathcal{S}_5)\,w^{4i,5j}, \tag{5.18}$$

are fully regulated and free of all divergences so that a numerical integration in four dimensions can be performed. The counterterms contain all these divergences and must be integrated over the phase space of the unresolved partons to manifest them.

Triple-Collinear Partitions – Sector $\Theta^{(a)}$ and Sector $\Theta^{(c)}$

Moving to sector (a) of the triple-collinear partition $w^{41,51}$, we use the projectors $\mathcal{C}_{51}$ and $\boldsymbol{\mathcal{C}}_1$ for extracting all collinear singularities. We find

$$\begin{aligned}
&\Big\langle (1-\boldsymbol{\mathcal{S}})\,(1-\mathcal{S}_5)\,w^{41,51}\Theta_1^{(a)} F_{\text{LM}}(1_{f_a},2_{f_b}\,|\,4_g,5_g)\Big\rangle \\
&= \big\langle (\boldsymbol{\mathcal{C}}_1+\mathcal{C}_{51}-\boldsymbol{\mathcal{C}}_1\mathcal{C}_{51})\,(1-\boldsymbol{\mathcal{S}})\,(1-\mathcal{S}_5)\,w^{41,51}\Theta_1^{(a)} F_{\text{LM}}(1_{f_a},2_{f_b}\,|\,4_g,5_g)\big\rangle \\
&\quad + \big\langle (1-\boldsymbol{\mathcal{C}}_1)\,(1-\mathcal{C}_{51})\,(1-\boldsymbol{\mathcal{S}})\,(1-\mathcal{S}_5)\,w^{41,51}\Theta_1^{(a)} F_{\text{LM}}(1_{f_a},2_{f_b}\,|\,4_g,5_g)\big\rangle \\
&= \big\langle (\boldsymbol{\mathcal{C}}_1+\mathcal{C}_{51}-\boldsymbol{\mathcal{C}}_1\mathcal{C}_{51})\,(1-\boldsymbol{\mathcal{S}})\,(1-\mathcal{S}_5)\,w^{41,51}\Theta_1^{(a)} F_{\text{LM}}(1_{f_a},2_{f_b}\,|\,4_g,5_g)\big\rangle \\
&\quad + \Big\langle \hat{\mathcal{O}}^{(1,a)}_{\text{NNLO}} F_{\text{LM}}(1_{f_a},2_{f_b}\,|\,4_g,5_g)\Big\rangle,
\end{aligned} \tag{5.19}$$

with the subtraction operator for sector (a),

$$\hat{\mathcal{O}}^{(i,a)}_{\text{NNLO}} = (1-\boldsymbol{\mathcal{C}}_i)\,(1-\mathcal{C}_{5i})\,(1-\boldsymbol{\mathcal{S}})\,(1-\mathcal{S}_5)\,w^{4i,5i}\Theta_i^{(a)}. \tag{5.20}$$

Considering the previous discussion, the singularities in sector (c) can be regulated straightforwardly by replacing parton 5 with parton 4 in the single-collinear projector everywhere in Eq. (5.19) which results in a similar NNLO subtraction operator ,

$$\hat{\mathcal{O}}^{(i,c)}_{\text{NNLO}} = (1-\boldsymbol{\mathcal{C}}_i)\,(1-\mathcal{C}_{4i})\,(1-\boldsymbol{\mathcal{S}})\,(1-\mathcal{S}_5)\,w^{4i,5i}\Theta_i^{(c)}. \tag{5.21}$$

The sectors (a) and (c) in the other triple-collinear partition, $w^{42,52}$, require an exchange of the indices 1 and 2 in the projectors of the corresponding term in partition $w^{41,51}$, as already indicated by the general expressions in Eq. (5.20) and Eq. (5.21) with the general index i that can be either 1 or 2.

Triple-Collinear Partitions – Sector $\Theta^{(b)}$ and Sector $\Theta^{(d)}$

Collinear singularities in sector (b) of the partition $w^{41,51}$ are regulated with $\mathcal{C}_{45}$ and $\boldsymbol{\mathcal{C}}_1$, resulting in

$$\begin{aligned}
&\Big\langle (1-\boldsymbol{\mathcal{S}})\,(1-\mathcal{S}_5)\,w^{41,51}\Theta_1^{(b)} F_{\text{LM}}(1_{f_a},2_{f_b}\,|\,4_g,5_g)\Big\rangle \\
&= \big\langle (\boldsymbol{\mathcal{C}}_1+\mathcal{C}_{45}-\boldsymbol{\mathcal{C}}_1\mathcal{C}_{45})\,(1-\boldsymbol{\mathcal{S}})\,(1-\mathcal{S}_5)\,w^{41,51}\Theta_1^{(b)} F_{\text{LM}}(1_{f_a},2_{f_b}\,|\,4_g,5_g)\big\rangle \\
&\quad + \big\langle (1-\boldsymbol{\mathcal{C}}_1)\,(1-\mathcal{C}_{45})\,(1-\boldsymbol{\mathcal{S}})\,(1-\mathcal{S}_5)\,w^{41,51}\Theta_1^{(b)} F_{\text{LM}}(1_{f_a},2_{f_b}\,|\,4_g,5_g)\big\rangle \\
&= \big\langle (\boldsymbol{\mathcal{C}}_1+\mathcal{C}_{45}-\boldsymbol{\mathcal{C}}_1\mathcal{C}_{45})\,(1-\boldsymbol{\mathcal{S}})\,(1-\mathcal{S}_5)\,w^{41,51}\Theta_1^{(b)} F_{\text{LM}}(1_{f_a},2_{f_b}\,|\,4_g,5_g)\big\rangle \\
&\quad + \Big\langle \hat{\mathcal{O}}^{(1,b)}_{\text{NNLO}} F_{\text{LM}}(1_{f_a},2_{f_b}\,|\,4_g,5_g)\Big\rangle,
\end{aligned} \tag{5.22}$$

where the subtraction operator reads

$$\hat{\mathcal{O}}^{(i,b)}_{\mathrm{NNLO}} = (1-\boldsymbol{\mathcal{C}}_i)\,(1-\mathcal{C}_{45})\,(1-\boldsymbol{\mathcal{S}})\,(1-\mathcal{S}_5)\,w^{4i,5i}\Theta_i^{(b)}. \tag{5.23}$$

The only difference in sector (d) lies in the interpretation of the action of $\mathcal{C}_{45}$. In sector (b), this operator acts on θ_5 approaching θ_4, while in sector (d), it acts on θ_4 approaching θ_5. Thus, the subtraction operator takes the same form as in Eq. (5.23),

$$\hat{\mathcal{O}}^{(i,d)}_{\mathrm{NNLO}} = (1-\boldsymbol{\mathcal{C}}_i)\,(1-\mathcal{C}_{45})\,(1-\boldsymbol{\mathcal{S}})\,(1-\mathcal{S}_5)\,w^{4i,5i}\Theta_i^{(d)}. \tag{5.24}$$

Consequently, also the counterterms exhibit the same shape as those in Eq. (5.22) by remembering the different action of $\mathcal{C}_{45}$ on the angles. Again, the expressions for partition $w^{42,52}$ can be obtained by the obvious exchange of indices of the two initial-state partons.

Cross Section

Combining all pieces, the final result for the double-real-emission cross section with fully-regulated matrix elements and their counterterms reads

$$\begin{aligned}
2\hat{s}\cdot \mathrm{d}\hat{\sigma}^{\mathrm{RR}}_{f_a f_b} = &\sum_{(i,j)\in \mathrm{dc}} \Big\langle \hat{\mathcal{O}}^{(i,j)}_{\mathrm{NNLO}} F_{\mathrm{LM}}(1_{f_a}, 2_{f_b} \,|\, 4_g, 5_g) \Big\rangle \\
&+ \sum_{i\in \mathrm{tc}} \Big\langle \Big(\hat{\mathcal{O}}^{(i,a)}_{\mathrm{NNLO}} + \hat{\mathcal{O}}^{(i,b)}_{\mathrm{NNLO}} + \hat{\mathcal{O}}^{(i,c)}_{\mathrm{NNLO}} + \hat{\mathcal{O}}^{(i,d)}_{\mathrm{NNLO}} \Big) F_{\mathrm{LM}}(1_{f_a}, 2_{f_b} \,|\, 4_g, 5_g) \Big\rangle \\
&+ \sum_{(i,j)\in \mathrm{dc}} \Big\langle (\mathcal{C}_{4i} + \mathcal{C}_{5j} - \mathcal{C}_{4i}\mathcal{C}_{5j})\,(1-\boldsymbol{\mathcal{S}})\,(1-\mathcal{S}_5)\,w^{4i,5j} \\
&\times F_{\mathrm{LM}}(1_{f_a}, 2_{f_b} \,|\, 4_g, 5_g) \Big\rangle + \sum_{i\in \mathrm{tc}} \Big\langle \Big(\mathcal{C}_{5i}\,\Theta_i^{(a)} + \mathcal{C}_{45}\,\Theta_i^{(b)} + \mathcal{C}_{4i}\,\Theta_i^{(c)} \\
&+ \mathcal{C}_{45}\,\Theta_i^{(d)} \Big) (1-\boldsymbol{\mathcal{S}})\,(1-\mathcal{S}_5)\,w^{4i,5i} F_{\mathrm{LM}}(1_{f_a}, 2_{f_b} \,|\, 4_g, 5_g) \Big\rangle \\
&- \sum_{i\in \mathrm{tc}} \Big\langle \boldsymbol{\mathcal{C}}_i \Big(\mathcal{C}_{5i}\,\Theta_i^{(a)} + \mathcal{C}_{45}\,\Theta_i^{(b)} + \mathcal{C}_{4i}\,\Theta_i^{(c)} + \mathcal{C}_{45}\,\Theta_i^{(d)} \Big) (1-\boldsymbol{\mathcal{S}}) \\
&\times (1-\mathcal{S}_5)\,w^{4i,5i} F_{\mathrm{LM}}(1_{f_a}, 2_{f_b} \,|\, 4_g, 5_g) \Big\rangle + \sum_{i\in \mathrm{tc}} \Big\langle \boldsymbol{\mathcal{C}}_i F_{\mathrm{LM}}(1_{f_a}, 2_{f_b} \,|\, 4_g, 5_g) \Big\rangle \\
&+ \Big\langle (1-\boldsymbol{\mathcal{S}})\,\mathcal{S}_5 F_{\mathrm{LM}}(1_{f_a}, 2_{f_b} \,|\, 4_g, 5_g) \Big\rangle + \Big\langle \boldsymbol{\mathcal{S}} F_{\mathrm{LM}}(1_{f_a}, 2_{f_b} \,|\, 4_g, 5_g) \Big\rangle.
\end{aligned} \tag{5.25}$$

Terms with NNLO subtraction operators, $\hat{\mathcal{O}}_{\mathrm{NNLO}}$, are free of all IR divergences, instead, all divergences are shifted into the rich counterterm structure.

5.2.1.4. Subtraction Functions

In order to calculate the $\hat{\mathcal{O}}_{\mathrm{NNLO}}$ terms, it is necessary to understand the action of all operators on the F_{LM} function. Moreover, the counterterms have to be integrated analytically. Since we are interested in the implementation of the Nested Soft-Collinear Subtraction scheme, we do not aim to recompute the latter or rederive the proof of analytic pole cancellation. We refrain from performing these analytic computations and focus on constructing the subtraction terms.

To determine the action of all combinations of NNLO IR operators, we first need to

know the action of the four basis operators, $\mathcal{S}_i$, $\boldsymbol{\mathcal{S}}$, $\mathcal{C}_{ji}$, and $\boldsymbol{\mathcal{C}}_i$. The projectors for the single-soft and the double-soft limits have been known for more than two decades. The NNLO Eikonal approximation of the former limit is given by

$$\begin{aligned}\mathcal{S}_5 F_{\mathrm{LM}}(1_{f_a}, 2_{f_b} \,|\, 4_g, 5_g) = g_{s,\epsilon}^2 \big[(2\,C_{\mathrm{F}} - C_{\mathrm{A}}) S_{12}(p_5) + C_{\mathrm{A}} \big(S_{14}(p_5) + S_{24}(p_5)\big)\big] \\ \times F_{\mathrm{LM}}(1_{f_a}, 2_{f_b} \,|\, 4_g),\end{aligned} \tag{5.26}$$

with the soft function

$$S_{ij}(p_k) = \frac{(p_i \cdot p_j)}{(p_i \cdot p_k)(p_j \cdot p_k)}. \tag{5.27}$$

Similar to the quadratic Casimir operator of the $\mathbf{SU}(\mathbf{3})$ color symmetry group with $N_c = 3$ colors in the fundamental representation, $C_{\mathrm{F}} = (N_c^2 - 1)/(2N_c)$, $C_{\mathrm{A}} = N_c$ is the quadratic Casimir operator of the same group in the adjoint representation.
The Eikonal factorization for the double-soft limit was calculated in Ref. [266] and reads in our notation

$$\boldsymbol{\mathcal{S}} F_{\mathrm{LM}}(1_{f_a}, 2_{f_b} \,|\, 4_g, 5_g) = g_{s,\epsilon}^4 \,\mathrm{Eik}_{gg}(p_1, p_2, p_4, p_5; \epsilon) F_{\mathrm{LM}}(1_{f_a}, 2_{f_b}), \tag{5.28}$$

with the Eikonal function for a soft gluon pair

$$\begin{aligned}\mathrm{Eik}_{gg}(p_1, p_2, p_4, p_5; \epsilon) = 4\,C_{\mathrm{F}}^2 S_{12}(p_4) S_{12}(p_5) \\ + C_{\mathrm{A}} C_{\mathrm{F}} \big(2\,S_{12}(p_4, p_5; \epsilon) - S_{11}(p_4, p_5; \epsilon) - S_{22}(p_4, p_5; \epsilon)\big),\end{aligned} \tag{5.29}$$

which depends on the soft function that was given in Eq. (5.27) and the double-soft function

$$\begin{aligned}S_{ij}(p_k, p_l; \epsilon) = S_{ij}^{\mathrm{s.o.}}(p_k, p_l) - \frac{2(p_i \cdot p_j)}{(p_k \cdot p_l)\,[p_i \cdot (p_k + p_l)]\,[p_j \cdot (p_k + p_l)]} \\ + \frac{(p_i \cdot p_k)(p_j \cdot p_l) + (p_i \cdot p_l)(p_j \cdot p_k)}{[p_i \cdot (p_k + p_l)]\,[p_j \cdot (p_k + p_l)]} \left(\frac{1 - \epsilon}{(p_k \cdot p_l)^2} - \frac{1}{2} S_{ij}^{\mathrm{s.o.}}(p_k, p_l)\right),\end{aligned} \tag{5.30}$$

which in turn depends on the strongly-ordered double-soft function

$$\begin{aligned}S_{ij}^{\mathrm{s.o.}}(p_k, p_l) = \frac{(p_i \cdot p_j)}{(p_k \cdot p_l)} \left(\frac{1}{(p_i \cdot p_k)(p_j \cdot p_l)} + \frac{1}{(p_i \cdot p_l)(p_j \cdot p_k)}\right) \\ - \frac{(p_i \cdot p_j)^2}{(p_i \cdot p_k)(p_j \cdot p_k)(p_i \cdot p_l)(p_j \cdot p_l)}.\end{aligned} \tag{5.31}$$

With the knowledge of the action of these two operators, we can construct a subtraction function where multiple projectors act on the F_{LM} function. In particular, the strongly-ordered soft limit can be obtained by the action of the double-soft operator on Eq. (5.26). After applying the operator $\mathcal{S}_5$, the limit as E_5 approaches zero is already carried out, and the operator $\boldsymbol{\mathcal{S}}$ extracts the limit for vanishing E_4. Therefore, $\boldsymbol{\mathcal{S}}\mathcal{S}_5$ acts in the same way as the combination of the two single-soft projectors $\mathcal{S}_4\mathcal{S}_5$, yielding

$$\begin{aligned}\boldsymbol{\mathcal{S}}\mathcal{S}_5 F_{\mathrm{LM}}(1_{f_a}, 2_{f_b} \,|\, 4_g, 5_g) &= \mathcal{S}_4\mathcal{S}_5 F_{\mathrm{LM}}(1_{f_a}, 2_{f_b} \,|\, 4_g, 5_g) \\ &= 2\,C_{\mathrm{F}}\, g_{s,\epsilon}^4 \big[(2\,C_{\mathrm{F}} - C_{\mathrm{A}}) S_{12}(p_5) + C_{\mathrm{A}} \big(S_{14}(p_5) + S_{24}(p_5)\big)\big] \\ &\quad \times S_{12}(p_4)\, F_{\mathrm{LM}}(1_{f_a}, 2_{f_b}).\end{aligned} \tag{5.32}$$

The action of $\mathcal{S}_4$ on $F_{\text{LM}}(1_{f_a}, 2_{f_b} \,|\, 4_g)$ in Eq. (5.26) is the usual limit at NLO introduced in Eq. (4.23), where the scalar products are expressed using the soft function in Eq. (5.27).
These are the operators without any collinear projector. Therefore, we need to understand the behavior of the collinear operators at NNLO in order to obtain the remaining subtraction functions. The simplest case occurs when one incoming parton and one real-emitted particle become collinear to each other. For instance, considering the scenario where the quark with index 1 emits the gluon with index 5, the limit reads

$$\mathcal{C}_{51} F_{\text{LM}}(1_{f_a}, 2_{f_b} \,|\, 4_g, 5_g) = g_{s,\epsilon}^2 \frac{1}{(p_1 \cdot p_5)} P_{qq}^{(0)}(z;\epsilon) \frac{F_{\text{LM}}(z \cdot 1_{f_a}, 2_{f_b} \,|\, 4_g)}{z}, \tag{5.33}$$

where the energy fraction is computed as $z = (E_1 - E_5)/E_1$. This limit retains structure as the related NLO limit in Eq. (4.27) and contains the same splitting function which we introduced in Eq. (4.29). The other initial-state-final-state collinear limits can be obtained by replacing the corresponding particle indices.
For the emission of a collinear gluon pair, spin correlations must be taken into account. Hence, we cannot use the spin-averaged splitting functions, and the factorization theorem becomes

$$\begin{aligned} \mathcal{C}_{45} F_{\text{LM}}(1_{f_a}, 2_{f_b} \,|\, 4_g, 5_g) &\overset{(b)}{=} g_{s,\epsilon}^2 \frac{1}{(p_4 \cdot p_5)} P_{gg,\mu\nu}(z, k_\perp;\epsilon) F_{\text{LM}}^{\mu\nu}\left(1_{f_a}, 2_{f_b} \,\middle|\, \frac{4_g}{z}\right) \\ &= g_{s,\epsilon}^2 \frac{1}{(p_4 \cdot p_5)} \left[\widetilde{P}_{gg}^{(0)}(z;\epsilon) F_{\text{LM}}\left(1_{f_a}, 2_{f_b} \,\middle|\, \frac{4_g}{z}\right) \right. \\ &\quad \left. + \widetilde{P}_{gg}^{\perp}(z;\epsilon) \kappa_{\perp,\mu} \kappa_{\perp,\nu} F_{\text{LM}}^{\mu\nu}\left(1_{f_a}, 2_{f_b} \,\middle|\, \frac{4_g}{z}\right) \right], \end{aligned} \tag{5.34}$$

where the energy fraction of the final-state partons is $z = E_4/(E_4 + E_5)$. The expression in Eq. (5.34) is valid in sector (b) as indicated by the symbol on top of the equal sign in the first line, to obtain the result in sector (d) the partons 4 and 5 should change their roles. However, for the further discussion we stay with the result of sector (b). The function $F_{\text{LM}}^{\mu\nu}$ represents the squared matrix element without the polarization vectors of the external gluon that decays collinearly. Its relation to the ordinary F_{LM} function is

$$F_{\text{LM}}\left(1_{f_a}, 2_{f_b} \,|\, 4_g\right) = \sum_\lambda \varepsilon_\mu^\lambda(p_4) \varepsilon_\nu^{*\lambda}(p_4) F_{\text{LM}}^{\mu\nu}\left(1_{f_a}, 2_{f_b} \,|\, 4_g\right), \tag{5.35}$$

with the polarization vector $\varepsilon_\mu^\lambda(p_4)$ of the gluon with momentum p_4. The sum runs over all polarizations λ in d dimensions. Moreover, the splitting function for a gluon decaying into a pair of gluons,

$$P_{gg}^{\mu\nu}(z, k_\perp;\epsilon) = -\widetilde{P}_{gg}^{(0)}(z;\epsilon)\, g^{\mu\nu} - \widetilde{P}_{gg}^{\perp}(z;\epsilon) \frac{k_\perp^\mu k_\perp^\nu}{k_\perp^2}, \tag{5.36}$$

is split into a term proportional to the d-dimensional metric tensor $g^{\mu\nu}$ and one proportional to the transverse momentum vector $k_\perp^\mu$, with the coefficients

$$\widetilde{P}_{gg}^{(0)}(z;\epsilon) = 2\, C_{\text{A}} \left(\frac{z}{1-z} + \frac{1-z}{z} \right) \quad \text{and} \quad \widetilde{P}_{gg}^{\perp}(z;\epsilon) = 4\, C_{\text{A}} \,(1-\epsilon)\, z\,(1-z). \tag{5.37}$$

The transverse momentum vector is defined through the Sudakov decomposition of momentum p_5 in terms of p_4,

$$p_5^\mu = \alpha\, p_4^\mu + \beta\, \bar{p}_4^{\,\mu} + k_\perp^\mu, \tag{5.38}$$

where $\bar{p}_4 = (E_4, -\vec{p}_4)$ and $k_\perp \cdot \bar{p}_4 = k_\perp \cdot p_4 = 0$. A more detailed explanation can be found in Appendix C[4]. Additionally, we introduce the normalized transverse momentum,

$$\kappa_\perp^\mu = \frac{k_\perp^\mu}{\sqrt{-k_\perp^2}}, \tag{5.39}$$

to write Eq. (5.34) more compactly. One crucial component of the subtraction scheme is a smart parametrization of this transverse momentum vector. Further explanations will be provided in chapter 6, where we describe the parametrization of the phase space. The next operator we consider describes the triple-collinear limit. When both final-state gluons become simultaneously collinear to the initial-state quark, we write

$$\boldsymbol{\mathcal{C}}_1 F_{\mathrm{LM}}(1_{f_a}, 2_{f_b} \,|\, 4_g, 5_g) = g_{s,\epsilon}^4 \left(\frac{2}{s_{145}}\right)^2 \hat{P}_{ggq}(p_4, p_5, -p_1) F_{\mathrm{LM}}(z \cdot 1_{f_a}, 2_{f_b}), \tag{5.40}$$

where the momentum fraction is given by $z = (E_1 - E_4 - E_5)/E_1$, and $s_{145} = s_{45} - s_{14} - s_{15}$ with the sub-energies $s_{ij} = (p_i + p_j)^2$. The triple-collinear splitting function has been computed in Ref. [267][5]. Due to its length, we point to Eq. (C.42) in Appendix C for the complete and detailed expression instead of presenting it here. The negative sign preceding the argument p_1 of the splitting function indicates that the momentum originates from an incoming particle.

We now have the ingredients to compute all other limits where at least two IR operators act on the F_{LM} function. First, we investigate the double-collinear limit, which arises when the process involves two collinear parton pairs as it appears in the double-collinear partitions. For example, in partition $w^{42,51}$, this limit can be calculated by applying $\mathcal{C}_{42}$ to Eq. (5.33). In the general case, we obtain

$$\mathcal{C}_{i1}\mathcal{C}_{j2} F_{\mathrm{LM}}(1_{f_a}, 2_{f_b} \,|\, 4_g, 5_g) = g_{s,\epsilon}^4 \frac{1}{(p_1 \cdot p_i)} P_{qq}^{(0)}(z;\epsilon) \frac{1}{(p_2 \cdot p_j)} P_{qq}^{(0)}(\bar{z};\epsilon) \frac{F_{\mathrm{LM}}(z \cdot 1_{f_a}, \bar{z} \cdot 2_{f_b})}{z\bar{z}}, \tag{5.41}$$

where the two momentum fractions are $z = (E_1 - E_i)/E_1$ and $\bar{z} = (E_2 - E_j)/E_2$ for $i, j \in \{4, 5\}$, but $i \neq j$. The order in which the limits are carried out does not affect the result and always leads to the same expression.

The strongly-ordered collinear limits must be distinguished for two scenarios in the triple-collinear partitions. First, when one final-state gluon becomes collinear to an initial-state parton before the second final-state gluon becomes collinear to them, as occurring in sectors (a) and (c). Second, both final-state gluons become collinear to each other and subsequently collinear to an initial-state parton, describing the situation in sectors (b) and (d). The limit in the former scenario can be understood as two

[4]Eq. (5.38) can be matched to the notation in Eq. (C.1) by setting $n^\mu = \bar{p}_4^{\,\mu}$. The factor α is only dependent on the momentum fraction z, which is here redefined with respect to the definition in Appendix C, and β is $\mathcal{O}(k_\perp^2)$. However, the explicit form of the prefactors is not important for our discussion.

[5]The triple-collinear splitting functions, averaged over the azimuthal angles, have been published for the first time in Ref. [268]. However, their expressions have been derived on the assumption that the factorization theorem holds without proving it.

subsequently performed single-collinear limits, *e.g.* in partition $w^{41,51}$, the strongly-ordered operator $\boldsymbol{\mathcal{C}}_1\mathcal{C}_{i1}$ can be rewritten as $\mathcal{C}_{j1}\mathcal{C}_{i1}$, where $i = 5$ and $j = 4$ in sector (a), or $i = 4$ and $j = 5$ in sector (c). Making use of the generalization of Eq. (5.33) we get

$$\boldsymbol{\mathcal{C}}_1\mathcal{C}_{i1}F_{\mathrm{LM}}(1_{f_a}, 2_{f_b} \,|\, 4_g, 5_g) = g_{s,\epsilon}^4 \frac{1}{z(p_1\cdot p_4)(p_1\cdot p_5)} P_{qq}^{(0)}(z;\epsilon) P_{qq}^{(0)}(\bar{z};\epsilon) \frac{F_{\mathrm{LM}}(z\bar{z}\cdot 1_{f_a}, 2_{f_b})}{z\bar{z}}, \tag{5.42}$$

with $z = (E_1 - E_i)/E_1$ and $\bar{z} = (E_1 - E_4 - E_5)/(E_1 - E_i)$. The subtraction functions for partition $w^{42,52}$ can be obtained by the obvious exchange of the indices 1 and 2.
If, first, both final-state partons become collinear to each other, spin-correlations need to be considered. The action of the triple-collinear operator on Eq. (5.34) can be expressed as an iterated limit $\boldsymbol{\mathcal{C}}_i\mathcal{C}_{45}$ which becomes $\mathcal{C}_{ji}\mathcal{C}_{45}$ with $i = 1$ in partition $w^{41,51}$, or $i = 2$ in partition $w^{42,52}$ as well as $j = 4$ in sector (b) or $j = 5$ in sector (d). The second single-collinear projector acts on the function $F_{\mathrm{LM}}^{\mu\nu}$, and the spin-averaged splitting functions cannot describe this limit. Instead, a polarized splitting function is necessary so that the strongly-ordered limit takes the shape

$$\begin{aligned}
\boldsymbol{\mathcal{C}}_1\mathcal{C}_{45}F_{\mathrm{LM}}(1_{f_a}, 2_{f_b} \,|\, 4_g, 5_g) &= g_{s,\epsilon}^4 \frac{1}{(p_1\cdot p_j)/z} \frac{1}{(p_4\cdot p_5)} P_{gg,\mu\nu}(z, k_\perp;\epsilon) P_{qq}^{\mu\nu}(\bar{z}, \bar{k}_\perp;\epsilon) \\
&\quad \times \frac{F_{\mathrm{LM}}(\bar{z}\cdot 1_{f_a}, 2_{f_b})}{\bar{z}} \\
&= g_{s,\epsilon}^4 \frac{1}{(p_1\cdot p_j)/z} \frac{1}{(p_4\cdot p_5)} \Big[P_{gg}^{(0)}(z;\epsilon) P_{qq}^{(0)}(\bar{z};\epsilon) \\
&\quad + \frac{1}{2(1-\epsilon)} \widetilde{P}_{gg}^{\perp}(z;\epsilon) \widetilde{P}_{qq}^{\perp}(\bar{z};\epsilon) \left(\big[\kappa_\perp\cdot\bar{\kappa}_\perp\big]^2 - \frac{1}{2(1-\epsilon)} \right) \Big] \\
&\quad \times \frac{F_{\mathrm{LM}}(\bar{z}\cdot 1_{f_a}, 2_{f_b})}{\bar{z}},
\end{aligned} \tag{5.43}$$

with $z = E_j/(E_4 + E_5)$ and $\bar{z} = (E_1 - E_4 - E_5)/E_1$. In the first line, we find the polarized initial-state splitting function for a quark decaying into a quark,

$$P_{qq}^{\mu\nu}(z, k_\perp;\epsilon) = \frac{1-\epsilon}{T_{\mathrm{R}}} C_{\mathrm{F}}(1-z) P_{qg}^{\mu\nu}\left(\frac{1}{1-z}, k_\perp;\epsilon\right), \tag{5.44}$$

which we obtain through crossing relations from the polarized final-state splitting function $P_{qg}^{\mu\nu}$ that is given in Eq. (C.5) of Appendix C. The prefactors on the right-hand side of Eq. (5.44) come from exchanging the initial-state gluon in $P_{qg}^{\mu\nu}$ with an initial-state quark in $P_{qq}^{\mu\nu}$. The factor $(1-\epsilon)/T_{\mathrm{R}}$ originates from the different number of spin and polarization states, and the factor C_{F} arises from the different number of color states. One minus sign comes from the spin-statistics theorem when crossing a fermion from a final into an initial state. Moreover, we use a slightly different normalization for initial-state and final-state splitting functions, introducing an additional factor $-(1-z)$.
One argument of the splitting function is the transverse vector $\bar{k}_\perp^\mu$, which, in analogy to the definition of $k_\perp^\mu$ that was given in Eq. (5.38), is obtained by the Sudakov decomposition of the collinear gluon pair's common momentum in terms of the momentum of the incoming parton. For the normalized transverse momenta, we use the κ notation again.
The third line of Eq. (5.43) contains the spin-averaged splitting functions $P_{qq}^{(0)}$ for a

quark decaying into a quark as well as $P_{gg}^{(0)}$ for a gluon decaying into a gluon, that reads

$$P_{gg}^{(0)}(z;\epsilon) = 2\,C_{\mathrm{A}}\left(\frac{z}{1-z} + \frac{1-z}{z} + z\,(1-z)\right). \tag{5.45}$$

Moreover, the product of the transverse coefficient functions $\widetilde{P}_{qq}^{\perp}$ and $\widetilde{P}_{gg}^{\perp}$ appears. While we have seen $\widetilde{P}_{gg}^{\perp}$ previously, this is the first appearance of $\widetilde{P}_{qq}^{\perp}$, which is given by

$$\widetilde{P}_{qq}^{\perp}(z;\epsilon) = 4\,C_{\mathrm{F}}\frac{z}{1-z}(1-\epsilon). \tag{5.46}$$

Furthermore, the strongly-ordered triple-collinear limits in the sectors (b) and (d) of partition $w^{42,52}$ can be obtained by interchanging indices of the initial-state quark and antiquark in Eq. (5.43).
Now, we can consider the limits where soft and collinear projectors act simultaneously on F_{LM}. These subtraction terms can be computed by nested applications of the singular operators. Due to color coherence, the order of applying soft or collinear projections does not matter. However, it is often convenient to extract soft limits first. All possible combinations of these limits arise when we collect them from all partitions and sectors in the quark-antiquark channel. For the sake of clarity, we structure the listing of the subtraction as follows:

First We begin by computing the subtraction terms that involve only single-collinear operators. We combine them first with a single-soft limit, then with the double-soft limit, and lastly with the strongly-ordered soft limit.

Second Next, we move on to the subtraction terms containing a triple-collinear operator. We combine this operator with the soft projectors in the same order as before.

Third Finally, we consider the subtraction terms involving a strongly-ordered triple-collinear limit in combination with the soft limits, following the same structure.

Additionally, we will present the subtraction functions for a specific limit when another limit can be obtained by exchanging indices. In cases where such symmetry relations exist, we briefly mention them without providing explicit expressions if they do not appear to be trivial.
For each of the three single-collinear operators $\mathcal{C}_{5i}$, $\mathcal{C}_{4i}$, and $\mathcal{C}_{45}$, with i being one of the initial-state partons in combination with $\mathcal{S}_5$, the single-soft single-collinear subtractions terms have different shapes. The subsequent application of $\mathcal{S}_5$ and $\mathcal{C}_{5i}$ or $\mathcal{S}_5$ and $\mathcal{C}_{45}$ on a double-real emission amplitude is proportional to a single-real emission amplitude. On the other hand, when $\mathcal{C}_{4i}$ is combined with $\mathcal{S}_5$, the multiplicity of final states in the matrix elements decreases by two, resulting in a subtraction term proportional to the LO process.
More concrete, if both projectors act on parton 5 and the collinear operator leaves parton 4 unchanged, the subtraction function takes the form

$$\mathcal{C}_{51}\mathcal{S}_5 F_{\mathrm{LM}}(1_{f_a}, 2_{f_b} \,|\, 4_g, 5_g) = C_{\mathrm{F}}\, g_{s,\epsilon}^2 \frac{1}{E_5^2 \eta_{15}} F_{\mathrm{LM}}(1_{f_a}, 2_{f_b} \,|\, 4_g). \tag{5.47}$$

If the collinear operator acts on parton 4 but not on parton 5, the limit is a product of a soft function times a splitting function. It reads

$$\mathcal{C}_{41}\mathcal{S}_5 F_{\mathrm{LM}}(1_{f_a}, 2_{f_b} \,|\, 4_g, 5_g) = 2\, C_{\mathrm{F}}\, g_{s,\epsilon}^4 S_{12}(p_5) \frac{1}{(p_1 \cdot p_4)} P_{qq}^{(0)}(z;\epsilon) \frac{F_{\mathrm{LM}}(z \cdot 1_{f_a}, 2_{f_b})}{z}, \quad (5.48)$$

with the energy fraction $z = (E_1 - E_4)/E_1$.
For collinear final-state gluons, where one of them is soft, we get

$$\mathcal{C}_{45}\mathcal{S}_5 F_{\mathrm{LM}}(1_{f_a}, 2_{f_b} \,|\, 4_g, 5_g) = C_{\mathrm{A}}\, g_{s,\epsilon}^2 \frac{1}{E_5^2 \eta_{45}} F_{\mathrm{LM}}(1_{f_a}, 2_{f_b} \,|\, 4_g). \quad (5.49)$$

The double-soft single-collinear subtraction terms, where initial-state parton 1 and final-state parton 4 or 5 become collinear to each other, are

$$\mathcal{C}_{41}\boldsymbol{\mathcal{S}} F_{\mathrm{LM}}(1_{f_a}, 2_{f_b} \,|\, 4_g, 5_g) = 2\, C_{\mathrm{F}}^2\, g_{s,\epsilon}^4 \frac{1}{E_4^2 \eta_{14}} S_{12}(p_5) F_{\mathrm{LM}}(1_{f_a}, 2_{f_b}), \quad (5.50a)$$

$$\mathcal{C}_{51}\boldsymbol{\mathcal{S}} F_{\mathrm{LM}}(1_{f_a}, 2_{f_b} \,|\, 4_g, 5_g) = 2\, C_{\mathrm{F}}^2\, g_{s,\epsilon}^4 \frac{1}{E_5^2 \eta_{15}} S_{12}(p_4) F_{\mathrm{LM}}(1_{f_a}, 2_{f_b}). \quad (5.50b)$$

For the case of two soft and collinear final-state gluons, spin correlations need to be taken into account, which results in

$$\begin{aligned} \mathcal{C}_{45}\boldsymbol{\mathcal{S}} F_{\mathrm{LM}}(1_{f_a}, 2_{f_b} \,|\, 4_g, 5_g) \overset{(b)}{=} g_s^4 \frac{1}{(p_4 \cdot p_5)} \Bigg[& 2\, C_{\mathrm{F}} S_{12}\Big(\frac{p_4}{z}\Big) \widetilde{P}_{gg}^{(0)}(z;\epsilon) \\ & + C_{\mathrm{F}} \left(\frac{(p_1 \cdot \kappa_\perp)}{(p_1 \cdot p_4)/z} - \frac{(p_2 \cdot \kappa_\perp)}{(p_2 \cdot p_4)/z} \right)^2 \widetilde{P}_{gg}^{\perp}(z;\epsilon) \Bigg] \\ & \times F_{\mathrm{LM}}(1_{f_a}, 2_{f_b}) \end{aligned} \quad (5.51)$$

with $z = E_4/(E_4 + E_5)$. The (b) on top of the equal sign indicates again that this expression is valid in sector (b), in sector (d) the soft function would depend on momentum p_5 instead of momentum p_4 and $z = E_5/(E_4 + E_5)$. The κ-vector is the same transverse momentum vector as in the limit $\vec{p}_4 \parallel \vec{p}_5$ with non-soft partons. A detailed explanation and the derivation of Eq. (5.51) is presented in Appendix D.
By applying $\boldsymbol{\mathcal{S}}$ to Eq. (5.47), Eq. (5.48), and Eq. (5.49) the strongly-ordered double-soft single-collinear subtraction terms can be computed,

$$\mathcal{C}_{41}\boldsymbol{\mathcal{S}}\mathcal{S}_5 F_{\mathrm{LM}}(1_{f_a}, 2_{f_b} \,|\, 4_g, 5_g) = C_{\mathrm{F}}^2\, g_{s,\epsilon}^4 \frac{1}{E_4^2 E_5^2 \eta_{14}\eta_{15}\eta_{25}} F_{\mathrm{LM}}(1_{f_a}, 2_{f_b}), \quad (5.52a)$$

$$\mathcal{C}_{51}\boldsymbol{\mathcal{S}}\mathcal{S}_5 F_{\mathrm{LM}}(1_{f_a}, 2_{f_b} \,|\, 4_g, 5_g) = C_{\mathrm{F}}^2\, g_{s,\epsilon}^4 \frac{1}{E_4^2 E_5^2 \eta_{14}\eta_{24}\eta_{15}} F_{\mathrm{LM}}(1_{f_a}, 2_{f_b}), \quad (5.52b)$$

$$\mathcal{C}_{45}\boldsymbol{\mathcal{S}}\mathcal{S}_5 F_{\mathrm{LM}}(1_{f_a}, 2_{f_b} \,|\, 4_g, 5_g) \overset{(b)}{=} C_{\mathrm{A}} C_{\mathrm{F}}\, g_{s,\epsilon}^4 \frac{1}{E_4^2 E_5^2 \eta_{14}\eta_{24}\eta_{45}} F_{\mathrm{LM}}(1_q, 2_q). \quad (5.52c)$$

On the other side, applying the collinear projector $\mathcal{C}_{52}$ to Eq. (5.48), we identify the single-soft double-collinear limit as it occurs in partition $w^{41,52}$ as

$$\mathcal{C}_{41}\mathcal{C}_{52}\mathcal{S}_5 F_{\mathrm{LM}}(1_{f_a}, 2_{f_b} \,|\, 4_g, 5_g) = C_{\mathrm{F}}\, g_{s,\epsilon}^4 \frac{1}{E_5^2 \eta_{25}} \frac{1}{(p_1 \cdot p_4)} P_{qq}^{(0)}(z;\epsilon) \frac{F_{\mathrm{LM}}(z \cdot 1_{f_a}, 2_{f_b})}{z}, \quad (5.53)$$

where $z = (E_1 - E_4)/E_1$.

Acting with $\mathcal{C}_{52}$ on Eq. (5.50a) we find the double-soft double-collinear limit of the partition $w^{41,52}$,

$$\mathcal{C}_{41}\mathcal{C}_{52}\boldsymbol{\mathcal{S}}F_{\mathrm{LM}}(1_{f_a},2_{f_b}\,|\,4_g,5_g) = C_{\mathrm{F}}^2\,g_{s,\epsilon}^4\frac{1}{E_4^2E_5^2\eta_{14}\eta_{25}}F_{\mathrm{LM}}(1_{f_a},2_{f_b}). \tag{5.54}$$

The corresponding strongly-ordered double-soft double-collinear limit can be obtained by the application of $\mathcal{C}_{52}$ on Eq. (5.52a), or $\boldsymbol{\mathcal{S}}$ on Eq. (5.53), or $\mathcal{S}_5$ on Eq. (5.54). All options lead to

$$\mathcal{C}_{41}\mathcal{C}_{52}\boldsymbol{\mathcal{S}}\mathcal{S}_5F_{\mathrm{LM}}(1_{f_a},2_{f_b}\,|\,4_g,5_g) = C_{\mathrm{F}}^2\,g_{s,\epsilon}^4\frac{1}{E_4^2E_5^2\eta_{14}\eta_{25}}F_{\mathrm{LM}}(1_{f_a},2_{f_b}). \tag{5.55}$$

The subtraction terms with a triple-collinear projector are missing now. In combination with a single-soft projector, the limit becomes

$$\begin{aligned}\boldsymbol{\mathcal{C}}_1\mathcal{S}_5F_{\mathrm{LM}}(1_{f_a},2_{f_b}\,|\,4_g,5_g) = g_{s,\epsilon}^4\frac{1}{2E_5^2}\left[(2\,C_{\mathrm{F}}-C_{\mathrm{A}})\frac{1}{\eta_{15}}+C_{\mathrm{A}}\left(\frac{1}{\eta_{45}}+\frac{\eta_{14}}{\eta_{15}\eta_{45}}\right)\right]\\ \times\frac{1}{(p_1\cdot p_4)}P_{qq}^{(0)}(z;\epsilon)\frac{F_{\mathrm{LM}}(z\cdot 1_{f_a},2_{f_b})}{z},\end{aligned} \tag{5.56}$$

with $z=(E_1-E_4)/E_1$, which can be computed on the basis of the single-soft limit in Eq. (5.26).
The simplest way to calculate the double-soft triple-collinear limit is the application of $\boldsymbol{\mathcal{S}}$ on Eq. (5.40). The result is

$$\boldsymbol{\mathcal{C}}_1\boldsymbol{\mathcal{S}}F_{\mathrm{LM}}(1_{f_a},2_{f_b}\,|\,4_g,5_g) = g_{s,\epsilon}^4\left(\frac{2}{\tilde{s}_{145}}\right)^2\hat{P}_{ggq}^{\boldsymbol{\mathcal{S}}}(p_4,p_5,-p_1)F_{\mathrm{LM}}(1_{f_a},2_{f_b}), \tag{5.57}$$

where $\tilde{s}_{145}=s_{14}+s_{15}$ with the same sub-energy definition as previously, $s_{ij}=(p_i+p_j)^2$. The double-soft limit of the triple-collinear splitting function is explicitly stated in Eq. (D.13) in Appendix D.
In the strongly-ordered double-soft triple-collinear limit, the subtraction function becomes more compact

$$\begin{aligned}\boldsymbol{\mathcal{C}}_1\boldsymbol{\mathcal{S}}\mathcal{S}_5F_{\mathrm{LM}}(1_{f_a},2_{f_b}\,|\,4_g,5_g) = C_{\mathrm{F}}\,g_{s,\epsilon}^4\left[(2\,C_{\mathrm{F}}-C_{\mathrm{A}})\frac{1}{\eta_{14}\eta_{15}}+C_{\mathrm{A}}\left(\frac{1}{\eta_{14}\eta_{45}}+\frac{1}{\eta_{15}\eta_{45}}\right)\right]\\ \times\frac{1}{2E_4^2E_5^2}F_{\mathrm{LM}}(1_{f_a},2_{f_b}).\end{aligned} \tag{5.58}$$

Moreover, the single-soft strongly-ordered triple-collinear limits are concise too,

$$\boldsymbol{\mathcal{C}}_1\mathcal{C}_{41}\mathcal{S}_5F_{\mathrm{LM}}(1_{f_a},2_{f_b}\,|\,4_g,5_g) = C_{\mathrm{F}}\,g_{s,\epsilon}^4\frac{1}{E_5^2\eta_{15}}\frac{1}{(p_1\cdot p_4)}P_{qq}^{(0)}(z;\epsilon)\frac{F_{\mathrm{LM}}(z\cdot 1_{f_a},2_{f_b})}{z}, \tag{5.59a}$$

$$\boldsymbol{\mathcal{C}}_1\mathcal{C}_{51}\mathcal{S}_5F_{\mathrm{LM}}(1_{f_a},2_{f_b}\,|\,4_g,5_g) = C_{\mathrm{F}}\,g_{s,\epsilon}^4\frac{1}{E_5^2\eta_{15}}\frac{1}{(p_1\cdot p_4)}P_{qq}^{(0)}(z;\epsilon)\frac{F_{\mathrm{LM}}(z\cdot 1_{f_a},2_{f_b})}{z}, \tag{5.59b}$$

$$\boldsymbol{\mathcal{C}}_1\mathcal{C}_{45}\mathcal{S}_5F_{\mathrm{LM}}(1_{f_a},2_{f_b}\,|\,4_g,5_g) \overset{(b)}{=} C_{\mathrm{A}}\,g_{s,\epsilon}^4\frac{1}{E_5^2\eta_{45}}\frac{1}{(p_1\cdot p_4)}P_{qq}^{(0)}(z;\epsilon)\frac{F_{\mathrm{LM}}(z\cdot 1_{f_a},2_{f_b})}{z}, \tag{5.59c}$$

with $z=(E_1-E_4)/E_1$ in all three expressions. It should be noticed that the first two results are equal, even though, once, the single-collinear operator acts on another

parton than the soft operator, and once, both act on the same parton. In Eq. (5.59c), we consider sector (b), while in sector (d), the scalar product in the denominator has to be replaced with $\{p_1 \cdot p_4\}_{4\|5}$, corresponding to the definition in Eq. (4.32).
In the double-soft strongly-ordered triple-collinear limits, the subtraction functions in the sectors (a) and (c) read

$$\boldsymbol{\mathcal{C}}_1\mathcal{C}_{41}\boldsymbol{\mathcal{S}}F_{\mathrm{LM}}(1_{f_a}, 2_{f_b} \,|\, 4_g, 5_g) = C_{\mathrm{F}}^2\, g_{s,\epsilon}^4 \frac{1}{E_4^2 E_5^2 \eta_{14}\eta_{15}} F_{\mathrm{LM}}(1_{f_a}, 2_{f_b}), \tag{5.60a}$$

$$\boldsymbol{\mathcal{C}}_1\mathcal{C}_{51}\boldsymbol{\mathcal{S}}F_{\mathrm{LM}}(1_{f_a}, 2_{f_b} \,|\, 4_g, 5_g) = C_{\mathrm{F}}^2\, g_{s,\epsilon}^4 \frac{1}{E_4^2 E_5^2 \eta_{14}\eta_{15}} F_{\mathrm{LM}}(1_{f_a}, 2_{f_b}), \tag{5.60b}$$

where again both expressions coincide with each other. When first the final-state gluons become collinear as in sector (b), spin correlations are present,

$$\begin{aligned}\boldsymbol{\mathcal{C}}_1\mathcal{C}_{45}\boldsymbol{\mathcal{S}}F_{\mathrm{LM}}(1_{f_a}, 2_{f_b} \,|\, 4_g, 5_g) \overset{(b)}{=} g_{s,\epsilon}^4 &\frac{1}{(E_4+E_5)^2\eta_{14}} \frac{1}{(p_4\cdot p_5)} \\ &\times \left[P_{gg}^{(0)}(z;\epsilon) + \widetilde{P}_{gg}^{\perp}(z;\epsilon)\left(\left[\kappa_\perp \cdot \bar{\kappa}_\perp\right]^2 - \frac{1}{2(1-\epsilon)}\right)\right] \\ &\times F_{\mathrm{LM}}(1_{f_a}, 2_{f_b}).\end{aligned} \tag{5.60c}$$

The transverse vectors remain unchanged with respect to the strongly-ordered triple-collinear limit and also $z = E_4/(E_4 + E_5)$ stays the same. By renaming index 4 in 5 and vice versa, the subtraction function for sector (d) can be recovered.
Finally, the strongly-ordered double-soft strongly-ordered triple-collinear limits involving each of the four basis operator types read

$$\boldsymbol{\mathcal{C}}_1\mathcal{C}_{41}\boldsymbol{\mathcal{S}}\mathcal{S}_5F_{\mathrm{LM}}(1_{f_a}, 2_{f_b} \,|\, 4_g, 5_g) = C_{\mathrm{F}}^2\, g_{s,\epsilon}^4 \frac{1}{E_4^2 E_5^2 \eta_{14}\eta_{15}} F_{\mathrm{LM}}(1_{f_a}, 2_{f_b}), \tag{5.61a}$$

$$\boldsymbol{\mathcal{C}}_1\mathcal{C}_{51}\boldsymbol{\mathcal{S}}\mathcal{S}_5F_{\mathrm{LM}}(1_{f_a}, 2_{f_b} \,|\, 4_g, 5_g) = C_{\mathrm{F}}^2\, g_{s,\epsilon}^4 \frac{1}{E_4^2 E_5^2 \eta_{14}\eta_{15}} F_{\mathrm{LM}}(1_{f_a}, 2_{f_b}), \tag{5.61b}$$

and

$$\boldsymbol{\mathcal{C}}_1\mathcal{C}_{45}\boldsymbol{\mathcal{S}}\mathcal{S}_5F_{\mathrm{LM}}(1_{f_a}, 2_{f_b} \,|\, 4_g, 5_g) \overset{(b)}{=} C_{\mathrm{A}}C_{\mathrm{F}}\, g_{s,\epsilon}^4 \frac{1}{E_4^2 E_5^2 \eta_{14}\eta_{45}} F_{\mathrm{LM}}(1_{f_a}, 2_{f_b}). \tag{5.61c}$$

The last equation holds in sector (b), but the result for sector (d) can be obtained by renaming the indices accordingly.
With all the terms collected, the next step would be to compute the counterterms by integrating over the unresolved phase space. However, instead of replicating this task here, we refer to the works of Refs. [38, 269, 270] where these computations have been carried out. They cleverly recombine the sectors and partitions to obtain concise expressions for the counterterms. In particular, the analytic integration of the counterterm with a single soft limit and a strongly-ordered soft limit, *i.e.* the term $\langle(1-\boldsymbol{\mathcal{S}})\,\mathcal{S}_5F_{\mathrm{LM}}\rangle$ in Eq. (5.7), is straightforward and has been performed in Ref. [38]. In the same reference, all counterterms containing single-collinear projectors, but no triple-collinear projectors, have been provided. The more complicated integral for the counterterm in the double-soft limit, corresponding to $\langle\boldsymbol{\mathcal{S}}F_{\mathrm{LM}}\rangle$, over the unresolved phase space of the soft partons was presented in Ref. [269]. The most challenging counterterms are those involving triple-collinear operators, their analytic solutions have been obtained in Ref. [270].

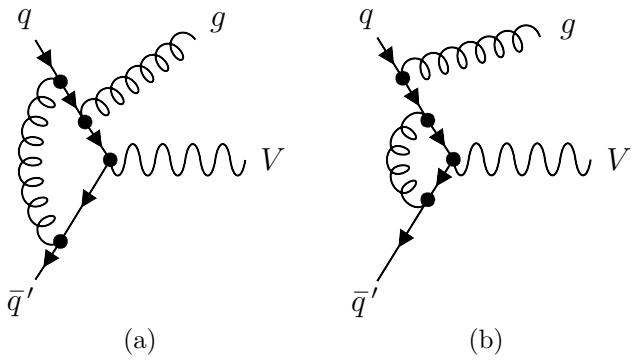

Figure 5.5.: Representative Feynman diagrams for real-virtual corrections to color-singlet production in the quark-antiquark channel.

However, even though we have examined the core aspects of the NNLO Nested Soft-Collinear Subtraction scheme, namely the manifestation of the double-real radiation singularities, we still need to address the real-virtual and the double-virtual contributions to extract their IR poles and combine all pieces into a finite remainder without divergences.

5.2.2. Real-Virtual Corrections

Mixed real-virtual contributions, illustrated in Figure 5.5, contain phase-space singularities from one real-emitted parton. Since the parton in our specific computation is a gluon, these singularities can be either of soft, collinear, or soft-collinear origin[6]. To regulate them, we need the same operators we introduced in chapter 4 and follow the same procedure we applied to single-real-emission amplitudes at NLO.

We define the real-virtual cross section in our notation as

$$\begin{aligned} 2\hat{s}\cdot \mathrm{d}\hat{\sigma}^{\mathrm{RV}}_{f_a f_b} &= \int [\mathrm{d}p_4] F_{\mathrm{LRV}}(1_{f_a}, 2_{f_b} \,|\, 4_g) \\ &= \big\langle F_{\mathrm{LRV}}(1_{f_a}, 2_{f_b} \,|\, 4_g) \big\rangle, \end{aligned} \tag{5.62}$$

with the function

$$\begin{aligned} F_{\mathrm{LRV}}(1_{f_a}, 2_{f_b} \,|\, 4_g) = \mathcal{N}\, \mathrm{d}\Pi^{(d)}_{\mathrm{B}}\, 2\, \mathfrak{Re}\Big\{ \mathcal{M}^{(1)}_{f_a f_b \to V+g}(p_1,p_2,p_3,p_4) \mathcal{M}^{*(0)}_{f_a f_b \to V+g}(p_1,p_2,p_3,p_4) \Big\} \\ \times F_J(p_1,p_2,p_3,p_4), \end{aligned} \tag{5.63}$$

which represents the interference between the one-loop real-virtual amplitudes and the single-real-emission tree-level diagrams. The Born phase-space element includes the momentum conserving δ-distribution,

$$\mathrm{d}\Pi^{(d)}_{\mathrm{B}} = \frac{\mathrm{d}^{d-1}p_3}{(2\pi)^{d-1} 2E_3} (2\pi)^d\, \delta^{(d)}(p_1 + p_2 - p_3 - p_4), \tag{5.64}$$

and describes the same phase-space configurations as Eq. (4.9).

[6] If the parton is a quark, soft singularities are forbidden by quark-number conservation and, hence, only collinear singularities are present.

In analogy to Eq. (4.25), the soft and collinear singularities can be extracted in a nested manner,

$$\begin{aligned} 2\hat{s}\cdot \mathrm{d}\hat{\sigma}^{\mathrm{RV}}_{f_a f_b} = &\left\langle \hat{\mathcal{O}}_{\mathrm{NLO}} F_{\mathrm{LRV}}(1_{f_a}, 2_{f_b} \,|\, 4_g) \right\rangle + \left\langle (\mathcal{C}_{41} + \mathcal{C}_{42})\, F_{\mathrm{LRV}}(1_{f_a}, 2_{f_b} \,|\, 4_g) \right\rangle \\ &+ \left\langle (1 - \mathcal{C}_{41} - \mathcal{C}_{42})\, \mathcal{S}_4 F_{\mathrm{LRV}}(1_{f_a}, 2_{f_b} \,|\, 4_g) \right\rangle, \end{aligned} \tag{5.65}$$

where the NLO subtraction operator $\hat{\mathcal{O}}_{\mathrm{NLO}}$ is defined in Eq. (4.26).
However, the action of the IR operators on the one-loop amplitudes differs from their action on the tree-level amplitudes. The soft-gluon current for general one-loop amplitudes has been studied in Refs. [271, 272] and reads for our process

$$\begin{aligned} \mathcal{S}_4 F_{\mathrm{LRV}}(1_{f_a}, 2_{f_b} \,|\, 4_g) = 2\, C_{\mathrm{F}}\, g_{s,\epsilon}^2 S_{12}(p_4) \Bigg\{ &F_{\mathrm{LV}}(1_{f_a}, 2_{f_b}) + [\alpha_{s,\epsilon}] \Bigg[c_\Gamma \left(\frac{S_{12}(p_4)}{2} \right)^{\epsilon} \\ &\times \mathrm{Eik}_g^{\mathrm{Loop}}(\epsilon) - \frac{\Gamma(1-\epsilon)}{\mu_{\mathrm{F}}^{2\epsilon} e^{\epsilon\gamma_{\mathrm{E}}}} \frac{\beta_0}{\epsilon} \Bigg] F_{\mathrm{LM}}(1_{f_a}, 2_{f_b}) \Bigg\}. \end{aligned} \tag{5.66}$$

The abbreviation $\mathrm{Eik}_g^{\mathrm{Loop}}$ in Eq. (5.66) corresponds to

$$\mathrm{Eik}_g^{\mathrm{Loop}}(\epsilon) = -C_{\mathrm{A}} \frac{1}{\epsilon^2} \frac{\Gamma^2(1-\epsilon)\Gamma^2(1+\epsilon)}{\Gamma(1-2\epsilon)\Gamma(1+2\epsilon)} \tag{5.67}$$

and c_Γ is a combination of Euler gamma functions,

$$c_\Gamma = \frac{\Gamma^3(1-\epsilon)\Gamma(1+\epsilon)}{\Gamma(1-2\epsilon)}. \tag{5.68}$$

The collinear limit of one-loop amplitudes has been known for more than two decades. Its general structure is very similar to the structure of the soft limit in Eq. (5.66). When the outgoing gluon becomes collinear to an incoming quark, the expression reads [217, 273–277]

$$\begin{aligned} \mathcal{C}_{41} F_{\mathrm{LRV}}(1_{f_a}, 2_{f_b} \,|\, 4_g) = g_{s,\epsilon}^2 \frac{1}{(p_1 \cdot p_4)} \Bigg\{ &P_{qq}^{(0)}(z;\epsilon) \frac{F_{\mathrm{LV}}(z \cdot 1_{f_a}, 2_{f_b})}{z} + [\alpha_{s,\epsilon}] \Bigg[c_\Gamma \left(\frac{1}{2(p_1 \cdot p_4)} \right)^{\epsilon} \\ &\times P_{qq}^{\mathrm{Loop}}(z;\epsilon) - \frac{\Gamma(1-\epsilon)}{\mu_{\mathrm{F}}^{2\epsilon} e^{\epsilon\gamma_{\mathrm{E}}}} \frac{\beta_0}{\epsilon} P_{qq}^{(0)}(z;\epsilon) \Bigg] \frac{F_{\mathrm{LM}}(z \cdot 1_{f_a}, 2_{f_b})}{z} \Bigg\}, \end{aligned} \tag{5.69}$$

where $z = (E_1 - E_4)/E_1$. The one-loop splitting function, P_{qq}^{Loop}, is given explicitly in Eq. (C.45) of Appendix C.
The last missing piece is the soft-collinear subtraction function, which can be derived from the soft subtraction function by isolating its leading singular behavior in the collinear limit. For the operator combination $\mathcal{C}_{41}\mathcal{S}_4$, it takes the form

$$\begin{aligned} \mathcal{C}_{41}\mathcal{S}_4 F_{\mathrm{LRV}}(1_{f_a}, 2_{f_b} \,|\, 4_g) = C_{\mathrm{F}}\, g_{s,\epsilon}^2 \frac{1}{E_4^2 \eta_{14}} \Bigg\{ &F_{\mathrm{LV}}(1_{f_a}, 2_{f_b}) + [\alpha_{s,\epsilon}] \Bigg[c_\Gamma \left(\frac{1}{4E_4^2 \eta_{14}} \right)^{\epsilon} \\ &\times \mathrm{Eik}_g^{\mathrm{Loop}}(\epsilon) - \frac{\Gamma(1-\epsilon)}{\mu_{\mathrm{F}}^{2\epsilon} e^{\epsilon\gamma_{\mathrm{E}}}} \frac{\beta_0}{\epsilon} \Bigg] F_{\mathrm{LM}}(1_{f_a}, 2_{f_b}) \Bigg\}. \end{aligned} \tag{5.70}$$

The explicit ϵ poles in these subtraction functions arise from the manifest IR singularities in the loop computation. Although we have regulated the IR divergencies coming from the phase-space integration, we cannot carry out the limit $d \to 4$ directly, and

the numerical evaluation of the $\hat{\mathcal{O}}_{\text{NLO}}$ term is not feasible. Instead, we need to compute a finite remainder of the one-loop amplitude, similarly to the procedure we applied in section 4.4. Analogously to Eq. (4.66), we define

$$F_{\text{LRV}}(1_{f_a}, 2_{f_b} \,|\, 4_g) = [\alpha_{s,\epsilon}]\, I_{qqg}(\epsilon) F_{\text{LM}}(1_{f_a}, 2_{f_b} \,|\, 4_g) + F^{\text{fin}}_{\text{LRV}}(1_{f_a}, 2_{f_b} \,|\, 4_g), \tag{5.71}$$

where we introduce the color-charge insertion operator [278]

$$\begin{aligned} I_{qqg}(\epsilon) = \cos(\epsilon\,\pi) \left(\frac{1}{\hat{s}}\right)^{\epsilon} \left(\frac{C_{\text{A}} - 2\,C_{\text{F}}}{\epsilon^2} + \frac{\chi_q - 2\,\gamma_q}{\epsilon}\right) \\ - \left[\left(-\frac{1}{\hat{t}}\right)^{\epsilon} + \left(-\frac{1}{\hat{u}}\right)^{\epsilon}\right] \left(\frac{C_{\text{A}}}{\epsilon^2} + \frac{\chi_q + \gamma_g}{2\epsilon}\right) \end{aligned} \tag{5.72}$$

with the usual conventions for the Mandelstam variables, $\hat{s} = (p_1 + p_2)^2$, $\hat{t} = (p_2 - p_4)^2$, and $\hat{u} = (p_1 - p_4)^2$. The anomalous dimensions of the quark and the gluon are denoted as $\gamma_q = 3\,C_{\text{F}}/2$ and $\gamma_g = \beta_0$, respectively, while $\chi_q = 3\,C_{\text{A}}/2$. In particular, it holds $\beta_0 = 11 C_{\text{A}}/6 - 2\,T_{\text{R}} n_f/3$, where β_0 is the first coefficients of the QCD beta function which is described in Appendix B.

Substituting Eq. (5.71) into Eq. (5.65), the NLO subtraction operator acts on the finite remainder of the real-virtual corrections, which is the only component containing the full information about the kinematics of the real-emitted gluon that is left after analytic pole cancellation. Due to the absence of explicit poles in the finite remainder, the phase space can be integrated numerically, as the operator $\hat{\mathcal{O}}_{\text{NLO}}$ regulates all phase-space singularities. However, this requires knowledge about the action of the IR projectors on $F^{\text{fin}}_{\text{LRV}}$.

For the soft limit, we find

$$\begin{aligned} \mathcal{S}_4 F^{\text{fin}}_{\text{LRV}}(1_{f_a}, 2_{f_b} \,|\, 4_g) = 2\,C_{\text{F}}\, g_s^2 S_{12}(p_4) \Big\{ F^{\text{fin}}_{\text{LV}}(1_{f_a}, 2_{f_b}) + \frac{\alpha_s(\mu_{\text{R}})}{2\pi} \\ \times \text{Eik}^{\text{Loop}}_{g,\text{F}}(p_1, p_2, p_4; \mu_{\text{F}}) F_{\text{LM}}(1_{f_a}, 2_{f_b}) \Big\}, \end{aligned} \tag{5.73}$$

with the finite one-loop Eikonal function

$$\begin{aligned} \text{Eik}^{\text{Loop}}_{g,\text{F}}(p_1, p_2, p_4; \mu_{\text{F}}) = C_{\text{A}} \left(\frac{5\pi^2}{6} + \frac{3}{4}\left[\ln\left(-\frac{\hat{s}}{\hat{t}}\right) + \ln\left(-\frac{\hat{s}}{\hat{u}}\right)\right] - \ln\left(-\frac{\hat{s}}{\hat{t}}\right) \ln\left(-\frac{\hat{s}}{\hat{u}}\right)\right) \\ + \frac{1}{2}\beta_0 \left[\ln\left(-\frac{\mu_{\text{F}}^2}{\hat{t}}\right) + \ln\left(-\frac{\mu_{\text{F}}^2}{\hat{u}}\right)\right]. \end{aligned} \tag{5.74}$$

The collinear limit reads

$$\begin{aligned} \mathcal{C}_{41} F^{\text{fin}}_{\text{LRV}}(1_{f_a}, 2_{f_b} \,|\, 4_g) = g_s^2 \frac{1}{(p_1 \cdot p_4)} \left(P^{(0)}_{qq}(z;0) \frac{F^{\text{fin}}_{\text{LV}}(z \cdot 1_{f_a}, 2_{f_b})}{z} + \frac{\alpha_s(\mu_{\text{R}})}{2\pi} \right. \\ \left. \times P^{\text{Loop}}_{qq,\text{F}}(p_1, p_2, p_4) \frac{F_{\text{LM}}(z \cdot 1_{f_a}, 2_{f_b})}{z} \right), \end{aligned} \tag{5.75}$$

with an unchanged energy fraction $z = (E_1 - E_4)/E_1$. The one-loop splitting function is explicitly given in Eq. (C.47).

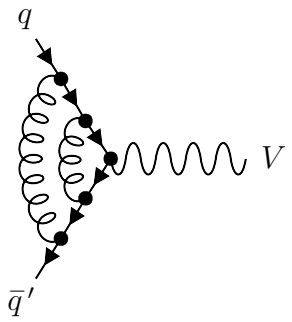

Figure 5.6.: Representative Feynman diagram for two-loop double-virtual corrections in color-singlet production.

Lastly, the overlapping soft-collinear limit becomes

$$\begin{aligned}\mathcal{C}_{41}\mathcal{S}_4 F^{\text{fin}}_{\text{LRV}}(1_{f_a},2_{f_b}\,|\,4_g) = C_{\text{F}}\,g_s^2\frac{1}{E_4^2\eta_{14}}\Big\{F^{\text{fin}}_{\text{LV}}(1_{f_a},2_{f_b}) + \frac{\alpha_s(\mu_{\text{R}})}{2\pi} \\ \times \text{Eik}^{\text{Loop},\mathcal{C}_{41}}_{g,\text{F}}(p_1,p_2,p_4;\mu_{\text{F}})F_{\text{LM}}(1_{f_a},2_{f_b})\Big\},\end{aligned} \tag{5.76}$$

with the modified Eikonal factor

$$\begin{aligned}\text{Eik}^{\text{Loop},\mathcal{C}_{41}}_{g,\text{F}}(p_1,p_2,p_4;\mu_{\text{F}}) = C_{\text{A}}\left[\frac{5\pi^2}{6} + \frac{3}{4}\ln\left(\frac{E_1E_2}{E_4^2\eta_{14}}\right) - \ln\left(\frac{E_1}{E_4}\right)\ln\left(\frac{E_2}{E_4\eta_{14}}\right)\right] \\ + \frac{1}{2}\beta_0\left[\ln\left(\frac{\mu_{\text{F}}^2}{4E_1E_4\eta_{14}}\right) + \ln\left(\frac{\mu_{\text{F}}^2}{4E_2E_4}\right)\right].\end{aligned} \tag{5.77}$$

As before, we do not aim to repeat the computation of the counterterms here, which can be done straightforwardly in a similar manner as presented in chapter 4 for the NLO case with single-real emission. The solutions have been presented in Ref. [38]. With the inclusion of these counterterms, we have accounted for all the essential components of the real-virtual contributions in the quark-antiquark channel. We can now proceed to examine the double-virtual corrections.

5.2.3. Double-Virtual Corrections

An exemplary Feynman diagram illustrating the two-loop contribution is depicted in Figure 5.6. The interferences between this type of diagrams and the amplitudes of the LO process lead, together with squared one-loop amplitudes, to the double-virtual corrections. The kinematics of the external particles remains the same as that of the Born process, ensuring that no singularities will spoil the phase-space integration. All IR singularities are encountered in the loop integrals. To identify them, we decompose the double-virtual contribution,

$$2\hat{s}\cdot\mathrm{d}\hat{\sigma}^{\text{VV}}_{f_af_b} = \big\langle F_{\text{LVV}}(1_{f_a},2_{f_b})\big\rangle + \big\langle F_{\text{LV}^2}(1_{f_a},2_{f_b})\big\rangle, \tag{5.78}$$

in a term that contains the UV-renormalized two-loop corrections,

$$F_{\text{LVV}}(1_{f_a},2_{f_b}) = \mathcal{N}\,\mathrm{d}\Pi^{(d)}_{\text{B}}\,2\,\mathfrak{Re}\Big\{\mathcal{M}^{(2)}_{f_af_b\to V}(p_1,p_2,p_3)\mathcal{M}^{*(0)}_{f_af_b\to V}(p_1,p_2,p_3)\Big\}\,F_J(p_1,p_2,p_3), \tag{5.79}$$

and another term with the squared one-loop diagrams,

$$F_{\mathrm{LV}^2}(1_{f_a}, 2_{f_b}) = \mathcal{N}\, \mathrm{d}\Pi_{\mathrm{B}}^{(d)} \left| \mathcal{M}^{(1)}_{f_a f_b \to V}(p_1, p_2, p_3) \right|^2 F_J(p_1, p_2, p_3). \tag{5.80}$$

The phase-space element corresponds to the one of the Born process in Eq. (4.3),

$$\mathrm{d}\Pi_{\mathrm{B}}^{(d)} = \frac{\mathrm{d}^{d-1}p_3}{(2\pi)^{d-1}2E_3}\,(2\pi)^d\,\delta^{(d)}(p_1 + p_2 - p_3), \tag{5.81}$$

where the momentum-conserving δ-distribution only contains the momenta of the incoming particles and the color singlet.
In Eq. (4.64), it was demonstrated how IR poles are extracted from the one-loop amplitude, allowing to separate the divergent part from the finite component in F_{LV^2}. This leads to the definition of the finite remainder,

$$F^{\mathrm{fin}}_{\mathrm{LV}^2}(1_{f_a}, 2_{f_b}) = \mathcal{N}\, \mathrm{d}\Pi_{\mathrm{B}}^{(d)} \left| \mathcal{M}^{(1),\mathrm{fin}}_{f_a f_b \to V}(p_1, p_2, p_3) \right|^2 F_J(p_1, p_2, p_3). \tag{5.82}$$

The IR structure of the two-loop amplitude is more intricate. It can be factorized according to [278]

$$\begin{aligned}\mathcal{M}^{(2)}(p_1, p_2, p_3) = {}& [\alpha_{s,\epsilon}]^2\, \mathcal{I}_2(\epsilon)\mathcal{M}^{(0)}(p_1, p_2, p_3) + [\alpha_{s,\epsilon}]\, \mathcal{I}_1(\epsilon)\mathcal{M}^{(1)}(p_1, p_2, p_3) \\ & + \mathcal{M}^{(2),\mathrm{fin}}(p_1, p_2, p_3),\end{aligned} \tag{5.83}$$

where all poles are contained in the two color-charge operators, so that $\mathcal{M}^{(2),\mathrm{fin}}$ is a finite UV and IR renormalized amplitude free of singularities in the regulator ϵ so that it can be computed in $d = 4$ dimensions. The first of the two insertion operators is known from the one-loop case and is given in Eq. (4.65). It extracts poles proportional to the one-loop amplitude.
The second operator, which acts on the tree-level amplitude, has the shape [278]

$$\begin{aligned}\mathcal{I}_2(\epsilon) = {}& -\frac{1}{2}\mathcal{I}_1(\epsilon)\left(\mathcal{I}_1(\epsilon) + 2\frac{\Gamma(1-\epsilon)}{\mu_{\mathrm{F}}^{2\epsilon} e^{\epsilon\gamma_{\mathrm{E}}}}\frac{\beta_0}{\epsilon}\right) + \frac{\Gamma(1-\epsilon)}{e^{\epsilon\gamma_{\mathrm{E}}}}\left(\frac{\beta_0}{\epsilon} + K\right)\mathcal{I}_1(2\epsilon) \\ & + \frac{1}{2\epsilon}\frac{\Gamma(1-\epsilon)}{e^{\epsilon\gamma_{\mathrm{E}}}}\mathcal{H}_2(\epsilon)\end{aligned} \tag{5.84}$$

and depends on another operator which reads

$$\begin{aligned}\mathcal{H}_2(\epsilon) = {}& e^{-2i\pi\epsilon}\left(\frac{1}{\hat{s}}\right)^{2\epsilon}\left[C_{\mathrm{F}}^2\left(-\frac{3}{8} + \frac{\pi^2}{2} - 6\zeta_3\right) + C_{\mathrm{A}}C_{\mathrm{F}}\left(\frac{245}{216} - \frac{23}{48}\pi^2 + \frac{13}{2}\zeta_3\right)\right. \\ & \left. + C_{\mathrm{F}}T_{\mathrm{R}}n_f\left(-\frac{25}{54} + \frac{\pi^2}{12}\right)\right].\end{aligned} \tag{5.85}$$

The explicit expression of $\mathcal{H}_2$ for our process is taken from Ref. [278], but it can also be obtained from its general, process-independent definition in Refs. [279, 280]. Lastly, the coefficient K in Eq. (5.84) is given by

$$K = \left(\frac{67}{18} - \frac{\pi^2}{6}\right)C_{\mathrm{A}} - \frac{10}{9}T_{\mathrm{R}}n_f. \tag{5.86}$$

With these expressions at hand, it is straightforward to determine a finite remainder for the two-loop contribution, which becomes

$$F^{\text{fin}}_{\text{LVV}}(1_{f_a},2_{f_b}) = \mathcal{N}\,\mathrm{d}\Pi^{(d)}_{\text{B}}\,2\,\mathfrak{Re}\Big\{\mathcal{M}^{(2),\text{fin}}_{f_af_b\to V}(p_1,p_2,p_3)\mathcal{M}^{*(0)}_{f_af_b\to V}(p_1,p_2,p_3)\Big\}\,F_J(p_1,p_2,p_3). \tag{5.87}$$

Finally, we have collected all the necessary ingredients for rewriting the double-virtual cross section, yielding the result

$$\begin{aligned}
2\hat{s}\cdot\mathrm{d}\hat{\sigma}^{\text{VV}}_{f_af_b} = &\left(\frac{\alpha_s(\mu_{\text{R}})}{2\pi}\right)^2\left(\frac{\mu_{\text{F}}^2}{\hat{s}}\right)^{2\epsilon}\Bigg\{\left(\frac{e^{\epsilon\gamma_{\text{E}}}}{\Gamma(1-\epsilon)}\right)^2\cos^2(\epsilon\pi)\,C_{\text{F}}^2\left(\frac{2}{\epsilon^4}+\frac{6}{\epsilon^3}+\frac{9}{2\epsilon^2}\right)\\
&+\frac{e^{\epsilon\gamma_{\text{E}}}}{\Gamma(1-\epsilon)}\cos(2\epsilon\pi)\Bigg[C_{\text{F}}^2\left(-\frac{3}{8\epsilon}+\frac{\pi^2}{2\epsilon}-\frac{6\zeta_3}{\epsilon}\right)+C_{\text{A}}C_{\text{F}}\left(-\frac{11}{12\epsilon^3}\right.\\
&\left.-\frac{83}{18\epsilon^2}+\frac{\pi^2}{12\epsilon^2}-\frac{961}{216\epsilon}-\frac{11\pi^2}{48\epsilon}+\frac{13\zeta_3}{2\epsilon}\right)+C_{\text{F}}T_{\text{R}}n_f\left(\frac{1}{3\epsilon^3}+\frac{14}{9\epsilon^2}\right.\\
&\left.+\frac{65}{54\epsilon}+\frac{\pi^2}{12\epsilon}\right)\Bigg]\Bigg\}\left\langle F_{\text{LM}}(1_{f_a},2_{f_b})\right\rangle+2\left(\frac{\alpha_s(\mu_{\text{R}})}{2\pi}\right)^2\left(\frac{\mu_{\text{F}}^2}{\hat{s}}\right)^{\epsilon}\frac{e^{\epsilon\gamma_{\text{E}}}}{\Gamma(1-\epsilon)}\\
&\times\cos(\epsilon\pi)\frac{\beta_0}{\epsilon}\left(\frac{C_{\text{F}}}{\epsilon^2}+\frac{3C_{\text{F}}}{2\epsilon}\right)\left\langle F_{\text{LM}}(1_{f_a},2_{f_b})\right\rangle-4\left(\frac{\alpha_s(\mu_{\text{R}})}{2\pi}\right)\left(\frac{\mu_{\text{F}}^2}{\hat{s}}\right)^{\epsilon}\\
&\times\frac{e^{\epsilon\gamma_{\text{E}}}}{\Gamma(1-\epsilon)}\cos(\epsilon\pi)\left(\frac{C_{\text{F}}}{\epsilon^2}+\frac{3C_{\text{F}}}{2\epsilon}\right)\left\langle F^{\text{fin}}_{\text{LV}}(1_{f_a},2_{f_b})\right\rangle+\left\langle F^{\text{fin}}_{\text{LV}^2}(1_{f_a},2_{f_b})\right\rangle\\
&+\left\langle F^{\text{fin}}_{\text{LVV}}(1_{f_a},2_{f_b})\right\rangle.
\end{aligned} \tag{5.88}$$

5.2.4. Fully-Differential Next-to-Next-to-Leading Order Cross Section

5.2.4.1. Quark-Quark Initiated Process

Apart from the double-real, real-virtual, and double-virtual corrections, an additional term arising from the collinear renormalization of the PDFs contributes to the cross section. When the renormalization scale equals the factorization scale, this term is necessary to prove analytic pole cancellation but does not contribute to the finite part. However, if the scales are different, an extra term proportional to the logarithm of their ratio appears as a leftover. The renormalization contribution can be computed using the equation

$$\begin{aligned}
2\hat{s}\cdot\mathrm{d}\hat{\sigma}^{\text{C}_{\text{NNLO}}}_{f_af_b} = &\frac{\alpha_s(\mu_{\text{R}})}{2\pi}2\hat{s}\cdot\left[\Gamma_1\otimes\mathrm{d}\hat{\sigma}^{\text{NLO}}_{f_af_b}+\mathrm{d}\hat{\sigma}^{\text{NLO}}_{f_af_b}\otimes\Gamma_1\right]-\left(\frac{\alpha_s(\mu_{\text{R}})}{2\pi}\right)^2\\
&\times 2\hat{s}\cdot\left[\Gamma_1\otimes\mathrm{d}\hat{\sigma}^{\text{LO}}_{f_af_b}\otimes\Gamma_1+\Gamma_2\otimes\mathrm{d}\hat{\sigma}^{\text{LO}}_{f_af_b}+\mathrm{d}\hat{\sigma}^{\text{LO}}_{f_af_b}\otimes\Gamma_2\right],
\end{aligned} \tag{5.89}$$

where the renormalization constants read

$$\Gamma_1(z)=\frac{\hat{P}^{(0)}_{qq}(z)}{\epsilon},\quad \Gamma_2(z)=\frac{\left(\hat{P}^{(0)}_{qq}\otimes\hat{P}^{(0)}_{qq}\right)(z)+\beta_0\hat{P}^{(0)}_{qq}(z)}{2\epsilon^2}-\frac{\hat{P}^{(1)}_{qq}(z)}{2\epsilon}. \tag{5.90}$$

The NLO Altarelli-Parisi splitting function $\hat{P}^{(1)}_{qq}$ can be found in Appendix C. After performing the convolution in Eq. (5.89) according to Eq. (4.13), the results for

$\mathrm{d}\hat{\sigma}^{\mathrm{RR}}_{f_af_b}$, $\mathrm{d}\hat{\sigma}^{\mathrm{RV}}_{f_af_b}$, $\mathrm{d}\hat{\sigma}^{\mathrm{VV}}_{f_af_b}$, and $\mathrm{d}\hat{\sigma}^{\mathrm{C_{NNLO}}}_{f_af_b}$ can be combined to obtain a finite expression for the fully-differential NNLO cross section of the quark-antiquark channel. However, for convenience, it is more suitable to present a finite remainder that combines the quark-antiquark and the quark-quark channel. To achieve this, we extend the cross section for double-real emission in Eq. (5.1) to get

$$\begin{aligned} 2\hat{s}\cdot\mathrm{d}\hat{\sigma}^{\mathrm{RR}}_{f_af_b} &= 2\int[\mathrm{d}p_4][\mathrm{d}p_5]\Theta(E_4-E_5)\,F_{\mathrm{LM}}(1_{f_a},2_{f_b}\,|\,4_g,5_g) \\ &\quad+\sum_{c\in\mathcal{Q}}\sum_{\substack{d\in\mathcal{Q}\\ d\geqslant c}}\int[\mathrm{d}p_4][\mathrm{d}p_5]F_{\mathrm{LM}}(1_{f_a},2_{f_b}\,|\,4_{f_c},5_{f_d}) \\ &=\big\langle F_{\mathrm{LM}}(1_{f_a},2_{f_b}\,|\,4_g,5_g)\big\rangle+\sum_{c\in\mathcal{Q}}\sum_{\substack{d\in\mathcal{Q}\\ d\geqslant c}}\big\langle F_{\mathrm{LM}}(1_{f_a},2_{f_b}\,|\,4_{f_c},5_{f_d})\big\rangle, \end{aligned} \tag{5.91}$$

with the F_{LM} function for the quark-quark channel

$$F_{\mathrm{LM}}(1_{f_a},2_{f_b}\,|\,4_{f_c},5_{f_d})=\mathcal{N}\,\mathrm{d}\Pi^{(d)}_{\mathrm{B}}\,|\mathcal{M}^{(0)}_{f_af_b\to V+f_cf_d}(p_1,p_2,p_3,p_4,p_5)|^2F_J(p_1,p_2,p_3,p_4,p_5), \tag{5.92}$$

which contains the same phase-space element introduced in Eq. (5.3). In the quark-quark channel, we removed the energy ordering used in the quark-antiquark channel. To regulate the IR divergences, we follow the same steps as in the quark-antiquark channel. Firstly, the soft singularities can be eliminated using the soft operators[7]. Next, the collinear singularities can be removed separately in each partition and sector using the collinear projectors. As the procedure is similar to what we have already explained and does not introduce new concepts, we refrain from a detailed discussion. However, the subtraction terms have a different form. They can be found in Appendix E.
The result of the NNLO contribution can be obtained according to Eq. (3.6) as the sum

$$\mathrm{d}\hat{\sigma}^{\mathrm{NNLO}}_{f_af_b}=\mathrm{d}\hat{\sigma}^{\mathrm{RR}}_{f_af_b}+\mathrm{d}\hat{\sigma}^{\mathrm{RV}}_{f_af_b}+\hat{\sigma}^{\mathrm{VV}}_{f_af_b}+\mathrm{d}\hat{\sigma}^{\mathrm{C_{NNLO}}}_{f_af_b}. \tag{5.93}$$

As shown in Ref. [116], where the results of Refs. [38, 269, 270] have been combined, the poles of the four terms on the right-hand side of this equation cancel each other analytically after the IR singularities were extracted based on the rules for the Nested Soft-Collinear Subtraction scheme. The remaining term is finite, and the phase-space integral can be performed in $d=4$ dimensions, allowing for numerical integration. Since soft and collinear singularities cancel out for each phase-space point due to the locality of the subtraction scheme, contributions proportional to matrix elements with different multiplicities must be finite on their own. In other words, terms involving $F_{\mathrm{LM}}(1_{f_a},2_{f_b}\,|\,4_g,5_g)$, $F_{\mathrm{LM}}(1_{f_a},2_{f_b}\,|\,4_g)$, $F_{\mathrm{LM}}(1_{f_a},2_{f_b})$, *etc.*, can be integrated separately. Therefore, we split the cross section into the finite contributions

$$\mathrm{d}\hat{\sigma}^{\mathrm{NNLO}}_{f_af_b}=\mathrm{d}\hat{\sigma}^{\mathrm{NNLO}}_{1245,f_af_b}+\mathrm{d}\hat{\sigma}^{\mathrm{NNLO}}_{124,f_af_b}+\mathrm{d}\hat{\sigma}^{\mathrm{NNLO}}_{12,f_af_b}. \tag{5.94}$$

The terms in $\mathrm{d}\hat{\sigma}^{\mathrm{NNLO}}_{1245,f_af_b}$ contain matrix elements where both real-emitted particles are resolved and need to be integrated over the phase-space with double-real emission. We refer to them as terms with NNLO kinematics. The second summand, $\mathrm{d}\hat{\sigma}_{124,f_af_b}$, includes matrix elements with single-real emission, originating either from real-virtual

[7] In the quark-quark channel, no single-soft singularities are present. Thus, the operator $\boldsymbol{\mathcal{S}}$ is the only operator necessary to isolate soft divergences. Consequently, there is no need to introduce a soft operator $\mathcal{S}_4$, even though we removed the energy ordering.

corrections or counterterms for double-real emission where one final-state parton remains unresolved. These contributions are referred to as terms with NLO kinematics. Finally, the terms with LO kinematics, $\mathrm{d}\hat{\sigma}^{\mathrm{NNLO}}_{12,f_af_b}$, require integration over the Born phase space. They arise from double-virtual corrections, counterterms for real-virtual corrections, and counterterms for double-real emission with two unresolved final-state partons. The results in the following are adapted from Ref. [116], but are modified to separate the factorization and renormalization scale dependencies from each other.

Terms with NNLO Kinematics

The terms with NNLO kinematics are all related to tree-level diagrams with double-real emission. The IR singularities are regulated by the $\hat{\mathcal{O}}_{\mathrm{NNLO}}$ operators introduced in the last section. They have different shapes in different partitions and sectors[8]. The finite remainder reads

$$\begin{aligned}
2\hat{s}\cdot\mathrm{d}\hat{\sigma}^{\mathrm{NNLO}}_{1245,f_af_b} = &\sum_{(i,j)\in\mathrm{dc}}\left\langle\hat{\mathcal{O}}^{(i,j)}_{\mathrm{NNLO}}F_{\mathrm{LM}}(1_{f_a},2_{f_b}\,|\,4_g,5_g)\right\rangle\\
&+\sum_{i\in\mathrm{tc}}\left\langle\left(\hat{\mathcal{O}}^{(i,a)}_{\mathrm{NNLO}}+\hat{\mathcal{O}}^{(i,b)}_{\mathrm{NNLO}}+\hat{\mathcal{O}}^{(i,c)}_{\mathrm{NNLO}}+\hat{\mathcal{O}}^{(i,d)}_{\mathrm{NNLO}}\right)F_{\mathrm{LM}}(1_{f_a},2_{f_b}\,|\,4_g,5_g)\right\rangle\\
&+\sum_{c\in\mathcal{Q}}\sum_{\substack{d\in\mathcal{Q}\\ d\geqslant c}}\Bigg\{\sum_{(i,j)\in\mathrm{dc}}\left\langle\hat{\mathcal{O}}^{(i,j)}_{\mathrm{NNLO}}F_{\mathrm{LM}}(1_{f_a},2_{f_b}\,|\,4_{f_c},5_{f_d})\right\rangle\\
&+\sum_{i\in\mathrm{tc}}\left\langle\left(\hat{\mathcal{O}}^{(i,a)}_{\mathrm{NNLO}}+\hat{\mathcal{O}}^{(i,b)}_{\mathrm{NNLO}}+\hat{\mathcal{O}}^{(i,c)}_{\mathrm{NNLO}}+\hat{\mathcal{O}}^{(i,d)}_{\mathrm{NNLO}}\right)F_{\mathrm{LM}}(1_{f_a},2_{f_b}\,|\,4_{f_c},5_{f_d})\right\rangle\Bigg\}.
\end{aligned}\tag{5.95}$$

Terms with NLO Kinematics

To handle the terms with NLO kinematics more conveniently, it is beneficial to split the cross section further into four independently finite pieces. This division includes terms where the tree-level NLO real-emission matrix elements are convoluted with a splitting function, terms where they appear without a splitting function, and terms involving the one-loop matrix element of the real-virtual corrections. We use the notation

$$\mathrm{d}\hat{\sigma}^{\mathrm{NNLO}}_{124,f_af_b}=\mathrm{d}\hat{\sigma}^{\mathrm{NNLO}}_{(z,2,4),f_af_b}+\mathrm{d}\hat{\sigma}^{\mathrm{NNLO}}_{(1,z,4),f_af_b}+\mathrm{d}\hat{\sigma}^{\mathrm{NNLO}}_{(1,2,4),f_af_b}+\mathrm{d}\hat{\sigma}^{\mathrm{NNLO}}_{\mathrm{virt}(1,2,4),f_af_b}.\tag{5.96}$$

Regarding the terms with boosted matrix elements, which are those convoluted with a splitting function, the finite remainder can be expressed as

$$\begin{aligned}
&2\hat{s}\cdot\left(\mathrm{d}\hat{\sigma}^{\mathrm{NNLO}}_{(z,2,4),f_af_b}+\mathrm{d}\hat{\sigma}^{\mathrm{NNLO}}_{(1,z,4),f_af_b}\right)\\
&=\frac{\alpha_s(\mu_{\mathrm{R}})}{2\pi}\int_0^1\mathrm{d}z\left\{\hat{P}^{(0)}_{qq,\mathrm{R}}(z)\left\langle\ln\!\left(\frac{\eta_{14}}{2}\right)\hat{\mathcal{O}}_{\mathrm{NLO}}\left(w^{41,51}_{5\|1}\frac{F_{\mathrm{LM}}(z\cdot 1_{f_a},2_{f_b}\,|\,4_g)}{z}\right)\right\rangle\right.\\
&\quad+\left[\mathcal{P}'_{qq}(z)-\hat{P}^{(0)}_{qq,\mathrm{R}}(z)\ln\!\left(\frac{\mu_{\mathrm{F}}^2}{\hat{s}}\right)\right]\left\langle\hat{\mathcal{O}}_{\mathrm{NLO}}\left(\frac{F_{\mathrm{LM}}(z\cdot 1_{f_a},2_{f_b}\,|\,4_g)}{z}\right)\right\rangle\\
&\quad\left.+\hat{P}^{(0)}_{qq,\mathrm{R}}(z)\left\langle\ln\!\left(\frac{\eta_{24}}{2}\right)\hat{\mathcal{O}}_{\mathrm{NLO}}\left(w^{42,52}_{5\|2}\frac{F_{\mathrm{LM}}(1_{f_a},z\cdot 2_{f_b}\,|\,4_g)}{z}\right)\right\rangle\right.
\end{aligned}$$

[8] As mentioned previously, the quark-quark channel is free of single-soft singularities. Therefore, it yields $\mathcal{S}_5F_{\mathrm{LM}}(1_{f_a},2_{f_b}\,|\,4_{f_c},5_{f_d})=0$, and the operators $\hat{\mathcal{O}}_{\mathrm{NNLO}}$ for the quark-antiquark channel extract the singularities of the quark-quark channel, too.

$$
\begin{aligned}
&+\left[\mathcal{P}'_{qq}(z)-\hat{P}^{(0)}_{qq,\mathrm{R}}(z)\ln\!\left(\frac{\mu_\mathrm{F}^2}{\hat{s}}\right)\right]\left\langle\hat{\mathcal{O}}_{\mathrm{NLO}}\left(\frac{F_{\mathrm{LM}}(1_{f_a},z\cdot 2_{f_b}\,|\,4_g)}{z}\right)\right\rangle\\
&+\hat{P}^{(0)}_{gq,\mathrm{R}}(z)\left\langle\ln\!\left(\frac{\eta_{14}}{2}\right)\hat{\mathcal{O}}_{\mathrm{NLO}}\left(w_{5\|1}^{41,51}\frac{F_{\mathrm{LM}}(z\cdot 1_g,2_{f_b}\,|\,4_{f_a})}{z}\right)\right\rangle\\
&+\left[\mathcal{P}'_{qq}(z)-\hat{P}^{(0)}_{qq,\mathrm{R}}(z)\ln\!\left(\frac{\mu_\mathrm{F}^2}{\hat{s}}\right)\right]\left\langle\hat{\mathcal{O}}_{\mathrm{NLO}}\left(\frac{F_{\mathrm{LM}}(z\cdot 1_g,2_{f_b}\,|\,4_{f_a})}{z}\right)\right\rangle\\
&+\hat{P}^{(0)}_{gq,\mathrm{R}}(z)\left\langle\ln\!\left(\frac{\eta_{24}}{2}\right)\hat{\mathcal{O}}_{\mathrm{NLO}}\left(w_{5\|2}^{42,52}\frac{F_{\mathrm{LM}}(1_{f_a},z\cdot 2_g\,|\,4_{f_b})}{z}\right)\right\rangle\\
&+\left[\mathcal{P}'_{qq}(z)-\hat{P}^{(0)}_{qq,\mathrm{R}}(z)\ln\!\left(\frac{\mu_\mathrm{F}^2}{\hat{s}}\right)\right]\left\langle\hat{\mathcal{O}}_{\mathrm{NLO}}\left(\frac{F_{\mathrm{LM}}(1_{f_a},z\cdot 2_g\,|\,4_{f_b})}{z}\right)\right\rangle\Bigg\}
\end{aligned}
\tag{5.97}
$$

with the collinear limit of the partition functions from Eq. (5.8),

$$
w_{k\|l}^{4i,5j}=\lim_{\eta_{lk}\to 0}w^{4i,5j}. \tag{5.98}
$$

The remainder of non-boosted terms with tree-level diagrams has the form

$$
\begin{aligned}
2\hat{s}\cdot\mathrm{d}\hat{\sigma}^{\mathrm{NNLO}}_{(1,2,4),f_af_b}=\frac{\alpha_s(\mu_\mathrm{R})}{2\pi}\Big\{&\big\langle\hat{\mathcal{O}}_{\mathrm{NLO}}\big(\Delta_q F_{\mathrm{LM}}(1_{f_a},2_{f_b}\,|\,4_g)\big)\big\rangle\\
&+\big\langle\hat{\mathcal{O}}_{\mathrm{NLO}}\big(\Delta_r r_\mu r_\nu F^{\mu\nu}_{\mathrm{LM}}(1_{f_a},2_{f_b}\,|\,4_g)\big)\big\rangle\\
&-\beta_0\ln\!\left(\frac{\mu_\mathrm{F}^2}{\mu_\mathrm{R}^2}\right)\big\langle\hat{\mathcal{O}}_{\mathrm{NLO}}\,F_{\mathrm{LM}}(1_{f_a},2_{f_b}\,|\,4_g)\big\rangle\Big\},
\end{aligned}
\tag{5.99}
$$

with the function

$$
\begin{aligned}
\Delta_q=\;&C_\mathrm{F}\left[\frac{2}{3}\pi^2-2L\left(w_{5\|1}^{41,51}\ln\!\left(\frac{\eta_{14}}{2}\right)+w_{5\|2}^{42,52}\ln\!\left(\frac{\eta_{24}}{2}\right)\right)\right]\\
&+C_\mathrm{A}\left[L\big(L+\ln(\eta_{14}\eta_{24})\big)-\ln(\eta_{14})\ln(\eta_{24})+\left(\frac{137}{18}-\frac{7}{6\pi^2}\right)\right]\\
&+\beta_0\left[w_{4\|5}^{41,51}\ln\!\left(\frac{\eta_{24}}{\eta_{14}}\right)+w_{4\|5}^{42,52}\ln\!\left(\frac{\eta_{14}}{\eta_{24}}\right)+\frac{\ln(\eta_{14}\eta_{24})}{2}-L-2\ln(2)\right]\\
&-\frac{13}{9}n_f+\chi_q\left[L+\frac{\ln(\eta_{14}\eta_{24})}{2}\right]-2\gamma_q\ln\!\left(\frac{\mu_\mathrm{F}^2}{\hat{s}}\right),
\end{aligned}
\tag{5.100}
$$

that depends on the logarithm

$$
L=\ln\!\left(\frac{2E_4}{\sqrt{\hat{s}}}\right). \tag{5.101}
$$

The second term on the right-hand side of Eq. (5.99) contains the object

$$
\Delta_r=-\frac{C_\mathrm{A}}{3}+\frac{n_f}{3}, \tag{5.102}
$$

as well as the squared matrix element without polarization vectors introduced in Eq. (5.35). This function is contracted with the vector r^μ. The vector r^μ is an artifact from averaging Eq. (5.34) over the transverse directions of $\kappa_\perp^\mu$ when using a proper phase-space parametrization[9]. In the subtraction terms, spin correlations must be considered to make the subtraction scheme local. However, the hard matrix elements

[9] We will discuss such a parametrization in chapter 6.

in the related counterterms depend only on the sum of both real-emitted partons and are independent of the azimuthal direction of the unresolved parton. This allows us to analytically average over these components before the numerical integration introducing the r^μ dependence[10]. The vector r^μ is a unit vector that spans the two-dimensional space orthogonal to the gluon momentum p_4^μ, satisfying $r^2 = -1$ and $r \cdot p_4 = 0$, so that it can be interpreted as the polarization vector of the gluon.
Finally, in analogy to the real-emission contributions at NLO, the real-virtual corrections are given by

$$2\hat{s} \cdot \mathrm{d}\hat{\sigma}^{\mathrm{NNLO}}_{\mathrm{virt}(1,2,4),f_a f_b} = \left\langle \hat{\mathcal{O}}_{\mathrm{NLO}} F^{\mathrm{fin}}_{\mathrm{LV}}(1_{f_a}, 2_{f_b} \,|\, 4_g) \right\rangle . \tag{5.103}$$

It is important to note that contrary to our observation in the NLO calculation in chapter 4, the soft and soft-collinear subtraction terms do not cancel each other in case of virtual corrections.

Terms with LO Kinematics

Similarly, as for the terms with NLO kinematics, the terms with LO kinematics can be divided into several independently finite pieces according to

$$\begin{aligned} \mathrm{d}\hat{\sigma}^{\mathrm{NNLO}}_{12,f_a f_b} = {} & \mathrm{d}\hat{\sigma}^{\mathrm{NNLO}}_{(z,\bar{z}),f_a f_b} + \mathrm{d}\hat{\sigma}^{\mathrm{NNLO}}_{(z,2),f_a f_b} + \mathrm{d}\hat{\sigma}^{\mathrm{NNLO}}_{(1,z),f_a f_b} + \mathrm{d}\hat{\sigma}^{\mathrm{NNLO}}_{(1,2),f_a f_b} \\ & + \mathrm{d}\hat{\sigma}^{\mathrm{NNLO}}_{\mathrm{virt}(z,2),f_a f_b} + \mathrm{d}\hat{\sigma}^{\mathrm{NNLO}}_{\mathrm{virt}(1,z),f_a f_b} + \mathrm{d}\hat{\sigma}^{\mathrm{NNLO}}_{\mathrm{virt}(1,2),f_a f_b}. \end{aligned} \tag{5.104}$$

The first finite term, containing two convolutions with splitting functions, is

$$\begin{aligned} 2\hat{s} \cdot \mathrm{d}\hat{\sigma}^{\mathrm{NNLO}}_{(z,\bar{z}),f_a f_b} = {} & \left(\frac{\alpha_s(\mu_{\mathrm{R}})}{2\pi}\right)^2 \int_0^1 \mathrm{d}z \, \mathrm{d}\bar{z} \left(\mathcal{P}'_{qq}(z) - \hat{P}^{(0)}_{qq,\mathrm{R}}(z) \ln\left(\frac{\mu_{\mathrm{F}}^2}{\hat{s}}\right)\right) \\ & \times \left\langle \frac{F_{\mathrm{LM}}(z \cdot 1_{f_a}, \bar{z} \cdot 2_{f_b})}{z} \right\rangle \left(\mathcal{P}'_{qq}(\bar{z}) - \hat{P}^{(0)}_{qq,\mathrm{R}}(\bar{z}) \ln\left(\frac{\mu_{\mathrm{F}}^2}{\hat{s}}\right)\right) \end{aligned} \tag{5.105}$$

The tree-level matrix elements that are convoluted with one splitting function lead to

$$\begin{aligned} 2\hat{s} \cdot \left(\mathrm{d}\hat{\sigma}^{\mathrm{NNLO}}_{(z,2),f_a f_b} + \mathrm{d}\hat{\sigma}^{\mathrm{NNLO}}_{(1,z),f_a f_b}\right) = {} & \left(\frac{\alpha_s(\mu_{\mathrm{R}})}{2\pi}\right)^2 \left\{ \sum_{x \in \mathcal{Q}} \int_0^1 \mathrm{d}z \left(\mathcal{T}_{f_x f_a}(z) \left\langle \frac{F_{\mathrm{LM}}(z \cdot 1_{f_x}, 2_{f_b})}{z} \right\rangle \right.\right. \\ & \left. + \left\langle \frac{F_{\mathrm{LM}}(1_{f_a}, z \cdot 2_{f_x})}{z} \right\rangle \mathcal{T}_{f_x f_b}(z) \right) - \beta_0 \ln\left(\frac{\mu_{\mathrm{F}}^2}{\mu_{\mathrm{R}}^2}\right) \\ & \times \int_0^1 \mathrm{d}z \left(\mathcal{P}'_{qq}(\bar{z}) - \hat{P}^{(0)}_{qq,\mathrm{R}}(\bar{z}) \ln\left(\frac{\mu_{\mathrm{F}}^2}{\hat{s}}\right)\right) \\ & \left.\times \left\langle \frac{F_{\mathrm{LM}}(z \cdot 1_{f_a}, 2_{f_b}) + F_{\mathrm{LM}}(1_{f_a}, z \cdot 2_{f_b})}{z} \right\rangle \right\}, \end{aligned} \tag{5.106}$$

where the lengthy expressions for the transition functions $\mathcal{T}_{ij}$ are publicly available as an ancillary file of Ref. [116]. They can be understood as generalizations of the NLO Altarelli-Parisi splitting functions. These transition functions have a non-trivial color structure and depend on the scale of the process, the representation of the partition functions, and the energy fraction z.

[10] The average over the transverse directions can be written as (*c.f.* Eq. (8.66) of Ref. [38])
$$\langle \kappa_\perp^\mu \kappa_\perp^\nu \rangle = -\tfrac{1}{2} g^{\mu\nu} + \epsilon \, r^\mu r^\nu .$$

Next, the finite remainder of the tree-level terms without boost can be written as

$$
\begin{aligned}
2\hat{s}\cdot \mathrm{d}\hat{\sigma}^{\mathrm{NNLO}}_{(1,2),f_af_b} = \left(\frac{\alpha_s(\mu_\mathrm{R})}{2\pi}\right)^2 \Bigg\{ C_\mathrm{F}^2 \Bigg[\frac{8\pi^4}{45} - (2\pi^2+16\zeta_3)\ln\left(\frac{\mu_\mathrm{F}^2}{\hat{s}}\right) + \left(\frac{9}{4}-\frac{2\pi^2}{3}\right) \\
\times \ln^2\left(\frac{\mu_\mathrm{F}^2}{\hat{s}}\right)\Bigg] + C_\mathrm{A}C_\mathrm{F}\Bigg[\frac{739}{81}+\frac{209\pi^2}{72}-\frac{7\pi^4}{80}+\ln(2)\left(\frac{4}{3}+\frac{11\pi^2}{9}\right. \\
\left.-\frac{7\zeta_3}{2}\right)+\ln^2(2)(\zeta_2-2)-\frac{1}{6}\ln^4(2)-\frac{407\zeta_3}{36}-4\,\mathrm{Li}_4\left(\frac{1}{2}\right) \\
+\ln\left(\frac{\mu_\mathrm{F}^2}{\hat{s}}\right)\left(-\frac{199}{54}+\frac{23\pi^2}{24}-7\zeta_3\right)-\frac{11}{4}\ln^2\left(\frac{\mu_\mathrm{F}^2}{\hat{s}}\right)\Bigg] + C_\mathrm{F}\,n_f \\
\times\Bigg[-\frac{214}{81}-\frac{7\pi^2}{18}-\ln(2)\left(\frac{4}{3}+\frac{2\pi^2}{9}\right)+2\ln^2(2)+\frac{37\zeta_3}{18} \\
+\ln\left(\frac{\mu_\mathrm{F}^2}{\hat{s}}\right)\left(\frac{17}{27}-\frac{\pi^2}{12}\right)+\frac{1}{2}\ln^2\left(\frac{\mu_\mathrm{F}^2}{\hat{s}}\right)\Bigg] + \Theta_{bd}\Bigg[C_\mathrm{F}\,n_f\frac{23}{72} \\
+C_\mathrm{A}C_\mathrm{F}\left(\frac{\pi^2}{6}-\frac{131}{72}\right)+C_\mathrm{F}\beta_0\ln(2)\Bigg]-\beta_0\ln\left(\frac{\mu_\mathrm{F}^2}{\mu_\mathrm{R}^2}\right)\Bigg[C_\mathrm{F}\frac{2\pi^2}{3} \\
-2\gamma_q\ln\left(\frac{\mu_\mathrm{F}^2}{\hat{s}}\right)\Bigg]\Bigg\}\left\langle F_{\mathrm{LM}}(1_{f_a},2_{f_b})\right\rangle,
\end{aligned}
\tag{5.107}
$$

with the partition-dependent term

$$
\begin{aligned}
\Theta_{bd} &= -\left\langle \left(1-\mathcal{C}_{41}-\mathcal{C}_{42}\right)\left(\frac{\eta_{12}}{\eta_{14}\eta_{24}}\left[w_{4\|5}^{41,51}\ln\left(\frac{\eta_{14}}{1-\eta_{14}}\right)+w_{4\|5}^{42,52}\ln\left(\frac{\eta_{24}}{1-\eta_{24}}\right)\right]\right)\right\rangle \\
&= 4-\frac{2\pi^2}{3},
\end{aligned}
\tag{5.108}
$$

where the last line follows immediately from the explicit parametrization in Eq. (5.11). The counterterms of the real-virtual corrections are proportional to boosted matrix elements of NLO virtual corrections. These terms are independently finite and read

$$
\begin{aligned}
2\hat{s}\cdot\left(\mathrm{d}\hat{\sigma}^{\mathrm{NNLO}}_{\mathrm{virt}(z,2),f_af_b}+\mathrm{d}\hat{\sigma}^{\mathrm{NNLO}}_{\mathrm{virt}(1,z),f_af_b}\right) = \frac{\alpha_s(\mu_\mathrm{R})}{2\pi}\int_0^1\mathrm{d}z\left(\mathcal{P}'_{qq}(z)-\hat{P}^{(0)}_{qq,\mathrm{R}}(z)\ln\left(\frac{\mu_\mathrm{F}^2}{\hat{s}}\right)\right) \\
\times\left\langle\frac{F^{\mathrm{fin}}_{\mathrm{LV}}(z\cdot 1_{f_a},2_{f_b})+F^{\mathrm{fin}}_{\mathrm{LV}}(1_{f_a},z\cdot 2_{f_b})}{z}\right\rangle.
\end{aligned}
\tag{5.109}
$$

Additionally, there are virtual corrections with LO kinematics without boosts. These contributions have the compact form

$$
\begin{aligned}
2\hat{s}\cdot\mathrm{d}\hat{\sigma}^{\mathrm{NNLO}}_{\mathrm{virt}(1,2),f_af_b} = \frac{\alpha_s(\mu_\mathrm{R})}{2\pi}\left[\frac{2\pi^2}{3}C_\mathrm{F}-2\gamma_q\ln\left(\frac{\mu_\mathrm{F}^2}{\hat{s}}\right)-\beta_0\ln\left(\frac{\mu_\mathrm{F}^2}{\mu_\mathrm{R}^2}\right)\right]\left\langle F^{\mathrm{fin}}_{\mathrm{LV}}(1_{f_a},2_{f_b})\right\rangle \\
+\left\langle F^{\mathrm{fin}}_{\mathrm{LV}^2}(1_{f_a},2_{f_b})\right\rangle+\left\langle F^{\mathrm{fin}}_{\mathrm{LVV}}(1_{f_a},2_{f_b})\right\rangle,
\end{aligned}
\tag{5.110}
$$

and contain the finite remainders of the double-virtual corrections as well as a counterterm proportional to the NLO one-loop finite remainder.

This completes the picture of the quark-antiquark as well as the quark-quark channel. The finite remainders can be evaluated numerically, providing finite results for arbitrary infrared-safe observables. However, for obtaining physically meaningful re-

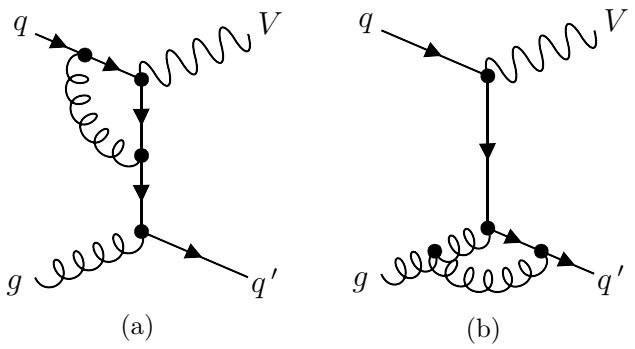

Figure 5.7.: Representative Feynman diagrams for real-virtual corrections in color-singlet production in the quark-gluon channel.

sults, the inclusion of the quark-gluon and the gluon-gluon channels are substantial as well. Similar to the quark-quark channel, we do not repeat the construction of the finite remainder as no new concepts are introduced in comparison to extensively discussed quark-antiquark channel. Instead, we directly present the finite results of the fully-differential NNLO cross section.

5.2.4.2. Quark-Gluon Initiated Process

To express the remainder of the quark-gluon channel, we need its F_{LM} function with the two-parton final state, which is given by

$$F_{\mathrm{LM}}(1_{f_a}, 2_g \,|\, 4_{f_x}, 5_g) = \mathcal{N} \mathrm{d}\Pi_{\mathrm{B}}^{(d)} \, |\mathcal{M}^{(0)}_{f_a g \to V + f_x g}(p_1, p_2, p_3, p_4, p_5)|^2 F_J(p_1, p_2, p_3, p_4, p_5), \tag{5.111}$$

where the energy ordering is not implied. Moreover, the virtual corrections of the diagrams that we already investigated at NLO, see Figure 5.7, are required, and have to be interfered with the corresponding tree-level amplitude,

$$\begin{aligned} F_{\mathrm{LRV}}(1_{f_a}, 2_g \,|\, 4_{f_x}) = \mathcal{N} \, \mathrm{d}\Pi_{\mathrm{B}}^{(d)} \, 2 \, \mathfrak{Re}\Big\{ \mathcal{M}^{(1)}_{f_a g \to V + f_x}(p_1, p_2, p_3, p_4) \mathcal{M}^{*(0)}_{f_a g \to V + f_x}(p_1, p_2, p_3, p_4) \Big\} \\ \times F_J(p_1, p_2, p_3, p_4). \end{aligned} \tag{5.112}$$

The phase-space element of the former process includes the full NNLO kinematics, while the one-loop process in the F_{LRV} function contains a phase-space element with NLO kinematics. Since the one-loop amplitudes have explicit IR poles encoded, we need to isolate and cancel them before an evaluation in four dimensions is possible. This can be achieved by the replacement

$$F_{\mathrm{LRV}}(1_{f_a}, 2_g \,|\, 4_{f_x}) = [\alpha_{s,\epsilon}] \, I_{qgq}(\epsilon) F_{\mathrm{LM}}(1_{f_a}, 2_g \,|\, 4_{f_x}) + F^{\mathrm{fin}}_{\mathrm{LRV}}(1_{f_a}, 2_g \,|\, 4_{f_x}), \tag{5.113}$$

with the color-charge insertion operator [278]

$$\begin{aligned} I_{qgq}(\epsilon) = \left(-\frac{1}{\hat{u}}\right)^{\epsilon} \left(\frac{C_{\mathrm{A}} - 2\, C_{\mathrm{F}}}{\epsilon^2} + \frac{\chi_q - 2\, \gamma_q}{\epsilon} \right) \\ - \left[\cos(\epsilon\, \pi) \left(\frac{1}{\hat{s}}\right)^{\epsilon} + \left(-\frac{1}{\hat{t}}\right)^{\epsilon} \right] \left(\frac{C_{\mathrm{A}}}{\epsilon^2} + \frac{\chi_q + \gamma_g}{2\epsilon} \right). \end{aligned} \tag{5.114}$$

With these definitions in place, we can further divide the finite remainder into independently finite terms based on the highest kinematical multiplicity of the matrix elements, resulting in

$$\mathrm{d}\hat{\sigma}^{\mathrm{NNLO}}_{f_a g} = \mathrm{d}\hat{\sigma}^{\mathrm{NNLO}}_{1245,f_a g} + \mathrm{d}\hat{\sigma}^{\mathrm{NNLO}}_{124,f_a g} + \mathrm{d}\hat{\sigma}^{\mathrm{NNLO}}_{12,f_a g}. \tag{5.115}$$

Terms with NNLO Kinematics

The terms with NNLO kinematics are divided into the four usual partitions, whereby the two triple-collinear partitions are further decomposed into the four sectors (a), (b), (c), and (d). The $\hat{\mathcal{O}}_{\mathrm{NNLO}}$ projectors, which are used for the extraction of the IR singularities arising during the phase-space integration, remain unchanged in this channel compared to the scenarios that we have discussed previously[11]. We find

$$\begin{aligned} 2\hat{s}\cdot \mathrm{d}\hat{\sigma}^{\mathrm{NNLO}}_{1245,f_a g} = \sum_{x\in\mathcal{Q}}\Bigg\{ & \sum_{(i,j)\in \mathrm{dc}} \left\langle \hat{\mathcal{O}}^{(i,j)}_{\mathrm{NNLO}} F_{\mathrm{LM}}(1_{f_a}, 2_g \,|\, 4_{f_x}, 5_g) \right\rangle \\ & + \sum_{i\in \mathrm{tc}} \left\langle \left(\hat{\mathcal{O}}^{(i,a)}_{\mathrm{NNLO}} + \hat{\mathcal{O}}^{(i,b)}_{\mathrm{NNLO}} + \hat{\mathcal{O}}^{(i,c)}_{\mathrm{NNLO}} + \hat{\mathcal{O}}^{(i,d)}_{\mathrm{NNLO}} \right) F_{\mathrm{LM}}(1_{f_a}, 2_g \,|\, 4_{f_x}, 5_g) \right\rangle \Bigg\}. \end{aligned} \tag{5.116}$$

Terms with NLO Kinematics

In the case of NLO kinematics, we have four separately finite structures depending on whether the F_{LM} functions are convoluted with splitting functions or not. Thus, we write

$$\mathrm{d}\hat{\sigma}^{\mathrm{NNLO}}_{124,f_a g} = \mathrm{d}\hat{\sigma}^{\mathrm{NNLO}}_{(z,2,4),f_a g} + \mathrm{d}\hat{\sigma}^{\mathrm{NNLO}}_{(1,z,4),f_a g} + \mathrm{d}\hat{\sigma}^{\mathrm{NNLO}}_{(1,2,4),f_a g} + \mathrm{d}\hat{\sigma}^{\mathrm{NNLO}}_{\mathrm{virt}(1,2,4),f_a g}. \tag{5.117}$$

The boosted contributions are

$$\begin{aligned} & 2\hat{s}\cdot\left(\mathrm{d}\hat{\sigma}^{\mathrm{NNLO}}_{(z,2,4),f_a g} + \mathrm{d}\hat{\sigma}^{\mathrm{NNLO}}_{(1,z,4),f_a g}\right) \\ & = \frac{\alpha_s(\mu_{\mathrm{R}})}{2\pi} \sum_{x\in\mathcal{Q}} \int_0^1 \mathrm{d}z \Bigg\{ \hat{P}^{(0)}_{qq,\mathrm{R}}(z) \left\langle \ln\!\left(\frac{\eta_{14}}{2}\right) \hat{\mathcal{O}}_{\mathrm{NLO}} \left(w_{5\|1}^{41,51} \frac{F_{\mathrm{LM}}\left(z\cdot 1_{f_a}, 2_g \,|\, 4_{f_x}\right)}{z} \right) \right\rangle \\ & + \left[\mathcal{P}'_{qq}(z) - \hat{P}^{(0)}_{qq,\mathrm{R}}(z) \ln\!\left(\frac{\mu_{\mathrm{F}}^2}{\hat{s}}\right) \right] \left\langle \hat{\mathcal{O}}_{\mathrm{NLO}} \left(\frac{F_{\mathrm{LM}}\left(z\cdot 1_{f_a}, 2_g \,|\, 4_{f_x}\right)}{z} \right) \right\rangle \\ & + \hat{P}^{(0)}_{qg,\mathrm{R}}(z) \left\langle \ln\!\left(\frac{\eta_{24}}{2}\right) \hat{\mathcal{O}}_{\mathrm{NLO}} \left(w_{5\|2}^{42,52} \frac{F_{\mathrm{LM}}\left(1_{f_a}, z\cdot 2_{f_x} \,|\, 4_g\right)}{z} \right) \right\rangle \\ & + \hat{P}^{(0)}_{gg,\mathrm{R}}(z) \left\langle \ln\!\left(\frac{\eta_{24}}{2}\right) \hat{\mathcal{O}}_{\mathrm{NLO}} \left(w_{5\|2}^{42,52} \frac{F_{\mathrm{LM}}\left(1_{f_a}, z\cdot 2_g \,|\, 4_{f_x}\right)}{z} \right) \right\rangle \\ & + \left[\mathcal{P}'_{qg}(z) - \hat{P}^{(0)}_{qg,\mathrm{R}}(z) \ln\!\left(\frac{\mu_{\mathrm{F}}^2}{\hat{s}}\right) \right] \left\langle \hat{\mathcal{O}}_{\mathrm{NLO}} \left(\frac{F_{\mathrm{LM}}\left(1_{f_a}, z\cdot 2_{f_x} \,|\, 4_g\right)}{z} \right) \right\rangle \\ & + \left[\mathcal{P}'_{gg}(z) - \hat{P}^{(0)}_{gg,\mathrm{R}}(z) \ln\!\left(\frac{\mu_{\mathrm{F}}^2}{\hat{s}}\right) \right] \left\langle \hat{\mathcal{O}}_{\mathrm{NLO}} \left(\frac{F_{\mathrm{LM}}\left(1_{f_a}, z\cdot 2_g \,|\, 4_{f_x}\right)}{z} \right) \right\rangle \Bigg\}, \end{aligned} \tag{5.118}$$

where all splitting functions appearing in this expression are listed in Appendix C.

[11] As in the quark-quark channel, there is no single-soft singularity for vanishing energy of a final-state quark. This can be deduced from quark-number conservation. Therefore, there is no need to introduce an operator $\mathcal{S}_4$.

The non-boosted term can be written as

$$\begin{aligned} 2\hat{s}\cdot \mathrm{d}\hat{\sigma}^{\mathrm{NNLO}}_{(1,2,4),f_a g} = \frac{\alpha_s(\mu_\mathrm{R})}{2\pi}\sum_{x\in\mathcal{Q}}\Big\{\Big\langle \hat{\mathcal{O}}_{\mathrm{NLO}}\left(\Delta_{qg} F_{\mathrm{LM}}\left(1_{f_a},2_g\,|\,4_{f_x}\right)\right)\Big\rangle \\ -\beta_0 \ln\!\left(\frac{\mu_\mathrm{F}^2}{\mu_\mathrm{R}^2}\right)\Big\langle \hat{\mathcal{O}}_{\mathrm{NLO}}\, F_{\mathrm{LM}}\left(1_{f_a},2_g\,|\,4_{f_x}\right)\Big\rangle\Big\}, \end{aligned} \tag{5.119}$$

with a factor depending on the process kinematics and the collinear partition functions defined in Eq. (5.98),

$$\begin{aligned} \Delta_{qg} = C_\mathrm{F}\Bigg[& L\big(L-2\ln(\eta_{14})-4\ln(2)\big)+\left(\frac{3}{2}-2L\right)\left(w_{4\|5}^{41,51}\ln\!\left(\frac{\eta_{24}}{\eta_{14}}\right)+w_{4\|5}^{42,52}\ln\!\left(\frac{\eta_{14}}{\eta_{24}}\right)\right) \\ & +\frac{13}{2}+3\ln(2)-\pi^2+3\ln(\eta_{14})+2\,\mathrm{Li}_2(\eta_{24})-\frac{3}{2}\ln\!\left(\frac{\mu_\mathrm{F}^2}{\hat{s}}\right)\Bigg] \\ & + C_\mathrm{A}\left[\frac{\pi^2}{3}-\frac{3}{4}\ln(\eta_{24})+\left(\frac{3}{2}-L\right)\ln\!\left(\frac{\eta_{24}}{\eta_{14}}\right)-\frac{3}{4}L+\mathrm{Li}_2(\eta_{14})-\mathrm{Li}_2(\eta_{24})\right] \\ & +\beta_0\left[\frac{1}{2}\big(L+\ln(\eta_{24})\big)-\ln\!\left(\frac{\mu_\mathrm{F}^2}{\hat{s}}\right)\right]. \end{aligned} \tag{5.120}$$

The logarithm L is the same as given in Eq. (5.101).
The virtual corrections are given by

$$2\hat{s}\cdot \mathrm{d}\hat{\sigma}^{\mathrm{NNLO}}_{\mathrm{virt}(1,2,4),f_a g} = \sum_{x\in\mathcal{Q}}\Big\langle \hat{\mathcal{O}}_{\mathrm{NLO}}\left(F^{\mathrm{fin}}_{\mathrm{LRV}}\left(1_{f_a},2_g\,|\,4_{f_x}\right)\right)\Big\rangle, \tag{5.121}$$

where the phase-space divergences are regulated by the NLO subtraction operator, $\hat{\mathcal{O}}_{\mathrm{NLO}}$ that was introduced in Eq. (4.26).

Terms with LO Kinematics

Since the quark-gluon process starts to contribute at NLO, there are no terms with LO kinematics without boost. Therefore, we have only three independent terms,

$$\mathrm{d}\hat{\sigma}^{\mathrm{NNLO}}_{12,f_a g} = \mathrm{d}\hat{\sigma}^{\mathrm{NNLO}}_{(z,\bar{z}),f_a g} + \mathrm{d}\hat{\sigma}^{\mathrm{NNLO}}_{(1,z),f_a g} + \mathrm{d}\hat{\sigma}^{\mathrm{NNLO}}_{\mathrm{virt}(1,z),f_a g}. \tag{5.122}$$

When the squared LO amplitudes are convoluted with two splitting functions, the contribution reads

$$\begin{aligned} 2\hat{s}\cdot \mathrm{d}\hat{\sigma}^{\mathrm{NNLO}}_{(z,\bar{z}),f_a g} = & \left(\frac{\alpha_s(\mu_\mathrm{R})}{2\pi}\right)^2\sum_{x\in\mathcal{Q}}\int_0^1 \mathrm{d}z\,\mathrm{d}\bar{z}\left(\mathcal{P}'_{qq}(z)-\hat{P}^{(0)}_{qq,\mathrm{R}}(z)\ln\!\left(\frac{\mu_\mathrm{F}^2}{\hat{s}}\right)\right) \\ & \times\left\langle\frac{F_{\mathrm{LM}}(z\cdot 1_{f_a},\bar{z}\cdot 2_{f_x})}{z\bar{z}}\right\rangle\left(\mathcal{P}'_{qg}(\bar{z})-\hat{P}^{(0)}_{qg,\mathrm{R}}(\bar{z})\ln\!\left(\frac{\mu_\mathrm{F}^2}{\hat{s}}\right)\right). \end{aligned} \tag{5.123}$$

If only the initial state gluon is convoluted, the contribution becomes

$$\begin{aligned} 2\hat{s}\cdot \mathrm{d}\hat{\sigma}^{\mathrm{NNLO}}_{(1,z),f_a g} = & \left(\frac{\alpha_s(\mu_\mathrm{R})}{2\pi}\right)^2\sum_{x\in\mathcal{Q}}\left\{\int_0^1 \mathrm{d}z\,\mathcal{T}_{qg}(z)\left\langle\frac{F_{\mathrm{LM}}(1_{f_a},z\cdot 2_{f_x})}{z}\right\rangle-\beta_0\ln\!\left(\frac{\mu_\mathrm{F}^2}{\mu_\mathrm{R}^2}\right)\right. \\ & \left.\times\int_0^1 \mathrm{d}z\left(\mathcal{P}'_{qg}(\bar{z})-\hat{P}^{(0)}_{qg,\mathrm{R}}(\bar{z})\ln\!\left(\frac{\mu_\mathrm{F}^2}{\hat{s}}\right)\right)\left\langle\frac{F_{\mathrm{LM}}(1_{f_a},z\cdot 2_{f_x})}{z}\right\rangle\right\}. \end{aligned} \tag{5.124}$$

The transition function $\mathcal{T}_{qg}$ is also part of the ancillary file of Ref. [116].

Finally, the term with virtual corrections is

$$2\hat{s}\cdot \mathrm{d}\hat{\sigma}^{\mathrm{NNLO}}_{\mathrm{virt}(1,z),f_a g} = \frac{\alpha_s(\mu_\mathrm{R})}{2\pi}\sum_{x\in\mathcal{Q}}\int_0^1 \mathrm{d}z\left(\mathcal{P}'_{qg}(z) - \hat{P}^{(0)}_{qg,\mathrm{R}}(z)\ln\left(\frac{\mu_\mathrm{F}^2}{\hat{s}}\right)\right)\left\langle \frac{F^{\mathrm{fin}}_{\mathrm{LV}}(1_{f_a}, z\cdot 2_{f_x})}{z}\right\rangle. \tag{5.125}$$

The results for interchanged roles of the two incoming partons, specifically, a gluon coming from the first hadron and the quark originating from the second hadron, can be obtained by relabeling the momenta 1 and 2.

5.2.4.3. Gluon-Gluon Initiated Process

The gluon-initiated process is newly rising at NNLO. Therefore, only tree-level amplitudes are necessary to describe the corresponding cross section. Its related F_{LM} function is given by

$$F_{\mathrm{LM}}(1_g, 2_g \,|\, 4_{f_x}, 5_{f_y}) = \mathcal{N}\mathrm{d}\Pi^{(d)}_{\mathrm{B}}\,|\mathcal{M}^{(0)}_{gg\to V+f_x f_y}(p_1,p_2,p_3,p_4,p_5)|^2 F_J(p_1,p_2,p_3,p_4,p_5). \tag{5.126}$$

Since this channel contributes for the first time, soft singularities and triple-collinear singularities are not present, making it much simpler than the other channels. However, to maintain the same structure as before, we separate independently finite pieces,

$$\mathrm{d}\hat{\sigma}^{\mathrm{NNLO}}_{gg} = \mathrm{d}\hat{\sigma}^{\mathrm{NNLO}}_{1245,gg} + \mathrm{d}\hat{\sigma}^{\mathrm{NNLO}}_{124,gg} + \mathrm{d}\hat{\sigma}^{\mathrm{NNLO}}_{12,gg}. \tag{5.127}$$

Terms with NNLO Kinematics

Due to the simplified structure of the gluon-gluon channel, a separation into different partitions or sectors is dispensable. Then, the terms with NNLO kinematics take the form

$$2\hat{s}\cdot \mathrm{d}\hat{\sigma}^{\mathrm{NNLO}}_{1245,gg} = \sum_{x\in\mathcal{Q}}\sum_{\substack{y\in\mathcal{Q}\\ y\geqslant x}}\left\langle \hat{\mathcal{O}}^{(g,g)}_{\mathrm{NNLO}} F_{\mathrm{LM}}(1_g, 2_g \,|\, 4_{f_x}, 5_{f_y})\right\rangle, \tag{5.128}$$

with the NNLO subtraction operator

$$\hat{\mathcal{O}}^{(g,g)}_{\mathrm{NNLO}} = \big(1 - \mathcal{C}_{41} - \mathcal{C}_{42} - \mathcal{C}_{51} - \mathcal{C}_{52} + \mathcal{C}_{41}\mathcal{C}_{52} + \mathcal{C}_{42}\mathcal{C}_{51}\big). \tag{5.129}$$

This projector does not contain overlapping singularities, supporting the argument that a phase-space division into different regions is unnecessary.

Terms with NLO Kinematics

The terms with NLO kinematics can only arise from counterterms of collinear limits, which implies that they have to be proportional to boosted matrix elements. Indeed, we find

$$\begin{aligned} 2\hat{s}\cdot \mathrm{d}\hat{\sigma}^{\mathrm{NNLO}}_{124,gg} = \frac{\alpha_s(\mu_\mathrm{R})}{2\pi}\sum_{x\in\mathcal{Q}}\sum_{y\in\mathcal{Q}}\int_0^1 \mathrm{d}z\left(\mathcal{P}'_{qg}(z) - \hat{P}^{(0)}_{qg,\mathrm{R}}(z)\ln\left(\frac{\mu_\mathrm{F}^2}{\hat{s}}\right)\right) \\ \times\left\langle \hat{\mathcal{O}}_{\mathrm{NLO}}\left(\frac{F_{\mathrm{LM}}(z\cdot 1_{f_x}, 2_g \,|\, 4_{f_y}) + F_{\mathrm{LM}}(1_g, z\cdot 2_{f_x} \,|\, 4_{f_y})}{z}\right)\right\rangle. \end{aligned} \tag{5.130}$$

Terms with LO Kinematics

The same holds for the terms with LO kinematics. They have their origin in counterterms of purely collinear limits, and consequently, they have to be proportional to double-boosted matrix elements,

$$2\hat{s}\cdot\mathrm{d}\hat{\sigma}^{\mathrm{NNLO}}_{12,gg} = \left(\frac{\alpha_s(\mu_\mathrm{R})}{2\pi}\right)^2 \sum_{x\in\mathcal{Q}}\sum_{y\in\mathcal{Q}} \int_0^1 \mathrm{d}z\,\mathrm{d}\bar{z} \left(\mathcal{P}'_{qg}(z) - \hat{P}^{(0)}_{qg,\mathrm{R}}(z)\ln\left(\frac{\mu_\mathrm{F}^2}{\hat{s}}\right)\right) \times \left\langle \hat{\mathcal{O}}_{\mathrm{NLO}}\left(\frac{F_{\mathrm{LM}}(z\cdot 1_{f_x}, \bar{z}\cdot 2_{f_y})}{z\bar{z}}\right)\right\rangle \left(\mathcal{P}'_{qg}(\bar{z}) - \hat{P}^{(0)}_{qg,\mathrm{R}}(\bar{z})\ln\left(\frac{\mu_\mathrm{F}^2}{\hat{s}}\right)\right). \tag{5.131}$$

5.2.4.4. Hadronic Process

In a last step, all channels can be combined and convoluted with the parton luminosity functions to find the expression for the NNLO cross section in proton-proton collisions,

$$\begin{aligned}\mathrm{d}\sigma^{\mathrm{NNLO}}_{pp} = &\sum_{a\in\mathcal{Q}}\sum_{b\in\mathcal{Q}}\int_0^1 \mathrm{d}\tau\,\frac{\mathrm{d}\mathcal{L}^{f_a f_b}_{pp}(\tau,\mu_\mathrm{F})}{\mathrm{d}\tau}\,\mathrm{d}\hat{\sigma}^{\mathrm{NNLO}}_{f_a f_b}(\tau,\mu_\mathrm{R},\mu_\mathrm{F}) \\ &+\sum_{a\in\mathcal{Q}}\int_0^1 \mathrm{d}\tau\,\frac{\mathrm{d}\mathcal{L}^{f_a g}_{pp}(\tau,\mu_\mathrm{F})}{\mathrm{d}\tau}\,\mathrm{d}\hat{\sigma}^{\mathrm{NNLO}}_{f_a g}(\tau,\mu_\mathrm{R},\mu_\mathrm{F}) \\ &+\sum_{b\in\mathcal{Q}}\int_0^1 \mathrm{d}\tau\,\frac{\mathrm{d}\mathcal{L}^{g f_b}_{pp}(\tau,\mu_\mathrm{F})}{\mathrm{d}\tau}\,\mathrm{d}\hat{\sigma}^{\mathrm{NNLO}}_{g f_b}(\tau,\mu_\mathrm{R},\mu_\mathrm{F}) \\ &+\int_0^1 \mathrm{d}\tau\,\frac{\mathrm{d}\mathcal{L}^{gg}_{pp}(\tau,\mu_\mathrm{F})}{\mathrm{d}\tau}\,\mathrm{d}\hat{\sigma}^{\mathrm{NNLO}}_{gg}(\tau,\mu_\mathrm{R},\mu_\mathrm{F})\,.\end{aligned} \tag{5.132}$$

With this result, we have completed the NNLO cross-section computation. We can head forward to its implementation into a Monte Carlo Event Generator for making experimentally relevant predictions of fully-differential IR-safe observables.

6

Phase-Space Integration

Contents

A crucial point for an efficient numerical evaluation of the cross sections lies in the parametrization of the phase space. In particular, the terms with NNLO kinematics require a smart handling of the angular parameters. In this chapter, we will discuss the implementation of the Nested Soft-Collinear Subtraction scheme on the basis of such a smart parametrization which was introduced in Refs. [34, 35]. We will focus the attention on the computation of color-singlet production with double-real radiation for the Drell-Yan-like process as the phase-space structure is the most complex one and all other phase-space parametrizations with a reduced number of final-state particles can be easily received with the in the following presented method.

6.1. Parametrization

In order to get the fully-differential hadronic cross section we aim to perform the phase-space integrals, the integrals from the convolution of the partonic cross section with the PDFs as well as the integration over the invariant mass of the final-state vector boson-Higgs system according to Eq. (2.9) numerically. Since the subtraction scheme is not Lorentz invariant and the counterterms of the subtraction functions were given in the partonic center-of-mass system, we parameterize our momenta in this frame,

$$p_1 = \frac{\sqrt{\hat{s}}}{2}\big(1,0,0,1\big)^{\mathrm{T}}, \tag{6.1}$$

$$p_2 = \frac{\sqrt{\hat{s}}}{2}\big(1,0,0,-1\big)^{\mathrm{T}}, \tag{6.2}$$

$$p_4 = E_4\big(1, \cos(\phi_4)\sin(\theta_4), \sin(\phi_4)\sin(\theta_4), \cos(\theta_4)\big)^{\mathrm{T}}, \tag{6.3}$$

$$p_5 = E_5\big(1, \cos(\phi_5)\sin(\theta_5), \sin(\phi_5)\sin(\theta_5), \cos(\theta_5)\big)^{\mathrm{T}}. \tag{6.4}$$

The momenta p_1 and p_2 are associated with the two colliding partons coming from the first or the second proton beam, respectively. Their energy is in the center-of-mass frame simply given by half of the partonic center-of-mass energy, $\sqrt{\hat{s}}$. The momenta p_4 and p_5 belong to the two real-emitted partons, each momentum has three independent degrees of freedom, which are the energies, E_i, and two angles, θ_i and ϕ_i, with $i \in \{4, 5\}$. The momentum of the color singlet is then fully determined by momentum conservation,

$$p_3 = p_1 + p_2 - p_4 - p_5. \tag{6.5}$$

However, for a numerical evaluation the parametrization in Eqs. (6.1) to (6.4) is not suitable and for each partition and sector we will use a proper substitution that we will describe in subsection 6.1.4. Before, we give a closer look to the integral over the invariant mass of the color singlet, the convolution of the PDFs, and the Born phase space.

6.1.1. Invariant Mass of the Color Singlet

The invariant mass of the final-state vector boson-Higgs system has to be in the range

$$q^2 \in \big[(M_V + M_H)^2, s\big)\,, \tag{6.6}$$

where the lower boundary comes from the minimal collision energy that is needed to produce the vector boson and the Higgs boson commonly on-shell. The upper boundary is the maximum energy of the hadronic collision, and, of course, the invariant mass of the final-state system is limited by this energy scale. In summary, we can write the integral over the invariant mass as

$$\int \mathrm{d}q^2 = \int_{(M_V+M_H)^2}^{s} \mathrm{d}q^2\, \Theta\big(\hat{s} - q^2\big)\,, \tag{6.7}$$

where the Heaviside function ensures that the partonic collision energy $\hat{s}$ is at least large enough to produce the color singlet with mass q.

6.1.2. Bjorken Variables

For carrying out the integration over the PDFs we have to plug in the luminosity function of Eq. (2.3) into Eq. (2.9). The τ integration can be eliminated by the δ-distribution so that we are left with two integrations over the Bjorken variables ξ_1 and ξ_2. It is convenient to rewrite them as

$$\begin{aligned} \xi_1 &= \sqrt{\frac{\hat{s}}{s}}\, e^{y}, \\ \xi_2 &= \sqrt{\frac{\hat{s}}{s}}\, e^{-y}. \end{aligned} \tag{6.8}$$

This choice of the Bjorken variables relates the hadronic collision energy, $\sqrt{s}$, to the partonic center-of-mass energy according to $\hat{s} = \xi_1\xi_2 s$. Moreover, y can be interpreted as the rapidity of the partonic center-of-mass system in the laboratory frame of the hadronic collision. It immediately follows that the integration over the momentum fractions can be replaced with an integration over $\hat{s}$ and y,

$$\mathrm{d}\xi_1\mathrm{d}\xi_2 = \frac{1}{s}\mathrm{d}\hat{s}\,\mathrm{d}y. \tag{6.9}$$

The integration boundaries can be obtained from the fact that $\xi_i \in (0,1)$ for both, $i = \{1,2\}$, which results in the boundary $\hat{s} \in (0,s)$, but this can be combined with the Heaviside function in Eq. (6.7) so that we find

$$\hat{s} \in \left[q^2, s\right) \quad \text{and} \quad y \in \left(\frac{1}{2}\ln(\tau), -\frac{1}{2}\ln(\tau)\right). \tag{6.10}$$

The parameter τ is the product of the two Bjorken variables, or simply expressed in terms of the energies $\tau = \hat{s}/s$.

6.1.3. Born Phase Space

The heart of the numerical integration is the phase-space evaluation. By the discussion up to here, it should have become clear that we want to split these integrations into the phase space of the Born process and the phase space of the real radiation. For double-real emission we have seen the Born phase-space element in Eq. (5.3). We want to perform the numerical computation in $d = 4$ dimensions, where the phase-space element reads[1]

$$\mathrm{d}\Pi_{\mathrm{B}}^{(4)} = \frac{\mathrm{d}^3p_3}{(2\pi)^3 2E_3}\,(2\pi)^4\,\delta^{(4)}(p_1 + p_2 - p_3 - p_4 - p_5). \tag{6.11}$$

Making use of the identity

$$\begin{aligned}\frac{\mathrm{d}^3p_3}{2E_3} &= \mathrm{d}^4p_3\,\delta\big(p_3^2 - q^2\big)\Theta(E_3)\\ &= \mathrm{d}^4p_3\,\frac{\hat{s}}{q^2}\,\delta\left(\hat{s} - \frac{q^2}{\hat{p}_3^2}\right)\Theta(E_3)\end{aligned} \tag{6.12}$$

the four-dimensional integral over the momentum of the color singlet can be used to eliminate the momentum-conserving δ-distribution in Eq. (6.11) which is consistent with the earlier claim in Eq. (6.5). In the second line of Eq. (6.12) we introduced the dimensionless auxiliary quantity $\hat{p}_3^2 = p_3^2/\hat{s}$ in order to reshape the δ-distribution, that now can be integrated out trivially by combining it with Eq. (6.9). The exact form of $\hat{p}_3$ will become clear in the next subsection when we parametrize the radiation phase space.

[1] For detailed explanations of the d-dimensional phase-space parametrization we want to point to Refs. [34, 35, 38].

6.1.4. Radiation Phase Space

To integrate over the final-state momenta of the emitted partons we consider their phase-space elements in four dimensions,

$$\begin{aligned}\lim_{d\to 4}\left[\mathrm{d}p_i\right] &= \frac{\mathrm{d}^3 p_i}{(2\pi)^3 2E_i}\,\Theta(E_{\max}-E_i)\\ &= \mathrm{d}E_i E_i \frac{\mathrm{d}\Omega_i^{(3)}}{2(2\pi)^3}\,\Theta(E_{\max}-E_i)\,,\end{aligned} \tag{6.13}$$

for $i \in \{4,5\}$. Since soft and collinear divergences do not mix in the formalism of the Nested Soft-Collinear Subtraction scheme, we can parameterize the energies and angles separately. While the energy parametrization is general, a proper choice of parameters for the angles depends on the sector under investigation.

Energy Integration

When the energies are decomposed as

$$E_4 = x_1 E_{\max}, \qquad E_5 = x_1 x_2 E_{\max}. \tag{6.14}$$

with $x_1, x_2 \in [0,1)$, the energy integrations can be written as

$$\mathrm{d}E_4 E_4\,\Theta(E_{\max}-E_4)\;\mathrm{d}E_5 E_5\,\Theta(E_4-E_5) = x_1^3 x_2 E_{\max}^4 \mathrm{d}x_1 \mathrm{d}x_2. \tag{6.15}$$

This parametrization assures the energy ordering $E_4 > E_5$ as we use it in the quark-antiquark channel. If no energy ordering is desired, the equation for E_5 has to be modified. From this definition it is implied that the soft singularities can be extracted by computing the limit in the related variable,

$$\begin{aligned}\mathcal{S}_5 A &= \lim_{x_2\to 0} A,\\ \boldsymbol{\mathcal{S}} A &= \lim_{x_1\to 0} A.\end{aligned} \tag{6.16}$$

Additionally, we are now able to determine the dimensionless variable $\hat{p}_3$, which fixes the partonic center-of-mass energy. As explained in detail below Eq. (4.48), the arbitrary energy scale $E_{\max}$ is set in our computations to the energy of the incoming partons, $E_{\max} = \sqrt{\hat{s}}/2$, so that from $p_3^2 = q^2$ follows[2]

$$\hat{s} = \frac{p_3^2}{\hat{p}_3^2} = \frac{q^2}{1 - x_1 - x_1 x_2 + x_1^2 x_2 \eta_{45}}. \tag{6.17}$$

Angular Integration

The angular measure over the surface of the unit sphere in three dimensions is given in the parametrization of Eqs. (6.3) and (6.4) as

$$\frac{\mathrm{d}\Omega_i^{(3)}}{2(2\pi)^3} = \frac{1}{(2\pi)^2}\frac{\mathrm{d}\cos(\theta_i)}{2}\frac{\mathrm{d}\phi_i}{2\pi}, \tag{6.18}$$

[2]It is trivial to see that Eq. (6.17) introduces additional constraints on the boundaries of the new integration variables, since $\hat{s}$ has to be larger or equal to q^2, and smaller than s. However, in the numerical MC integration this condition can be simply included by discarding all phase-space points that do not pass the check $s > \hat{s} > q^2$.

with $\theta_i \in [0,\pi)$ and $\phi_i \in [0,2\pi)$, for both final-state partons $i \in \{4,5\}$[3]. However, as mentioned earlier, this parametrization is not perfectly suited to separate overlapping singularities an should be adjusted in the four sectors of the two triple-collinear partitions. But first we give a look to the simpler double-collinear partitions.

1) Double-Collinear Partitions

In both double-collinear partitions, $w^{41,52}$ and $w^{42,51}$, the only collinear divergences that appear are divergences where an initial-state particle and a final-state particle become collinear to each other, but not when two final-state partons become collinear. These partitions do not include overlapping singularities by construction and, thus, the angles of the partons can be generated independently. A simple mapping for the polar angles that we choose is

$$\cos(\theta_4) = 1 - 2x_3, \qquad \cos(\theta_5) = 1 - 2x_4 \tag{6.19}$$

with $x_3, x_4 \in [0,1)$, while we perform the mapping of the azimuthal angles linearly. The angular integral then can be written as

$$\frac{\mathrm{d}\Omega_4^{(3)}}{2(2\pi)^3}\frac{\mathrm{d}\Omega_5^{(3)}}{2(2\pi)^3} = \frac{1}{(2\pi)^4}\mathrm{d}x_3\mathrm{d}x_4\frac{\mathrm{d}\phi_4}{2\pi}\frac{\mathrm{d}\phi_5}{2\pi}. \tag{6.20}$$

Summarized, we find in the double-collinear partitions the four-dimensional radiation-phase-space element

$$\lim_{d\to 4}[\mathrm{d}p_4][\mathrm{d}p_5]\Theta(E_4 - E_5) = \frac{\hat{s}^2}{16(2\pi)^4}x_1^3 x_2\,\mathrm{d}x_1\mathrm{d}x_2\mathrm{d}x_3\mathrm{d}x_4\frac{\mathrm{d}\phi_4}{2\pi}\frac{\mathrm{d}\phi_5}{2\pi}. \tag{6.21}$$

Also all independent momenta are fixed by the integrations variables[4],

$$\begin{aligned} &p_1(x_1,x_2,x_3,x_4,\phi_4,\phi_5), \qquad &&p_2(x_1,x_2,x_3,x_4,\phi_4,\phi_5),\\ &p_4(x_1,x_2,x_3,x_4,\phi_4,\phi_5), \qquad &&p_5(x_1,x_2,x_3,x_4,\phi_4,\phi_5). \end{aligned} \tag{6.22}$$

In particular, the dependence of the initial-state momenta on the variables of the radiation-phase-space parametrization comes from the dependence of the partionic center-of-mass energy on them. For the same reason also the boundaries of the rapidity integration and the two Bjorken variables depend on them.

Up to here, we considered the integration over the phase space for double-real radiation with two resolved partons. Based on the previous discourse, we are now able to parameterize the phase space of the subtraction functions where at least one parton is unresolved. The provided definitions yield $\eta_{14} = x_3$ and $\eta_{15} = x_4$, enabling us to derive the collinear limits with

$$\begin{aligned} \mathcal{C}_{41}A &= \lim_{x_3\to 0} A, \qquad &\mathcal{C}_{42}A &= \lim_{x_3\to 1} A,\\ \mathcal{C}_{51}A &= \lim_{x_4\to 0} A, \qquad &\mathcal{C}_{52}A &= \lim_{x_4\to 1} A. \end{aligned} \tag{6.23}$$

[3]Momentum conservation will give additional, non-trivial boundaries for physically meaningful angles. Instead of generating this complicated integration contour, we will simply check each phase-space point for physical correctness in the MC integrator (*i.e.* the only non-trivial condition that needs to be checked is $E_3 \pm p_{3,z} > 0$).

[4]We omit here the explicit dependence on the invariant mass integration variable q to avoid an overloaded notation and focus on the dependencies that are more relevant for the further discussion.

To express the momenta for the subtraction terms related to an IR projector $\hat{\mathcal{O}}$ in a compact form, we introduce the symbol

$$p_i^{\hat{\mathcal{O}}} = \hat{\mathcal{O}}\, p_i. \tag{6.24}$$

In the single-soft limit, we get the set of momenta

$$\begin{aligned} p_1^{\mathcal{S}_5}(x_1,x_2,x_3,x_4,\phi_4,\phi_5) &= p_1(x_1,0,x_3,x_4,\phi_4,\phi_5),\\ p_2^{\mathcal{S}_5}(x_1,x_2,x_3,x_4,\phi_4,\phi_5) &= p_2(x_1,0,x_3,x_4,\phi_4,\phi_5),\\ p_4^{\mathcal{S}_5}(x_1,x_2,x_3,x_4,\phi_4,\phi_5) &= p_4(x_1,0,x_3,x_4,\phi_4,\phi_5),\\ p_5^{\mathcal{S}_5}(x_1,x_2,x_3,x_4,\phi_4,\phi_5) &= p_5(x_1,0,x_3,x_4,\phi_4,\phi_5), \end{aligned} \tag{6.25}$$

and in the double-soft limit

$$\begin{aligned} p_1^{\boldsymbol{\mathcal{S}}}(x_1,x_2,x_3,x_4,\phi_4,\phi_5) &= p_1(0,x_2,x_3,x_4,\phi_4,\phi_5),\\ p_2^{\boldsymbol{\mathcal{S}}}(x_1,x_2,x_3,x_4,\phi_4,\phi_5) &= p_2(0,x_2,x_3,x_4,\phi_4,\phi_5),\\ p_4^{\boldsymbol{\mathcal{S}}}(x_1,x_2,x_3,x_4,\phi_4,\phi_5) &= p_4(0,x_2,x_3,x_4,\phi_4,\phi_5),\\ p_5^{\boldsymbol{\mathcal{S}}}(x_1,x_2,x_3,x_4,\phi_4,\phi_5) &= p_5(0,x_2,x_3,x_4,\phi_4,\phi_5). \end{aligned} \tag{6.26}$$

Following the same strategy we generate the momenta in the collinear limit, *i.e.* for the parton 5 collinear to initial-state parton 1,

$$\begin{aligned} p_1^{\mathcal{C}_{51}}(x_1,x_2,x_3,x_4,\phi_4,\phi_5) &= p_1(x_1,x_2,x_3,0,\phi_4,\phi_5),\\ p_2^{\mathcal{C}_{51}}(x_1,x_2,x_3,x_4,\phi_4,\phi_5) &= p_2(x_1,x_2,x_3,0,\phi_4,\phi_5),\\ p_4^{\mathcal{C}_{51}}(x_1,x_2,x_3,x_4,\phi_4,\phi_5) &= p_4(x_1,x_2,x_3,0,\phi_4,\phi_5),\\ p_5^{\mathcal{C}_{51}}(x_1,x_2,x_3,x_4,\phi_4,\phi_5) &= p_5(x_1,x_2,x_3,0,\phi_4,\phi_5), \end{aligned} \tag{6.27}$$

and, consequently,

$$\begin{aligned} p_1^{\mathcal{C}_{51}\boldsymbol{\mathcal{S}}}(x_1,x_2,x_3,x_4,\phi_4,\phi_5) &= p_1(0,x_2,x_3,0,\phi_4,\phi_5),\\ p_2^{\mathcal{C}_{51}\boldsymbol{\mathcal{S}}}(x_1,x_2,x_3,x_4,\phi_4,\phi_5) &= p_2(0,x_2,x_3,0,\phi_4,\phi_5),\\ p_4^{\mathcal{C}_{51}\boldsymbol{\mathcal{S}}}(x_1,x_2,x_3,x_4,\phi_4,\phi_5) &= p_4(0,x_2,x_3,0,\phi_4,\phi_5),\\ p_5^{\mathcal{C}_{51}\boldsymbol{\mathcal{S}}}(x_1,x_2,x_3,x_4,\phi_4,\phi_5) &= p_5(0,x_2,x_3,0,\phi_4,\phi_5). \end{aligned} \tag{6.28}$$

The momenta as well as the integration boundaries for the y integral and the momentum fractions $\xi_{1/2}$ in all singular limits can be obtained by applying similar rules.
It is important to note, that first the leading singularities need to be extracted before the corresponding parameter is set to zero, for instance

$$\mathcal{C}_{51} F_{\mathrm{LM}}(1_{f_a}, 2_{f_b} \,|\, 4_g, 5_g) \sim \frac{1}{(p_1 \cdot p_5)} \sim \frac{1}{\eta_{51}} = \frac{1}{x_4}, \tag{6.29}$$

where we keep $x_4 \neq 0$ for the divergent term and set $x_4 = 0$ everywhere else.
Additionally, in some subtraction terms for the collinear limits spin correlations need to be taken into account (*c.f.* Eq. (E.34)). Therefore, the knowledge of the vector $\kappa_\perp^\mu$ is required. In the limit $5 \parallel 1$ this vector can be computed by the parametrization of the momentum p_5 in the Sudakov decomposition in terms of the momentum p_1. We find

$$\kappa_\perp^\mu = \big(0, \cos(\phi_5), \sin(\phi_5), 0\big)^{\mathrm{T}}. \tag{6.30}$$

2) Triple-Collinear Partitions

As example for a triple-collinear partition we consider $w^{41,51}$ in the parametrization that was suggested in Refs. [34, 35]. The polar angles in the four sectors can be written as

$$\begin{aligned}
&\text{Sector } (a): && \eta_{14} = x_3, && \eta_{15} = \frac{x_3 x_4}{2},\\
&\text{Sector } (b): && \eta_{14} = x_3, && \eta_{15} = x_3\left(1 - \frac{x_4}{2}\right),\\
&\text{Sector } (c): && \eta_{14} = \frac{x_3 x_4}{2}, && \eta_{15} = x_3,\\
&\text{Sector } (d): && \eta_{14} = x_3\left(1 - \frac{x_4}{2}\right), && \eta_{15} = x_3,
\end{aligned} \tag{6.31}$$

with $x_3, x_4 \in [0, 1)$. This parameter choice guaranties the angular ordering in each sector. Moreover, the symmetry between the sectors (a) and (c), as well as (b) and (d) can be observed easily. Since the meaning of η_{14} and η_{15} is simply exchanged, the angle between the two final-state partons in the related sectors is the same. This angle is given in terms of their polar angles and the difference of their azimuthal angles, ϕ_{45}, so that

$$\phi_5 = \phi_4 + \phi_{45}. \tag{6.32}$$

If the angle between parton 4 and parton 5 is given as

$$\begin{aligned}
&\text{Sectors } (a)\&(c): && \eta_{45} = \frac{x_3(1 - x_4/2)^2}{N_{\mathrm{F}}(x_3, x_4/2, \lambda)},\\
&\text{Sectors } (b)\&(d): && \eta_{45} = \frac{x_3(x_4/2)^2}{N_{\mathrm{F}}(x_3, 1 - x_4/2, \lambda)},
\end{aligned} \tag{6.33}$$

where $\lambda \in [0, 1)$ and

$$N_{\mathrm{F}}(x_3, x_4, \lambda) = 1 + x_4(1 - 2x_3) - 2(1 - 2\lambda)\sqrt{x_4(1 - x_3)(1 - x_3 x_4)}, \tag{6.34}$$

the parameter λ fixes ϕ_{45}. We find

$$\begin{aligned}
\text{Sectors } (a)\&(c): \qquad \sin(\phi_{45}) &= \frac{2\sqrt{\lambda(1-\lambda)}(1 - x_4/2)}{N_{\mathrm{F}}(x_3, x_4/2, \lambda)},\\
\cos(\phi_{45}) &= \pm\sqrt{1 - \sin^2(\phi_{45})},
\end{aligned} \tag{6.35}$$

where the negative sign for the cosine is selected if

$$\frac{2(1 - x_4/2)^2}{N_{\mathrm{F}}(x_3, x_4/2, \lambda)} > 2 + x_4(1 - 2x_3). \tag{6.36}$$

Similarly holds

$$\begin{aligned}
\text{Sectors } (b)\&(d): \qquad \sin(\phi_{45}) &= \frac{2\sqrt{\lambda(1-\lambda)}(x_4/2)}{N_{\mathrm{F}}(x_3, 1 - x_4/2, \lambda)}\\
\cos(\phi_{45}) &= \pm\sqrt{1 - \sin^2(\phi_{45})}
\end{aligned} \tag{6.37}$$

with the minus sign in the second line if

$$\frac{2(x_4/2)^2}{N_{\mathrm{F}}(x_3,1-x_4/2,\lambda)} > 2+(2-x_4)(1-2x_3). \tag{6.38}$$

The angular integrals read in total

$$\begin{aligned}
\frac{\mathrm{d}\Omega_4^{(3)}}{2(2\pi)^3}\frac{\mathrm{d}\Omega_5^{(3)}}{2(2\pi)^3}\Theta_1^{(a/c)} &= \frac{1}{(2\pi)^4}\frac{x_3(1-x_4/2)}{2N_{\mathrm{F}}(x_3,x_4/2,\lambda)}\mathrm{d}x_3\mathrm{d}x_4\frac{\mathrm{d}\phi_4}{2\pi}\frac{\mathrm{d}\lambda}{\pi\sqrt{\lambda(1-\lambda)}},\\
\frac{\mathrm{d}\Omega_4^{(3)}}{2(2\pi)^3}\frac{\mathrm{d}\Omega_5^{(3)}}{2(2\pi)^3}\Theta_1^{(b/d)} &= \frac{1}{(2\pi)^4}\frac{x_3(x_4/2)}{2N_{\mathrm{F}}(x_3,1-x_4/2,\lambda)}\mathrm{d}x_3\mathrm{d}x_4\frac{\mathrm{d}\phi_4}{2\pi}\frac{\mathrm{d}\lambda}{\pi\sqrt{\lambda(1-\lambda)}}.
\end{aligned} \tag{6.39}$$

The notation $\Theta_1^{(a/c)}$ imposes that the equation is valid for both sectors, (a) and (c) of partition $w^{41,51}$, which are defined through the symbols $\Theta_1^{(a)}$ and $\Theta_1^{(c)}$ in Eq. (5.13), respectively. In the second line we use the same notation, just for the sectors (b) and (d) instead of the sectors (a) and (c).
In summary, the radiation phase space for double-real emission in the triple-collinear partition $w^{41,51}$ in the sectors (a) and (c) can be parametrized as

$$\begin{aligned}
\lim_{d\to 4}[\mathrm{d}p_4][\mathrm{d}p_5]\Theta(E_4-E_5)\Theta^{(a/c)} = {}& \frac{\hat{s}^2}{16(2\pi)^4}\frac{x_1^3x_2x_3(1-x_4/2)}{2N_{\mathrm{F}}(x_3,x_4/2,\lambda)}\\
&\times \mathrm{d}x_1\mathrm{d}x_2\mathrm{d}x_3\mathrm{d}x_4\frac{\mathrm{d}\phi_4}{2\pi}\frac{\mathrm{d}\lambda}{\pi\sqrt{\lambda(1-\lambda)}}.
\end{aligned} \tag{6.40}$$

The phase space for the sectors (b) and (d) of the same partition is given by

$$\begin{aligned}
\lim_{d\to 4}[\mathrm{d}p_4][\mathrm{d}p_5]\Theta(E_4-E_5)\Theta^{(b/d)} = {}& \frac{\hat{s}^2}{16(2\pi)^4}\frac{x_1^3x_2x_3(x_4/2)}{2N_{\mathrm{F}}(x_3,1-x_4/2,\lambda)}\\
&\times \mathrm{d}x_1\mathrm{d}x_2\mathrm{d}x_3\mathrm{d}x_4\frac{\mathrm{d}\phi_4}{2\pi}\frac{\mathrm{d}\lambda}{\pi\sqrt{\lambda(1-\lambda)}}.
\end{aligned} \tag{6.41}$$

In analogy to Eq. (6.22) the momenta are now all parametrized in terms of the integration variables,

$$\begin{aligned}
&p_1(x_1,x_2,x_3,x_4,\phi_4,\lambda), \qquad && p_2(x_1,x_2,x_3,x_4,\phi_4,\lambda),\\
&p_4(x_1,x_2,x_3,x_4,\phi_4,\lambda), && p_5(x_1,x_2,x_3,x_4,\phi_4,\lambda).
\end{aligned} \tag{6.42}$$

Also the collinear limits are encoded in the boundaries of these parameters, but they differ in the two sector categories. Next, we will investigate sector (a) representatively for the category of the sectors (a) and (c). Subsequently, we give a closer look to sector (b) as an example for the sectors (b) and (d).

2.1) Collinear Limits in Sector (a)

Soft limits are unchanged with respect to the double-collinear partitions. The relevant collinear limits are

$$\mathcal{C}_{51}A = \lim_{x_4\to 0}A, \qquad \boldsymbol{\mathcal{C}}_1A = \lim_{x_3\to 0}A. \tag{6.43}$$

The momenta for the subtraction terms are then constructed along the same lines as we have shown in Eqs. (6.25) to (6.28) and leading divergences are kept as in the example

of Eq. (6.29). Particularly, the angles of the momenta in the argument of the triple-collinear splitting function cannot be set to zero since this function describes such a leading singularity.
It is important to note that, due to the dependence of the azimuthal angle ϕ_5 on x_3 and x_4, its value will change in the collinear limits. This is contrary to the behavior we have seen in the double-collinear partitions and will not just lead to a change of the treatment of this angle in the construction of the momentum p_5 in the collinear limits, it also has an effect on the transverse κ-vector that appear in the spin correlated limits. In the single-collinear case, where x_4 is going to zero, this vector reads

$$\kappa_\perp^\mu = \Big(0, \cos\big(\phi_5^{\mathcal{C}_{51}}\big), \sin\big(\phi_5^{\mathcal{C}_{51}}\big), 0\Big)^{\mathrm{T}}, \tag{6.44}$$

with

$$\phi_5^{\mathcal{C}_{51}} = \phi_4 + \phi_{45}^{\mathcal{C}_{51}}. \tag{6.45}$$

The angle ϕ_4 is of course not effected by this limit, but ϕ_{45} becomes

$$\sin\big(\phi_{45}^{\mathcal{C}_{51}}\big) = \sqrt{4\lambda(1-\lambda)} \quad \wedge \quad \cos\big(\phi_{45}^{\mathcal{C}_{51}}\big) = -1 + 2\lambda, \tag{6.46}$$

which follows immediately from setting $x_4 = 0$ in Eq. (6.35).
The scalar product of the two κ-vectors in the strongly-ordered triple-collinear limits (*c.f.* Eq. (E.55)) then reads

$$[\kappa_\perp \cdot \bar{\kappa}_\perp]^2 = (-1+2\lambda)^2(1-x_3). \tag{6.47}$$

2.2) Collinear Limits in Sector (b)

In sector (b) the collinear limits can be extracted with the operators

$$\mathcal{C}_{45}A = \lim_{x_4\to 0} A, \qquad \boldsymbol{\mathcal{C}}_1 A = \lim_{x_3\to 0} A. \tag{6.48}$$

In particular, the single-collinear limit fulfills $\eta_{15} \to \eta_{14}$ as well as $\eta_{45} \to 0$. Of course, the soft limits are the same as in the other scenarios that we already discussed. With these relations between the limits and parametrization all momenta as well as the integration boundaries can be obtained through the same strategy that we applied previously. However, the angles have to be kept in the arguments of the triple-collinear splitting function. It is just important to note, that the leading divergence of the angle between both final-state partons has to be taken carefully in the single-collinear limit,

$$\mathcal{C}_{45}F_{\mathrm{LM}}(1_{f_a}, 2_{f_b} \,|\, 4_g, 5_g) \sim \mathcal{C}_{45}\frac{1}{(p_4\cdot p_5)} \sim \mathcal{C}_{45}\frac{1}{\eta_{45}} = \frac{1}{\eta_{45}^{\mathcal{C}_{45}}}, \tag{6.49}$$

with

$$\eta_{45}^{\mathcal{C}_{45}} = \mathcal{C}_{45}\eta_{45} = \frac{x_3(x_4/2)^2}{N_{\mathrm{F}}(x_3,1,\lambda)} = \frac{x_3(x_4/2)^2}{4\lambda(1-x_3)}. \tag{6.50}$$

Hence, the angular parameter η_{45} is not the same in the single-collinear limit and in the fully-resolved phase space as maybe naively expected and as it was in the previously shown single-collinear limits. This difference comes from the fact, that the azimuthal angle is considered to be zero in the single-collinear limit,

$$\phi_{45}^{\mathcal{C}_{45}} = 0. \tag{6.51}$$

For the κ-vector that appears in several single-collinear limits it is convenient to introduce a decomposition of the structure

$$\kappa_\perp^\mu = \sqrt{\lambda}\, r^\mu + \sqrt{1-\lambda}\, a^\mu, \tag{6.52}$$

where the vector r^μ is the same that is present in the counterterm in Eq. (5.99) and was described in detail below Eq. (5.102)[5],

$$r^\mu = \big(0, -\cos(\phi_4)\cos(\theta_4), -\sin(\phi_4)\cos(\theta_4), \sin(\theta_4)\big)^{\mathrm{T}}. \tag{6.53}$$

The auxiliary vector a^μ is another unit vector, $a^2 = -1$, which reads

$$a^\mu = \big(0, -\sin(\phi_4), \cos(\phi_4), 0\big)^{\mathrm{T}}. \tag{6.54}$$

In the strongly-ordered triple-collinear limit the scalar product of the transverse vectors is

$$[\kappa_\perp \cdot \overline{\kappa}_\perp]^2 = \lambda(1-x_3). \tag{6.55}$$

The parametrization of the subtraction functions in the remaining sectors is straightforward by applying symmetry relations. Finally, the other triple-collinear partition, $w^{42,52}$, can be obtained by replacing the indices 1 and 2 with each other everywhere.
At this point we have completed the theoretical picture of the Nested Soft-Collinear Subtraction scheme and combined it with a suitable phase-space decomposition in the spirit of the original Sector-Improved Residue Subtraction scheme. These results can be implemented in a numerical code in order to make predictions for fully-differential cross sections with NNLO QCD precision.

6.2. Implementation

We implemented the Nested Soft-Collinear Subtraction scheme in a `FORTRAN` code with the aim to build a flexible tool that gives the opportunity for evaluating Higgs-Strahlung cross sections in the SM, but also in theories beyond the SM. Moreover, we construct the code in a way that it can be easily extended to other arbitrary processes with a colorless final state at Born level.

6.2.1. Phase-Space Mapping

For the prediction of color-singlet cross sections we have to face an integration over the phase space, the invariant mass and the rapidity of the color singlet, ending up in an eight-dimensional integral. To solve such high dimensional integrals Monte Carlo (MC) approaches are suited best. They deliver precise results in reasonable computation time. In particular, we perform the integrations with the widely used `VEGAS` algorithm [281, 282] by a link of our tool to its implementation in the `Cuba` library [283, 284]. This well-established library comes with the advantage that it is parallelized and allows for a fast evaluation of the integrand while using the hardware resources efficiently. Based on importance sampling [285, 286], a random number r is generated in the range 0 to 1

[5] In sector (d) the vector r^μ reads

$$r^\mu = \big(0, \cos(\phi_4)\cos(\theta_5), \sin(\phi_4)\cos(\theta_5), -\sin(\theta_5)\big)^{\mathrm{T}}.$$

for each dimension of the integral. These numbers have to be mapped to the integration variables. For most of them this mapping is trivial, but, anyhow, we think it is worth to spend a few words about it:

Generating the Invariant Mass of the Color Singlet

The first integration variable that we generate is the invariant mass of the color singlet. The lower boundary is given by $q_{\min} = M_V + M_H$, the upper boundary is the hadronic center-of-mass energy, $q_{\max} = \sqrt{s}$, *c.f.* subsection 6.1.1. An invariant mass in this range can be linked to the random number $r^{(q)}$ as

$$q^2 = (s - q_{\min}^2)\, r^{(q)} + q_{\min}^2, \quad \text{with} \quad r^{(q)} \in (0,1), \tag{6.56}$$

which introduces an additional Jacobian weight factor according to

$$\mathrm{d}q^2 = (s - q_{\min}^2)\, \mathrm{d}r^{(q)}. \tag{6.57}$$

Generating the Radiation Phase Space

The next random numbers can be used to generate the phase space of the real-emitted partons. For the energy parameters the mapping is trivial,

$$\begin{aligned} x_1 &= r^{(1)}, \quad \text{with} \quad r^{(1)} \in (0,1), \\ x_2 &= r^{(2)}, \quad \text{with} \quad r^{(2)} \in (0,1), \end{aligned} \tag{6.58}$$

as well as for the parameters that characterize the polar coordinates,

$$\begin{aligned} x_3 &= r^{(3)}, \quad \text{with} \quad r^{(3)} \in (0,1), \\ x_4 &= r^{(4)}, \quad \text{with} \quad r^{(4)} \in (0,1). \end{aligned} \tag{6.59}$$

These substitutions have also trivial weights,

$$\mathrm{d}x_i = \mathrm{d}r^{(i)}, \quad \text{for} \quad i \in \{1,2,3,4\}. \tag{6.60}$$

The azimuthal angle ϕ_4 in the range 0 to 2π can be related to $r^{(\phi)}$ by a linear rescaling,

$$\phi_4 = 2\pi r^{(\phi)}, \quad \text{with} \quad r^{(\phi)} \in (0,1), \tag{6.61}$$

and the replacement

$$\frac{\mathrm{d}\phi_4}{2\pi} = \mathrm{d}r^{(\phi)}. \tag{6.62}$$

In the double-collinear partition the second azimuthal angle, ϕ_5, can obviously be constructed with a similar relation. More interesting is the situation in the triple-collinear partitions. There, the azimuthal angle is associated with the parameter that we called λ. Even though λ receives values between 0 and 1, it is more convenient to write it as

$$\lambda = \sin^2\left(\frac{\pi}{2} r^{(\lambda)}\right), \quad \text{with} \quad r^{(\lambda)} \in (0,1), \tag{6.63}$$

so that

$$\frac{\mathrm{d}\lambda}{\pi\sqrt{\lambda(1-\lambda)}} = \mathrm{d}r^{(\lambda)}. \tag{6.64}$$

The reason for this mapping lies in the better numerical stability, because of the integrable singularities that show up in the denominator of the last equation in the limits λ going to zero or λ close to one which can be avoided in this way.

Generating the Rapidity of the Color Singlet

Up to here, the order of the integration-parameter mapping has not been important and we have the freedom to generate the previous variables in arbitrary order. For the y integration the situation is different since its boundary conditions depend on all before fixed values. The mapping can be done according to

$$y = \ln(\tau)\left(\frac{1}{2} - r^{(y)}\right), \quad \text{with} \quad r^{(y)} \in (0,1) \tag{6.65}$$

with the replacement

$$\mathrm{d}y = |\ln(\tau)|\,\mathrm{d}r^{(y)}. \tag{6.66}$$

As seen in below Eq. (6.10), τ is the ratio of the partonic center-of-mass energy and the hadronic collision energy. The partonic center-of-mass energy is computed according to Eq. (6.17) which in turn depends on η_{45} which is determined by Eq. (6.33). Following this chain of substitutions, it becomes obvious that τ relies on all previously introduced random numbers.

Constituents of the Color Singlet

The described procedure provides us with the full knowledge about the momentum of the color singlet as a single particle, as well as the momenta of all involved partons. But, in order to get the entire information about the kinematics of the final state, the momenta of the constituents that together build the color singlet is required. These momenta can be constructed with the help of standard phase-space generators. In our tool we use an algorithm for MC generators that was proposed in Ref. [287]. For the Higgs-Strahlung process, where the color singlet consists out of two particles, the idea is to generate the momenta of the vector boson and the Higgs boson in the rest frame of the color singlet and subsequently boost them into the partonic center-of-mass system. The advantage of this method lies in the simplicity of the two-particle phase space in their common rest frame. As an additional feature, the before mentioned algorithm extends the strategy for generating phase-space momenta by iterative generation of two-particle decays and boosts to an arbitrary number of final-state particles and, thus, provides an ideal, but also simple, tool for possible extension to more complex color singlets in future applications of our code. The construction of the vector boson and Higgs momenta introduces two new degrees of freedom, so that the total number of integration parameters adds up to ten for the Higgs-Strahlung production mechanism in its most complex contribution.

6.2.2. Matrix Elements

When a phase-space point is generated, the momenta have to be plugged in into the squared matrix elements. We computed the squared matrix elements for LO and NLO diagrams with the Feynman rules which are listed in Appendix A. These computations are straightforward and standard, they do not come with any complications. The same is also true for squared tree-level single-real emission amplitudes with spin correlations,

the only difference to the standard approach for computing squared matrix elements is the replacement of the gluon polarization vectors. For the subtraction terms they have to be replaced by the corresponding κ-vector, in the related counterterm we need a replacement of the polarization vector with the vector r^μ. In contrast to the LO and NLO amplitudes, we rely on known results for most of the NNLO matrix elements and just recompute them for the real-virtual corrections. The interference term of the one-loop real-virtual corrections with the tree-level single-real emission diagrams were calculated with the help of the `Mathematica` [252] library `Package-X` [288, 289] analytically. The validity of our results was cross checked with high numerical precision against `OpenLoops` [290] as well as another independent analytic computation [291], finding full agreement. The form factors for NNLO double-virtual corrections where taken from Ref. [56], they multiply with the squared LO matrix element that we calculated by ourselves as mentioned before. For completeness we recapitulate them in section B.2. For an efficient evaluation of tree-level amplitudes with double-real radiation we use `MadGraph`'s [292] standalone matrix element option that is based on `ALOHA` [293] which automatically writes a `HELAS` [294] library for Feynman diagrams in the helicity-matrix-element formalism.

6.2.3. Links to External Libraries

Next to the links of our Event Generator to the `Cuba` and `HELAS` libraries, we make connections to other established libraries to ensure efficiency and compatibility to common scientific standard.

Parton Distribution Functions

Since standardized PDF sets in agreement with the Les Houches Accords are provided as numerical grids in the `LHAPDF` format, we connect our tool with the `LHAPDF` [295, 296] framework. This gives us the freedom to use a wide range of modern PDF sets from various collaborations like CTEQ [297], MSHT [298, 299], NNPDF [300], and many others.

Polylogarithms

One of the main bottlenecks for a good performance of our program is the evaluation of polylogarithms. In NNLO calculations they appear up to weight four. We use an implementation provided by the `Polylogarithm` package [301] that is highly optimized for fast numerical evaluation. This implementation is an adaption of the algorithms presented in Refs. [302, 303] and inspired by `SPheno` [304, 305].

Passarino-Veltman Integrals

Beyond the calculation of Drell-Yan-like Higgs-Strahlung we adapt the implementation of the gluon-initiated Higgs-Strahlung process for ZH production at $\mathcal{O}(\alpha_s^2)$ from `vh@nnlo`[6]. We modify the phase-space integration so that we are able to compute distributions for arbitrary IR-safe observables. The amplitudes for this implementation were

[6] We do not include the K-factor to obtain an approximation of the $\mathcal{O}(\alpha_s^3)$ corrections in the heavy top-mass limit as done in `vh@nnlo`. These corrections are very large, they are usually around 100 %, but the K-factor is in general not flat bin-by-bin for differential cross sections and would skew our results.

taken from Ref. [109]. They are expressed in terms of scalar Passarino-Veltman integrals [306]. In order to evaluate these one-loop integrals we link our code to `LoopTools` [307].

6.2.4. Differential Cross Sections

The histograms for differential cross sections are filled with information from the `VEGAS` implementation that `Cuba` provides. In particular, we need the weight of each phase-space point so that we can evaluate the integral value and the corresponding uncertainty in each bin of the histogram independently as `Cuba` will return the total inclusive cross section only. Additionally, the parallelization feature requires the usage of inter-process communication (IPC) techniques for saving the histograms at the end of the integration procedure. We use IPC shared memory which is not natively available in `FORTRAN`, but can be made accessible by a wrapper written in `C`.
The binning itself is performed in two steps: First, the integrand is evaluated in several iterations with the aim to optimize the grid of the `VEGAS` integration. Subsequently, the optimized grid is used for the actual event generation in a single iteration. Only events that are generated during the second step are included in the histograms.

7 Results

Contents

In this chapter, we apply our implementation of the Nested Soft-Collinear Subtraction scheme to predict differential cross sections for Higgs-Strahlung. In section 7.1, we consider the SM and verify the correctness of our code with cross-checks against established tools. That at hand, we move on in section 7.2 to study differential cross sections taking into account phenomenological effects of BSM theories.
All distributions in the following are evaluated for 13.6 TeV proton-proton collisions, using the `PDF4LHC21_40` PDF set. Moreover, the factorization and renormalization scales are set both equal to the invariant mass of the Higgs-vector boson system, $\mu_{\mathrm{F}} = \mu_{\mathrm{R}} = M_{VH}$.

7.1. Differential Cross Sections in the Standard Model

To validate the implementation of the subtraction scheme, we compare the output with results that can be produced with `vh@nnlo`. Next to the fully-inclusive cross sections that are found to be in perfect agreement for different parameter settings, the most important check concerns the differential cross section for the VH system's invariant mass spectrum as an analytic computation of it is accessible with `vh@nnlo`[1].
In the first test, we compare the NNLO QCD distributions for the Drell-Yan-like mechanism of our new implementation in `history` with `vh@nnlo` for WH and ZH production as illustrated in Figure 7.1 and Figure 7.2, respectively. It is notable that the analytic results with `vh@nnlo` for each bin is approximated as a Riemann sum of five invariant mass values that are equally distributed over the bin itself. For both distributions this leads us to the conclusion that `history` is able to reproduce the spectra ideally. A systematic mismatch in the first bin, that can be observed for WH as well as ZH creation, is expected due to the approximation of the result with `vh@nnlo` since the VH

[1] Analytic computation means in this context, that the differential partonic cross section is evaluated by fixing the integration over the virtuality q^2 to M_{VH}^2 with a δ-distribution,

$$\frac{\mathrm{d}\hat{\sigma}}{\mathrm{d}M_{VH}} \sim \int \mathrm{d}q^2\, \delta\big(q^2 - M_{VH}^2\big).$$

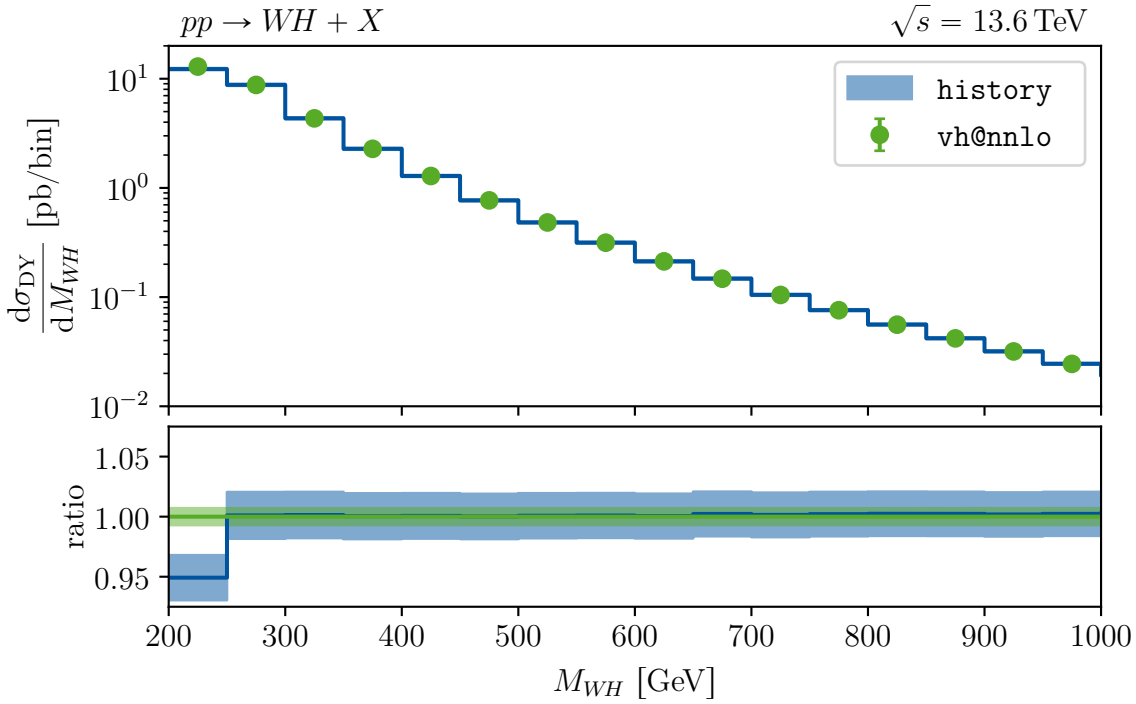

Figure 7.1.: Invariant mass spectrum for the Drell-Yan-like cross section $pp \to WH + X$ at NNLO in the SM. The upper panel shows the spectra computed with `history` (blue line) and `vh@nnlo` (green dots). The lower panel the illustrates their ratios normalized to the `vh@nnlo` distribution. The shaded band indicates the statistical MC uncertainty.

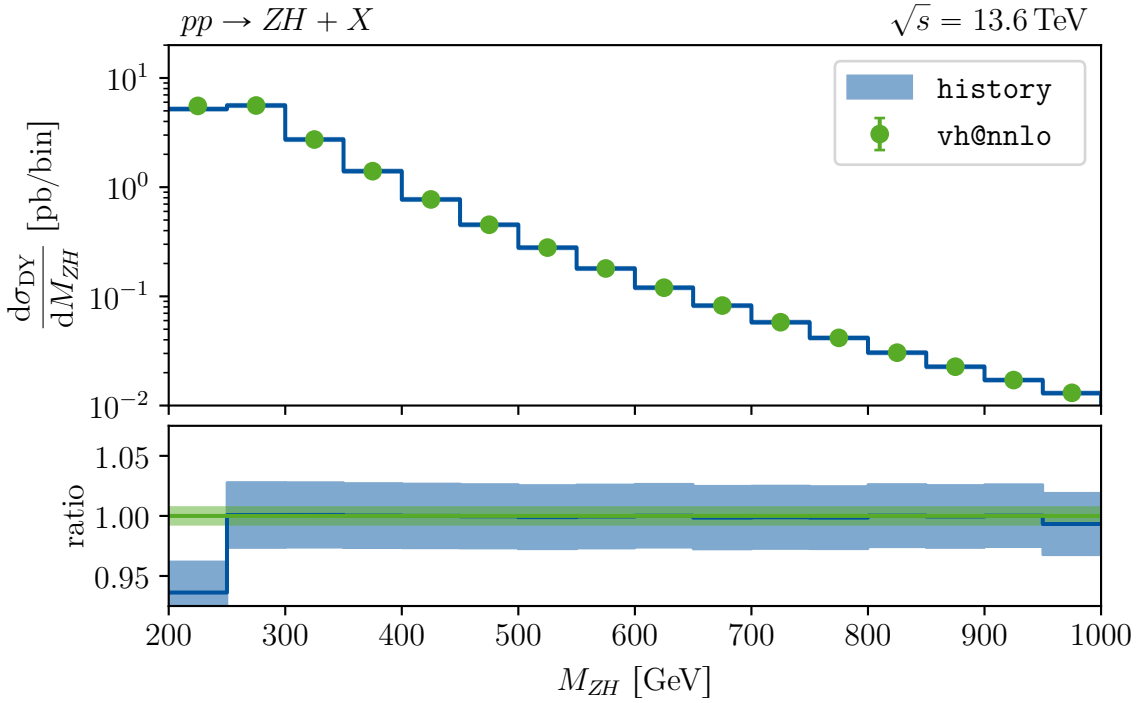

Figure 7.2.: Invariant mass spectrum for the Drell-Yan-like cross section $pp \to ZH + X$ at NNLO in the SM. The upper panel shows the spectra computed with `history` (blue line) and `vh@nnlo` (green dots). The lower panel the illustrates their ratios normalized to the `vh@nnlo` distribution. The shaded band indicates the statistical MC uncertainty.

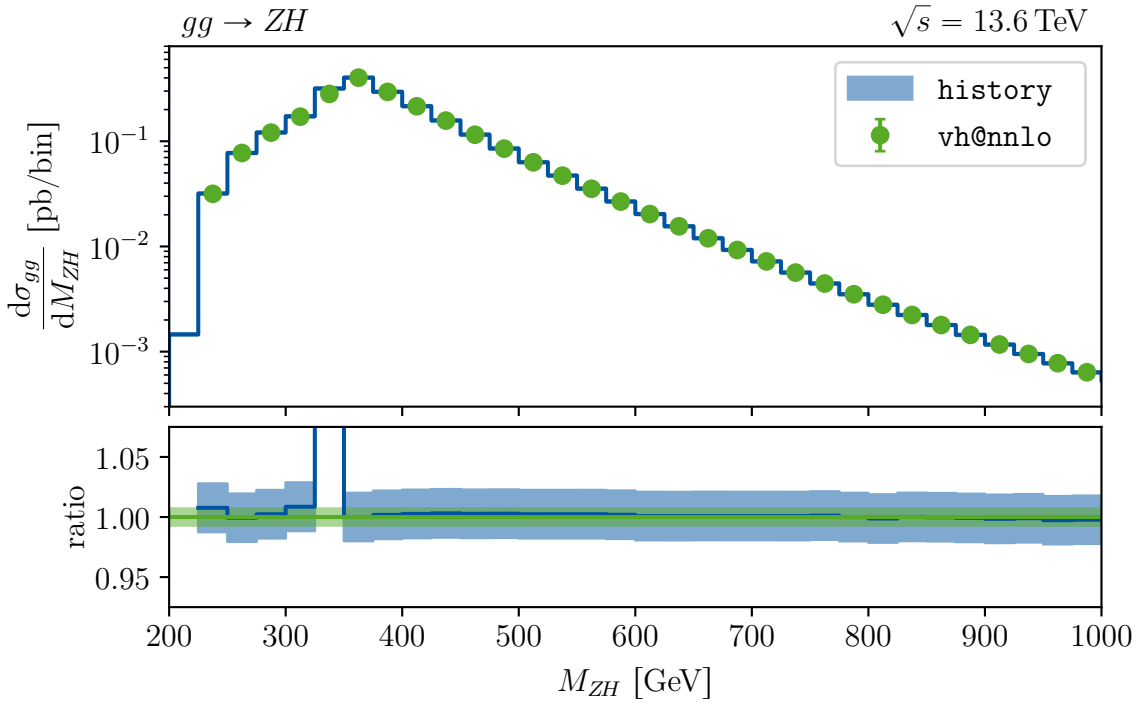

Figure 7.3.: Invariant mass spectrum for the gluon-induced cross section $gg \to ZH$ at $\mathcal{O}(\alpha_s^2)$ in the SM. The upper panel shows the spectra computed with `history` (blue line) and `vh@nnlo` (green dots). The lower panel the illustrates their ratios normalized to the `vh@nnlo` distribution. The shaded band indicates the statistical MC uncertainty.

production threshold lies inside. In case of a WH final state, just four of the five points that are evaluated in this bin are unequal to zero, for ZH only three do not vanish. Moreover, the chosen invariant mass values for the `vh@nnlo` calculation are not equally distributed over the non-vanishing part of the bin anymore. However, in all other bins in the distributions, the agreement between `history` and `vh@nnlo` is at the permille level and deviations of the results are around 0.2 %. This is significantly better than the estimated MC uncertainties in the shaded band let expect, which are of the order 1 to 2 %. Hence, we conclude that our estimates of statistical errors are too conservative and the performance of `history` is even better than indicated.

Another important cross-check verifies the correctness of the phase-space integration and histogramming procedure for the gluon-induced mode. As mentioned in the last chapter, the matrix elements for the $\mathcal{O}(\alpha_s^2)$ contribution were taken from `vh@nnlo`, but the phase-space integration was modified in order to allow for the extraction of fully-differential cross sections. Even though this is just a $2 \to 2$ process without IR singularities so that no subtraction is necessary, we have to ensure that no mistakes are made. The flawless implementation is confirmed by the results shown in Figure 7.3, where the `history` output matches the one of `vh@nnlo` again perfectly. The two outliers in the first bin and in the bin around an invariant mass value of 350 GeV originate again from the approach that we use to obtain the values with the analytic computation. In particular, we have chosen smaller bins and approximated their results with `vh@nnlo` using just a single value in its center. Since the center of the first bin is below the ZH threshold, no number is provided by `vh@nnlo` and no comparison for it can be

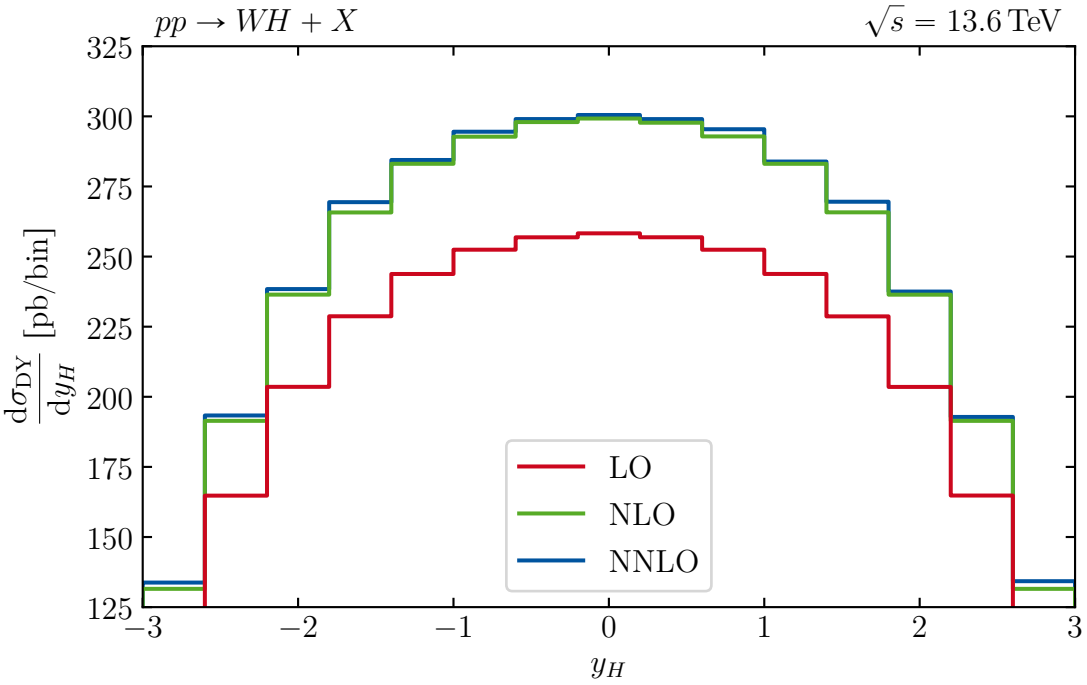

Figure 7.4.: Higgs rapidity spectrum for the Drell-Yan-like cross section of the process $pp \to WH + X$ at LO (red line), NLO (green line), and NNLO (blue line) in the SM.

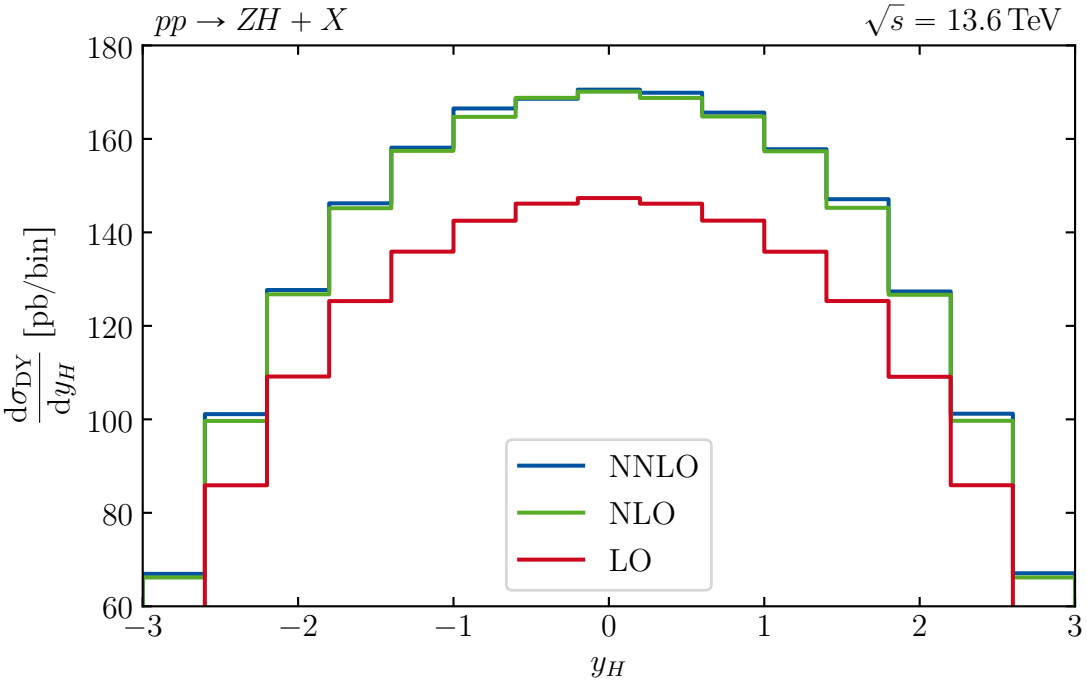

Figure 7.5.: Higgs rapidity spectrum for the Drell-Yan-like cross section of the process $pp \to ZH + X$ at LO (red line), NLO (green line), and NNLO (blue line) in the SM.

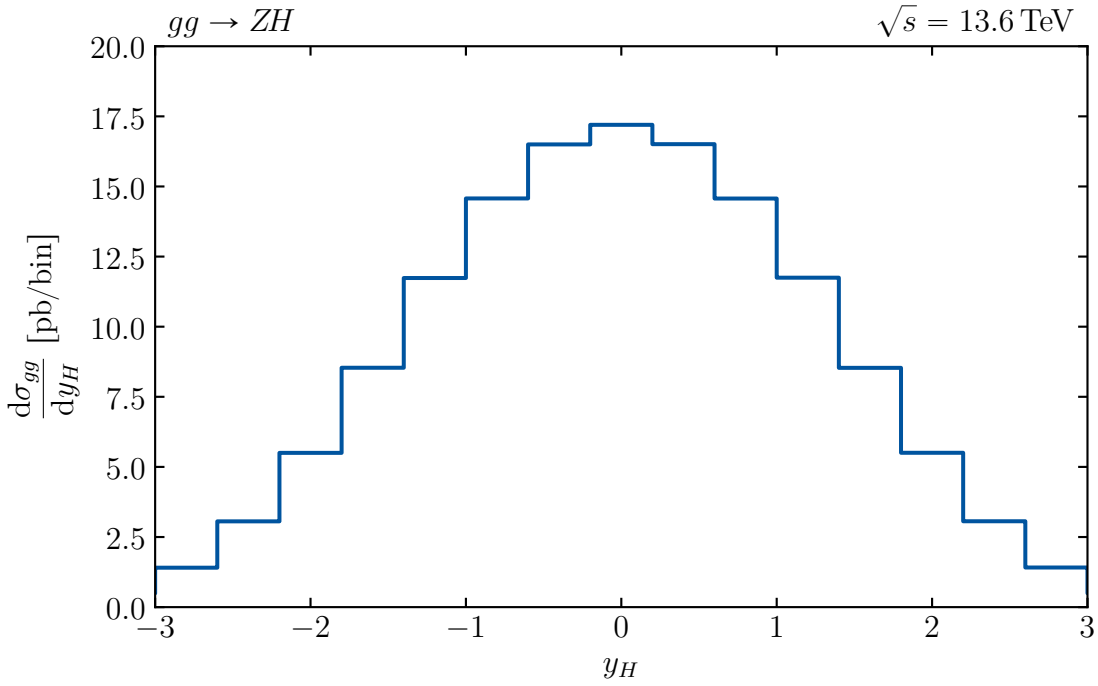

Figure 7.6.: Higgs rapidity spectrum for the gluon-induced cross section $gg \to ZH$ at $\mathcal{O}(\alpha_s^2)$ in the SM.

made. The other bin where `history` and `vh@nnlo` do not agree is around the top-pair production threshold at which a resonance of the triangle and box diagrams with top-quark loops arises. While `history` covers this resonance, the `vh@nnlo` result does not resolve it by construction and thus underestimates the bin content. However, the fully inclusive cross sections calculated with both programs do not show any deviations. As a final remark, we notice again that in all other bins the numbers coincide at permille level while statistical MC uncertainties are overestimated in agreement with the previous observation that we handle them too conservative.
Convinced by the validity of our code, we study a differential cross section for an observable that cannot be investigated with `vh@nnlo`, only with other tools like `MCFM`. As an example, the spectra for the rapidity of the Higgs boson, denoted by y_H, in case of Drell-Yan-like production for WH and ZH final states are given in Figure 7.4 and Figure 7.5, respectively. The symmetry in shape for both Drell-Yan-like processes can be clearly seen and, additionally, the well-known behavior of having large NLO corrections, but good convergence at NNLO can be recognized. In contrast, the gluon-induced component, *cf.* Figure 7.6, has a sharper peak at $y_H = 0$ in its rapidity distribution and is falling steeper when approaching higher absolute values.

7.2. Differential Cross Sections Beyond the Standard Model

Beside fully-differential cross section for Higgs-Strahlung in the SM, `history` allows to make predictions for the Drell-Yan-like contributions in the 2HDM and the B–L Model. For the 2HDM these results can be obtained by rescaling the SM distribution, so we

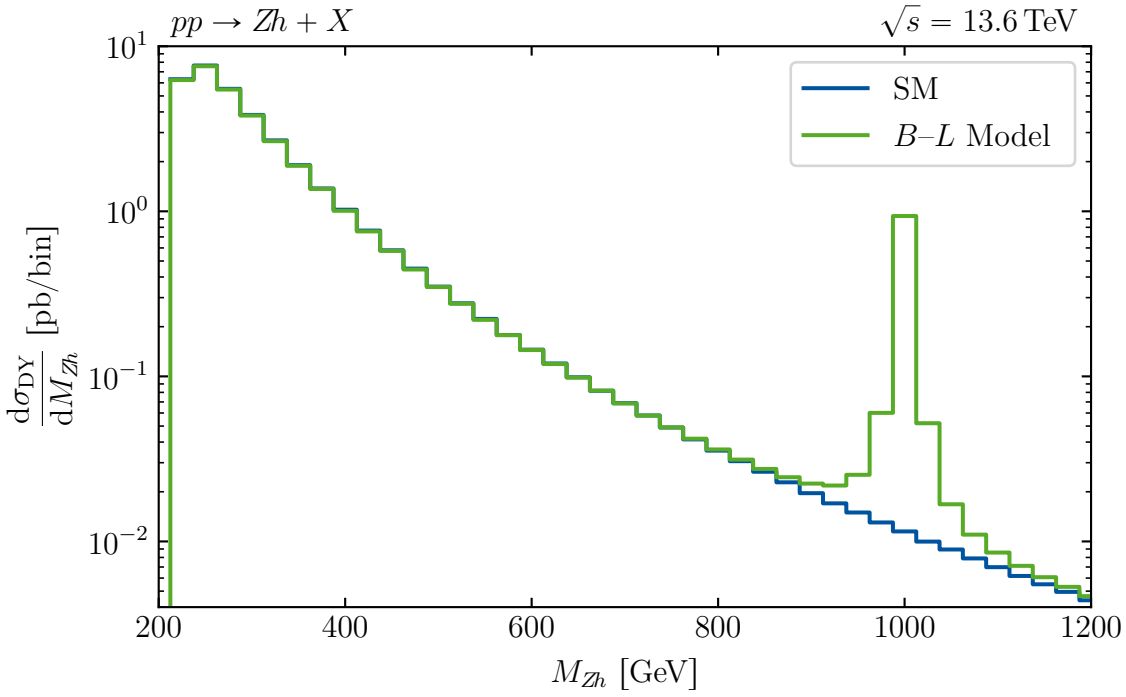

Figure 7.7.: Invariant mass spectrum for the Drell-Yan-like cross section $pp \to Zh + X$ at NNLO in the SM (blue line) and the B–L Model (green line).

refrain from showing them here. As discussed in subsection 2.2.3, the modifications of the Drell-Yan-like mechanism in the B–L Model are more complex. We will shown an exemplary distribution to outline the phenomenological impact of introducing the local $\mathbf{U}(\mathbf{1})_{B-L}$ symmetry in subsection 7.2.1. Finally, in subsection 7.2.2, we return to the primary motivation of this project and extend the set of observables that are used to investigate the R^{VH} double ratio that we have seen in section 2.3.

7.2.1. B–L Model

Due to the presence of the Z' boson, kinematic distributions in the B–L Model have different shapes compared to the SM. Current experimental searches reveal that this new boson most likely is very heavy if it exists. The final data from LEP2 [308] give constraints for a lower bound on the B–L breaking scale $v' = M_{Z'}/(2g_1') \geqslant 3.45\,\text{TeV}$ at 95 % confidence level for $M_{Z'} \gg 200\,\text{GeV}$ [309]. To gain a feeling for the qualitative impact of the B–L Model in our theoretical case study we fix the mass of the Z' boson to $M_{Z'} = 1\,\text{TeV}$, its decay width to $\Gamma_{Z'} = 5\,\text{GeV}$, and choose the new coupling parameter to be $g_1' = 0.145$, so that v' takes the lowest possible value[2]. Here, we are interested in the lighter, SM-like Higgs boson h that corresponds to the observed scalar boson with a mass of $M_h = 125\,\text{GeV}$. This Higgs boson differs from the SM Higgs since its mass eigenstate is a mixture of two isospin eigenstates, where the second one originates from the newly introduced scalar singlet. We set the related mixing angle to $\alpha = 0.11$.
A comparison of the invariant mass spectra of this model and the SM is shown in Fig-

[2]Measurements in hadron collisions with the ATLAS and CMS experiments hint for even larger masses of the Z' bosons, $M_{Z'} > 4\,\text{TeV}$ [310, 311].

ure 7.7. The low invariant mass region is very similar for both models and effects from the heavy Z' bosons grow when the invariant mass increases, leading to a resonance peak when the s-channel Z' boson is produced on-shell. Even though the change in the total cross section is small comparing the SM and B–L Model, the large invariant mass region is highly sensitive to this New Physics scenario.

7.2.2. R^{VH} Double Ratio

Turning to the double ratio, it is worth to mention that it for the first time has been used to extensively study the phenomenological impact of the 2HDM on inclusive Higgs-Strahlung cross sections in Ref. [99], leading to the conclusion that further studies in particular kinematic regions of differential cross sections can improve the experimental and theoretical significance of the effects observed therein. The follow-up study in Ref. [115] then has been extended the double ratio of inclusive cross sections to differential cross sections, as described in section 2.3, for two selected observables. The observables that have been chosen were the invariant mass of the Higgs-vector boson system and the transverse momentum of the Higgs boson. Moreover, Ref. [115] did not just investigate the impact of the 2HDM, instead more possible BSM scenarios have been taken into account, *e.g.* higher dimensional operator, vector-like quarks, and others. The exciting results of this work led to the conclusion that studying more observables and models is convenient. However, the framework consisting out of `vh@nnlo` linked to `MCFM` used in the original work does not easily allow for the necessary flexibility that is needed for this purpose. As we have now the full control within the `history` framework we can perform such analyses in future projects.
As a first result, we present the R^{VH} double ratio for the same models as shown in Figure 2.7 in chapter 2, but as a rapidity spectrum of the Higgs boson instead of the invariant mass distribution. To recapitulate, the three models in the previous plot are the SM itself, as well as SMs with a modified top-to-Higgs Yukawa coupling, which is denoted by y_t. The first modification does not have such a coupling, $y_t = 0$. The second model has a doubled Yukawa coupling with respect to the SM, $y_t = 2y_t^{\mathrm{SM}}$, where y_t^{SM} is the usual SM value. The outcome is depicted in Figure 7.8. Of course, the symmetry of the distributions is not broken by New Physics effects, but it can be clearly observed that the double ratio falls steeper for increasing absolute values of the Higgs rapidity when the Yukawa coupling decreases. Additionally, the ratio is significantly larger for small top-to-Higgs couplings. That means that the non-Drell-Yan-like contribution, which is here just the gluon-induced component, has a higher impact on the total cross section. This stems from the behavior we have discussed in chapter 2, arguing that the triangle and box diagrams interfere destructively in the SM. These destructive interference effects are enhanced when the Yukawa coupling increases, lowering the non-Drell-Yan-like contribution, while destructive interference effects are not present when the box diagrams vanish due to a zero Yukawa coupling, giving rise to larger non-Drell-Yan-like contributions. The Drell-Yan-like component instead is not affected at all by the change of the Yukawa coupling and, hence, the same in all three models. It corresponds to the NNLO distribution in Figure 7.5. In summary, the double ratio in Figure 7.8 reveals also for the rapidity spectrum high sensitivity to BSM physics making it an interesting observable for experimental searches.

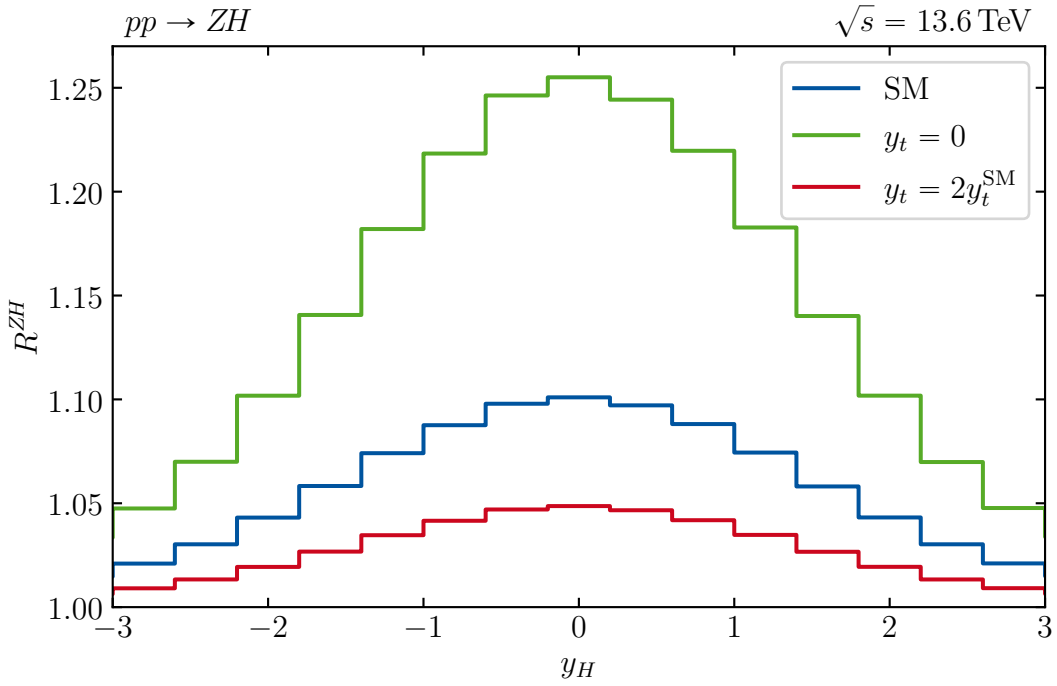

Figure 7.8.: Higgs rapidity spectrum of the double ratio $R^{ZH} \equiv R^{ZH}(y_H)$. The blue line shows the SM prediction, the green line represents a modified SM without a top-quark Yukawa coupling, and the red line a model with a top-quark Yukawa coupling that is the double of the SM value.

8 Conclusion

In this thesis, we investigated the Higgs-Strahlung production mechanism, where a Higgs boson is produced in association with a massive vector boson. Its phenomenological importance in the SM is due to a distinctive experimental signature of the tag on the vector boson. This helps to separate the Higgs signal from the background noise. Therefore, the measurement in the Higgs-Strahlung channel has taken a leading role in the breakthrough discovery of the Higgs decay into a pair of bottom quarks, $H \to b\bar{b}$. With the increasing precision of collider experiments, the Higgs-Strahlung process can also serve as a discovery tool in the search for New Physics. Particularly, the gluon-induced subprocess is sensitive to various possible BSM phenomena. To make these effects experimentally accessible, an observable such as the R^{VH} double ratio is key. With the `history` framework that was developed in this project, the set of kinematic distributions of the double ratio can be extended to arbitrary observables. The presented framework is designed to be flexible, so that new models can be easily incorporated and studied. Here, we have, for the first time, looked at the double ratio of the Higgs rapidity spectrum and compared the SM with two simple theories that have modified top-to-Higgs Yukawa couplings. We have demonstrated that this double ratio also shows different characteristics for the different models, making it an interesting observable for experimental measurements in the hunt for New Physics. Although the choice of models for this study was driven by theoretical motivations to investigate the qualitative behavior of BSM effects, our tool can be used to study phenomenologically more relevant theories.

For this purpose, the 2HDM and the B–L Model are implemented, but further extensions are planned. The changes coming with the B–L Model significantly impact the Drell-Yan-like Higgs-Strahlung subprocess and not only the gluon-induced contribution. Thus, we have also studied them in this work. As expected, the presence of the newly introduced heavy Z' vector boson leads to an s-channel resonance, which can be observed in the invariant mass distribution of the cross section.

The program `history` itself is based on the Nested Soft-Collinear Subtraction scheme, enabling calculations of fully differential cross sections up to NNLO precision. We have reviewed the concepts and ideas of this scheme based on a small number of guiding principles. Then we presented in detail all the ingredients, including the full list of subtraction terms and an in-depth description of the phase-space parametrization, necessary for an actual implementation of color-singlet production that is initiated by a quark-antiquark pair at LO, such as Drell-Yan-like Higgs-Strahlung. The outcome is an efficient and flexible tool. Indeed, all plots made with `history` in this thesis were produced with a single laptop with an Intel® Core™ i7-12700H processor without using computer-cluster resources.

With this novel program at hand, the phenomenology of Higgs-Strahlung can be explored in a wide variety of theories in the future, and extensions to include models

like the MSSM or model-independent approaches like SMEFT seem to be the natural next step. In this regard, the inclusion of bottom quark-induced Higgs-Strahlung, $b\bar{b} \to VH + X$, where the Higgs couples directly to an incoming bottom or antibottom quark, would be beneficial. These contributions are negligible in the SM, but the bottom-to-Higgs Yukawa coupling is enhanced in many BSM scenarios giving rise to substantial impact of these terms. In addition, a deeper analysis of the models that are already part of `history` would be desirable, *i.e.* the 2HDM and the B–L Model could be systematically studied to enlarge the set of observables that could be used in experimental searches for New Physics exploiting the full potential of the R^{VH} double ratio.
The current version of `history` is private, but we aim to merge it with `vh@nnlo` and `SusHi` with the goal of providing a user-friendly open-source code to the particle physics community. In this context, it would be advantageous to enlarge the number of processes to allow for fully-differential predictions of cross sections for Higgs production via gluon fusion. However, this is beyond the scope of this thesis.

A

Feynman Rules

Contents

In this appendix, we summarize the Feynman rules for computing the diagrams that contribute to the Higgs-Strahlung process. In section A.1 we show the set of rules for computations in the SM. The rules for the BSM theories discussed in this thesis are given in section A.2 and section A.3 for the 2HDM and the B–L Model, respectively. In the literature many different signs and conventions are used. In order to avoid confusion, our notation can be matched with the resource for Feynman rules presented in Ref. [312] by fixing their general sign parameters to $\eta = \eta_Z = 1$.
Additionally, we want to recap the usual relations among the parameters in the EW sector to make results easier comparable,

$$e = g\sin(\theta_{\mathrm{W}}), \qquad \cos(\theta_{\mathrm{W}}) = \frac{M_W}{M_Z},$$
$$M_W = \frac{v}{2}g, \qquad G_{\mathrm{F}} = \frac{\sqrt{2}}{8M_W^2}g^2.$$

Above, e is the elementary electric charge of a single proton which is related to the coupling constant of the $\mathbf{SU}(\mathbf{2})_{\mathrm{L}}$ gauge group g through the Weinberg angle θ_{W} whose cosine is the ratio of the W boson's mass and the Z boson's mass. The third relation connects the mass of the W boson with the coupling g and the SM vacuum expectation value v, while the last relation provides the definition of Fermi's coupling constant G_{F}.

A.1. Standard Model

Propagators

In SM computations of Higgs-Strahlung diagrams without considering EW corrections only three different types of particles can appear as internal lines. These are fermions, weak gauge bosons, and gluons. The propagators read

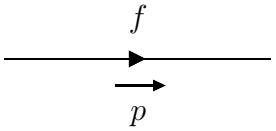

$$= i\frac{\not{p} + m_f}{p^2 - m_f^2 + i\varepsilon}, \tag{A.1}$$

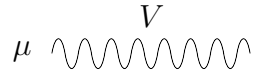

$$= -i\frac{1}{p^2 - M_V^2 + i\varepsilon}\left(g_{\mu\nu} - (1-\xi_V)\frac{p_\mu p_\nu}{p^2 - \xi_V M_V^2}\right), \tag{A.2}$$

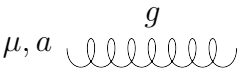

$$= -i\delta^{ab}\left(\frac{g_{\mu\nu}}{p^2 + i\varepsilon} - (1-\xi_g)\frac{p_\mu p_\nu}{(p^2)^2}\right). \tag{A.3}$$

The Feynman rule (A.1) for the fermion propagator uses the Feynman slash notation which is defined for a covariant vector a as

$$\not{a} = \gamma_\mu a^\mu$$

with the Dirac gamma matrices γ_μ. The boson propagators in (A.2) and (A.3) are both given in R_ξ gauge. The greek letters μ and ν indicate Lorentz indices, for the latter propagator the latin letters a and b represent color indices. The same conventions will also be used in the following.

Fermion-Gauge Couplings

All particles in the vertex Feynman rules are consider to be incoming. The first type of vertices that we are interested in describe the couplings between a pair of fermions an a weak gauge boson. For the charged W bosons the Feynman rules are

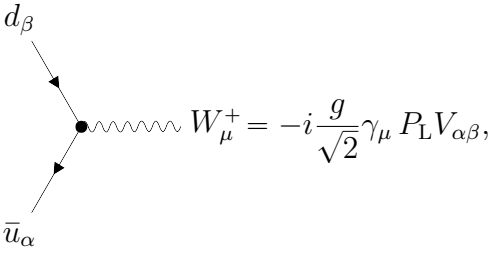

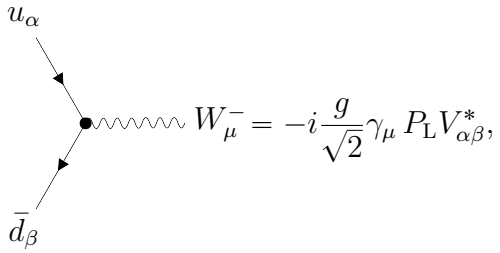

(A.4)

with the left projector

$$P_\mathrm{L} = \frac{1-\gamma_5}{2}$$

and the CKM matrix elements $V_{\alpha\beta}$, where α and β are the fermion generation indices of the up-type quarks and down-type quarks, respectively.
The vertex that couples a fermion-antifermion pair to a neutral Z boson is given by

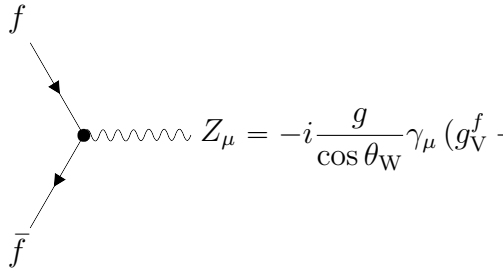

(A.5)

where the vectorial and axial coupling constants are

$$g_\mathrm{V}^f = \frac{1}{2}T_f^3 - Q_f \sin^2(\theta_\mathrm{W}), \qquad g_\mathrm{A}^f = \frac{1}{2}T_f^3.$$

In the couplings, T_f^3 is the third component of the fermion's weak isospin and Q_f its electric charge.

Higgs-Gauge Couplings
Next, we consider the SM vertex of the Higgs boson to two massive gauge bosons. In both cases, for $V = W^{\pm}$ and $V = Z$, the Feynman rule is given by

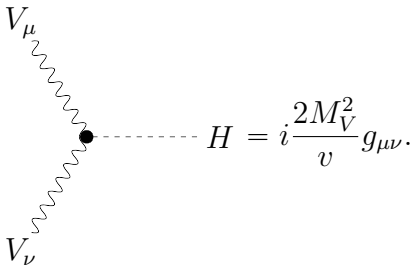

(A.6)

Yukawa Couplings
Finally, the Yukawa couplings have the form

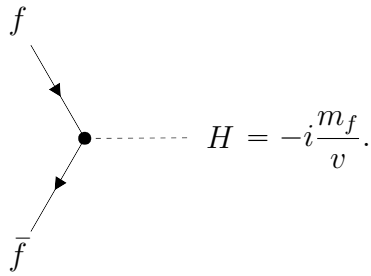

(A.7)

A.2. Two-Higgs-Doublet Model

The new free parameters of the 2HDM that are relevant for computing Higgs-Strahlung cross sections are the masses of the Higgs boson, M_h, M_H, and M_A, as well as the mixing angle α that rotates the two $\mathcal{CP}$-even Higgs bosons from the isospin basis into the physical mass basis and the angle β whose tangent is given as the ratio of the two vacuum expectation values,

$$\tan(\beta) = \frac{v_2}{v_1}.$$

Here, we will just present the Feynman rules that are either new or differ from the previously shown SM rules.

Propagators
In the 2HDM additional propagating Higgs bosons can appear in s-channel diagrams. If the mass of the new bosons are higher than the production threshold for the final states, this can lead to resonances and we introduce Breit-Wigner propagators to tame potential divergences,

$$= i\frac{1}{p^2 - M_\phi^2 + iM_\phi\Gamma_\phi + i\varepsilon}, \tag{A.8}$$

where $\phi \in \{h, H, A\}$ and Γ_ϕ represents the decay width of the corresponding Higgs boson.

Higgs-Gauge Couplings

The couplings of the Higgs bosons to a pair of vector bosons can be obtained by multiplying the analog SM coupling with a factor g_{VV}^{ϕ},

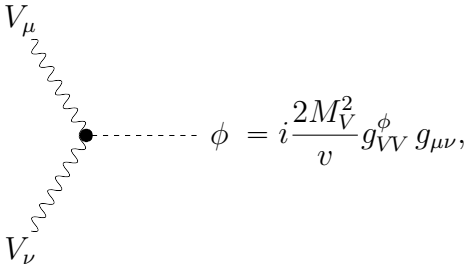

$$= i\frac{2M_V^2}{v} g_{VV}^{\phi}\, g_{\mu\nu}, \tag{A.9}$$

where again $\phi \in \{h, H, A\}$ and $V \in \{W^{\pm}, Z\}$. In particular, these factors do not depend on the vector boson type and read

$$g_{VV}^{h} = \sin(\beta - \alpha), \qquad g_{VV}^{H} = \cos(\beta - \alpha), \qquad g_{VV}^{A} = 0.$$

Tri-Linear Couplings

Moreover, the 2HDM provides a new tri-linear coupling, that connects one of the two $\mathcal{CP}$-even Higgs bosons with the $\mathcal{CP}$-odd boson and the Z boson. The Feynman rule is given by

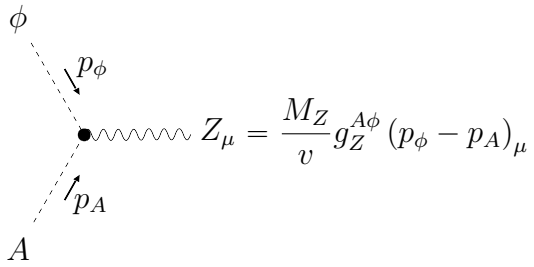

$$= \frac{M_Z}{v} g_Z^{A\phi} \left(p_\phi - p_A\right)_\mu \tag{A.10}$$

with $\phi \in \{h, H\}$ and

$$g_Z^{Ah} = \cos(\beta - \alpha), \qquad g_Z^{AH} = -\sin(\beta - \alpha).$$

Yukawa

The Yukawa couplings differ for the scalar and the pseudoscalar Higgs bosons. They are

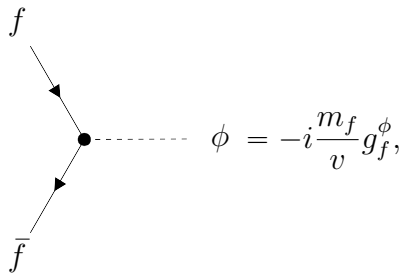

$$= -i\frac{m_f}{v} g_f^{\phi}, \tag{A.11}$$

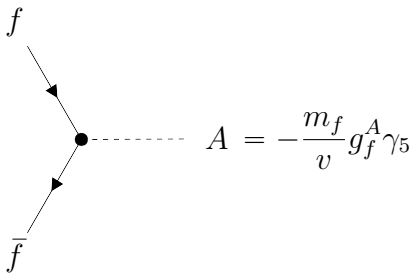

$$= -\frac{m_f}{v} g_f^{A} \gamma_5,$$

Table A.1.: Overview of the Yukawa coupling constants in the 2HDM related to the Feynman rules (A.11). The indices u, d, and e stand for all up-type quarks, down-type quarks, and charged leptons, respectively, independent of the generation.

	Type I	Type II	Lepton-specific	Flipped
g_u^h	$\cos(\alpha)/\sin(\beta)$	$\cos(\alpha)/\sin(\beta)$	$\cos(\alpha)/\sin(\beta)$	$\cos(\alpha)/\sin(\beta)$
g_u^H	$\sin(\alpha)/\sin(\beta)$	$\sin(\alpha)/\sin(\beta)$	$\sin(\alpha)/\sin(\beta)$	$\sin(\alpha)/\sin(\beta)$
g_u^A	$\cot(\beta)$	$\cot(\beta)$	$\cot(\beta)$	$\cot(\beta)$
g_d^h	$\cos(\alpha)/\sin(\beta)$	$-\sin(\alpha)/\cos(\beta)$	$\cos(\alpha)/\sin(\beta)$	$-\sin(\alpha)/\cos(\beta)$
g_d^H	$\sin(\alpha)/\sin(\beta)$	$\cos(\alpha)/\cos(\beta)$	$\sin(\alpha)/\sin(\beta)$	$\cos(\alpha)/\cos(\beta)$
g_d^A	$-\cot(\beta)$	$\tan(\beta)$	$-\cot(\beta)$	$\tan(\beta)$
g_e^h	$\cos(\alpha)/\sin(\beta)$	$-\sin(\alpha)/\cos(\beta)$	$-\sin(\alpha)/\cos(\beta)$	$\cos(\alpha)/\sin(\beta)$
g_e^H	$\sin(\alpha)/\sin(\beta)$	$\cos(\alpha)/\cos(\beta)$	$\cos(\alpha)/\cos(\beta)$	$\sin(\alpha)/\sin(\beta)$
g_e^A	$-\cot(\beta)$	$\tan(\beta)$	$\tan(\beta)$	$-\cot(\beta)$

where the factors depend on the type of the 2HDM. All factors are listed in Table A.1. Since we are not interested in Yukawa couplings to leptons, the lepton-specific and flipped 2HDM are the same as the type I and type II 2HDM, respectively[1].

A.3. B–L Model

Due to the introduction of a new symmetry group and a complex scalar singlet, the Higgs-Strahlung process in B–L Model depends on the new free parameters for the masses of the two Higgs bosons, M_h and M_h, the mass of the new neutral vector boson, $M_{Z'}$, and on the mixing angle α that is used to transform the two Higgs bosons from the isospin basis into the mass basis. Moreover, the $\mathbf{U}(\mathbf{1})_{B-L}$ symmetry group introduces the coupling constant g_1'.
As before, we present in this subsection only Feynman rules that appear newly or that are changed with respect to the SM.

Propagators

Since the Z' boson can occur as internal particle, its propagator is needed. Experimental constaints reveal, that the mass of the Z' boson has to be larger than the threshold for Zh production, thus, s-channel resonance are present in this model and a Breit-Wigner propagator is used, which reads in R_ξ gauge

$$\mu \overset{Z'}{\sim\!\sim\!\sim} \nu = -i\frac{1}{p^2 - M_{Z'}^2 + iM_{Z'}\Gamma_{Z'} + i\varepsilon} \times \left(g_{\mu\nu} - (1-\xi_{Z'})\frac{p_\mu p_\nu}{p^2 - \xi_{Z'}(M_{Z'}^2 - iM_{Z'}\Gamma_{Z'})}\right), \tag{A.12}$$

[1] An implicit difference comes from different decay widths of the Higgs bosons in the lepton-specific and the type I 2HDM or the flipped and the type II 2HDM, but these parameters are inputs of our tool, so we do not distinguish these models and leave the task to care about this to the user.

where $\Gamma_{Z'}$ is the decay width of the Z' boson.

Fermion-Gauge Couplings

The coupling of the Z' boson to a fermion-antifermion pair is

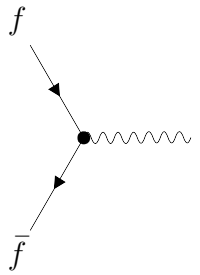

$$= -i\frac{g}{\cos\theta_{\mathrm{W}}}\gamma_\mu\,(g'^{f}_{\mathrm{V}} - g'^{f}_{\mathrm{A}}\gamma_5), \tag{A.13}$$

where the vectorial and axial coupling constants in a pure B–L Model[2] are

$$g'^{f}_{\mathrm{V}} = \frac{g'_1}{g}\cos(\theta_{\mathrm{W}})\,Y^{f}_{B-L}, \qquad g'^{f}_{\mathrm{A}} = 0.$$

It holds $Y^{f}_{B-L} = B^f - L^f$, with the fermion's baryon number B^f and its lepton number L^f, so that for a quark-antiquark pair follows $Y^{q}_{B-L} = 1/3$.

Higgs-Gauge Couplings

Compared to the SM, the couplings of the Higgs bosons to the SM's weak bosons can be obtained by rescaling due to

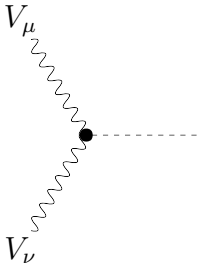

$$= i\frac{2M_V^2}{v}g^{\phi}_{VV}\,g_{\mu\nu}, \tag{A.14}$$

with $\phi \in \{h, H\}$ and the factors

$$g^{h}_{VV} = \cos(\alpha), \qquad g^{H}_{VV} = \sin(\alpha).$$

A new vertex, that connects one of the Higgs bosons to the Z boson and the Z' boson is very similar to that,

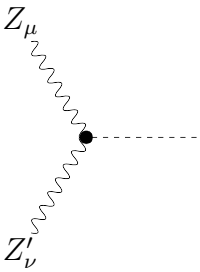

$$= i\frac{2M_Z^2}{v}g^{\phi}_{ZZ'}\,g_{\mu\nu}, \tag{A.15}$$

[2] In a more general B–L Model that allows for a mixing of the Z and Z' bosons the axial coupling does not vanish and the coupling constants become more complex. Moreover, the $f\bar{f}Z$ vertex would also differ from the SM vertex.

where again $\phi \in \{h, H\}$. The explicit expressions for the coupling factors are

$$g^h_{ZZ'} = \frac{v g'_1}{M_Z} \cos(\alpha), \qquad g^H_{ZZ'} = \frac{v g'_1}{M_Z} \sin(\alpha).$$

Yukawa

Lastly, the Yukawa couplings are also a rescaling of their SM pedant,

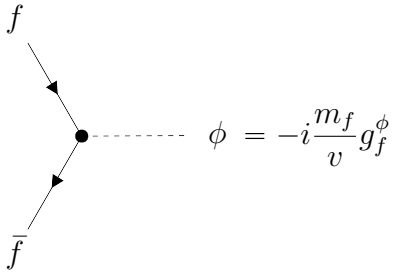

(A.16)

with the factors

$$g^h_f = \cos(\alpha), \qquad g^H_f = \sin(\alpha).$$

B

Renormalization

Contents

The first part of this appendix concerns the UV renormalization for color-singlet production in the Drell-Yan-like which requires up to NNLO QCD only the renormalization of the strong coupling constant. Moreover, we list in the second part of this appendix the UV- and IR-renormalized finite remainders for the purely virtual corrections for color-singlet production in the Drell-Yan-like process.

B.1. Strong Coupling Constant

The relation between the bare coupling constant, α_s^{B} and the UV renormalized coupling constant α_s at a renormalization scale μ_{R} in the $\overline{\mathrm{MS}}$ scheme reads

$$\alpha_s^{\mathrm{B}}\, S_\epsilon = \alpha_s(\mu_{\mathrm{R}})\, \mu_{\mathrm{R}}^{2\epsilon} \left(1 - \frac{\alpha_s(\mu_{\mathrm{R}})}{2\pi} \frac{\beta_0}{\epsilon} + \mathcal{O}(\alpha_s^2)\right), \tag{B.1}$$

with $S_\epsilon = (4\pi)^\epsilon e^{-\epsilon\gamma_{\mathrm{E}}}$, and γ_{E} is the Euler–Mascheroni constant.
The running between two scales is described by the renormalization group equation

$$\frac{\partial \alpha_s}{\partial \ln(\mu^2)} = \beta(\alpha_s), \tag{B.2}$$

where the QCD beta function can be written in expansion of the coupling constant itself as

$$\beta(\alpha_s) = -2\pi \sum_{i=0}^{\infty} \left(\frac{\alpha_s}{2\pi}\right)^{i+2} \beta_i. \tag{B.3}$$

Since our LO process is α_s independent, the NNLO process is of $\mathcal{O}(\alpha_s^2)$. Consequently, we just need to consider the first coefficient of the QCD beta function. Up to the required order the solution is given by

$$\frac{\alpha_s(\mu)}{2\pi} = \frac{\alpha_s(\mu_0)}{2\pi} \left\{1 - \frac{\alpha_s(\mu_0)}{2\pi} \beta_0 \ln\left(\frac{\mu^2}{\mu_0^2}\right) + \mathcal{O}(\alpha_s^2)\right\}. \tag{B.4}$$

The explicit expression for the first coefficients of the beta function is

$$\beta_0 = \frac{11}{6} C_\mathrm{A} - \frac{2}{3} T_\mathrm{R} n_f. \tag{B.5}$$

In our calculations, we perform the factorization of the IR singularities at the factorization scale μ_F which is in general different from the renormalization scale. Consequently, in these expressions, the bare quantity g_s^B reads

$$\begin{aligned} g_s^\mathrm{B} &= \sqrt{4\pi\alpha_s^\mathrm{B}} \\ &= \sqrt{4\pi\alpha_s(\mu_\mathrm{F})\frac{\mu_\mathrm{F}^{2\epsilon}}{S_\epsilon}} \left(1 - \frac{\alpha_s(\mu_\mathrm{F})}{2\pi}\frac{\beta_0}{2\epsilon} + \mathcal{O}(\alpha_s^2)\right) \\ &= \sqrt{4\pi\alpha_s(\mu_\mathrm{R})\frac{\mu_\mathrm{F}^{2\epsilon}}{S_\epsilon}} \left(1 - \frac{\alpha_s(\mu_\mathrm{R})}{2\pi}\frac{\beta_0}{2}\ln\left(\frac{\mu_\mathrm{F}^2}{\mu_\mathrm{R}^2}\right) - \frac{\alpha_s(\mu_\mathrm{R})}{2\pi}\frac{\beta_0}{2\epsilon} + \mathcal{O}(\alpha_s^2)\right) \\ &\equiv g_{s,\epsilon}. \end{aligned} \tag{B.6}$$

In the third line, we use the evolution of Eq. (B.4) to restore the renormalization scale dependence for taking into account that the UV renormalization of the strong coupling constant is carried out at that energy scale.
This definition of $g_{s,\epsilon}$ implies the useful relation

$$\begin{aligned} [\alpha_{s,\epsilon}] &= \left[\frac{g_{s,\epsilon}^2}{8\pi^2}\frac{(4\pi)^\epsilon}{\Gamma(1-\epsilon)}\right] \\ &= \frac{\alpha_s(\mu_\mathrm{R})}{2\pi}\frac{\mu_\mathrm{F}^{2\epsilon}}{S_\epsilon}\frac{(4\pi)^\epsilon}{\Gamma(1-\epsilon)} \left(1 - \frac{\alpha_s(\mu_\mathrm{R})}{2\pi}\beta_0 \ln\left(\frac{\mu_\mathrm{F}^2}{\mu_\mathrm{R}^2}\right) - \frac{\alpha_s(\mu_\mathrm{R})}{2\pi}\frac{\beta_0}{\epsilon} + \mathcal{O}(\alpha_s^2)\right), \end{aligned} \tag{B.7}$$

that appears over and over in our computations.

B.2. Finite Remainders of Virtual Corrections

Purely virtual corrections can be related to the tree-level process with the same final state by the introduction of so-called form factors. For Drell-Yan-like color-singlet production at NLO the interference of the one-loop matrix element and the tree-level diagram results in

$$F_\mathrm{LV}^\mathrm{fin}(1_{f_a}, 2_{f_b}) = -8\, C_\mathrm{F} \left(\frac{\alpha_s(\mu_\mathrm{R})}{2\pi}\right) F_\mathrm{LM}(1_{f_a}, 2_{f_b}) + \mathcal{O}(\epsilon). \tag{B.8}$$

At NNLO the squared one-loop contributions can be simply expressed as

$$F_\mathrm{LV^2}^\mathrm{fin}(1_{f_a}, 2_{f_b}) = 16\, C_\mathrm{F}^2 \left(\frac{\alpha_s(\mu_\mathrm{R})}{2\pi}\right)^2 F_\mathrm{LM}(1_{f_a}, 2_{f_b}) + \mathcal{O}(\epsilon), \tag{B.9}$$

the interference of two-loop amplitudes and tree-level amplitudes has the form

$$F_\mathrm{LVV}^\mathrm{fin}(1_{f_a}, 2_{f_b}) = \left(\frac{\alpha_s(\mu_\mathrm{R})}{2\pi}\right)^2 \left[C_\mathrm{F}^2 \left(\frac{255}{16} + \frac{29\pi^2}{12} - 15\zeta_3 - \frac{11\pi^4}{90}\right)\right.$$

$$
\begin{aligned}
&+ C_{\mathrm{A}} C_{\mathrm{F}} \left(-\frac{51157}{1296} - \frac{107\pi^2}{72} + \frac{659\zeta_3}{36} + \frac{31\pi^4}{240} \right) \\
&+ C_{\mathrm{F}}\, n_f \left(\frac{4085}{648} + \frac{7\pi^2}{36} - \frac{\zeta_3}{18} \right) \Bigg] F_{\mathrm{LM}}(1_{f_a}, 2_{f_b}) \\
&+ \left(\frac{\alpha_s(\mu_{\mathrm{R}})}{2\pi} \right) \beta_0 \ln\left(\frac{\mu_{\mathrm{R}}^2}{\hat{s}} \right) F_{\mathrm{LV}}^{\mathrm{fin}}(1_{f_a}, 2_{f_b}) + \mathcal{O}(\epsilon).
\end{aligned}
\tag{B.10}
$$

The form factors were computed in Ref. [56] and can also be found in the Appendix of Ref. [116]. Moreover, we restored the full scale dependence in Eq. (B.10) with help of the renormalization group equation for the strong coupling constant, *cf.* Eq. (B.4). The first two expressions, Eq. (B.8) and Eq. (B.9), do not have any scale dependence since no QCD couplings are involved in the LO color-singlet production mechanism.

C

Splitting Functions

Contents

In this appendix, we list the splitting functions that appear in the collinear renormalization procedure of the PDFs for NNLO color singlet production. All these splitting functions can either be found in literature [121, 217, 266, 267, 273–277, 313] or they can be obtained along the lines described therein.

C.1. Collinear Splitting Functions

When a final state parton a_1 with momentum p_1 becomes collinear to another final state parton a_2 with momentum p_2 and they are emitted from the same parent parton a with momentum p we can make use of the Sudakov parametrization to express the momenta as

$$\begin{aligned} p_1^\mu &= zp^\mu + k_\perp^\mu - \frac{k_\perp^2}{z}\frac{n^\mu}{2\,p{\cdot}n}, & p_2^\mu &= (1-z)p^\mu - k_\perp^\mu - \frac{k_\perp^2}{1-z}\frac{n^\mu}{2\,p{\cdot}n}, \\ s_{12} &= 2\,p_1{\cdot}p_2 = -\frac{k_\perp^2}{z(1-z)}, & k_\perp^\mu &\to 0, \end{aligned} \tag{C.1}$$

with the light-like momentum p in the collinear direction, $p^2 = 0$, $k_\perp$ a momentum in the transverse direction which specifies how the collinear limit is approached, and an auxiliary light-like vector n, $n^2 = 0$, which is necessary to define $k_\perp$ through the conditions $k_\perp{\cdot}p = k_\perp{\cdot}n = 0$. In this limit the squared matrix element factorizes as

$$|\mathcal{M}_{ij\to X+a_1a_2}(\dots,p_1,p_2)|^2 \simeq g_s^2\frac{2}{s_{12}}\left\langle \mathcal{M}_{ij\to X+a}(\dots,p)\right| \hat{\boldsymbol{P}}_{a_1a}\left|\mathcal{M}_{ij\to X+a}(\dots,p)\right\rangle, \tag{C.2}$$

where the d dimensional kernel $\hat{\boldsymbol{P}}_{a_1a}$ for the splitting

$$a(p) \to a_1\big(zp + k_\perp + \mathcal{O}\left(k_\perp^2\right)\big) + a_2\big((1-z)p - k_\perp + \mathcal{O}\left(k_\perp^2\right)\big) \tag{C.3}$$

is an operator in spin space. It acts on the spin of the parton a that is connected to the hard process,

$$\langle s|\, \hat{\boldsymbol{P}}_{a_1 a}\, |s'\rangle = P^{ss'}_{a_1 a}. \tag{C.4}$$

Due to these spin correlations, spin-averaged squared amplitudes do not simply factorize into spin-averaged amplitudes with reduced parton number and the splitting function in Eq. (D.1).
The expressions for the splitting functions in Eq. (C.36) are

$$\begin{aligned}
P^{ss'}_{qq}(z,k_\perp;\epsilon) &= \delta^{ss'} C_\mathrm{F} \left(\frac{1+z^2}{1-z} - \epsilon\,(1-z) \right), \\
P^{\mu\nu}_{qg}(z,k_\perp;\epsilon) &= T_\mathrm{R} \left(-g^{\mu\nu} + 4\,z\,(1-z)\,\frac{k_\perp^\mu k_\perp^\nu}{k_\perp^2} \right), \\
P^{ss'}_{gq}(z,k_\perp;\epsilon) &= \delta^{ss'} C_\mathrm{F} \left(\frac{1+(1-z)^2}{z} - \epsilon\, z \right), \\
P^{\mu\nu}_{gg}(z,k_\perp;\epsilon) &= 2\,C_\mathrm{A} \left(-g^{\mu\nu} \left(\frac{z}{1-z} + \frac{1-z}{z} \right) - 2\,(1-\epsilon)\,z\,(1-z)\,\frac{k_\perp^\mu k_\perp^\nu}{k_\perp^2} \right),
\end{aligned} \tag{C.5}$$

where we use the spin indices s and s' if the parent parton is a quark and μ and ν if the parent parton is a gluon. Sometimes we find it convenient to rewrite the two splitting functions for gluon parents as

$$\begin{aligned}
P^{\mu\nu}_{qg}(z,k_\perp;\epsilon) &= -\widetilde{P}^{(0)}_{qg}(z;\epsilon)\, g^{\mu\nu} - \widetilde{P}^{\perp}_{qg}(z;\epsilon) \frac{k_\perp^\mu k_\perp^\nu}{k_\perp^2}, \\
P^{\mu\nu}_{gg}(z,k_\perp;\epsilon) &= -\widetilde{P}^{(0)}_{gg}(z;\epsilon)\, g^{\mu\nu} - \widetilde{P}^{\perp}_{gg}(z;\epsilon) \frac{k_\perp^\mu k_\perp^\nu}{k_\perp^2},
\end{aligned} \tag{C.6}$$

with terms proportional to the metric tensor and to the transverse vector,

$$\begin{aligned}
\widetilde{P}^{(0)}_{qg}(z;\epsilon) &= T_\mathrm{R}, & \widetilde{P}^{\perp}_{qg}(z;\epsilon) &= -4\,T_\mathrm{R}\,z\,(1-z), \\
\widetilde{P}^{(0)}_{gg}(z;\epsilon) &= 2\,C_\mathrm{A} \left(\frac{z}{1-z} + \frac{1-z}{z} \right), & \widetilde{P}^{\perp}_{gg}(z;\epsilon) &= 4\,C_\mathrm{A}\,(1-\epsilon)\,z\,(1-z).
\end{aligned} \tag{C.7}$$

Often we are interested the splitting functions averaged over the transverse direction. These averaged splitting functions can be calculated with

$$\begin{aligned}
\left\langle \hat{\boldsymbol{P}}_{ig}(z;\epsilon) \right\rangle &= \frac{1}{d-2} d_{\mu\nu}(p) P^{\mu\nu}_{ig}(z,k_\perp;\epsilon) = \widetilde{P}^{(0)}_{ig} + \frac{1}{2\,(1-\epsilon)} \widetilde{P}^{\perp}_{ig}, \\
\left\langle \hat{\boldsymbol{P}}_{iq}(z;\epsilon) \right\rangle &= \frac{1}{2} \delta_{ss'} P^{ss'}_{iq}(z,k_\perp;\epsilon),
\end{aligned} \tag{C.8}$$

where the gluon polarization tensor is given by

$$d_{\mu\nu}(p) = -g_{\mu\nu} + \frac{p^\mu n^\nu + p^\nu n^\mu}{p{\cdot}n} \tag{C.9}$$

and read

$$\left\langle \hat{\boldsymbol{P}}_{qq}(z;\epsilon) \right\rangle = C_\mathrm{F} \left(\frac{1+z^2}{1-z} - \epsilon\,(1-z) \right),$$

$$\begin{aligned}
\left\langle \hat{\boldsymbol{P}}_{qg}(z;\epsilon) \right\rangle &= T_{\mathrm{R}} \left(1 - \frac{2\,z\,(1-z)}{1-\epsilon} \right), \\
\left\langle \hat{\boldsymbol{P}}_{gq}(z;\epsilon) \right\rangle &= C_{\mathrm{F}} \left(\frac{1+(1-z)^2}{z} - \epsilon\,z \right), \\
\left\langle \hat{\boldsymbol{P}}_{gg}(z;\epsilon) \right\rangle &= 2\,C_{\mathrm{A}} \left(\frac{z}{1-z} + \frac{1-z}{z} + z\,(1-z) \right).
\end{aligned} \tag{C.10}$$

Here we computed the final-state, or time-like, splitting functions, but mostly we need the initial-state, or space-like, splitting functions which can be obtained by crossing symmetries which are equivalent to the Drell-Levy-Yan relation [314, 315]

$$\hat{\boldsymbol{P}}_{a_1 a} \to (-1)^{2s_a + 2s_{a_1}} \hat{\boldsymbol{P}}_{a_1 a}, \tag{C.11}$$

which lead to the replacement

$$z = \frac{E_1}{E_1 + E_2} \in [0,1] \to z = \frac{E_1}{E_1 - E_2} \in [1,\infty), \tag{C.12}$$

with the spins s_a and s_{a_1} of the partons a and a_1, respectively, as well as the energies E_1, E_2 of parton a_1 and a_2, respectively. However, for the spin-averaged space-like splitting functions we use in all our computations a redefinition so that they coincide with the spin-averaged time-like splitting functions[1],

$$\begin{aligned}
P^{(0)}_{qq}(z;\epsilon) &= C_{\mathrm{F}} \left(\frac{1+z^2}{1-z} - \epsilon\,(1-z) \right), \\
P^{(0)}_{qg}(z;\epsilon) &= T_{\mathrm{R}} \left(1 - \frac{2\,z\,(1-z)}{1-\epsilon} \right), \\
P^{(0)}_{gq}(z;\epsilon) &= C_{\mathrm{F}} \left(\frac{1+(1-z)^2}{z} - \epsilon\,z \right), \\
P^{(0)}_{gg}(z;\epsilon) &= 2\,C_{\mathrm{A}} \left(\frac{z}{1-z} + \frac{1-z}{z} + z\,(1-z) \right).
\end{aligned} \tag{C.13}$$

A detailed discussion about the relations between time-like and space-like splitting functions can be found for example in Ref. [316], where also the conventional rules for the redefinition that we apply here are described.

C.2. Altarelli-Parisi Splitting Functions

For the collinear renormalization up to NNLO in QCD the space-like Altrarelli-Parisi splitting functions are needed up to $\mathcal{O}(\alpha_s)$,

$$\begin{aligned}
\hat{P}_{q_i q_j}(z) &= \delta_{ij} \hat{P}^{(0)}_{qq}(z) + \frac{\alpha_s}{2\pi} \hat{P}^{(1)}_{q_i q_j}(z) + \mathcal{O}\left(\alpha_s^2\right), \\
\hat{P}_{qg}(z) &= \hat{P}^{(0)}_{qg}(z) + \frac{\alpha_s}{2\pi} \hat{P}^{(1)}_{qg}(z) + \mathcal{O}\left(\alpha_s^2\right), \\
\hat{P}_{gq}(z) &= \hat{P}^{(0)}_{gq}(z) + \frac{\alpha_s}{2\pi} \hat{P}^{(1)}_{gq}(z) + \mathcal{O}\left(\alpha_s^2\right), \\
\hat{P}_{gg}(z) &= \hat{P}^{(0)}_{gg}(z) + \frac{\alpha_s}{2\pi} \hat{P}^{(1)}_{gg}(z) + \mathcal{O}\left(\alpha_s^2\right).
\end{aligned} \tag{C.14}$$

[1] For non-averaged splitting functions we do not use this redefinition. In the cases where we need them we have to use Eq. (D.1) and explicitly perform the crossing in Eq. (C.11).

It is convenient to decompose the LO Altarelli-Parisi splitting functions according to

$$\hat{P}_{ij}^{(0)}(z) = \hat{P}_{ij,\mathrm{R}}^{(0)}(z) + \hat{P}_{ij,\delta}^{(0)}\,\delta(1-z) \tag{C.15}$$

into a regular term

$$\begin{aligned}
\hat{P}_{qq,\mathrm{R}}^{(0)}(z) &= C_\mathrm{F}\left(\frac{2}{[1-z]_+} - (1+z)\right),\\
\hat{P}_{qg,\mathrm{R}}^{(0)}(z) &= T_\mathrm{R}\left(z^2 + (1-z)^2\right),\\
\hat{P}_{gq,\mathrm{R}}^{(0)}(z) &= C_\mathrm{F}\left(\frac{1+(1-z)^2}{z}\right),\\
\hat{P}_{gg,\mathrm{R}}^{(0)}(z) &= 2\,C_\mathrm{A}\left(\frac{1}{[1-z]_+} + \frac{1}{z} + z\,(1-z) - 2\right),
\end{aligned} \tag{C.16}$$

and a piece containing the soft limit, $z = 1$,

$$\begin{aligned}
\hat{P}_{qq,\delta}^{(0)} &= \gamma_q = \frac{3}{2}C_\mathrm{F},\\
\hat{P}_{qg,\delta}^{(0)} &= 0,\\
\hat{P}_{gq,\delta}^{(0)} &= 0,\\
\hat{P}_{gg,\delta}^{(0)} &= \gamma_g = \beta_0 = \frac{11}{6}C_\mathrm{A} - \frac{2}{3}T_\mathrm{R}n_f.
\end{aligned} \tag{C.17}$$

The NLO Altarelli-Parisi splitting functions, which are taken from Refs. [121, 313], are also divided into regular terms and terms proportional to the δ-distribution,

$$\hat{P}_{ij}^{(1)}(z) = \hat{P}_{ij,\mathrm{R}}^{(1)}(z) + \hat{P}_{ij,\delta}^{(1)}\,\delta(1-z). \tag{C.18}$$

Moreover, it is convenient to separate the splitting function for a quark decaying into a quark in flavor singlet (S) and non-singlet (V) contributions,

$$\begin{aligned}
\hat{P}_{q_iq_j}^{(1)}(z) &= \delta_{ij}\left(\hat{P}_{qq,\mathrm{R}}^{\mathrm{V}(1)}(z) + \hat{P}_{qq,\delta}^{(1)}\,\delta(1-z)\right) + \hat{P}_{qq,\mathrm{R}}^{\mathrm{S}(1)}(z),\\
\hat{P}_{q_i\bar{q}_j}^{(1)}(z) &= \delta_{ij}\hat{P}_{q\bar{q},\mathrm{R}}^{\mathrm{V}(1)}(z) + \hat{P}_{q\bar{q},\mathrm{R}}^{\mathrm{S}(1)}(z).
\end{aligned} \tag{C.19}$$

The non-singlet term for a quark decaying into a quark is given by

$$\begin{aligned}
\hat{P}_{qq,\mathrm{R}}^{\mathrm{V}(1)}(z) = C_\mathrm{F}^2\Bigg[&-\left(2\ln(z)\ln(1-z) + \frac{3}{2}\ln(z)\right)p_{qq}(z) - \left(\frac{3}{2} + \frac{7}{2}z\right)\ln(z)\\
&-\frac{1}{2}(1+z)\ln^2(z) - 5(1-z)\Bigg] + C_\mathrm{A}C_\mathrm{F}\Bigg[\left(\frac{1}{2}\ln^2(z) + \frac{11}{6}\ln(z)\right.\\
&\left.+\frac{67}{18} - \frac{\pi^2}{6}\right)p_{qq}(z) + (1+z)\ln(z) + \frac{20}{3}(1-z)\Bigg] + C_\mathrm{F}T_\mathrm{R}n_f\\
&\times\left[-\left(\frac{2}{3}\ln(z) + \frac{10}{9}\right)p_{qq}(z) - \frac{4}{3}(1-z)\right].
\end{aligned} \tag{C.20}$$

For a quark decaying into an antiquark the non-singlet term reads

$$\hat{P}_{q\bar{q},\mathrm{R}}^{\mathrm{V}(1)}(z) = C_\mathrm{F}\left(C_\mathrm{F} - \frac{1}{2}C_\mathrm{A}\right)\left[2\,p_{qq}(-z)\,S_2(z) + 2\,(1+z)\ln(z) + 4\,(1-z)\right]. \tag{C.21}$$

The singlet contributions are the same in both cases,

$$\hat{P}^{\mathrm{S}\,(1)}_{qq,\mathrm{R}}(z) = C_{\mathrm{F}}T_{\mathrm{R}}\left[-2+\frac{20}{9z}+6z-\frac{56}{9}z^2+\left(1+5z+\frac{8}{3}z^2\right)\ln(z)-(1+z)\ln^2(z)\right], \tag{C.22}$$

so that holds

$$\hat{P}^{\mathrm{S}\,(1)}_{q\bar{q},\mathrm{R}}(z) = \hat{P}^{\mathrm{S}\,(1)}_{qq,\mathrm{R}}(z). \tag{C.23}$$

The NLO Altarelli-Parisi splitting function for a gluon decaying into a quark is

$$\begin{aligned}\hat{P}^{(1)}_{qg,\mathrm{R}}(z) = \frac{1}{2}C_{\mathrm{F}}T_{\mathrm{R}}\Big[&4-9z-(1-4z)\ln(z)-(1-2z)\ln^2(z)+4\ln(1-z)\\&+\left(2\ln^2\left(\frac{1-z}{z}\right)-4\ln\left(\frac{1-z}{z}\right)-\frac{2\pi^2}{3}+10\right)p_{qg}(z)\Big]\\&+\frac{1}{2}C_{\mathrm{A}}T_{\mathrm{R}}\Big[\frac{182}{9}+\frac{14}{9}z+\frac{40}{9z}+\left(\frac{136}{3}z-\frac{38}{3}\right)\ln(z)-4\ln(1-z).\\&-(2+8z)\ln^2(z)+2\,p_{qg}(-z)\,S_2(z)+\Big(-\ln^2(z)+\frac{44}{3}\ln(z)\\&-2\ln^2(1-z)+4\ln(1-z)+\frac{\pi^2}{3}-\frac{218}{9}\Big)p_{qg}(z)\Big]\end{aligned} \tag{C.24}$$

If instead a quark splits into a gluon, the NLO Altarelli-Parisi splitting function reads

$$\begin{aligned}\hat{P}^{(1)}_{gq,\mathrm{R}}(z) = C_{\mathrm{F}}^2\Big[&-\frac{5}{2}-\frac{7}{2}z+\left(2+\frac{7}{2}z\right)\ln(z)-\left(1-\frac{1}{2}z\right)\ln^2(z)-2z\ln(1-z)\\&-\big(3\ln(1-z)+\ln^2(1-z)\big)\,p_{gq}(z)\Big]+C_{\mathrm{A}}C_{\mathrm{F}}\Big[\frac{28}{9}+\frac{65}{18}z+\frac{44}{9}z^2\\&-\left(12+5z+\frac{8}{3}z^2\right)\ln(z)+(4+z)\ln^2(z)+2z\ln(1-z)\\&+S_2(z)\,p_{gq}(-z)+\Big(\frac{1}{2}-2\ln(z)\ln(1-z)+\frac{1}{2}\ln^2(z)+\frac{11}{3}\ln(1-z)\\&+\ln^2(1-z)-\frac{\pi^2}{6}\Big)p_{gq}(z)\Big]+C_{\mathrm{F}}T_{\mathrm{R}}n_f\Big[-\frac{4}{3}z-\left(\frac{20}{9}+\frac{4}{3}\ln(1-z)\right)\\&\times p_{gq}(z)\Big].\end{aligned} \tag{C.25}$$

The NLO contribution for gluon going into a gluon is

$$\begin{aligned}\hat{P}^{(1)}_{gg,\mathrm{R}}(z) = C_{\mathrm{A}}^2\Big[&\frac{27}{2}(1-z)+\frac{67}{9}\left(z^2-\frac{1}{z}\right)-\left(\frac{25}{3}-\frac{11}{3}z+\frac{44}{3}z^2\right)\ln(z)\\&+4(1+z)\ln^2(z)+2\,p_{gg}(-z)\,S_2(z)+\Big(\frac{67}{9}-4\ln(z)\ln(1-z)\\&+\ln^2(z)-\frac{\pi^2}{3}\Big)p_{gg}(z)\Big]+C_{\mathrm{F}}T_{\mathrm{R}}n_f\Big[-16+8z+\frac{20}{3}z^2+\frac{4}{3z}\\&-(6+10z)\ln(z)-2(1+z)\ln^2(z)\Big]+C_{\mathrm{A}}T_{\mathrm{R}}n_f\Big[2(1-z)\\&+\frac{26}{9}\left(z^2-\frac{1}{z}\right)-\frac{4}{3}(1+z)\ln(z)-\frac{20}{9}p_{gg}(z)\Big].\end{aligned} \tag{C.26}$$

In the previous expressions we used the short notations

$$S_2(z) = -2\,\mathrm{Li}_2(-z) + \frac{1}{2}\ln^2(z) - 2\ln(z)\ln(1+z) - \frac{\pi^2}{6} \tag{C.27}$$

and

$$\begin{aligned} p_{qq}(z) &= \frac{2}{[1-z]_+} - 1 - z, \\ p_{qg}(z) &= z^2 + (1-z)^2, \\ p_{gq}(z) &= \frac{1+(1-z^2)}{z}, \\ p_{gg}(z) &= \frac{1}{[1-z]_+} + \frac{1}{z} - 2 + z(1-z). \end{aligned} \tag{C.28}$$

If the argument of p_{qq} or p_{gg} has a negative sign, the plus-distributions are removed,

$$\begin{aligned} p_{qq}(-z) &= \frac{2}{1+z} - 1 + z, \\ p_{gg}(-z) &= \frac{1}{1+z} - \frac{1}{z} - 2 - z(1+z). \end{aligned} \tag{C.29}$$

The δ-terms are

$$\begin{aligned} \hat{P}^{(1)}_{qq,\delta} &= C_\mathrm{F}^2\left(\frac{3}{8} - \frac{\pi^2}{2} + 6\zeta_3\right) + C_\mathrm{F}C_\mathrm{A}\left(\frac{17}{24} + \frac{11\pi^2}{18} - 3\zeta_3\right) - C_\mathrm{F}T_\mathrm{R}n_f\left(\frac{1}{6} + \frac{2\pi^2}{9}\right), \\ \hat{P}^{(1)}_{qg,\delta} &= 0, \\ \hat{P}^{(1)}_{gq,\delta} &= 0, \\ \hat{P}^{(1)}_{gg,\delta} &= C_\mathrm{A}^2\left(\frac{8}{3} + 3\zeta_3\right) - C_\mathrm{F}T_\mathrm{R}n_f - \frac{4}{3}C_\mathrm{A}T_\mathrm{R}n_f. \end{aligned} \tag{C.30}$$

C.3. Generalized Splitting Functions

Besides the usual Altarelli-Parisi splitting functions also generalized splitting functions appear in our computations. They are defined as

$$\mathcal{P}_{ij}(z;\epsilon) = \hat{P}^{(0)}_{ij}(z) - \epsilon\,\mathcal{P}'_{ij}(z) + \mathcal{O}\left(\epsilon^2\right), \tag{C.31}$$

with the $\mathcal{O}(\epsilon)$ related terms

$$\begin{aligned} \mathcal{P}'_{qq}(z) &= C_\mathrm{F}\left(4\left[\frac{\ln(1-z)}{1-z}\right]_+ - 2(1+z)\ln(1-z) + (1-z)\right), \\ \mathcal{P}'_{qg}(z) &= T_\mathrm{R}\left(2\left[z^2 + (1-z)^2\right]\ln(1-z) + 2\,z\,(1-z)\right), \\ \mathcal{P}'_{gq}(z) &= C_\mathrm{F}\left(2\left[\frac{1+(1-z)^2}{z}\right]\ln(1-z) + z\right), \\ \mathcal{P}'_{gg}(z) &= 2\,C_\mathrm{A}\left(2\left[\frac{\ln(1-z)}{1-z}\right]_+ + 2\left[\frac{1}{z} + z\,(1-z) - 2\right]\ln(1-z)\right). \end{aligned} \tag{C.32}$$

C.4. Triple-Collinear Splitting Functions

In analogy to Eq. (D.1) the squared matrix element factorizes in the triple-collinear limit,

$$\begin{aligned} &\left|\mathcal{M}_{ij\to X+a_1a_2a_3}(\dots,p_1,p_2,p_3)\right|^2 \\ &\simeq g_s^4\left(\frac{2}{s_{123}}\right)^2 \left\langle \mathcal{M}_{ij\to X+a}(\dots,x\,p)\right| \hat{\boldsymbol{P}}_{a_1a_2a_3} \left|\mathcal{M}_{ij\to X+a}(\dots,x\,p)\right\rangle . \end{aligned} \tag{C.33}$$

The momenta for the flavor conserving splitting

$$a(p) \to a_1(p_1) + a_2(p_2) + a_3(p_3) \tag{C.34}$$

are defined as

$$p_i^\mu = x_i\,p^\mu + k_{\perp i}^\mu - \frac{k_{\perp i}^2}{x_i}\frac{n^\mu}{2\,p{\cdot}n}, \tag{C.35}$$

with the light-like vector p^μ in the collinear direction, $p^2 = 0$, and the light-like auxiliary vector n^μ, $n^2 = 0$, so that $k_{\perp i}{\cdot}p = k_{\perp i}{\cdot}n = 0$. The Lorentz-invariant sub-energy s_{123} in Eq. (C.33) is defined as $s_{123} = (p_1+p_2+p_3)^2$ and the momentum fraction x is given by $x = x_1 + x_2 + x_3$.
The splitting kernel is again an operator in the spin space of the parent parton a,

$$\left\langle s\right| \hat{\boldsymbol{P}}_{a_1a_2a_3} \left|s'\right\rangle = P^{ss'}_{a_1a_2a_3}. \tag{C.36}$$

The explicit expressions of all kernels can be found in Ref. [267], here we just need the spin-averaged triple-collinear splitting functions with initial state quarks. To keep the expressions compact it is convenient to introduce the abbreviations,

$$\begin{aligned} z_i &= \frac{x_i}{\sum_{j=1}^3 x_j}, \\ t_{ij,k} &= 2\,\frac{z_i s_{jk} - z_j s_{ik}}{z_i + z_j} + \frac{z_i - z_j}{z_i + z_j} s_{ij}, \end{aligned} \tag{C.37}$$

with the definition of the sub-energies $s_{ij} = (p_i + p_j)^2$ which coincides also with the definition in Eq. (4.24).
Similarly to Eq. (C.11), initial state splitting functions can be obtained by a crossing relation ($a \leftrightarrow a_i$),

$$\hat{\boldsymbol{P}}_{a_1a_2a_3} \to (-1)^{2s_a+2s_{a_i}}\,\hat{\boldsymbol{P}}_{a_1a_2a_3}, \tag{C.38}$$

with the spins s_a and s_{a_i} of particle a and a_i, respectively.

Non-Identical Fermions: $q \to \bar{q}_1' q_2' q_3$

For the splitting process with non-identical fermions, $q' \neq q$, the spin-averaged splitting functions reads[2],

$$\hat{P}_{\bar{q}_1'q_2'q_3} = \frac{1}{2}C_\mathrm{F}T_\mathrm{R}\frac{s_{123}}{s_{12}}\left(-\frac{t_{12,3}^2}{s_{12}s_{123}} + \frac{4z_3 + (z_1-z_2)^2}{z_1+z_2} + (1-2\epsilon)\left[z_1+z_2-\frac{s_{12}}{s_{123}}\right]\right). \tag{C.39}$$

[2]For preventing an overload of the expressions we discard the explicit dependence of the splitting functions on the momenta. The splitting functions $\hat{P}_{a_1a_2a_3}$ should be understood as $\hat{P}_{a_1a_2a_3}(p_1,p_2,p_3)$.

Identical Fermions: $q \to \bar{q}_1 q_2 q_3$

If the fermions are identical the triple-collinear splitting becomes,

$$\hat{P}_{\bar{q}_1 q_2 q_3} = \left(\hat{P}_{\bar{q}_1' q_2' q_3} + (2 \leftrightarrow 3)\right) + \hat{P}^{(\mathrm{id})}_{\bar{q}_1 q_2 q_3}, \tag{C.40}$$

with

$$\begin{aligned}\hat{P}^{(\mathrm{id})}_{\bar{q}_1 q_2 q_3} = C_\mathrm{F}\left(C_\mathrm{F} - \frac{1}{2}C_\mathrm{A}\right)\Bigg((1-\epsilon)\left[\frac{2s_{23}}{s_{12}} - \epsilon\right] \\ + \frac{s_{123}}{s_{12}}\left[\frac{1+z_1^2}{1-z_2^2} - \frac{2z_2}{1-z_3} - \epsilon\left(\frac{(1-z_3)^2}{1-z_2} + 1 + z_1 - \frac{2z_2}{1-z_3}\right) - \epsilon^2(1-z_3)\right] \\ - \frac{s_{123}^2}{s_{12}s_{13}}\frac{z_1}{2}\left[\frac{1+z_1^2}{(1-z_2)(1-z_3)} - \epsilon\left(1 + 2\frac{1-z_2}{1-z_3}\right) - \epsilon^2\right]\Bigg) + (2 \leftrightarrow 3)\,.\end{aligned} \tag{C.41}$$

The symbol $(i \leftrightarrow j)$ means that the same term has to be added again by exchanging the meaning of the indices i and j.

Collinear Gluon Pair: $q \to g_1 g_2 q_3$:

In case the parent quark emits a collinear gluon pair the splitting function

$$\hat{P}_{g_1 g_2 q_3} = C_\mathrm{F}^2 \hat{P}^{(\mathrm{ab})}_{g_1 g_2 q_3} + C_\mathrm{F} C_\mathrm{A} \hat{P}^{(\mathrm{nab})}_{g_1 g_2 q_3} \tag{C.42}$$

can be divided into an abelian term,

$$\begin{aligned}\hat{P}^{(\mathrm{ab})}_{g_1 g_2 q_3} = \Bigg(\frac{s_{123}^2}{2s_{13}s_{23}} z_3\left[\frac{1+z_3^2}{z_1 z_2} - \epsilon\frac{z_1^2+z_2^2}{z_1 z_2} - \epsilon(1+\epsilon)\right] \\ + \frac{s_{123}}{s_{13}}\left[\frac{z_3(1-z_1)+(1-z_2)^3}{z_1 z_2} + \epsilon^2(1+z_3) - \epsilon(z_1^2+z_1 z_2+z_2^2)\frac{1-z_2}{z_1 z_2}\right] \\ + (1-\epsilon)\left[\epsilon - (1-\epsilon)\frac{s_{23}}{s_{13}}\right]\Bigg) + (1 \leftrightarrow 2),\end{aligned} \tag{C.43}$$

and a non-abelian term,

$$\begin{aligned}\hat{P}^{(\mathrm{nab})}_{g_1 g_2 q_3} = \Bigg((1-\epsilon)\left[\frac{t_{12,3}^2}{4s_{12}^2} + \frac{1}{4} - \frac{\epsilon}{2}\right] + \frac{s_{123}^2}{2s_{12}s_{13}}\left[\frac{(1-z_3)^2(1-\epsilon)+2z_3}{z_2}\right. \\ \left. + \frac{z_2^2(1-\epsilon)+2(1-z_2)}{1-z_3}\right] - \frac{s_{123}^2}{4s_{13}s_{23}} z_3\left[\frac{(1-z_3)^2(1-\epsilon)+2z_3}{z_1 z_2} + \epsilon(1-\epsilon)\right] \\ + \frac{s_{123}}{2s_{12}}\left[(1-\epsilon)\frac{z_1(2-2z_1+z_1^2) - z_2(6-6z_2+z_2^2)}{z_2(1-z_3)} + 2\epsilon\,\frac{z_3(z_1-2z_2)-z_2}{z_2(1-z_3)}\right] \\ + \frac{s_{123}}{2s_{13}}\left[(1-\epsilon)\frac{(1-z_2)^3+z_3^2-z_2}{z_2(1-z_3)} - \epsilon\left(\frac{2(1-z_2)(z_2-z_3)}{z_2(1-z_3)} - z_1 + z_2\right)\right. \\ \left. - \frac{z_3(1-z_1)+(1-z_2)^3}{z_1 z_2} + \epsilon(1-z_2)\left(\frac{z_1^2+z_2^2}{z_1 z_2} - \epsilon\right)\right]\Bigg) + (1 \leftrightarrow 2).\end{aligned} \tag{C.44}$$

C.5. One-Loop Splitting Functions

The one-loop splitting functions were studied in Refs. [217, 273–277]. We adapt them for the splitting of a quark into a quark,

$$\begin{aligned} P_{qq}^{\text{Loop}}(z;\epsilon) = P_{qq}^{(0)}(z;\epsilon) \Bigg\{ & -\frac{C_\text{A}}{\epsilon^2} + \frac{C_\text{A}\ln(1-z) - 2\,C_\text{F}\ln(z)}{\epsilon} \\ & + C_\text{A}\left[\frac{\pi^2}{3} - \frac{1}{2}\ln^2(1-z) - 2\,\text{Li}_2(1-z)\right] + 2\,C_\text{F}\,\text{Li}_2(1-z) \\ & + \epsilon\left[C_\text{A}\ln(1-z)\left(-\frac{\pi^3}{3} + \frac{1}{6}\ln^2(1-z)\right) + 2\,C_\text{F}\,\text{Li}_3(1-z)\right]\Bigg\} \\ & - C_\text{F}\,(C_\text{A} - C_\text{F})\left(z + \epsilon(1+z)\right) + \mathcal{O}\left(\epsilon^2\right), \end{aligned} \tag{C.45}$$

and for the splitting of a gluon into a quark,

$$\begin{aligned} P_{qg}^{\text{Loop}}(z;\epsilon) = P_{qg}^{(0)}(z;\epsilon) \Bigg\{ & -\frac{C_\text{A}}{\epsilon^2} - \frac{(C_\text{A} - 2\,C_\text{F})\ln(1-z) + 2\,C_\text{F}\,\ln(z)}{\epsilon} \\ & + (C_\text{A} - 2\,C_\text{F})\left[-\frac{\pi^2}{3} + \frac{1}{2}\ln^2(1-z) + 2\,\text{Li}_2(1-z)\right] + 2\,C_\text{F}\,\text{Li}_2(1-z) \\ & + \epsilon\left[(C_\text{A} - 2\,C_\text{F})\ln(1-z)\left(\frac{\pi^3}{3} - \frac{1}{6}\ln^2(1-z)\right) + 2\,C_\text{F}\,\text{Li}_3(1-z)\right]\Bigg\} \\ & + T_\text{R}\,(C_\text{A} - C_\text{F})\left(z - \epsilon(1-3z)\right) + \mathcal{O}\left(\epsilon^2\right). \end{aligned} \tag{C.46}$$

The corresponding one-loop splitting function of the finite remainder have the shape

$$\begin{aligned} P_{qq,\text{F}}^{\text{Loop}}(p_1,p_2,p_4) = P_{qq}^{(0)}(z;0) \Bigg\{ & C_\text{A}\Bigg[\frac{5\pi^2}{6} + \frac{3}{4}\ln\left(\frac{s_{12}}{s_{14}}\right) + \frac{1}{4}\ln(1-z) \\ & \times\left(-3 + 4\ln\left(\frac{s_{12}}{s_{14}}\right)\right) - 2\,\text{Li}_2(1-z)\Bigg] - C_\text{F}\Bigg[\ln(z) \\ & \times\left(-3 + \ln(z) + 2\ln\left(\frac{s_{12}}{s_{14}}\right)\right) - 2\,\text{Li}_2(1-z)\Bigg] - \frac{\beta_0}{2} \\ & \times\left[\ln(1-z) - \ln\left(\frac{\mu_\text{R}^2}{s_{12}}\right) - \ln\left(\frac{\mu_\text{R}^2}{s_{14}}\right)\right]\Bigg\} - z\,C_\text{F}\,(C_\text{A} - C_\text{F}) \end{aligned} \tag{C.47}$$

for the decay of a quark into a quark, and the shape

$$\begin{aligned} P_{qg,\text{F}}^{\text{Loop}}(p_1,p_2,p_4) = P_{qg}^{(0)}(z;0) \Bigg\{ & -C_\text{A}\Bigg[\frac{5\pi^2}{6} - \frac{3}{4}\ln\left(\frac{s_{12}}{s_{14}}\right) + \frac{1}{2}\ln(1-z) \\ & \times\left(-3 + 2\ln\left(\frac{s_{12}}{s_{14}}\right)\right) - 2\,\text{Li}_2(1-z)\Bigg] + C_\text{F}\Bigg[\frac{5\pi^2}{3} \\ & - \ln\left(\frac{z}{1-z}\right)\left(-3 + \ln(z) + 2\ln\left(\frac{s_{12}}{s_{14}}\right)\right) - \ln(z) \\ & \times\ln(1-z) - 2\,\text{Li}_2(1-z)\Bigg] + \frac{\beta_0}{2}\left[\ln\left(\frac{\mu_\text{R}^2}{s_{12}}\right) + \ln\left(\frac{\mu_\text{R}^2}{s_{14}}\right)\right]\Bigg\} \\ & + z\,T_\text{R}\,(C_\text{A} - C_\text{F}) \end{aligned} \tag{C.48}$$

for the decay of a gluon into a quark. In both splitting functions of the finite remainder the energy fraction is given by

$$z = \frac{E_1 - E_4}{E_1}. \tag{C.49}$$

D

Soft Singularities

Contents

We collect here some useful expressions that regularly appear in the subtraction functions where soft projectors are involved. Moreover, we give some more insight in the general properties of soft-parton emission.

D.1. Soft Gluon Emission

A matrix element factorizes as

$$|\mathcal{M}_{ij\to X+g}(\dots,q)\rangle \simeq g_s\,\boldsymbol{J}_\mu(q)\,\varepsilon^\mu_\lambda(q)\,|\mathcal{M}_{ij\to X}(\dots)\rangle \tag{D.1}$$

when a soft gluon with momentum q is emitted. The soft current is an operator in color space according to

$$\boldsymbol{J}^\mu(q) = \sum_i \boldsymbol{T}_i \frac{p_i^\mu}{(p_i\cdot q)}, \tag{D.2}$$

where the sum runs over all possible emitter particles i of the hard process with momentum p_i and $\boldsymbol{T}_i$ is the related color-charge operator.

Example:
Color singlet production with emission of a soft gluon, $q(p_1)\bar{q}'(p_2) \to V(p_3) + g(q)$.

$$\begin{aligned}
|\mathcal{M}_{q\bar{q}'\to V+g}|^2 &\simeq g_s^2 \sum_\lambda \langle \mathcal{M}_{q\bar{q}'\to V}|\,\boldsymbol{J}^\dagger_\mu(q)\,\varepsilon^{*\mu}_\lambda(q)\varepsilon^\nu_\lambda(q)\,\boldsymbol{J}_\nu(q)\,|\mathcal{M}_{q\bar{q}'\to V}\rangle \\
&= g_s^2 \,\langle \mathcal{M}_{q\bar{q}'\to V}|\,\boldsymbol{J}^\dagger_\mu(q)\,d^{\mu\nu}(q)\,\boldsymbol{J}_\nu(q)\,|\mathcal{M}_{q\bar{q}'\to V}\rangle \\
&= g_s^2 \,\langle \mathcal{M}_{q\bar{q}'\to V}|\,2\,\boldsymbol{T}_q^2 \frac{(p_1\cdot p_2)}{(p_1\cdot q)(p_2\cdot q)}\,|\mathcal{M}_{q\bar{q}'\to V}\rangle \\
&= 2\,C_\mathrm{F}\,g_s^2 \frac{(p_1\cdot p_2)}{(p_1\cdot q)(p_2\cdot q)}\,|\mathcal{M}_{q\bar{q}'\to V}|^2
\end{aligned} \tag{D.3}$$

with

$$\sum_{\lambda} \varepsilon_{\lambda}^{*\mu}(q)\varepsilon_{\lambda}^{\nu}(q) = d^{\mu\nu}(q), \tag{D.4}$$

where $d_{\mu\nu}$ is the gluon polarization tensor in Eq. (C.9), and

$$\boldsymbol{J}_{\mu}^{\dagger}(q)\, d^{\mu\nu}(q)\, \boldsymbol{J}_{\nu}(q) = 2\,\boldsymbol{T}_{q}^{2}\frac{(p_1\cdot p_2)}{(p_1\cdot q)(p_2\cdot q)} \tag{D.5}$$

by making use of color conservation $\boldsymbol{T}_{\bar{q}'} = -\boldsymbol{T}_q$ and $\boldsymbol{T}_q^2 = C_{\mathrm{F}}$ in intermediate steps.

D.2. Double-Soft Single-Collinear Limit

In the double-soft single collinear limit, where a gluon with momentum $q = q_1 + q_2$ is the mediator particle that decays in the soft parton pair, where the both particles have the momenta q_1 and q_2, the squared matrix element factorizes in the following way,

$$\begin{aligned}
&\left|\mathcal{M}_{ij\to X+a_1a_2}(\ldots, q_1, q_2)\right|^2 \\
&\simeq g_s^4 \frac{2}{s_{12}} \sum_{\lambda} \langle \mathcal{M}_{ij\to X}(\ldots)|\, \boldsymbol{J}_{\mu}^{\dagger}(q)\, \varepsilon_{\lambda}^{*\mu}(q) \hat{\boldsymbol{P}}_{a_1a}\, \varepsilon_{\lambda}^{\nu}(q)\, \boldsymbol{J}_{\nu}(q)\, |\mathcal{M}_{ij\to X}(\ldots)\rangle \\
&= g_s^4 \frac{2}{s_{12}} \langle \mathcal{M}_{ij\to X}(\ldots)|\, \boldsymbol{J}_{\mu}^{\dagger}(q)\, \hat{P}_{a_1a}^{\mu\nu}(z, k_\perp; \epsilon)\, \boldsymbol{J}_{\nu}(q)\, |\mathcal{M}_{ij\to X}(\ldots)\rangle \\
&= g_s^4 \frac{2}{s_{12}} \langle \mathcal{M}_{ij\to X}(\ldots)|\, \boldsymbol{J}_{\mu}^{\dagger}(q)\, \boldsymbol{J}^{\mu}(q) \widetilde{P}_{a_1a}^{(0)}(z;\epsilon) - \frac{1}{k_\perp^2}\big(\boldsymbol{J}_{\mu} k_\perp^{\mu}\big)^2 \widetilde{P}_{a_1a}^{\perp}(z;\epsilon)\, |\mathcal{M}_{ij\to X}(\ldots)\rangle\,.
\end{aligned} \tag{D.6}$$

The polarized splitting function is contracted with two soft current functions. Double-soft singularities can originate either from a soft gluon pair or a soft quark-antiquark pair. They can never come from a soft quark-gluon pair, since this would violate quark-number conservation.

Example:
Considering color singlet production with emission of a double-soft collinear gluon pair, $q(p_1)\bar{q}'(p_2) \to V(p_3) + g(q_1)g(q_2)$ and $q = q_1 + q_2$, it is then straightforward to find

$$\begin{aligned}
&\left|\mathcal{M}_{q\bar{q}'\to V+gg}\right|^2 \\
&\simeq g_s^4 \frac{2}{s_{12}} \left[2\, C_{\mathrm{F}} \frac{(p_1\cdot p_2)}{(p_1\cdot q)(p_2\cdot q)} \widetilde{P}_{gg}^{(0)}(z;\epsilon) - C_{\mathrm{F}} \frac{1}{k_\perp^2} \left(\frac{(p_1\cdot k_\perp)}{(p_1\cdot q)} - \frac{(p_2\cdot k_\perp)}{(p_2\cdot q)} \right)^2 \widetilde{P}_{gg}^{\perp}(z;\epsilon) \right] \\
&\quad \times \left|\mathcal{M}_{q\bar{q}'\to V}\right|^2.
\end{aligned} \tag{D.7}$$

D.3. Soft Functions

At NLO the soft function

$$S_{ij}(p_k) = \frac{(p_i\cdot p_j)}{(p_i\cdot p_k)(p_j\cdot p_k)}. \tag{D.8}$$

describes the emission of a soft gluon.

At NNLO double-soft singularities are present. They are characterized by the soft function

$$\begin{aligned} S_{ij}(p_k,p_l;\epsilon) = S_{ij}^{\text{s.o.}}(p_k,p_l) &- \frac{2(p_i\cdot p_j)}{(p_k\cdot p_l)\left[p_i\cdot(p_k+p_l)\right]\left[p_j\cdot(p_k+p_l)\right]} \\ &+ \frac{(p_i\cdot p_k)(p_j\cdot p_l)+(p_i\cdot p_l)(p_j\cdot p_k)}{\left[p_i\cdot(p_k+p_l)\right]\left[p_j\cdot(p_k+p_l)\right]}\left(\frac{1-\epsilon}{(p_k\cdot p_l)^2}-\frac{1}{2}S_{ij}^{\text{s.o.}}(p_k,p_l)\right), \end{aligned} \tag{D.9}$$

which depends on the strongly-ordered soft function

$$\begin{aligned} S_{ij}^{\text{s.o.}}(p_k,p_l) = \frac{(p_i\cdot p_j)}{(p_k\cdot p_l)}&\left(\frac{1}{(p_i\cdot p_k)(p_j\cdot p_l)}+\frac{1}{(p_i\cdot p_l)(p_j\cdot p_k)}\right) \\ &- \frac{(p_i\cdot p_j)^2}{(p_i\cdot p_k)(p_j\cdot p_k)(p_i\cdot p_l)(p_j\cdot p_l)}, \end{aligned} \tag{D.10}$$

if a soft gluon pair is emitted.
If a soft quark pair is emitted, the soft function reads

$$I_{ij}(p_k,p_l) = \frac{(p_i\cdot p_k)(p_j\cdot p_l)+(p_i\cdot p_l)(p_j\cdot p_k)-(p_i\cdot p_j)(p_k\cdot p_l)}{(p_k\cdot p_l)^2\left[p_i\cdot(p_k+p_l)\right]\left[p_j\cdot(p_k+p_l)\right]}. \tag{D.11}$$

D.4. Double-Soft Triple-Collinear Limit

In the double-soft triple-collinear limit the double soft operator has to act on the triple-collinear splitting function. The relevant results for color singlet production are[1]

$$\begin{aligned} \hat{P}^{\boldsymbol{\mathcal{S}}}_{g_1g_2q_3} &= \boldsymbol{\mathcal{S}}\hat{P}_{g_1g_2q_3}, \\ \hat{P}^{\boldsymbol{\mathcal{S}}}_{\bar{q}_1'q_2'q_3} &= \boldsymbol{\mathcal{S}}\hat{P}_{\bar{q}_1'q_2'q_3}, \\ \hat{P}^{\boldsymbol{\mathcal{S}}}_{\bar{q}_1q_2q_3} &= \boldsymbol{\mathcal{S}}\hat{P}_{\bar{q}_1q_2q_3}. \end{aligned} \tag{D.12}$$

The first expression can be write according to Eq. (C.42) as

$$\hat{P}^{\boldsymbol{\mathcal{S}}}_{g_1g_2q_3} = C_{\text{F}}^2\hat{P}^{\boldsymbol{\mathcal{S}}\,(\text{ab})}_{ggq} + C_{\text{F}}C_{\text{A}}\hat{P}^{\boldsymbol{\mathcal{S}}\,(\text{nab})}_{g_1g_2q_3}. \tag{D.13}$$

with the abelian term

$$\hat{P}^{\boldsymbol{\mathcal{S}}\,(\text{ab})}_{g_1g_2q_3} = 4\frac{\tilde{s}_{123}^2}{z_1z_2s_{13}s_{23}} \tag{D.14}$$

and the non-abelian piece

$$\begin{aligned} \hat{P}^{\boldsymbol{\mathcal{S}}\,(\text{nab})}_{g_1g_2q_3} = \frac{\tilde{t}_{12,3}^2}{2s_{12}^2}(1-\epsilon) &+ \frac{\tilde{s}_{123}^2}{s_{12}}\left(\frac{1}{z_2s_{13}}+\frac{1}{z_1s_{23}}\right)+\frac{\tilde{s}_{123}^2}{z_{12}s_{12}}\left(\frac{1}{s_{13}}+\frac{1}{s_{23}}\right) \\ &- \frac{\tilde{s}_{123}^2}{z_1z_2s_{13}s_{23}}+\frac{\tilde{s}_{123}}{z_{12}s_{12}}\left(\frac{z_1}{z_2}+\frac{z_2}{z_1}-6\right)+\frac{\tilde{s}_{123}}{z_{12}}\left(\frac{1}{z_2s_{13}}+\frac{1}{z_1s_{23}}\right) \\ &- \frac{\tilde{s}_{123}}{z_1z_2}\left(\frac{1}{s_{13}}+\frac{1}{s_{23}}\right). \end{aligned} \tag{D.15}$$

[1] We omit the explicit functional dependence on the momenta in order to keep the result in the same notation as in Appendix C.

The double-soft triple-collinear limit for a quark decaying into non-identical quarks is

$$\hat{P}^{\boldsymbol{\mathcal{S}}}_{\bar{q}_1' q_2' q_3} = \frac{1}{2} C_{\mathrm{F}} T_{\mathrm{R}} \frac{\tilde{s}_{123}}{s_{12}} \left(-\frac{\tilde{t}^2_{12,3}}{\tilde{s}_{123} s_{12}} + \frac{4}{z_{12}} \right), \tag{D.16}$$

which coincides with the decay into identical quarks

$$\hat{P}^{\boldsymbol{\mathcal{S}}}_{\bar{q}_1 q_2 q_3} = \hat{P}^{\boldsymbol{\mathcal{S}}}_{\bar{q}_1' q_2' q_3}. \tag{D.17}$$

As abbreviations we use $\tilde{s}_{123} = s_{13} + s_{23}$ for the subenergy, where $s_{ij} = (p_i + p_j)^2$, and the energy fractions

$$z_1 = \frac{E_1}{E_3}, \quad z_2 = \frac{E_2}{E_3}, \quad z_{12} = z_1 + z_2, \tag{D.18}$$

as well as

$$\tilde{t}_{12,3} = 2 \frac{z_1 s_{23} - z_2 s_{13}}{z_{12}}. \tag{D.19}$$

E

Infrared Limits

Contents

In this appendix, we give an overview of the subtraction functions up to NNLO QCD precision for color-singlet production that is initiated by a quark-antiquark pair at LO. We will repeat the functions for the quark-antiquark channel that we already presented in the main text in a compact form, but also show the solutions for the other channels that were not discussed in detail before.
We show the action for each possible IR operator combination in the following for one non-redundant exemplary subtraction function so that all not listed functions can be trivially obtained by renaming of indices. All relevant splitting functions that will show up in the subtraction functions can be found in Appendix C, the soft functions are given in Appendix D.
IR limits are studied extensively in literature, *cf.* Refs. [121, 217, 266, 267, 271–278, 313], and are adopted by us as pointed out in the main text of this work wherever a results is overtaken. The results of these sources build also the basis of the here presented projections.

E.1. Next-to-Leading Order Projections

Functions with NLO kinematics appear either at tree-level, see subsection E.1.2, or as one-loop functions, see subsection E.1.3. The two projectors for extracting the leading singularities are listed in subsection E.1.1.

E.1.1. Projectors

The leading soft singularities can be extracted with the operator

$$\mathcal{S}_i A = \lim_{E_i \to 0} A. \tag{E.1}$$

For obtaining leading collinear singularities we use the operator

$$\mathcal{C}_{ji} A = \lim_{\eta_{ij} \to 0} A. \tag{E.2}$$

E.1.2. Leading Singularities of Tree-Level F_{LM} Functions

The action of the above defined projectors on squared tree-level matrix elements is then given by the following expressions:

Soft Limit

The soft limit is just allowed in the quark-antiquark channel. The result reads

$$\mathcal{S}_4 F_{\mathrm{LM}}(1_{f_a}, 2_{f_b} \,|\, 4_g) = 2\, C_{\mathrm{F}}\, g_{s,\epsilon}^2 S_{12}(p_4) F_{\mathrm{LM}}(1_{f_a}, 2_{f_b}). \tag{E.3}$$

Collinear Limit

Collinear limits are present in the quark-antiquark channel,

$$\mathcal{C}_{41} F_{\mathrm{LM}}(1_{f_a}, 2_{f_b} \,|\, 4_g) = g_{s,\epsilon}^2 \frac{1}{(p_1 \cdot p_4)} P_{qq}^{(0)}(z;\epsilon) \frac{F_{\mathrm{LM}}(z \cdot 1_{f_a}, 2_{f_b})}{z}, \tag{E.4}$$

with the energy fraction

$$z = \frac{E_1 - E_4}{E_1}, \tag{E.5}$$

and in the quark-gluon channel,

$$\mathcal{C}_{42} F_{\mathrm{LM}}(1_{f_a}, 2_g \,|\, 4_{f_x}) = g_{s,\epsilon}^2 \frac{1}{(p_2 \cdot p_4)} P_{qg}^{(0)}(z;\epsilon) \frac{F_{\mathrm{LM}}(1_{f_a}, z \cdot 2_{\bar{f}_x})}{z}, \tag{E.6}$$

where the momentum fraction is given by

$$z = \frac{E_2 - E_4}{E_2}. \tag{E.7}$$

Soft-Collinear Limit

The combined soft-collinear limit is again only divergent in the quark-antiquark process,

$$\mathcal{C}_{41} \mathcal{S}_4 F_{\mathrm{LM}}(1_{f_a}, 2_{f_b} \,|\, 4_g) = C_{\mathrm{F}}\, g_{s,\epsilon}^2 \frac{1}{E_4^2 \eta_{14}} F_{\mathrm{LM}}(1_{f_a}, 2_{f_b}). \tag{E.8}$$

E.1.3. Leading Singularities of Real-Virtual F_{LRV} Functions

In case the projectors act on the interference of one-loop matrix elements with tree-level matrix elements the results are usually shown in literature before the manifest IR poles of the loops are isolated. However, in our computation we need also the subtraction functions for projectors acting on the finite remainders, so we will give the solutions for both scenarios.

Soft Limit

Soft limits lead only in the quark-antiquark channel to divergences, the related subtraction function reads

$$\begin{aligned}\mathcal{S}_4 F_{\mathrm{LRV}}(1_{f_a}, 2_{f_b} \,|\, 4_g) = 2\, C_{\mathrm{F}}\, g_{s,\epsilon}^2 S_{12}(p_4) \Bigg\{ & F_{\mathrm{LV}}(1_{f_a}, 2_{f_b}) + [\alpha_{s,\epsilon}] \\ & \times \left[c_\Gamma \left(\frac{S_{12}(p_4)}{2} \right)^{\epsilon} \mathrm{Eik}_g^{\mathrm{Loop}}(\epsilon) - \frac{\Gamma(1-\epsilon)}{\mu_{\mathrm{F}}^{2\epsilon} e^{\epsilon\gamma_{\mathrm{E}}}} \frac{\beta_0}{\epsilon} \right] \\ & \times F_{\mathrm{LM}}(1_{f_a}, 2_{f_b}) \Bigg\},\end{aligned} \tag{E.9}$$

with the one-loop Eikonal function

$$\mathrm{Eik}_g^{\mathrm{Loop}}(\epsilon) = -C_{\mathrm{A}} \frac{1}{\epsilon^2} \frac{\Gamma^2(1-\epsilon)\Gamma^2(1+\epsilon)}{\Gamma(1-2\epsilon)\Gamma(1+2\epsilon)}. \tag{E.10}$$

Collinear Limit

Collinear limits appear again in the quark-antiquark channel,

$$\begin{aligned}\mathcal{C}_{41} F_{\mathrm{LRV}}(1_{f_a}, 2_{f_b} \,|\, 4_g) = g_{s,\epsilon}^2 \frac{1}{(p_1 \cdot p_4)} \Bigg\{ & P_{qq}^{(0)}(z;\epsilon) \frac{F_{\mathrm{LV}}(z \cdot 1_{f_a}, 2_{f_b})}{z} + [\alpha_{s,\epsilon}] \\ & \times \left[c_\Gamma \left(\frac{1}{2(p_1 \cdot p_4)} \right)^{\epsilon} P_{qq}^{\mathrm{Loop}}(z;\epsilon) - \frac{S_\epsilon}{\mu_{\mathrm{R}}^{2\epsilon}} \frac{\Gamma(1-\epsilon)}{(4\pi)^\epsilon} \frac{\beta_0}{\epsilon} P_{qq}^{(0)}(z;\epsilon) \right] \\ & \times \frac{F_{\mathrm{LM}}(z \cdot 1_{f_a}, 2_{f_b})}{z} \Bigg\},\end{aligned} \tag{E.11}$$

with the energy fraction

$$z = \frac{E_1 - E_4}{E_1}, \tag{E.12}$$

as well as in the quark-gluon channel,

$$\begin{aligned}\mathcal{C}_{42} F_{\mathrm{LRV}}(1_{f_a}, 2_g \,|\, 4_{f_x}) = g_{s,\epsilon}^2 \frac{1}{(p_2 \cdot p_4)} \Bigg\{ & P_{qg}^{(0)}(z;\epsilon) \frac{F_{\mathrm{LV}}(1_{f_a}, z \cdot 2_{\bar{f}_x})}{z} + [\alpha_{s,\epsilon}] \\ & \times \left[c_\Gamma \left(\frac{1}{2(p_2 \cdot p_4)} \right)^{\epsilon} P_{qg}^{\mathrm{Loop}}(z;\epsilon) - \frac{S_\epsilon}{\mu_{\mathrm{R}}^{2\epsilon}} \frac{\Gamma(1-\epsilon)}{(4\pi)^\epsilon} \frac{\beta_0}{\epsilon} P_{qg}^{(0)}(z;\epsilon) \right] \\ & \times \frac{F_{\mathrm{LM}}(1_{f_a}, z \cdot 2_{\bar{f}_x})}{z} \Bigg\},\end{aligned} \tag{E.13}$$

with

$$z = \frac{E_2 - E_4}{E_2}. \tag{E.14}$$

Soft-Collinear Limit

The soft-collinear limit in the quark-antiquark channel is

$$\begin{aligned}\mathcal{C}_{41}\mathcal{S}_4 F_{\mathrm{LRV}}(1_{f_a}, 2_{f_b} \,|\, 4_g) = C_{\mathrm{F}}\, g_{s,\epsilon}^2 \frac{1}{E_4^2 \eta_{14}} \Bigg\{ & F_{\mathrm{LV}}(1_{f_a}, 2_{f_b}) + [\alpha_{s,\epsilon}] \left[c_\Gamma \left(\frac{1}{4E_4^2 \eta_{14}} \right)^{\epsilon} \right. \\ & \left. \times \mathrm{Eik}_g^{\mathrm{Loop}}(\epsilon) - \frac{\Gamma(1-\epsilon)}{\mu_{\mathrm{F}}^{2\epsilon} e^{\epsilon\gamma_{\mathrm{E}}}} \frac{\beta_0}{\epsilon} \right] F_{\mathrm{LM}}(1_{f_a}, 2_{f_b}) \Bigg\},\end{aligned} \tag{E.15}$$

with the same Eikonal function as in Eq. (E.10).

Soft Limit of the Finite Remainder

For the finite remainder we find the soft subtraction term

$$\begin{aligned}\mathcal{S}_4 F^{\text{fin}}_{\text{LRV}}(1_{f_a},2_{f_b}\,|\,4_g) = 2\,C_{\text{F}}\,g_s^2 S_{12}(p_4)\Big\{F^{\text{fin}}_{\text{LV}}(1_{f_a},2_{f_b}) + \frac{\alpha_s(\mu_{\text{R}})}{2\pi} \\ \times \text{Eik}^{\text{Loop}}_{g,\text{F}}(p_1,p_2,p_4;\mu_{\text{F}})F_{\text{LM}}(1_{f_a},2_{f_b})\Big\},\end{aligned} \tag{E.16}$$

and the Eikonal function

$$\begin{aligned}\text{Eik}^{\text{Loop}}_{g,\text{F}}(p_1,p_2,p_4;\mu_{\text{F}}) = C_{\text{A}}\left\{\frac{5\pi^2}{6} + \frac{3}{4}\left[\ln\left(-\frac{\hat{s}}{\hat{t}}\right)+\ln\left(-\frac{\hat{s}}{\hat{u}}\right)\right] - \ln\left(-\frac{\hat{s}}{\hat{t}}\right)\ln\left(-\frac{\hat{s}}{\hat{u}}\right)\right\} \\ + \frac{1}{2}\beta_0\left[\ln\left(-\frac{\mu_{\text{F}}^2}{\hat{t}}\right)+\ln\left(-\frac{\mu_{\text{F}}^2}{\hat{u}}\right)\right].\end{aligned} \tag{E.17}$$

Collinear Limit of the Finite Remainder

The collinear limit of the finite remainder in the quark-antiquark channel is

$$\begin{aligned}\mathcal{C}_{41}F^{\text{fin}}_{\text{LRV}}(1_{f_a},2_{f_b}\,|\,4_g) = g_s^2\frac{1}{(p_1\cdot p_4)}\left\{P^{(0)}_{qq}(z;0)\frac{F^{\text{fin}}_{\text{LV}}(z\cdot 1_{f_a},2_{f_b})}{z}\right. \\ \left. + \frac{\alpha_s(\mu_{\text{R}})}{2\pi}P^{\text{Loop}}_{qq,\text{F}}(p_1,p_2,p_4)\frac{F_{\text{LM}}(z\cdot 1_{f_a},2_{f_b})}{z}\right\},\end{aligned} \tag{E.18}$$

where

$$z = \frac{E_1 - E_4}{E_1}. \tag{E.19}$$

In the quark-gluon channel this limit reads[1]

$$\begin{aligned}\mathcal{C}_{42}F^{\text{fin}}_{\text{LRV}}(1_{f_a},2_g\,|\,4_{f_x}) = g_s^2\frac{1}{(p_2\cdot p_4)}\left\{P^{(0)}_{qg}(z;0)\frac{F^{\text{fin}}_{\text{LV}}(1_{f_a},z\cdot 2_{\bar{f}_x})}{z}\right. \\ \left. + \frac{\alpha_s(\mu_{\text{R}})}{2\pi}P^{\text{Loop}}_{qg,\text{F}}(p_2,p_1,p_4)\frac{F_{\text{LM}}(1_{f_a},z\cdot 2_{\bar{f}_x})}{z}\right\},\end{aligned} \tag{E.20}$$

where

$$z = \frac{E_2 - E_4}{E_2}. \tag{E.21}$$

Soft-Collinear Limit of the Finite Remainder

In the quark-antiquark channel the soft-collinear limit is

$$\begin{aligned}\mathcal{C}_{41}\mathcal{S}_4 F^{\text{fin}}_{\text{LRV}}(1_{f_a},2_{f_b}\,|\,4_g) = C_{\text{F}}\,g_s^2\frac{1}{E_4^2\eta_{14}}\Big\{F^{\text{fin}}_{\text{LV}}(1_{f_a},2_{f_b}) + \frac{\alpha_s(\mu_{\text{R}})}{2\pi} \\ \times \text{Eik}^{\text{Loop},\mathcal{C}_{41}}_{g,\text{F}}(p_1,p_2,p_4;\mu_{\text{F}})F_{\text{LM}}(1_{f_a},2_{f_b})\Big\},\end{aligned} \tag{E.22}$$

[1] Note the order of the momenta arguments of the one-loop splitting function.

with the function

$$\begin{aligned}\mathrm{Eik}_{g,\mathrm{F}}^{\mathrm{Loop},\mathcal{C}_{41}}(p_1,p_2,p_4;\mu_\mathrm{F}) = C_\mathrm{A}\left[\frac{5\pi^2}{6}+\frac{3}{4}\ln\!\left(\frac{E_1E_2}{E_4^2\eta_{14}}\right)-\ln\!\left(\frac{E_1}{E_4}\right)\ln\!\left(\frac{E_2}{E_4\eta_{14}}\right)\right]\\ +\frac{1}{2}\beta_0\left[\ln\!\left(\frac{\mu_\mathrm{F}^2}{4E_1E_4\eta_{14}}\right)+\ln\!\left(\frac{\mu_\mathrm{F}^2}{4E_2E_4}\right)\right].\end{aligned} \tag{E.23}$$

E.2. Next-to-Next-to-Leading Order Projections

To NNLO kinematics just tree-level functions can contribute. The IR projectors that are necessary to extract their singularities are defined in subsection E.2.1. The following subtractions terms are presented in subsection E.2.2.

E.2.1. Projectors

The operators for extracting the single-soft and double-soft divergences are

$$\begin{aligned}\mathcal{S}_i A &= \lim_{E_i\to 0} A,\\ \boldsymbol{\mathcal{S}} A &= \lim_{E_4,E_5\to 0} A, \text{ at fixed ratio } \frac{E_5}{E_4},\end{aligned} \tag{E.24}$$

respectively. The collinear divergences are extracted with the projectors

$$\begin{aligned}\mathcal{C}_{ji} A &= \lim_{\eta_{ij}\to 0} A,\\ \boldsymbol{\mathcal{C}}_i A &= \lim_{\eta_{i4},\eta_{i5}\to 0} A, \text{ with non-vanishing ratios } \frac{\eta_{i4}}{\eta_{i5}}, \frac{\eta_{45}}{\eta_{i4}}, \frac{\eta_{45}}{\eta_{i5}},\end{aligned} \tag{E.25}$$

in case of single-collinear and triple-collinear limits, respectively.

E.2.2. Leading Singularities of Tree-Level F_{LM} Functions

Single-Soft Limits

If a single gluon becomes soft, the factorization in the quark-antiquark channel reads

$$\begin{aligned}\mathcal{S}_5 F_{\mathrm{LM}}(1_{f_a},2_{f_b}\,|\,4_g,5_g) = g_{s,\epsilon}^2\left[(2\,C_\mathrm{F}-C_\mathrm{A})S_{12}(p_5)+C_\mathrm{A}\big(S_{14}(p_5)+S_{24}(p_5)\big)\right]\\ \times F_{\mathrm{LM}}(1_{f_a},2_{f_b}\,|\,4_g).\end{aligned} \tag{E.26}$$

The result in the quark gluon channel is

$$\begin{aligned}\mathcal{S}_5 F_{\mathrm{LM}}(1_{f_a},2_g\,|\,4_{f_x},5_g) = g_{s,\epsilon}^2\left[(2\,C_\mathrm{F}-C_\mathrm{A})S_{14}(p_5)+C_\mathrm{A}\big(S_{12}(p_5)+S_{24}(p_5)\big)\right]\\ \times F_{\mathrm{LM}}(1_{f_a},2_g\,|\,4_{f_x}).\end{aligned} \tag{E.27}$$

Double-Soft Limits

Double-soft singularities can show up either in the quark-antiquark channel,

$$\boldsymbol{\mathcal{S}} F_{\mathrm{LM}}(1_{f_a},2_{f_b}\,|\,4_g,5_g) = g_{s,\epsilon}^4\,\mathrm{Eik}_{gg}(p_1,p_2,p_4,p_5;\epsilon)F_{\mathrm{LM}}(1_{f_a},2_{f_b}), \tag{E.28}$$

with the Eikonal function for a soft gluon pair,

$$\begin{aligned}\mathrm{Eik}_{gg}(p_1,p_2,p_4,p_5;\epsilon) = C_\mathrm{F}\,C_\mathrm{A}\big(2\,S_{12}(p_4,p_5;\epsilon) - S_{11}(p_4,p_5;\epsilon) - S_{22}(p_4,p_5;\epsilon)\big)\\ + 4\,C_\mathrm{F}^2 S_{12}(p_4)S_{12}(p_5),\end{aligned} \tag{E.29}$$

or in the quark-quark channel,

$$\boldsymbol{\mathcal{S}} F_\mathrm{LM}(1_{f_a},2_{f_b}\,|\,4_{f_c},5_{\bar{f}_c}) = g_{s,\epsilon}^4\,\mathrm{Eik}_{qq}(p_1,p_2,p_4,p_5;\epsilon)F_\mathrm{LM}(1_{f_a},2_{f_b}), \tag{E.30}$$

where the Eikonal function for a soft quark pair is given by

$$\mathrm{Eik}_{qq}(p_1,p_2,p_4,p_5;\epsilon) = -C_\mathrm{F}T_\mathrm{R}\big(2\,I_{12}(p_4,p_5;\epsilon) - I_{11}(p_4,p_5;\epsilon) - I_{22}(p_4,p_5;\epsilon)\big). \tag{E.31}$$

Strongly-Ordered Double-Soft Limits

The strongly-ordered double-soft limit instead, is only present in the quark-antiquark channel,

$$\begin{aligned}\boldsymbol{\mathcal{S}}\mathcal{S}_5 F_\mathrm{LM}(1_q,2_q\,|\,4_g,5_g) = 2\,C_\mathrm{F}\,g_{s,\epsilon}^4\big[(2\,C_\mathrm{F}-C_\mathrm{A})S_{12}(p_5) + C_\mathrm{A}\big(S_{14}(p_5)+S_{24}(p_5)\big)\big]\\ \times S_{12}(p_4)\,F_\mathrm{LM}(1_q,2_q).\end{aligned} \tag{E.32}$$

Single-Collinear Limits

Single collinear limits appear in all channels. In the quark-antiquark channel they are

$$\mathcal{C}_{51}F_\mathrm{LM}(1_{f_a},2_{f_b}\,|\,4_g,5_g) = g_{s,\epsilon}^2\frac{1}{(p_1\cdot p_5)}P_{qq}^{(0)}(z;\epsilon)\frac{F_\mathrm{LM}(z\cdot 1_{f_a},2_{f_b}\,|\,4_g)}{z}, \tag{E.33a}$$

$$\begin{aligned}\mathcal{C}_{45}F_\mathrm{LM}(1_{f_a},2_{f_b}\,|\,4_g,5_g) &\overset{(b)}{=} g_{s,\epsilon}^2\frac{1}{(p_4\cdot p_5)}P_{gg,\mu\nu}(z,k_\perp;\epsilon)F_\mathrm{LM}^{\mu\nu}\left(1_{f_a},2_{f_b}\,\middle|\,\frac{4_g}{z}\right)\\ &= g_{s,\epsilon}^2\frac{1}{(p_4\cdot p_5)}\left[\widetilde{P}_{gg}^{(0)}(z;\epsilon)F_\mathrm{LM}\left(1_{f_a},2_{f_b}\,\middle|\,\frac{4_g}{z}\right)\right.\\ &\quad\left.+\widetilde{P}_{gg}^{\perp}(z;\epsilon)\kappa_{\perp,\mu}\kappa_{\perp,\nu}F_\mathrm{LM}^{\mu\nu}\left(1_{f_a},2_{f_b}\,\middle|\,\frac{4_g}{z}\right)\right],\end{aligned} \tag{E.33b}$$

with the energy fractions $z = \dfrac{E_1-E_5}{E_1}$ in Eq. (E.33a) or $z = \dfrac{E_4}{E_4+E_5}$ in Eq. (E.33b). The notation (b) on top of the equal sign indicates that this limit is valid in sector (b), while the limit in sector (d) can be extracted by exchanging the indices properly.
In the quark-antiquark channel collinear singularities show up when an initial-state quark and a final-state quark become collinear to each other,

$$\begin{aligned}\mathcal{C}_{51}F_\mathrm{LM}(1_{f_a},2_{f_b}\,|\,4_{f_c},5_{f_a}) &= g_{s,\epsilon}^2\frac{1}{(p_1\cdot p_5)}P_{gq,\mu\nu}(z,k_\perp;\epsilon)\frac{F_\mathrm{LM}^{\mu\nu}\,(z\cdot 1_g,2_{f_b}\,|\,4_{f_c})}{z}\\ &= g_{s,\epsilon}^2\frac{1}{(p_1\cdot p_5)}\left[\widetilde{P}_{gq}^{(0)}(z;\epsilon)\frac{F_\mathrm{LM}\,(z\cdot 1_g,2_{f_b}\,|\,4_{f_c})}{z}\right.\\ &\quad\left.+\widetilde{P}_{gq}^{\perp}(z;\epsilon)\kappa_{\perp,\mu}\kappa_{\perp,\nu}\frac{F_\mathrm{LM}^{\mu\nu}\,(z\cdot 1_g,2_{f_b}\,|\,4_{f_c})}{z}\right],\end{aligned} \tag{E.34}$$

where $z = \dfrac{E_1 - E_5}{E_1}$. The splitting function here reads

$$P_{gq}^{\mu\nu}(z, k_\perp; \epsilon) = \frac{1-\epsilon}{T_\mathrm{R}} C_\mathrm{F}\, z\, P_{qg}^{\mu\nu}\left(\frac{1}{z}, k_\perp; \epsilon\right), \tag{E.35}$$

which can be decomposed into

$$\begin{aligned} \widetilde{P}_{gq}^{(0)}(z;\epsilon) &= C_\mathrm{F}\, z\,(1-\epsilon), \\ \widetilde{P}_{gq}^{\perp}(z;\epsilon) &= 4\, C_\mathrm{F} \frac{1-z}{z}(1-\epsilon). \end{aligned} \tag{E.36}$$

In the quark-gluon channel the collinear limits have many different forms,

$$\mathcal{C}_{42} F_\mathrm{LM}(1_{f_a}, 2_g \,|\, 4_{f_x}, 5_g) = g_{s,\epsilon}^2 \frac{1}{(p_2 \cdot p_4)} P_{qg}^{(0)}(z;\epsilon) \frac{F_\mathrm{LM}(1_{f_a}, z \cdot 2_{\bar{f}_x} \,|\, 5_g)}{z}, \tag{E.37a}$$

$$\mathcal{C}_{51} F_\mathrm{LM}(1_{f_a}, 2_g \,|\, 4_{f_x}, 5_g) = g_{s,\epsilon}^2 \frac{1}{(p_1 \cdot p_5)} P_{qq}^{(0)}(z;\epsilon) \frac{F_\mathrm{LM}(z \cdot 1_{f_a}, 2_g \,|\, 4_{f_x})}{z}, \tag{E.37b}$$

$$\begin{aligned} \mathcal{C}_{52} F_\mathrm{LM}(1_{f_a}, 2_g \,|\, 4_{f_x}, 5_g) &= -g_{s,\epsilon}^2 \frac{1}{(p_2 \cdot p_5)} P_{gg,\mu\nu}\left(\frac{1}{z}, k_\perp; \epsilon\right) F_\mathrm{LM}^{\mu\nu}\left(1_{f_a}, z \cdot 2_g \,|\, 4_{f_x}\right) \\ &= -g_{s,\epsilon}^2 \frac{1}{(p_2 \cdot p_5)} \left[\widetilde{P}_{gg}^{(0)}\left(\frac{1}{z};\epsilon\right) F_\mathrm{LM}\left(1_{f_a}, z \cdot 2_g \,|\, 4_{f_x}\right) \right. \\ &\quad \left. + \widetilde{P}_{gg}^{\perp}\left(\frac{1}{z};\epsilon\right) \kappa_{\perp,\mu} \kappa_{\perp,\nu} F_\mathrm{LM}^{\mu\nu}\left(1_{f_a}, z \cdot 2_g \,|\, 4_{f_x}\right) \right], \end{aligned} \tag{E.37c}$$

$$\mathcal{C}_{45} F_\mathrm{LM}(1_{f_a}, 2_g \,|\, 4_{f_x}, 5_g) \overset{(b)}{=} g_{s,\epsilon}^2 \frac{1}{(p_4 \cdot p_5)} P_{qq}^{(0)}(z;\epsilon) F_\mathrm{LM}\left(1_{f_a}, 2_g \,\middle|\, \frac{4_{f_x}}{z}\right), \tag{E.37d}$$

$$\mathcal{C}_{45} F_\mathrm{LM}(1_{f_a}, 2_g \,|\, 4_{f_x}, 5_g) \overset{(d)}{=} g_{s,\epsilon}^2 \frac{1}{(p_4 \cdot p_5)} P_{qg}^{(0)}(z;\epsilon) F_\mathrm{LM}\left(1_{f_a}, 2_g \,\middle|\, \frac{5_{f_x}}{z}\right), \tag{E.37e}$$

with $z = \dfrac{E_2 - E_4}{E_2}$ in Eq. (E.37a), $z = \dfrac{E_1 - E_5}{E_1}$ in Eq. (E.37b), $z = \dfrac{E_2 - E_5}{E_2}$ in Eq. (E.37c), $z = \dfrac{E_4}{E_4 + E_5}$ in Eq. (E.37d) for sector (b), and $z = \dfrac{E_5}{E_4 + E_5}$ in Eq. (E.37e) for sector (d). The argument of the splitting function in the collinear limit $\mathcal{C}_{52}$ is the inverse of the energy fraction z, this is due to the fact that we use a final-state splitting function for describing an initial-state splitting and thus have to apply a crossing relation. This is also the origin of the additional minus sign.
In the gluon-gluon channel the limit is simply

$$\mathcal{C}_{51} F_\mathrm{LM}(1_g, 2_g \,|\, 4_{f_x}, 5_{f_y}) = g_{s,\epsilon}^2 \frac{1}{(p_1 \cdot p_5)} P_{qg}^{(0)}(z;\epsilon) \frac{F_\mathrm{LM}(z \cdot 1_{\bar{f}_y}, 2_g \,|\, 4_{f_x})}{z}, \tag{E.38}$$

with $z = \dfrac{E_1 - E_5}{E_1}$.

Double-Collinear Limits

Double-collinear limits are obtained by application of two single-collinear limits. In the quark-antiquark channel we get

$$\mathcal{C}_{41}\mathcal{C}_{52}F_{\mathrm{LM}}(1_{f_a},2_{f_b}\,|\,4_g,5_g) = g_{s,\epsilon}^4\frac{1}{(p_1\cdot p_4)}P_{qq}^{(0)}(z;\epsilon)\frac{1}{(p_2\cdot p_5)}P_{qq}^{(0)}(\bar{z};\epsilon)\frac{F_{\mathrm{LM}}(z\cdot 1_{f_a},\bar{z}\cdot 2_{f_b})}{z\bar{z}}, \tag{E.39}$$

with $z=\dfrac{E_1-E_4}{E_1}$ and $\bar{z}=\dfrac{E_2-E_5}{E_2}$.
In the quark-gluon channel we find

$$\mathcal{C}_{51}\mathcal{C}_{42}F_{\mathrm{LM}}(1_{f_a},2_g\,|\,4_{f_x},5_g) = g_{s,\epsilon}^4\frac{1}{(p_1\cdot p_5)}P_{qq}^{(0)}(z;\epsilon)\frac{1}{(p_2\cdot p_4)}P_{qg}^{(0)}(\bar{z};\epsilon)\frac{F_{\mathrm{LM}}(z\cdot 1_{f_a},\bar{z}\cdot 2_{\bar{f}_x})}{z\bar{z}}, \tag{E.40}$$

where $z=\dfrac{E_1-E_5}{E_1}$ and $\bar{z}=\dfrac{E_2-E_4}{E_2}$.
In the gluon-gluon channel the double-collinear limit is

$$\mathcal{C}_{41}\mathcal{C}_{52}F_{\mathrm{LM}}(1_g,2_g\,|\,4_{f_x},5_{f_y}) = g_{s,\epsilon}^4\frac{1}{(p_1\cdot p_4)}P_{qg}^{(0)}(z;\epsilon)\frac{1}{(p_2\cdot p_5)}P_{qg}^{(0)}(\bar{z};\epsilon)\frac{F_{\mathrm{LM}}(z\cdot 1_{\bar{f}_x},\bar{z}\cdot 2_{\bar{f}_y})}{z\bar{z}}, \tag{E.41}$$

with $z=\dfrac{E_1-E_4}{E_1}$ and $\bar{z}=\dfrac{E_2-E_5}{E_2}$.

Single-Soft Single-Collinear Limits

The combination of a single-soft and a single-collinear limit can take many different shapes. In the quark-antiquark the three different forms are

$$\mathcal{C}_{51}\mathcal{S}_5F_{\mathrm{LM}}(1_{f_a},2_{f_b}\,|\,4_g,5_g) = C_{\mathrm{F}}\,g_{s,\epsilon}^2\frac{1}{E_5^2\eta_{15}}F_{\mathrm{LM}}(1_{f_a},2_{f_b}\,|\,4_g), \tag{E.42a}$$

$$\mathcal{C}_{41}\mathcal{S}_5F_{\mathrm{LM}}(1_{f_a},2_{f_b}\,|\,4_g,5_g) = 2\,C_{\mathrm{F}}\,g_{s,\epsilon}^4S_{12}(p_5)\frac{1}{(p_1\cdot p_4)}P_{qq}^{(0)}(z;\epsilon)\frac{F_{\mathrm{LM}}(z\cdot 1_{f_a},2_{f_b})}{z}, \tag{E.42b}$$

$$\mathcal{C}_{45}\mathcal{S}_5F_{\mathrm{LM}}(1_{f_a},2_{f_b}\,|\,4_g,5_g) = C_{\mathrm{A}}\,g_{s,\epsilon}^2\frac{1}{E_5^2\eta_{45}}F_{\mathrm{LM}}(1_{f_a},2_{f_b}\,|\,4_g), \tag{E.42c}$$

with $z=\dfrac{E_1-E_4}{E_1}$ in Eq. (E.42b).
In the quark-gluon channel four different scenarios are possible,

$$\mathcal{C}_{42}\mathcal{S}_5F_{\mathrm{LM}}(1_{f_a},2_g\,|\,4_{f_x},5_g) = 2\,C_{\mathrm{F}}\,g_{s,\epsilon}^4S_{12}(p_5)\frac{1}{(p_2\cdot p_4)}P_{qg}^{(0)}(z;\epsilon)F_{\mathrm{LM}}(1_{f_a},z\cdot 2_{\bar{f}_x}), \tag{E.43a}$$

$$\mathcal{C}_{51}\mathcal{S}_5F_{\mathrm{LM}}(1_{f_a},2_g\,|\,4_{f_x},5_g) = C_{\mathrm{F}}\,g_{s,\epsilon}^2\frac{1}{E_5^2\eta_{15}}F_{\mathrm{LM}}(1_{f_a},2_g\,|\,4_{f_x}), \tag{E.43b}$$

$$\mathcal{C}_{52}\mathcal{S}_5F_{\mathrm{LM}}(1_{f_a},2_g\,|\,4_{f_x},5_g) = C_{\mathrm{A}}\,g_{s,\epsilon}^2\frac{1}{E_5^2\eta_{15}}F_{\mathrm{LM}}(1_{f_a},2_g\,|\,4_{f_x}), \tag{E.43c}$$

$$\mathcal{C}_{45}\mathcal{S}_5F_{\mathrm{LM}}(1_{f_a},2_g\,|\,4_{f_x},5_g) = C_{\mathrm{F}}\,g_{s,\epsilon}^2\frac{1}{E_5^2\eta_{45}}F_{\mathrm{LM}}(1_{f_a},2_g\,|\,4_{f_x}), \tag{E.43d}$$

where the energy fraction in Eq. (E.43a) is $z=\dfrac{E_2-E_4}{E_2}$.

Double-Soft Single-Collinear Limits

Double-soft single-collinear limits are only in the quark-antiquark channel present. They are

$$\mathcal{C}_{51}\boldsymbol{\mathcal{S}}F_{\mathrm{LM}}(1_{f_a},2_{f_b}\,|\,4_g,5_g) = 2\,C_{\mathrm{F}}^2\,g_{s,\epsilon}^4\frac{1}{E_5^2\eta_{15}}S_{12}(p_4)F_{\mathrm{LM}}(1_{f_a},2_{f_b}), \tag{E.44a}$$

$$\begin{aligned}\mathcal{C}_{45}\boldsymbol{\mathcal{S}}F_{\mathrm{LM}}(1_{f_a},2_{f_b}\,|\,4_g,5_g) &\overset{(b)}{=} g_s^4\frac{1}{(p_4\cdot p_5)}\Bigg[2\,C_{\mathrm{F}}S_{12}\Big(\frac{p_4}{z}\Big)\,\widetilde{P}_{gg}^{(0)}(z;\epsilon)\\ &\quad + C_{\mathrm{F}}\left(\frac{(p_1\cdot\kappa_\perp)}{(p_1\cdot p_4)/z}-\frac{(p_2\cdot\kappa_\perp)}{(p_2\cdot p_4)/z}\right)^2\widetilde{P}_{gg}^{\perp}(z;\epsilon)\Bigg]\\ &\quad\times F_{\mathrm{LM}}(1_{f_a},2_{f_b}),\end{aligned} \tag{E.44b}$$

with $z=\dfrac{E_4}{E_4-E_5}$ in the latter case.

Strongly-Ordered Double-Soft Single-Collinear Limits

Since double-soft single-collinear limits are only in the quark-antiquark channel present, also the stongly-ordered double-soft single-collinear limits show up just in this channel. They read

$$\mathcal{C}_{41}\boldsymbol{\mathcal{S}}\mathcal{S}_5F_{\mathrm{LM}}(1_{f_a},2_{f_b}\,|\,4_g,5_g) = 2\,C_{\mathrm{F}}^2\,g_{s,\epsilon}^4\frac{1}{E_4^2\eta_{14}}S_{12}(p_5)F_{\mathrm{LM}}(1_{f_a},2_{f_b}), \tag{E.45a}$$

$$\mathcal{C}_{51}\boldsymbol{\mathcal{S}}\mathcal{S}_5F_{\mathrm{LM}}(1_{f_a},2_{f_b}\,|\,4_g,5_g) = 2\,C_{\mathrm{F}}^2\,g_{s,\epsilon}^4\frac{1}{E_5^2\eta_{15}}S_{12}(p_4)F_{\mathrm{LM}}(1_{f_a},2_{f_b}), \tag{E.45b}$$

$$\mathcal{C}_{45}\boldsymbol{\mathcal{S}}\mathcal{S}_5F_{\mathrm{LM}}(1_{f_a},2_{f_b}\,|\,4_g,5_g) = 2\,C_{\mathrm{A}}C_{\mathrm{F}}\,g_{s,\epsilon}^4\frac{1}{E_5^2\eta_{45}}S_{12}(p_4)F_{\mathrm{LM}}(1_{f_a},2_{f_b}). \tag{E.45c}$$

Single-Soft Double-Collinear Limits

One soft final-state gluon in combination with a double-collinear limit can appear in the quark-antiquark channel,

$$\mathcal{C}_{41}\mathcal{C}_{52}\mathcal{S}_5F_{\mathrm{LM}}(1_{f_a},2_{f_b}\,|\,4_g,5_g) = C_{\mathrm{F}}\,g_{s,\epsilon}^4\frac{1}{E_5^2\eta_{25}}\frac{1}{(p_1\cdot p_4)}P_{qq}^{(0)}(z;\epsilon)\frac{F_{\mathrm{LM}}(z\cdot 1_{f_a},2_{f_b})}{z}, \tag{E.46}$$

where $z=\dfrac{E_1-E_4}{E_1}$, and in the quark-gluon channel,

$$\mathcal{C}_{51}\mathcal{C}_{42}\mathcal{S}_5F_{\mathrm{LM}}(1_{f_a},2_g\,|\,4_{f_x},5_g) = C_{\mathrm{F}}\,g_{s,\epsilon}^4\frac{1}{E_5^2\eta_{15}}\frac{1}{(p_2\cdot p_4)}P_{qg}^{(0)}(z;\epsilon)\frac{F_{\mathrm{LM}}(1_{f_a},z\cdot 2_{\bar{f}_x})}{z}, \tag{E.47}$$

with $z=\dfrac{E_2-E_4}{E_2}$.

Double-Soft Double-Collinear Limits

The double-soft double-collinear limit in the quark-antiquark channel is

$$\mathcal{C}_{41}\mathcal{C}_{52}\boldsymbol{\mathcal{S}}F_{\mathrm{LM}}(1_{f_a},2_{f_b}\,|\,4_g,5_g) = C_{\mathrm{F}}^2\,g_{s,\epsilon}^4\frac{1}{E_4^2E_5^2\eta_{14}\eta_{25}}F_{\mathrm{LM}}(1_{f_a},2_{f_b}). \tag{E.48}$$

Strongly-Ordered Double-Soft Double-Collinear Limits

If the double-soft double-collinear limit is strongly ordered, we find

$$\mathcal{C}_{41}\mathcal{C}_{52}\boldsymbol{\mathcal{S}}\mathcal{S}_5 F_{\mathrm{LM}}(1_{f_a}, 2_{f_b} \,|\, 4_g, 5_g) = C_{\mathrm{F}}^2\, g_{s,\epsilon}^4 \frac{1}{E_4^2 E_5^2 \eta_{14}\eta_{25}} F_{\mathrm{LM}}(1_{f_a}, 2_{f_b}). \tag{E.49}$$

Triple-Collinear Limits

Triple-collinear limits are again present in all channels but the gluon-gluon channel. In the quark-antiquark channel this limit reads

$$\boldsymbol{\mathcal{C}}_1 F_{\mathrm{LM}}(1_{f_a}, 2_{f_b} \,|\, 4_g, 5_g) = g_{s,\epsilon}^4 \left(\frac{2}{s_{145}}\right)^2 \hat{P}_{ggq}(p_4, p_5, -p_1) F_{\mathrm{LM}}(z \cdot 1_{f_a}, 2_{f_b}), \tag{E.50}$$

where $z = \dfrac{E_1 - E_4 - E_5}{E_1}$, and $s_{145} = s_{45} - s_{14} - s_{15}$ with $s_{ij} = (p_i + p_j)^2$.
In the quark-quark channel different triple-collinear splitting functions have to be used, depending on the involved quark flavors. If the three involved quarks are from the same flavor type, the two possible limits are

$$\boldsymbol{\mathcal{C}}_1 F_{\mathrm{LM}}(1_{f_a}, 2_{f_b} \,|\, 4_{f_a}, 5_{\bar{f}_a}) = g_{s,\epsilon}^4 \left(\frac{2}{s_{145}}\right)^2 \hat{P}_{\bar{q}qq}(p_4, p_5, -p_1) F_{\mathrm{LM}}(z \cdot 1_{f_a}, 2_{f_b}), \tag{E.51a}$$

$$\boldsymbol{\mathcal{C}}_1 F_{\mathrm{LM}}(1_{f_a}, 2_{f_b} \,|\, 4_{f_a}, 5_{f_a}) = g_{s,\epsilon}^4 \left(\frac{2}{s_{145}}\right)^2 \hat{P}_{\bar{q}qq}(-p_1, p_4, p_5) F_{\mathrm{LM}}(z \cdot 1_{\bar{f}_a}, 2_{f_b}). \tag{E.51b}$$

The former limit has to be taken when the quarks in the final state build a quark-antiquark pair, the latter when the are of the same kind. If non-identical quark flavors ($|a| \neq |c|$) are involved, the limits become

$$\boldsymbol{\mathcal{C}}_1 F_{\mathrm{LM}}(1_{f_a}, 2_{f_b} \,|\, 4_{f_c}, 5_{\bar{f}_c}) = g_{s,\epsilon}^4 \left(\frac{2}{s_{145}}\right)^2 \hat{P}_{\bar{q}'q'q}(p_4, p_5, -p_1) F_{\mathrm{LM}}(z \cdot 1_{f_a}, 2_{f_b}), \tag{E.52a}$$

$$\boldsymbol{\mathcal{C}}_1 F_{\mathrm{LM}}(1_{f_a}, 2_{f_b} \,|\, 4_{f_a}, 5_{f_c}) = g_{s,\epsilon}^4 \left(\frac{2}{s_{145}}\right)^2 \hat{P}_{\bar{q}'q'q}(-p_1, p_4, p_5) F_{\mathrm{LM}}(z \cdot 1_{\bar{f}_c}, 2_{f_b}). \tag{E.52b}$$

The energy fraction z and the subenergy s_{145} is in all four expressions the same as defined below Eq. (E.50).
In the quark-gluon channel the triple-collinear limit is given by

$$\boldsymbol{\mathcal{C}}_2 F_{\mathrm{LM}}(1_{f_a}, 2_g \,|\, 4_{f_x}, 5_g) = -g_{s,\epsilon}^4 \left(\frac{2}{s_{245}}\right)^2 \frac{T_{\mathrm{R}}}{(1-\epsilon)C_{\mathrm{F}}} \hat{P}_{ggq}(-p_2, p_5, p_4) F_{\mathrm{LM}}(1_{f_a}, z \cdot 2_{\bar{f}_x}), \tag{E.53}$$

where $z = \dfrac{E_2 - E_4 - E_5}{E_2}$, and $s_{245} = s_{45} - s_{24} - s_{25}$. The minus sign and the color factor come from the crossing of an initial-state quark in the definition of the triple collinear splitting function in Appendix C with a final-state gluon, so that we can describe an initial-state gluon splitting into a triple-collinear quark-antiquark-gluon state.

Strongly-Ordered Triple-Collinear Limits

The strongly-ordered triple-collinear limits shows up in different ways. In the quark-antiquark channel we find

$$\begin{aligned}
\boldsymbol{\mathcal{C}}_1\mathcal{C}_{51}F_{\mathrm{LM}}(1_{f_a},2_{f_b}\,|\,4_g,5_g) &= g_{s,\epsilon}^4\frac{1}{(p_1\cdot p_5)}\frac{1}{z(p_1\cdot p_4)}P_{qq}^{(0)}(z;\epsilon)P_{qq}^{(0)}(\bar{z};\epsilon) \\
&\quad\times\frac{F_{\mathrm{LM}}(z\bar{z}\cdot 1_{f_a},2_{f_b})}{z\bar{z}}, \qquad \text{(E.54a)}\\
\boldsymbol{\mathcal{C}}_1\mathcal{C}_{45}F_{\mathrm{LM}}(1_{f_a},2_{f_b}\,|\,4_g,5_g) &\overset{(b)}{=} g_{s,\epsilon}^4\frac{1}{(p_4\cdot p_5)}\frac{1}{(p_1\cdot p_4)/z}P_{gg,\mu\nu}(z,k_\perp;\epsilon)P_{qq}^{\mu\nu}(\bar{z},\bar{k}_\perp;\epsilon) \\
&\quad\times\frac{F_{\mathrm{LM}}(\bar{z}\cdot 1_{f_a},2_{f_b})}{\bar{z}} \\
&= g_{s,\epsilon}^4\frac{1}{(p_4\cdot p_5)}\frac{1}{(p_1\cdot p_4)/z}\Big[P_{gg}^{(0)}(z;\epsilon)P_{qq}^{(0)}(\bar{z};\epsilon) \qquad \text{(E.54b)}\\
&\quad+\frac{1}{2(1-\epsilon)}\widetilde{P}_{gg}^{\perp}(z;\epsilon)\widetilde{P}_{qq}^{\perp}(\bar{z};\epsilon)\left(\left[\kappa_\perp\cdot\bar{\kappa}_\perp\right]^2-\frac{1}{2(1-\epsilon)}\right)\Big] \\
&\quad\times\frac{F_{\mathrm{LM}}(\bar{z}\cdot 1_{f_a},2_{f_b})}{\bar{z}}.
\end{aligned}$$

In Eq. (E.54a) the energy fractions are $z=\dfrac{E_1-E_5}{E_1}$ and $\bar{z}=\dfrac{E_1-E_4-E_5}{E_1-E_5}$, in Eq. (E.54b) the energy fractions are $z=\dfrac{E_4}{E_4+E_5}$ and $\bar{z}=\dfrac{E_1-E_4-E_5}{E_1}$.

The quark-quark channel has the strongly-ordered triple-collinear limit

$$\begin{aligned}
\boldsymbol{\mathcal{C}}_1\mathcal{C}_{51}F_{\mathrm{LM}}(1_{f_a},2_{f_b}\,|\,4_{f_c},5_{f_a}) &= g_{s,\epsilon}^4\frac{1}{(p_1\cdot p_5)}\frac{1}{z(p_1\cdot p_4)}P_{gq,\mu\nu}(z,k_\perp;\epsilon)P_{qg}^{\mu\nu}(\bar{z},\bar{k}_\perp;\epsilon) \\
&\quad\times\frac{F_{\mathrm{LM}}(z\bar{z}\cdot 1_{\bar{f}_c},2_{f_b})}{z\bar{z}} \\
&= g_{s,\epsilon}^4\frac{1}{(p_1\cdot p_5)}\frac{1}{z(p_1\cdot p_4)}\Big[P_{gq}^{(0)}(z;\epsilon)P_{qg}^{(0)}(\bar{z};\epsilon) \\
&\quad+\frac{1}{2(1-\epsilon)}\widetilde{P}_{gq}^{\perp}(z;\epsilon)\widetilde{P}_{qg}^{\perp}(\bar{z};\epsilon)\left(\left[\kappa_\perp\cdot\bar{\kappa}_\perp\right]^2-\frac{1}{2(1-\epsilon)}\right)\Big] \\
&\quad\times\frac{F_{\mathrm{LM}}(z\bar{z}\cdot 1_{\bar{f}_c},2_{f_b})}{z\bar{z}},
\end{aligned} \qquad \text{(E.55)}$$

with $z=\dfrac{E_1-E_5}{E_1}$ and $\bar{z}=\dfrac{E_1-E_4-E_5}{E_1-E_5}$.

In the quark-gluon channel we find

$$\begin{aligned}
\boldsymbol{\mathcal{C}}_2\mathcal{C}_{42}F_{\mathrm{LM}}(1_{f_a},2_g\,|\,4_{f_x},5_g) &= g_{s,\epsilon}^2\frac{1}{(p_2\cdot p_4)}\frac{1}{z(p_2\cdot p_5)}P_{qg}^{(0)}(z;\epsilon)P_{qq}^{(0)}(\bar{z};\epsilon) \qquad \text{(E.56a)}\\
&\quad\times\frac{F_{\mathrm{LM}}(1_{f_a},z\bar{z}\cdot 2_{\bar{f}_x})}{z\bar{z}}, \\
\boldsymbol{\mathcal{C}}_2\mathcal{C}_{52}F_{\mathrm{LM}}(1_{f_a},2_g\,|\,4_{f_x},5_g) &= -g_{s,\epsilon}^4\frac{1}{(p_2\cdot p_5)}\frac{1}{z(p_2\cdot p_4)}P_{gg,\mu\nu}\left(\frac{1}{z},k_\perp;\epsilon\right)P_{qg}^{\mu\nu}(\bar{z},\bar{k}_\perp;\epsilon) \\
&\quad\times\frac{F_{\mathrm{LM}}(1_{f_a},z\bar{z}\cdot 2_{\bar{f}_x})}{\bar{z}}
\end{aligned}$$

$$= -g_{s,\epsilon}^4 \frac{1}{(p_2\cdot p_5)} \frac{1}{z(p_2\cdot p_4)} \left[P_{gg}^{(0)}\left(\frac{1}{z};\epsilon\right) P_{qg}^{(0)}(\bar{z};\epsilon) \right. \tag{E.56b}$$
$$\left. + \frac{1}{2(1-\epsilon)} \widetilde{P}_{gg}^{\perp}\left(\frac{1}{z};\epsilon\right) \widetilde{P}_{qg}^{\perp}(\bar{z};\epsilon) \left(\left[\kappa_\perp\cdot\bar{\kappa}_\perp\right]^2 - \frac{1}{2(1-\epsilon)} \right) \right]$$
$$\times \frac{F_{\mathrm{LM}}(1_{f_q}, z\bar{z}\cdot 2_{\bar{f}_x})}{\bar{z}},$$

$$\boldsymbol{\mathcal{C}}_2\mathcal{C}_{45} F_{\mathrm{LM}}(1_{f_a}, 2_g \,|\, 4_{f_x}, 5_g) \overset{(b)}{=} g_{s,\epsilon}^4 \frac{1}{(p_4\cdot p_5)} \frac{1}{(p_2\cdot p_4)/z} P_{qq}(z;\epsilon) P_{qg}(\bar{z};\epsilon) \tag{E.56c}$$
$$\times \frac{F_{\mathrm{LM}}(1_{f_a}, \bar{z}\cdot 2_{\bar{f}_x})}{\bar{z}},$$

$$\boldsymbol{\mathcal{C}}_2\mathcal{C}_{45} F_{\mathrm{LM}}(1_{f_a}, 2_g \,|\, 4_{f_x}, 5_g) \overset{(d)}{=} g_{s,\epsilon}^4 \frac{1}{(p_4\cdot p_5)} \frac{1}{(p_2\cdot p_5)/z} P_{gq}(z;\epsilon) P_{qg}(\bar{z};\epsilon) \tag{E.56d}$$
$$\times \frac{F_{\mathrm{LM}}(1_{f_a}, \bar{z}\cdot 2_{\bar{f}_x})}{\bar{z}}.$$

The energy fractions in Eq. (E.56a) are $z = \dfrac{E_2 - E_4}{E_2}$ and $\bar{z} = \dfrac{E_2 - E_4 - E_5}{E_2 - E_4}$. In Eq. (E.56b) the energy fractions are given by $z = \dfrac{E_2 - E_5}{E_2}$ and $\bar{z} = \dfrac{E_2 - E_4 - E_5}{E_2 - E_5}$. In sector (b), *cf.* Eq. (E.56c), the energy fractions are $z = \dfrac{E_4}{E_4 + E_5}$ and $\bar{z} = \dfrac{E_2 - E_4 - E_5}{E_2}$, while in sector (d), referring to Eq. (E.56d), the first energy fraction has to be replaced with $z = \dfrac{E_5}{E_4 + E_5}$.

Single-Soft Triple-Collinear Limits

A soft quark in combination with a triple-collinear limit in the quark-antiquark channel has the shape

$$\boldsymbol{\mathcal{C}}_1\mathcal{S}_5 F_{\mathrm{LM}}(1_{f_a}, 2_{f_b} \,|\, 4_g, 5_g) = g_{s,\epsilon}^4 \frac{1}{2E_5^2} \left[\left(2\,C_{\mathrm{F}} - C_{\mathrm{A}}\right) \frac{1}{\eta_{15}} + C_{\mathrm{A}} \left(\frac{1}{\eta_{45}} + \frac{\eta_{14}}{\eta_{15}\eta_{45}} \right) \right]$$
$$\times \frac{1}{(p_1\cdot p_4)} P_{qq}^{(0)}(z;\epsilon) \frac{F_{\mathrm{LM}}(z\cdot 1_{f_a}, 2_{f_b})}{z}, \tag{E.57}$$

with $z = \dfrac{E_1 - E_4}{E_1}$.

In the quark-gluon channel this limit reads

$$\boldsymbol{\mathcal{C}}_2\mathcal{S}_5 F_{\mathrm{LM}}(1_{f_a}, 2_g \,|\, 4_{f_x}, 5_g) = g_{s,\epsilon}^4 \frac{1}{2E_5^2} \left[\left(2\,C_{\mathrm{F}} - C_{\mathrm{A}}\right) \frac{1}{\eta_{45}} + C_{\mathrm{A}} \left(\frac{1}{\eta_{25}} + \frac{\eta_{24}}{\eta_{25}\eta_{45}} \right) \right]$$
$$\times \frac{1}{(p_2\cdot p_4)} P_{qg}^{(0)}(z;\epsilon) \frac{F_{\mathrm{LM}}(1_{f_a}, z\cdot 2_{\bar{f}_x})}{z}, \tag{E.58}$$

where $z = \dfrac{E_2 - E_4}{E_2}$.

Double-Soft Triple-Collinear Limits

A soft gluon pair in combination with a triple-collinear limit appear in the quark-antiquark channel,

$$\boldsymbol{\mathcal{C}}_1\boldsymbol{\mathcal{S}}F_{\mathrm{LM}}(1_{f_a},2_{f_b}\,|\,4_g,5_g) = g_{s,\epsilon}^4\left(\frac{2}{\tilde{s}_{145}}\right)^2 \hat{P}^{\boldsymbol{\mathcal{S}}}_{ggq}(p_4,p_5,-p_1)F_{\mathrm{LM}}(1_{f_a},2_{f_b}), \tag{E.59}$$

where $\tilde{s}_{145} = s_{14} + s_{15}$ and $s_{ij} = (p_i + p_j)^2$.
A soft quark-antiquark pair in combination with a triple-collinear limit can appear in two different forms in the quark-quark channel. The quarks of the final-state pair can have the same flavor as the initial-state quark that is collinear with that pair, or it has another flavor. The limits are

$$\boldsymbol{\mathcal{C}}_1\boldsymbol{\mathcal{S}}F_{\mathrm{LM}}(1_{f_a},2_{f_b}\,|\,4_{f_a},5_{\bar{f}_a}) = g_{s,\epsilon}^4\left(\frac{2}{\tilde{s}_{145}}\right)^2 \hat{P}^{\boldsymbol{\mathcal{S}}}_{\bar{q}qq}(p_4,p_5,-p_1)F_{\mathrm{LM}}(1_{f_a},2_{f_b}), \tag{E.60a}$$

$$\boldsymbol{\mathcal{C}}_1\boldsymbol{\mathcal{S}}F_{\mathrm{LM}}(1_{f_a},2_{f_b}\,|\,4_{f_c},5_{\bar{f}_c}) = g_{s,\epsilon}^4\left(\frac{2}{\tilde{s}_{145}}\right)^2 \hat{P}^{\boldsymbol{\mathcal{S}}}_{\bar{q}'q'q}(p_4,p_5,-p_1)F_{\mathrm{LM}}(1_{f_a},2_{f_b}), \tag{E.60b}$$

respectively. However, it can easily be shown that both limits have to coincide with each other.

Strongly-Ordered Double-Soft Triple-Collinear Limits

In the quark-antiquark channel the strongly-ordered double-soft triple-collinear Limit is given by

$$\begin{aligned}\boldsymbol{\mathcal{C}}_1\boldsymbol{\mathcal{S}}\mathcal{S}_5F_{\mathrm{LM}}(1_{f_a},2_{f_b}\,|\,4_g,5_g) = C_{\mathrm{F}}\,g_{s,\epsilon}^4\left[(2\,C_{\mathrm{F}} - C_{\mathrm{A}})\frac{1}{\eta_{14}\eta_{15}} + C_{\mathrm{A}}\left(\frac{1}{\eta_{14}\eta_{45}} + \frac{1}{\eta_{15}\eta_{45}}\right)\right] \\ \times\,\frac{1}{2E_4^2E_5^2}F_{\mathrm{LM}}(1_{f_a},2_{f_b}).\end{aligned} \tag{E.61}$$

Single-Soft Strongly-Ordered Triple-Collinear Limits

The single-soft strongly-ordered triple-collinear limits in the quark-antiquark channel are

$$\boldsymbol{\mathcal{C}}_1\mathcal{C}_{41}\mathcal{S}_5F_{\mathrm{LM}}(1_{f_a},2_{f_b}\,|\,4_g,5_g) = C_{\mathrm{F}}\,g_{s,\epsilon}^4\frac{1}{E_5^2\eta_{15}}\frac{1}{(p_1\cdot p_4)}P_{qq}^{(0)}(z;\epsilon)\frac{F_{\mathrm{LM}}(z\cdot 1_{f_a},2_{f_b})}{z}, \tag{E.62a}$$

$$\boldsymbol{\mathcal{C}}_1\mathcal{C}_{51}\mathcal{S}_5F_{\mathrm{LM}}(1_{f_a},2_{f_b}\,|\,4_g,5_g) = C_{\mathrm{F}}\,g_{s,\epsilon}^4\frac{1}{E_5^2\eta_{15}}\frac{1}{(p_1\cdot p_4)}P_{qq}^{(0)}(z;\epsilon)\frac{F_{\mathrm{LM}}(z\cdot 1_{f_a},2_{f_b})}{z}, \tag{E.62b}$$

$$\boldsymbol{\mathcal{C}}_1\mathcal{C}_{45}\mathcal{S}_5F_{\mathrm{LM}}(1_{f_a},2_{f_b}\,|\,4_g,5_g) \overset{(b)}{=} C_{\mathrm{A}}\,g_{s,\epsilon}^4\frac{1}{E_5^2\eta_{45}}\frac{1}{(p_1\cdot p_4)}P_{qq}^{(0)}(z;\epsilon)\frac{F_{\mathrm{LM}}(z\cdot 1_{f_a},2_{f_b})}{z}, \tag{E.62c}$$

$$\boldsymbol{\mathcal{C}}_1\mathcal{C}_{45}\mathcal{S}_5F_{\mathrm{LM}}(1_{f_a},2_{f_b}\,|\,4_g,5_g) \overset{(d)}{=} C_{\mathrm{A}}\,g_{s,\epsilon}^4\frac{1}{E_5^2\eta_{45}}\frac{1}{2E_1E_4\eta_{15}}P_{qq}^{(0)}(z;\epsilon)\frac{F_{\mathrm{LM}}(z\cdot 1_{f_a},2_{f_b})}{z}, \tag{E.62d}$$

with the energy fraction $z = \dfrac{E_1 - E_4}{E_1}$ in all four expressions.

The four limits in the quark-gluon channel are

$$\boldsymbol{\mathcal{C}}_2\mathcal{C}_{42}\mathcal{S}_5 F_{\mathrm{LM}}(1_{f_a},2_g\,|\,4_{f_x},5_g) = C_{\mathrm{F}}\, g_{s,\epsilon}^4 \frac{1}{E_5^2\eta_{25}}\frac{1}{(p_2\cdot p_4)} P_{qg}^{(0)}(z;\epsilon)\frac{F_{\mathrm{LM}}(1_{f_a},z\cdot 2_{\bar{f}_x})}{z}, \tag{E.63a}$$

$$\boldsymbol{\mathcal{C}}_2\mathcal{C}_{52}\mathcal{S}_5 F_{\mathrm{LM}}(1_{f_a},2_g\,|\,4_{f_x},5_g) = C_{\mathrm{A}}\, g_{s,\epsilon}^4 \frac{1}{E_5^2\eta_{25}}\frac{1}{(p_2\cdot p_4)} P_{qg}^{(0)}(z;\epsilon)\frac{F_{\mathrm{LM}}(1_{f_a},z\cdot 2_{\bar{f}_x})}{z}, \tag{E.63b}$$

$$\boldsymbol{\mathcal{C}}_2\mathcal{C}_{45}\mathcal{S}_5 F_{\mathrm{LM}}(1_{f_a},2_g\,|\,4_{f_x},5_g) \overset{(b)}{=} C_{\mathrm{F}}\, g_{s,\epsilon}^4 \frac{1}{E_5^2\eta_{45}}\frac{1}{(p_2\cdot p_4)} P_{qg}^{(0)}(z;\epsilon)\frac{F_{\mathrm{LM}}(1_{f_a},z\cdot 2_{\bar{f}_x})}{z}, \tag{E.63c}$$

$$\boldsymbol{\mathcal{C}}_2\mathcal{C}_{45}\mathcal{S}_5 F_{\mathrm{LM}}(1_{f_a},2_g\,|\,4_{f_x},5_g) \overset{(d)}{=} C_{\mathrm{F}}\, g_{s,\epsilon}^4 \frac{1}{E_5^2\eta_{45}}\frac{1}{2E_2E_4\eta_{25}} P_{qg}^{(0)}(z;\epsilon)\frac{F_{\mathrm{LM}}(1_{f_a},z\cdot 2_{\bar{f}_x})}{z}, \tag{E.63d}$$

with $z = \dfrac{E_2 - E_4}{E_2}$ everywhere.

Double-Soft Strongly-Ordered Triple-Collinear Limits

Double-soft strongly-ordered triple-collinear limits appear in the quark-antiquark channel. They are

$$\boldsymbol{\mathcal{C}}_1\mathcal{C}_{51}\boldsymbol{\mathcal{S}} F_{\mathrm{LM}}(1_{f_a},2_{f_b}\,|\,4_g,5_g) = C_{\mathrm{F}}^2\, g_{s,\epsilon}^4 \frac{1}{E_4^2E_5^2\eta_{14}\eta_{15}} F_{\mathrm{LM}}(1_{f_a},2_{f_b}), \tag{E.64a}$$

$$\begin{aligned}\boldsymbol{\mathcal{C}}_1\mathcal{C}_{45}\boldsymbol{\mathcal{S}} F_{\mathrm{LM}}(1_{f_a},2_{f_b}\,|\,4_g,5_g) &\overset{(b)}{=} g_{s,\epsilon}^4 \frac{1}{(E_4+E_5)^2\eta_{14}}\frac{1}{(p_4\cdot p_5)} \\ &\quad\times\left[P_{gg}^{(0)}(z;\epsilon) + \widetilde{P}_{gg}^{\perp}(z;\epsilon)\left(\left[\kappa_\perp\cdot\bar{\kappa}_\perp\right]^2 - \frac{1}{2(1-\epsilon)}\right)\right] \\ &\quad\times F_{\mathrm{LM}}(1_{f_a},2_{f_b}).\end{aligned} \tag{E.64b}$$

In the second equation we have $z = \dfrac{E_4}{E_4+E_5}$.

Strongly-Ordered Double-Soft Strongly-Ordered Triple-Collinear Limits

The strongly-ordered double-soft strongly-ordered triple-collinear limits in the quark-antiquark channel are given by

$$\boldsymbol{\mathcal{C}}_1\mathcal{C}_{41}\boldsymbol{\mathcal{S}}\mathcal{S}_5 F_{\mathrm{LM}}(1_{f_a},2_{f_b}\,|\,4_g,5_g) = C_{\mathrm{F}}^2\, g_{s,\epsilon}^4 \frac{1}{E_4^2E_5^2\eta_{14}\eta_{15}} F_{\mathrm{LM}}(1_{f_a},2_{f_b}), \tag{E.65a}$$

$$\boldsymbol{\mathcal{C}}_1\mathcal{C}_{51}\boldsymbol{\mathcal{S}}\mathcal{S}_5 F_{\mathrm{LM}}(1_{f_a},2_{f_b}\,|\,4_g,5_g) = C_{\mathrm{F}}^2\, g_{s,\epsilon}^4 \frac{1}{E_4^2E_5^2\eta_{14}\eta_{15}} F_{\mathrm{LM}}(1_{f_a},2_{f_b}), \tag{E.65b}$$

$$\boldsymbol{\mathcal{C}}_1\mathcal{C}_{45}\boldsymbol{\mathcal{S}}\mathcal{S}_5 F_{\mathrm{LM}}(1_{f_a},2_{f_b}\,|\,4_g,5_g) = C_{\mathrm{A}}C_{\mathrm{F}}\, g_{s,\epsilon}^4 \frac{1}{E_4^2E_5^2\eta_{14}\eta_{45}} F_{\mathrm{LM}}(1_{f_a},2_{f_b}). \tag{E.65c}$$

Acknowledgments

It is a great pleasure to thank Prof. Robert V. Harlander for providing me with the opportunity to work on this exciting research topic. Under your guidance, I was granted a remarkable degree of autonomy in shaping the project, fostering my growth to become an independent researcher.

Furthermore, I would like to express my gratitude to Prof. Michał Czakon. Beyond your role as my second reporter, I am truly grateful for the invaluable knowledge and expertise you shared with me, which played a pivotal role in steering this project toward its successful conclusion.

I must also acknowledge Prof. Alexander Schmidt, who took on the role of my second advisor during these years. Our collaboration in linking theory and experiment served as a constant source of motivation, as I saw the meaningful contribution my results can make to cutting-edge research.

Special recognitions go to Prof. Robert V. Harlander, Prof. Alexander Schmidt, and Prof. Michael Krämer, who penned excellent recommendation letters. This support paved the way for me to pursue my passion for physics as a postdoctoral researcher in Paris.

I take great pleasure in extending my heartfelt thanks to Prof. Raoul Röntsch. I deeply appreciate your immense support in implementing the Nested Soft-Collinear Subtraction scheme. Your kind advices and provision of independent cross-checks have not only been crucial in validating my results but have also been a guiding light in identifying and fixing numerous issues that arose. It is undeniable that without your contributions, this project would not have achieved the remarkable success it has.

I would like to thank Marco Bonetti. We had numerous useful discussions and you gave me many detailed explanations during the early stages of my doctoral studies. Thanks also for organizing many social events, with your Italian mentality you always guided us to discover the finest pizza restaurants in Aachen, resulting in many great evenings.

I also wish to thank Terry Generet for sharing your expertise about subtraction schemes and the help you provided me in understanding `OpenLoops`.

Moreover, it was a pleasure to collaborate with Dmitrii Korneev.

I owe a debt of gratitude to Sven Yannick Klein, whose exceptional proofreading skills and passion for punctuation greatly improved this write-up. Every comma in this thesis is dedicated to you.

I warmly thank my friend Colomba Brancaccio. Our insightful discussions on both physics-related and non-physics topics made sharing an office with you an enriching experience where the work never became boring. Staying connected, especially during the challenging times of the pandemic, consistently motivated me and was indispensable in leading this journey to a successful end.

Mein allergrößtes Dankeschön gilt meiner Familie. Meinen Eltern Johann und Martina danke ich von Herzen für die beste Unterstützung, die ich mir über all die Jahre nur wünschen konnte - von einer wundervollen Kindheit, über die schöne Schulzeit, das

anspruchsvolle Studium, die herausfordernde Promotionszeit und bis heute. Meinem Bruder und Freund Martin möchte ich ebenso meinen aufrichtigen Dank aussprechen, für jeden Ratschlag, die unermüdliche Motivation und dafür, dass du immer an mich geglaubt hast. Gleiches gilt auch für Bina, danke für all deine warmen Worte der Aufmunterung, wann immer ich diese benötigt habe. Abschließend danke ich meiner Patentochter Maria und meinem Neffen Friedrich für jedes Lächeln und die willkommene Ablenkung in stressigen Zeiten bei jedem Besuch.

Bibliography

[1] R.P. Feynman and M. Gell-Mann, *Theory of the Fermi Interaction*, *Phys. Rev.* **109** (1958) 193–198.

[2] S.L. Glashow, *Partial-symmetries of weak interactions*, *Nucl. Phys.* **22** (1961) 579–588.

[3] J. Goldstone, A. Salam, and S. Weinberg, *Broken Symmetries*, *Phys. Rev.* **127** (1962) 965–970.

[4] S. Weinberg, *A Model of Leptons*, *Phys. Rev. Lett.* **19** (1967) 1264–1266.

[5] A. Salam, *Weak and Electromagnetic Interactions*, *Conf. Proc. C* **680519** (1968) 367–377.

[6] P.W. Higgs, *Broken symmetries, massless particles and gauge fields*, *Phys. Lett.* **12** (1964) 132–133.

[7] P.W. Higgs, *Broken Symmetries and the Masses of Gauge Bosons*, *Phys. Rev. Lett.* **13** (1964) 508–509.

[8] P.W. Higgs, *Spontaneous Symmetry Breakdown without Massless Bosons*, *Phys. Rev.* **145** (1966) 1156–1163.

[9] F. Englert and R. Brout, *Broken Symmetry and the Mass of Gauge Vector Mesons*, *Phys. Rev. Lett.* **13** (1964) 321–323.

[10] G.S. Guralnik, C.R. Hagen, and T.W.B. Kibble, *Global Conservation Laws and Massless Particles*, *Phys. Rev. Lett.* **13** (1964) 585–587.

[11] M. Gell-Mann, *Symmetries of Baryons and Mesons*, *Phys. Rev.* **125** (1962) 1067–1084.

[12] H. Fritzsch, M. Gell-Mann, and H. Leutwyler, *Advantages of the color octet gluon picture*, *Phys. Lett. B* **47** (1973) 365–368.

[13] G. Arnison *et al.* [UA1 Collaboration], *Experimental observation of isolated large transverse energy electrons with associated missing energy at* $\sqrt{s} = 540\ GeV$, *Phys. Lett. B* **122** (1983) 103–116.

[14] M. Banner *et al.* [UA2 Collaboration], *Observation of single isolated electrons of high transverse momentum in events with missing transverse energy at the CERN* $\bar{p}p$ *collider*, *Phys. Lett. B* **122** (1983) 476–485.

[15] G. Arnison *et al.* [UA1 Collaboration], *Experimental observation of lepton pairs of invariant mass around* $95\ GeV/c^2$ *at the CERN SPS collider*, *Phys. Lett. B* **126** (1983) 398–410.

[16] P. Bagnaia *et al.* [UA2 Collaboration], *Evidence for* $Z^0 \to e^+e^-$ *at the CERN* $\bar{p}p$ *collider*, *Phys. Lett. B* **129** (1983) 130–140.

[17] F. Abe *et al.* [CDF Collaboration], *Observation of Top Quark Production in* $\bar{p}p$ *Collisions with the Collider Detector at Fermilab*, *Phys. Rev. Lett.* **74** (1995) 2626–2631, `arXiv:hep-ex/9503002`.

[18] S. Abachi *et al.* [D0 Collaboration], *Observation of the Top Quark*, *Phys. Rev. Lett.* **74** (1995) 2632–2637, arXiv:hep-ex/9503003.

[19] K. Kodama *et al.* [DONUT Collaboration], *Observation of tau neutrino interactions*, *Phys. Lett. B* **504** (2001) 218–224, arXiv:hep-ex/0012035.

[20] G. Aad *et al.* [ATLAS Collaboration], *Observation of a new particle in the search for the Standard Model Higgs boson with the ATLAS detector at the LHC*, *Phys. Lett. B* **716** (2012) 1–29, arXiv:1207.7214.

[21] S. Chatrchyan *et al.* [CMS Collaboration], *Observation of a new boson at a mass of 125 GeV with the CMS experiment at the LHC*, *Phys. Lett. B* **716** (2012) 30–61, arXiv:1207.7235.

[22] N. Aghanim *et al.* [Planck Collaboration], *Planck 2018 results. VI. Cosmological parameters*, *A&A* **641** (2020) A6, arXiv:1807.06209.

[23] Y. Fukuda *et al.* [Super-Kamiokande Collaboration], *Evidence for Oscillation of Atmospheric Neutrinos*, *Phys. Rev. Lett.* **81** (1998) 1562–1567, arXiv:hep-ex/9807003.

[24] Q.R. Ahmad *et al.* [SNO Collaboration], *Measurement of the Rate of* $\nu_e + d \to p + p + e^-$ *Interactions Produced by* ^8B *Solar Neutrinos at the Sudbury Neutrino Observatory*, *Phys. Rev. Lett.* **87** (2001) 071301, arXiv:nucl-ex/0106015.

[25] Q.R. Ahmad *et al.* [SNO Collaboration], *Direct Evidence for Neutrino Flavor Transformation from Neutral-Current Interactions in the Sudbury Neutrino Observatory*, *Phys. Rev. Lett.* **89** (2002) 011301, arXiv:nucl-ex/0204008.

[26] M. Aker *et al.* [KATRIN Collaboration], *Direct neutrino-mass measurement with sub-electronvolt sensitivity*, *Nature Phys.* **18** (2022) 160–166, arXiv:2105.08533.

[27] J.H. Christenson, J.W. Cronin, V.L. Fitch, and R. Turlay, *Evidence for the* 2π *Decay of the* K_2^0 *Meson*, *Phys. Rev. Lett.* **13** (1964) 138–140.

[28] K. Abe *et al.* [T2K Collaboration], *Constraint on the matter–antimatter symmetry-violating phase in neutrino oscillations*, *Nature* **580** (2020) 339–344, arXiv:1910.03887.

[29] S. Catani and M. Grazzini, *Next-to-Next-to-Leading-Order Subtraction Formalism in Hadron Collisions and its Application to Higgs-Boson Production at the Large Hadron Collider*, *Phys. Rev. Lett.* **98** (2007) 222002, arXiv:hep-ph/0703012.

[30] J. Gaunt, M. Stahlhofen, F.J. Tackmann, and J. Walsh, *N-jettiness subtractions for NNLO QCD calculations*, *JHEP* **05** (2015) 058, arXiv:1505.04794.

[31] A. Gehrmann-De Ridder, T. Gehrmann, and E.N. Glover, *Antenna subtraction at NNLO*, *JHEP* **09** (2005) 056, arXiv:hep-ph/0505111.

[32] G. Heinrich, *A numerical method for NNLO calculations*, *Nucl. Phys. B Proc. Suppl.* **116** (2003) 368–372, arXiv:hep-ph/0211144.

[33] G. Heinrich, *Sector Decomposition*, *Int. J. Mod. Phys. A* **23** (2008) 1457–1486, arXiv:0803.4177.

[34] M. Czakon, *A novel subtraction scheme for double-real radiation at NNLO*, *Phys. Lett. B* **693** (2010) 259–268, arXiv:1005.0274.

[35] M. Czakon, *Double-real radiation in hadronic top quark pair production as a proof of a certain concept*, *Nucl. Phys. B* **849** (2011) 250–295, arXiv:1101.0642.

[36] G. Somogyi and Z. Trócsányi, *A New subtraction scheme for computing QCD jet cross sections at next-to-leading order accuracy* (2006) arXiv:hep-ph/0609041.

[37] M. Cacciari *et al.*, *Fully Differential Vector-Boson-Fusion Higgs Production at Next-to-Next-to-Leading Order*, *Phys. Rev. Lett.* **115** (2015) 082002, arXiv:1811.07918.

[38] F. Caola, K. Melnikov, and R. Röntsch, *Nested soft-collinear subtractions in NNLO QCD computations*, *Eur. Phys. J. C* **77** (2017) 248, arXiv:1702.01352.

[39] F. Herzog, *Geometric IR subtraction for final state real radiation*, *JHEP* **08** (2018) 006, arXiv:1804.07949.

[40] L. Magnea *et al.*, *Local analytic sector subtraction at NNLO*, *JHEP* **12** (2018) 107, arXiv:1806.09570.

[41] A.B. Goncharov, M. Spradlin, C. Vergu, and A. Volovich, *Classical Polylogarithms for Amplitudes and Wilson Loops*, *Phys. Rev. Lett.* **105** (2010) 151605, arXiv:1006.5703.

[42] S. Müller-Stach, S. Weinzierl, and R. Zayadeh, *Picard–Fuchs Equations for Feynman Integrals*, *Commun. Math. Phys.* **326** (2013) 237–249, arXiv:1212.4389.

[43] J.M. Henn, *Multiloop Integrals in Dimensional Regularization Made Simple*, *Phys. Rev. Lett.* **110** (2013) 251601, arXiv:1304.1806.

[44] J. Broedel, C. Duhr, F. Dulat, and L. Tancredi, *Elliptic polylogarithms and iterated integrals on elliptic curves I: general formalism*, *JHEP* **05** (2018) 093, arXiv:1712.07089.

[45] J. Broedel, C. Duhr, F. Dulat, and L. Tancredi, *Elliptic polylogarithms and iterated integrals on elliptic curves II: an application to the sunrise integral*, *Phys. Rev. D* **97** (2018) 116009, arXiv:1712.07095.

[46] S. Weinzierl, *Feynman Integrals - A Comprehensive Treatment for Students and Researchers*, *Springer Cham* (2022) 1–857, arXiv:2201.03593.

[47] M. Aaboud *et al.* [ATLAS Collaboration], *Evidence for the $H \to b\bar{b}$ decay with the ATLAS detector*, *JHEP* **12** (2017) 024, arXiv:1708.03299.

[48] M. Aaboud *et al.* [ATLAS Collaboration], *Observation of $H \to b\bar{b}$ decays and VH production with the ATLAS detector*, *Phys. Lett. B* **786** (2018) 59–86, arXiv:1808.08238.

[49] A.M. Sirunyan *et al.* [CMS Collaboration], *Evidence for the Higgs boson decay to a bottom quark–antiquark pair*, *Phys. Lett. B* **780** (2018) 501–532, arXiv:1709.07497.

[50] A.M. Sirunyan *et al.* [CMS Collaboration], *Observation of Higgs boson decay to bottom quarks*, *Phys. Rev. Lett.* **121** (2018) 121801, arXiv:1808.08242.

[51] T. Han and S. Willenbrock, *QCD correction to the $pp \to WH$ and ZH total cross sections*, *Phys. Lett. B* **273** (1991) 167–172.

[52] J. Ohnemus and W.J. Stirling, *Order-α_s corrections to the differential cross section for the* WH *intermediate-mass Higgs-boson signal*, *Phys. Rev. D* **47** (1993) 2722–2729.

[53] H. Baer, B. Bailey, and J.F. Owens, *$\mathcal{O}(\alpha_s)$ Monte Carlo approach to $W+$ Higgs-boson associated production at hadron supercolliders*, *Phys. Rev. D* **47** (1993) 2730–2734.

[54] O. Brein, A. Djouadi, and R.V. Harlander, *NNLO QCD corrections to the Higgs-strahlung processes at hadron colliders*, *Phys. Lett. B* **579** (2004) 149–156, arXiv:hep-ph/0307206.

[55] O. Brein, R.V. Harlander, and T.J.E. Zirke, *vh@nnlo - Higgs Strahlung at hadron colliders*, *Comput. Phys. Commun.* **184** (2013) 998–1003, arXiv:1210.5347.

[56] R. Hamberg, W.L. van Neerven, and T. Matsuura, *A complete calculation of the order α_s^2 correction to the Drell-Yan K-factor*, *Nucl. Phys. B* **359** (1991) 343–405.

[57] G. Ferrera, M. Grazzini, and F. Tramontano, *Associated Higgs-W-Boson Production at Hadron Colliders: A Fully Exclusive QCD Calculation at NNLO*, *Phys. Rev. Lett.* **107** (2011) 152003, arXiv:1107.1164.

[58] G. Ferrera, M. Grazzini, and F. Tramontano, *Higher-order QCD effects for associated WH production and decay at the LHC*, *JHEP* **04** (2014) 039, arXiv:1312.1669.

[59] G. Ferrera, M. Grazzini, and F. Tramontano, *Associated ZH production at hadron colliders: The fully differential NNLO QCD calculation*, *Phys. Lett. B* **740** (2015) 51–55, arXiv:1407.4747.

[60] J.M. Campbell, R.K. Ellis, and C. Williams, *Associated production of a Higgs boson at NNLO*, *JHEP* **06** (2016) 179, arXiv:1601.00658.

[61] G. Ferrera, G. Somogyi, and F. Tramontano, *Associated production of a Higgs boson decaying into bottom quarks at the LHC in full NNLO QCD*, *Phys. Lett. B* **780** (2018) 346–351, arXiv:1705.10304.

[62] F. Caola, G. Luisoni, K. Melnikov, and R. Röntsch, *NNLO QCD corrections to associated WH production and $H \to b\bar{b}$ decay*, *Phys. Rev. D* **97** (2018) 074022, arXiv:1712.06954.

[63] A. Behring and W. Bizoń, *Higgs decay into massive b-quarks at NNLO QCD in the nested soft-collinear subtraction scheme*, *JEHP* **01** (2020) 189, arXiv:1911.11524.

[64] A. Behring *et al.*, *Bottom quark mass effects in associated WH production with the $H \to b\bar{b}$ decay through NNLO QCD*, *Phys. Rev. D* **101** (2020) 114012, arXiv:2003.08321.

[65] K. Asteriadis, F. Caola, K. Melnikov, and R. Röntsch, *NNLO QCD corrections to weak boson fusion Higgs boson production in the $H \to b\bar{b}$ and $H \to WW^* \to 4l$ decay channels*, *JHEP* **02** (2022) 046, arXiv:2110.02818.

[66] R. Gauld *et al.*, *Associated production of a Higgs boson decaying into bottom quarks and a weak vector boson decaying leptonically at NNLO in QCD*, *JHEP* **10** (2019) 002, arXiv:1907.05836.

[67] S. Dawson *et al.*, *Resummation effects in vector-boson and Higgs associated production*, *Phys. Rev. D* **86** (2012) 074007, arXiv:1207.4207.

[68] R. Gauld *et al.*, *Precise predictions for WH+jet production at the LHC*, *Phys. Lett. B* **817** (2021) 136335, arXiv:2009.14209.

[69] R. Gauld *et al.*, *VH+jet production in hadron-hadron collisions up to order α_s^3 in perturbative QCD*, *JHEP* **03** (2022) 008, arXiv:2110.12992.

[70] J. Baglio, C. Duhr, B. Mistlberger, and R. Szafron, *Inclusive production cross sections at N^{3}LO*, *JHEP* **12** (2022) 066, arXiv:2209.06138.

[71] M.L. Ciccolini, S. Dittmaier, and M. Krämer, *Electroweak radiative corrections to associated WH and ZH production at hadron colliders*, *Phys. Rev. D* **68** (2003) 073003, arXiv:hep-ph/0306234.

[72] A. Denner, S. Dittmaier, S. Kallweit, and A. Mück, *Electroweak corrections to Higgs-strahlung off W/Z bosons at the Tevatron and the LHC with Hawk*, *JHEP* **03** (2012) 075, arXiv:1112.5142.

[73] A. Denner, S. Dittmaier, S. Kallweit, and A. Mück, *HAWK 2.0: A Monte Carlo program for Higgs production in vector-boson fusion and Higgs-strahlung at hadron colliders*, *Comput. Phys. Commun.* **195** (2015) 161–171, arXiv:1412.5390.

[74] G. Luisoni, P. Nason, C. Oleari, and F. Tramontano, *$HW \pm/HZ$ + 0 and 1 jet at NLO with the POWHEG BOX interfaced to GoSam and their merging within MiNLO*, *JHEP* **10** (2013) 083, arXiv:1306.2542.

[75] D. Gonçalves, F. Krauss, S. Kuttimalai, and P. Maierhöfer, *Higgs-Strahlung: Merging the NLO Drell-Yan and loop-induced $0+1$ jet multiplicities*, *Phys. Rev. D* **92** (2015) 073006, arXiv:1509.01597.

[76] B. Hespel, F. Maltoni, and E. Vryonidou, *Higgs and Z boson associated production via gluon fusion in the SM and the 2HDM*, *JHEP* **06** (2015) 065, arXiv:1503.01656.

[77] W. Astill, W. Bizoń, E. Re, and G. Zanderighi, *NNLOPS accurate associated HW production*, *JHEP* **06** (2016) 154, arXiv:1603.01620.

[78] W. Astill, W. Bizoń, E. Re, and G. Zanderighi, *NNLOPS accurate associated HZ production with $H \to b\bar{b}$ decay at NLO*, *JHEP* **11** (2018) 157, arXiv:1804.08141.

[79] S. Alioli *et al.*, *Higgsstrahlung at* NNLL$'$ + NNLO *matched to parton showers in GENEVA*, *Phys. Rev. D* **100** (2019) 096016, arXiv:1909.02026.

[80] W. Bizoń, E. Re, and G. Zanderighi, *NNLOPS description of the $H \to b\bar{b}$ decay with MiNLO*, *JHEP* **06** (2020) 006, arXiv:1912.09982.

[81] S. Zanoli *et al.*, *Next-to-next-to-leading order event generation for VH production with $H \to b\bar{b}$ decay*, *JHEP* **07** (2022) 008, arXiv:2112.04168.

[82] F. Granata, J.M. Lindert, C. Oleari, and S. Pozzorini, *NLO QCD+EW predictions for HV and HV+jet production including parton-shower effects*, *JHEP* **09** (2017) 012, arXiv:1706.03522.

[83] V.D. Barger *et al.*, *Higgs Boson Z^0 Associated Production From Fourth Generation Quarks at Super Collider Energies*, *Phys. Rev. Lett.* **57** (1986) 1672.

[84] D.A. Dicus and C. Kao, *Higgs-boson–Z^0 production from gluon fusion*, *Phys. Rev. D* **38** (1988) 1008–1011.

[85] B.A. Kniehl, *Associated Production of Higgs and Z Bosons From Gluon Fusion in Hadron Collisions*, *Phys. Rev. D* **42** (1990) 2253–2258.

[86] L. Altenkamp *et al.*, *Gluon-induced Higgs-strahlung at next-to-leading order QCD*, *JHEP* **02** (2013) 078, arXiv:1211.5015.

[87] R.V. Harlander, J. Klappert, S. Liebler, and L. Simon, *vh@nnlo-v2: New physics in Higgs Strahlung*, *JHEP* **05** (2018) 089, arXiv:1802.04817.

[88] A. Hasselhuhn, T. Luthe, and M. Steinhauser, *On top quark mass effects to $gg \to ZH$ at NLO*, *JHEP* **01** (2017) 073, arXiv:1611.05881.

[89] L. Alasfar *et al.*, *Virtual corrections to $gg \to ZH$ via a transverse momentum expansion*, *JHEP* **05** (2021) 168, arXiv:2103.06225.

[90] J. Davies, G. Mishima, and M. Steinhauser, *Virtual corrections to $gg \to ZH$ in the high-energy and large-m_t limits*, *JHEP* **03** (2021) 034.

[91] L. Bellafronte *et al.*, *Gluon fusion production at NLO: merging the transverse momentum and the high-energy expansions*, *JHEP* **07** (2022) 069, arXiv:2202.12157.

[92] G. Degrassi, R. Gröber, M. Vitti, and X. Zhao, *On the NLO QCD corrections to gluon-initiated ZH production*, *JHEP* **08** (2022) 009, arXiv:2205.02769.

[93] G. Wang, X. Xu, Y. Xu, and L.L. Yang, *Next-to-leading order corrections for $gg \to ZH$ with top quark mass dependence*, *Phys. Lett. B* **829** (2022) 137087, arXiv:2107.08206.

[94] L. Chen *et al.*, *ZH production in gluon fusion at NLO in QCD*, *JHEP* **08** (2022) 056, arXiv:2204.05225.

[95] L. Chen *et al.*, *ZH production in gluon fusion: two-loop amplitudes with full top quark mass dependence*, *JHEP* **03** (2021) 125, arXiv:2011.12325.

[96] R.V. Harlander, A. Kulesza, V. Theeuwes, and T.J.E. Zirke, *Soft gluon resummation for gluon-induced Higgs Strahlung*, *JHEP* **11** (2014) 082, arXiv:1410.0217.

[97] O. Brein, R.V. Harlander, M. Wiesemann, and T. Zirke, *Top-quark mediated effects in hadronic Higgs-Strahlung*, *Eur. Phys. J. C* **72** (2012) 1868, arXiv:1111.0761.

[98] J.M. Butterworth, A.R. Davison, M. Rubin, and G.P. Salam, *Jet substructure as a new Higgs search channel at the LHC*, *Phys. Rev. Lett.* **100** (2008) 242001, arXiv:0802.2470.

[99] R.V. Harlander, S. Liebler, and T.J.E. Zirke, *Higgs Strahlung at the Large Hadron Collider in the 2-Higgs-Doublet Model*, *JHEP* **02** (2014) 023, arXiv:1307.8122.

[100] C. Englert, M. McCullough, and M. Spannowsky, *Gluon-initiated associated production boosts Higgs physics*, *Phys. Rev. D* **89** (2014) 013013, arXiv:1310.4828.

[101] C. Kao, *Production of a pseudoscalar Higgs boson with a Z boson from gluon fusion*, *Phys. Rev. D* **46** (1992) 4907–4913.

[102] Y. Jun, M. Wen-Gan, Z. Ren-You, and H. Hong-Sheng, *A^0Z^0 associated production at the CERN Large Hadron Collider in the minimal supersymmetric standard model*, *Phys. Rev. D* **66** (2002) 095008, arXiv:hep-ph/0209279.

[103] C. Kao, G. Lovelace, and L.H. Orr, *Detecting a Higgs pseudoscalar with a Z boson at the LHC*, *Phys. Lett. B* **567** (2003) 259–264, arXiv:hep-ph/0305028.

[104] C. Kao and S. Sachithanandam, *Detecting a Higgs pseudoscalar with a Z boson produced in bottom quark fusion*, *Phys. Lett. B* **620** (2005) 80–87, arXiv:hep-ph/0411331.

[105] L.L. Yang, C.S. Li, J.J. Liu, and L.G. Jin, *Production of scalar Higgs bosons associated with Z^0 boson at the CERN LHC in the MSSM*, *J. Phys. G* **30** (2004) 1821–1833, arXiv:hep-ph/0312179.

[106] Q. Li *et al.*, *Next-to-leading order QCD predictions for A^0Z^0 associated production at the CERN Large Hadron Collider*, *Phys. Rev. D* **72** (2005) 034032, arXiv:hep-ph/0501070.

[107] A. Djouadi and M. Spira, *Supersymmetric QCD corrections to Higgs boson production at hadron colliders*, *Phys. Rev. D* **62** (2000) 014004, arXiv:hep-ph/9912476.

[108] A. Djouadi, *The Anatomy of electro-weak symmetry breaking. II. The Higgs bosons in the minimal supersymmetric model*, *Phys. Rept.* **459** (2008) 1–241, arXiv:hep-ph/0503173.

[109] B.A. Kniehl and C.P. Palisoc, *Associated production of Z and neutral Higgs bosons at the CERN Large Hadron Collider*, *Phys. Rev. D* **85** (2012) 075027, arXiv:1112.1575.

[110] W. Buchmüller and D. Wyler, *Effective Lagrangian Analysis of New Interactions and Flavor Conservation*, *Nucl. Phys. B* **268** (1986) 621–653.

[111] B. Grzadkowski, M. Iskrzyński, M. Misiak, and J. Rosiek, *Dimension-six terms in the Standard Model Lagrangian*, *JHEP* **10** (2010) 085, arXiv:1008.4884.

[112] I. Brivio and M. Trott, *The standard model as an effective field theory*, *Phys. Rep.* **793** (2019) 1–98, arXiv:1706.08945.

[113] K. Mimasu, V. Sanz, and C. Williams, *Higher order QCD predictions for associated Higgs production with anomalous couplings to gauge bosons*, *JHEP* **08** (2016) 039, arXiv:1512.02572.

[114] W. Bizoń, F. Caola, K. Melnikov, and R. Röntsch, *Anomalous couplings in associated VH production with Higgs boson decay to massive b quarks at NNLO in QCD*, *Phys. Rev. D* **105** (2022) 014023, arXiv:2106.06328.

[115] R.V. Harlander, J. Klappert, C. Pandini, and A. Papaefstathiou, *Exploiting the WH/ZH symmetry in the search for new physics*, *Eur. Phys. J. C* **78** (2018) 760, arXiv:1804.02299.

[116] F. Caola, K. Melnikov, and R. Röntsch, *Analytic results for color-singlet production at NNLO QCD with the nested soft-collinear subtraction scheme*, *Eur. Phys. J. C* **79** (2019) 386, arXiv:1902.02081.

[117] F. Caola, K. Melnikov, and R. Röntsch, *Analytic results for decays of color singlets to gg and $q\bar{q}$ final states at NNLO QCD with the nested soft-collinear subtraction scheme*, *Eur. Phys. J. C* **79** (2019) 1013, arXiv:1907.05398.

[118] K. Asteriadis, F. Caola, K. Melnikov, and R. Röntsch, *Analytic results for deep-inelastic scattering at NNLO QCD with the nested soft-collinear subtraction scheme*, *Eur. Phys. J. C* **80** (2020) 8, arXiv:1910.13761.

[119] R.V. Harlander, S. Liebler, and H. Mantler, *SusHi: A program for the calculation of Higgs production in gluon fusion and bottom-quark annihilation in the Standard Model and the MSSM*, *Comput. Phys. Commun.* **184** (2013) 1605–1617, arXiv:1212.3249.

[120] R.V. Harlander, S. Liebler, and H. Mantler, *SusHi Bento: Beyond NNLO and the heavy- top limit*, *Comput. Phys. Commun.* **212** (2017) 239–257, arXiv:1605.03190.

[121] M. Czakon and D. Heymes, *Four-dimensional formulation of the sector-improved residue subtraction scheme*, *Nucl. Phys. B* **890** (2015) 152–227, arXiv:1408.2500.

[122] A. Behring, M. Czakon, and R. Poncelet, *Sector-improved residue subtraction: Improvements and Applications*, *PoS* **LL2018** (2018) 024, arXiv:1808.07656.

[123] J.C. Collins, D.E. Soper, and G.F. Sterman, *Factorization of Hard Processes in QCD*, *Adv. Ser. Direct. High Energy Phys.* **5** (1989) 1–91, arXiv:hep-ph/0409313.

[124] G. 't Hooft and M.J.G. Veltman, *Regularization and renormalization of gauge fields*, *Nucl. Phys. B* **44** (1972) 189–213.

[125] S.D. Drell and T.M. Yan, *Massive Lepton-Pair Production in Hadron-Hadron Collisions at High Energies*, *Phys. Rev. Lett.* **25** (1970) 316–320.

[126] R. Harlander, S. Klein, and M. Lipp, *FeynGame*, *Comput. Phys. Commun.* **256** (2020) 107465, arXiv:2003.00896.

[127] E. Fermi, *Versuch einer Theorie der β-Strahlen. I*, *Z. Phys.* **88** (1934) 161–177.

[128] T.D. Lee, *A Theory of Spontaneous T Violation*, *Phys. Rev. D* **8** (1973) 1226–1239.

[129] J.F. Gunion, H.E. Haber, G.L. Kane, and S. Dawson, *The Higgs Hunter's Guide*, *Front.Phys.* **80** (2000) 1–404.

[130] A. Akeroyd, *Non-minimal neutral Higgs bosons at LEP2*, *Phys. Lett. B* **377** (1996) 95–101, arXiv:hep-ph/9603445.

[131] A.G. Akeroyd, *Fermiophobic and other non-minimal neutral Higgs bosons at the LHC*, *J. Phys. G: Nucl. Part. Phys.* **24** (1998) 1983–1994, arXiv:hep-ph/9803324.

[132] M. Aoki, S. Kanemura, K. Tsumura, and K. Yagyu, *Models of Yukawa interaction in the two Higgs doublet model, and their collider phenomenology*, *Phys. Rev. D* **80** (2009) 015017, arXiv:0902.4665.

[133] G. Branco *et al.*, *Theory and phenomenology of two-Higgs-doublet models*, *Phys. Rep.* **516** (2012) 1–102, arXiv:1106.0034.

[134] N. Craig and S. Thomas, *Exclusive signals of an extended Higgs sector*, *JHEP* **11** (2012) 083, arXiv:1207.4835.

[135] G. Bhattacharyya and D. Das, *Scalar sector of two-Higgs-doublet models: A minireview*, *Pramana* **87** (2016) 40, arXiv:1507.06424.

[136] L. Wang, J.M. Yang, and Y. Zhang, *Two-Higgs-doublet models in light of current experiments: a brief review*, *Commun. Theor. Phys.* **74** (2022) 097202, arXiv:2203.07244.

[137] N.G. Deshpande and E. Ma, *Pattern of symmetry breaking with two Higgs doublets*, *Phys. Rev. D* **18** (1978) 2574–2576.

[138] L.L. Honorez, E. Nezri, J.F. Oliver, and M.H.G. Tytgat, *The inert doublet model: an archetype for dark matter*, *JCAP* **02** (2007) 028, arXiv:hep-ph/0612275.

[139] J. Rosiek, *Complete set of Feynman rules for the minimal supersymmetric extension of the standard model*, *Phys. Rev. D* **41** (1990) 3464–3501, arXiv:hep-ph/9511250.

[140] M. Drees, R. Godbole, and P. Roy, *Theory and phenomenology of sparticles: An account of four-dimensional N=1 supersymmetry in high energy physics*, *Hackensack, USA: World Scientific* (2004) 1–555.

[141] S.L. Glashow and S. Weinberg, *Natural conservation laws for neutral currents*, *Phys. Rev. D* **15** (1977) 1958–1965.

[142] E.A. Paschos, *Diagonal neutral currents*, *Phys. Rev. D* **D 15** (1977) 1966–1972.

[143] E. Jenkins, *Searching for a (B–L) gauge boson in $p\bar{p}$ collisions*, *Phys. Lett. B* **192** (1987) 219–222.

[144] W. Buchmüller, C. Greub, and P. Minkowski, *Neutrino masses, neutral vector bosons and the scale of B–L breaking*, *Phys. Lett. B* **267** (1991) 395–399.

[145] S. Khalil, *Low-scale B–L extension of the standard model*, *J. Phys. G: Nucl. Part. Phys.* **35** (2008) 055001, arXiv:hep-ph/0611205.

[146] L. Basso, *Phenomenology of the minimal B–L extension of the Standard Model at the LHC*, PhD thesis, University of Southampton, School of Physics and Astronomy (2011). arXiv:1106.4462.

[147] J.L. Díaz-Cruz, J.M. Hernández-López, and J.A. Orduz-Ducuara, *An extra Z' gauge boson as a source of Higgs particles*, *J. Phys. G: Nucl. Part. Phys.* **40** (2013) 125002, arXiv:1304.0016.

[148] A. Gutiérrez-Rodríguez and M.A. Hernández-Ruiz, *Resonance and Associated Production at Future Higgs Boson Factory: ILC and CLIC*, *Adv. High Energy Phys.* **2015** (2015) 593898, arXiv:1506.07575.

[149] F. Ramírez-Sánchez, A. Gutiérrez-Rodríguez, and M.A. Hernández-Ruíz, *Higgs bosons production and decay at future e^+e^- linear colliders as a probe of the B–L model*, *J. Phys. G: Nucl. Part. Phys.* **43** (2016) 095003, arXiv:1606.04144.

[150] S.Y. Zhao, C.X. Yue, and Y. Yu, *The HZZ' Coupling and the Higgs-Strahlung Production $pp \to ZH$ at the LHC*, *Int. J. Theor. Phys.* **55** (2016) 648–657.

[151] R.D. Ball *et al.* [NNPDF Collaboration], *The PDF4LHC21 combination of global PDF fits for the LHC Run III**, *J. Phys. G: Nucl. Part. Phys.* **49** (2022) 080501, arXiv:2203.05506.

[152] F. Bloch and A. Nordsieck, *Note on the Radiation Field of the Electron*, *Phys. Rev.* **52** (1937) 54–59.

[153] T. Kinoshita, *Mass singularities of Feynman amplitudes*, *J. Math. Phys.* **3** (1962) 650–677.

[154] T.D. Lee and M. Nauenberg, *Degenerate Systems and Mass Singularities*, *Phys. Rev.* **133** (1964) B1549–B1562.

[155] Z. Kunszt and D.E. Soper, *Calculation of jet cross-sections in hadron collisions at order α_s^3*, *Phys. Rev. D* **46** (1992) 192–221.

[156] K. Fabricius, I. Schmitt, G. Kramer, and G. Schierholz, *Higher Order Perturbative QCD Calculation of Jet Cross-Sections in e^+e^- Annihilation*, *Z. Phys. C* **11** (1982) 315–333.

[157] H. Baer, J. Ohnemus, and J.F. Owens, *Next-to-leading-logarithm calculation of jet photoproduction*, *Phys. Rev. D* **40** (1989) 2844–2855.

[158] W.T. Giele and E.W.N. Glover, *Higher-order corrections to jet cross sections in e^+e^- annihilation*, *Phys. Rev. D* **46** (1992) 1980–2010.

[159] W. Giele, E. Glover, and D.A. Kosower, *Higher-order corrections to jet cross sections in hadron colliders*, *Nucl. Phys. B* **403** (1993) 633–667, arXiv:hep-ph/9302225.

[160] X. Chen *et al.*, *Dilepton Rapidity Distribution in Drell-Yan Production to Third Order in QCD*, *Phys. Rev. Lett.* **128** (2022) 052001, arXiv:2107.09085.

[161] G. Billis *et al.*, *Higgs p_T Spectrum and Total Cross Section with Fiducial Cuts at Third Resummed and Fixed Order in QCD*, *Phys. Rev. Lett.* **127** (2021) 072001, arXiv:2102.08039.

[162] S. Camarda, L. Cieri, and G. Ferrera, *Drell–Yan lepton-pair production: q_T resummation at N^{3}LL accuracy and fiducial cross sections at N^{3}LO*, *Phys. Rev. D* **104** (2021) L111503, arXiv:2103.04974.

[163] G. Bozzi, S. Catani, D. de Florian, and M. Grazzini, *Transverse-momentum resummation and the spectrum of the Higgs boson at the LHC*, *Nucl. Phys. B* **737** (2006) 73–120, arXiv:hep-ph/0508068.

[164] S. Catani *et al.*, *Universality of transverse-momentum resummation and hard factors at the NNLO*, *Nucl. Phys. B* **881** (2014) 414–443, arXiv:1311.1654.

[165] M. Grazzini, S. Kallweit, and M. Wiesemann, *Fully differential NNLO computations with MATRIX*, *Eur. Phys. J. C* **78** (2018) 537, arXiv:1711.06631.

[166] R. Boughezal *et al.*, *Higgs boson production in association with a jet at NNLO using jettiness subtraction*, *Phys. Lett. B* **748** (2015) 5–8, arXiv:1505.03893.

[167] R. Boughezal, X. Liu, and F. Petriello, *N-jettiness soft function at next-to-next-to-leading order*, *Phys. Rev. D* **91** (2015) 094035, arXiv:1504.02540.

[168] I.W. Stewart, F.J. Tackmann, and W.J. Waalewijn, *N-Jettiness: An Inclusive Event Shape to Veto Jets*, *Phys. Rev. Lett.* **105** (2010) 092002, arXiv:1004.2489.

[169] R. Boughezal *et al.*, *Color-singlet production at NNLO in MCFM*, *Eur. Phys. J. C* **77** (2016) 7, arXiv:1605.08011.

[170] S. Dittmaier, *A general approach to photon radiation off fermions*, *Nucl. Phys. B* **565** (2000) 69–122, arXiv:hep-ph/9904440.

[171] T. Eynck, E. Laenen, L. Phaf, and S. Weinzierl, *Comparison of phase space slicing and dipole subtraction methods for $\gamma^* \to Q\bar{Q}$*, *Eur. Phys. J. C* **23** (2002) 259–266, arXiv:hep-ph/0109246.

[172] M. Butenschoen and B.A. Kniehl, *Dipole subtraction vs. phase space slicing in NLO NRQCD heavy-quarkonium production calculations*, *Nucl. Phys. B* **957** (2020) 115056, arXiv:2003.01014.

[173] D.A. Kosower, *Antenna factorization of gauge-theory amplitudes*, *Phys. Rev. D* **57** (1998) 5410–5416, arXiv:hep-ph/9710213.

[174] D.A. Kosower, *Antenna factorization in strongly ordered limits*, *Phys. Rev. D* **71** (2005) 045016, arXiv:hep-ph/0311272.

[175] A. Gehrmann-De Ridder, T. Gehrmann, and G. Heinrich, *Four-particle phase space integrals in massless QCD*, *Nucl. Phys. B* **682** (2004) 265–288, arXiv:hep-ph/0311276.

[176] A. Daleo, T. Gehrmann, and D. Maître, *Antenna subtraction with hadronic initial states*, *JHEP* **04** (2007) 016, arXiv:hep-ph/0612257.

[177] A. Daleo, A. Gehrmann-De Ridder, T. Gehrmann, and G. Luisoni, *Antenna subtraction at NNLO with hadronic initial states: initial-final configurations*, *JHEP* **01** (2010) 118, arXiv:0912.0374.

[178] R. Boughezal, A. Gehrmann-De Ridder, and M. Ritzmann, *Antenna subtraction at NNLO with hadronic initial states: double real radiation for initial-initial configurations with two quark flavours*, *JHEP* **02** (2011) 098, arXiv:1011.6631.

[179] A. Gehrmann-De Ridder, T. Gehrmann, and M. Ritzmann, *Antenna subtraction at NNLO with hadronic initial states: double real initial-initial configurations*, *JHEP* **10** (2012) 047, arXiv:1207.5779.

[180] T. Gehrmann and P.F. Monni, *Antenna subtraction at NNLO with hadronic initial states: real-virtual initial-initial configurations*, *JHEP* **12** (2011) 049, arXiv:1107.4037.

[181] A. Gehrmann-De Ridder, T. Gehrmann, and M. Ritzmann, *Antenna subtraction at NNLO with hadronic initial states: double real initial-initial configurations*, *JHEP* **10** (2012) 047, arXiv:1207.5779.

[182] J. Currie, E.W.N. Glover, and S. Wells, *Infrared structure at NNLO using antenna subtraction*, *JHEP* **04** (2013) 066, arXiv:1301.4693.

[183] A. Gehrmann-De Ridder, T. Gehrmann, E.W.N. Glover, and J. Pires, *Second-Order QCD Corrections to Jet Production at Hadron Colliders: The All-Gluon Contribution*, *Phys. Rev. Lett.* **110** (2013) 162003, arXiv:1301.7310.

[184] J. Currie, *Colourful antenna subtraction for gluon scattering*, *PoS* **RADCOR2013** (2013) 001, arXiv:1311.6113.

[185] J. Currie, A. Gehrmann-De Ridder, E.W.N. Glover, and J. Pires, *NNLO QCD corrections to jet production at hadron colliders from gluon scattering*, *JHEP* **01** (2014) 110, arXiv:1310.3993.

[186] A. Gehrmann-De Ridder, T. Gehrmann, E.N. Glover, and G. Heinrich, *Infrared structure of $e^+e^- \to 3$ jets at NNLO*, *JHEP* **11** (2007) 058, arXiv:0710.0346.

[187] A. Gehrmann-De Ridder, T. Gehrmann, E.W.N. Glover, and G. Heinrich, *Second-Order QCD Corrections to the Thrust Distribution in Electron-Positron Annihilation*, *Phys. Rev. Lett.* **99** (2007) 132002, arXiv:0707.1285.

[188] A. Gehrmann-De Ridder, T. Gehrmann, E. Glover, and G. Heinrich, *NNLO corrections to event shapes in e^+e^- annihilation*, *JHEP* **12** (2007) 094, arXiv:0711.4711.

[189] A. Gehrmann-De Ridder, T. Gehrmann, E.W.N. Glover, and G. Heinrich, *Jet Rates in Electron-Positron Annihilation at $\mathcal{O}(\alpha_s^3)$ in QCD*, *Phys. Rev. Lett.* **100** (2008) 172001, arXiv:0802.0813.

[190] A. Gehrmann-De Ridder, T. Gehrmann, E. Glover, and G. Heinrich, *NNLO moments of event shapes in e^+e^- annihilation*, *JHEP* **05** (2009) 106, arXiv:0903.4658.

[191] S. Weinzierl, *Next-to-Next-to-Leading Order Corrections to Three-Jet Observables in Electron-Positron Annihilation*, *Phys. Rev. Lett.* **101** (2008) 162001, arXiv:0807.3241.

[192] S. Weinzierl, *Event shapes and jet rates in electron-positron annihilation at NNLO*, *JHEP* **06** (2009) 041, arXiv:0904.1077.

[193] S. Weinzierl, *The infrared structure of $e^+e^- \to 3$ jets at NNLO reloaded*, *JHEP* **07** (2009) 009, arXiv:0904.1145.

[194] S. Weinzierl, *Moments of event shapes in electron-positron annihilation at next-to-next-to-leading order*, *Phys. Rev. D* **80** (2009) 094018, arXiv:0909.5056.

[195] E.W.N. Glover and J. Pires, *Antenna subtraction for gluon scattering at NNLO*, *JHEP* **06** (2010) 096, arXiv:1003.2824.

[196] A. Gehrmann-De Ridder, E.W.N. Glover, and J. Pires, *Real-virtual corrections for gluon scattering at NNLO*, *JHEP* **02** (2012) 141, arXiv:1112.3613.

[197] G. Abelof and A. Gehrmann-De Ridder, *Antenna subtraction for the production of heavy particles at hadron colliders*, *JHEP* **04** (2011) 063, arXiv:1102.2443.

[198] W. Bernreuther, C. Bogner, and O. Dekkers, *The real radiation antenna function for $S \to Q\bar{Q}q\bar{q}$ at NNLO QCD*, *JHEP* **06** (2011) 032, arXiv:1105.0530.

[199] G. Abelof and A. Gehrmann-De Ridder, *Double real radiation corrections to $t\bar{t}$ production at the LHC: the $gg \to t\bar{t}q\bar{q}$ channel*, *JHEP* **11** (2012) 074, arXiv:1207.6546.

[200] G. Abelof, O. Dekkers, and A. Gehrmann-De Ridder, *Antenna subtraction with massive fermions at NNLO: double real initial-final configurations*, *JHEP* **12** (2012) 107, arXiv:1210.5059.

[201] O. Dekkers and W. Bernreuther, *The real-virtual antenna functions for $S \to Q\bar{Q}X$ at NNLO QCD*, *Phys. Lett. B* **738** (2014) 325–333, arXiv:1409.3124.

[202] G. Abelof, A. Gehrmann-De Ridder, and I. Majer, *Top quark pair production at NNLO in the quark-antiquark channel*, *JHEP* **12** (2015) 074, arXiv:1506.04037.

[203] X. Chen *et al.*, *NNLO QCD corrections to Higgs boson production at large transverse momentum*, *JHEP* **10** (2016) 066, arXiv:1607.08817.

[204] A. Gehrmann-De Ridder *et al.*, *Precise QCD Predictions for the Production of a Z Boson in Association with a Hadronic Jet*, *Phys. Rev. Lett.* **117** (2016) 022001, arXiv:1507.02850.

[205] A. Gehrmann-De Ridder *et al.*, *The NNLO QCD corrections to Z boson production at large transverse momentum*, *JHEP* **07** (2016) 133, arXiv:1605.04295.

[206] A. Gehrmann-De Ridder *et al.*, *NNLO QCD corrections for Drell-Yan p_T^Z and ϕ^* observables at the LHC*, *JHEP* **11** (2016) 094, arXiv:1610.01843.

[207] R. Gauld *et al.*, *Precise predictions for the angular coefficients in Z-boson production at the LHC*, *JHEP* **11** (2017) 003, arXiv:1708.00008.

[208] A. Gehrmann-De Ridder *et al.*, *Next-to-Next-to-Leading-Order QCD Corrections to the Transverse Momentum Distribution of Weak Gauge Bosons*, *Phys. Rev. Lett.* **120** (2018) 122001, arXiv:1712.07543.

[209] J. Currie, T. Gehrmann, and J. Niehues, *Precise QCD Predictions for the Production of Dijet Final States in Deep Inelastic Scattering*, *Phys. Rev. Lett.* **117** (2016) 042001, arXiv:1606.03991.

[210] J. Currie, T. Gehrmann, A. Huss, and J. Niehues, *NNLO QCD corrections to jet production in deep inelastic scattering*, *JHEP* **07** (2017) 018, arXiv:1703.05977.

[211] J. Currie, E. Glover, and J. Pires, *Next-to-Next-to Leading Order QCD Predictions for Single Jet Inclusive Production at the LHC*, *Phys. Rev. Lett.* **118** (2017) 072002, arXiv:1611.01460.

[212] J. Currie *et al.*, *Precise Predictions for Dijet Production at the LHC*, *Phys. Rev. Lett.* **119** (2017) 152001, arXiv:1705.10271.

[213] T. Gehrmann *et al.*, *NNLO QCD corrections to event orientation in e^+e^- annihilation*, *Phys. Lett. B* **775** (2017) 185–189, arXiv:1709.01097.

[214] X. Chen, T. Gehrmann, E.W.N. Glover, and J. Mo, *Antenna subtraction for jet production observables in full colour at NNLO*, *JHEP* **10** (2022) 040, arXiv:2208.02115.

[215] S. Borowka *et al.*, *pySecDec: A toolbox for the numerical evaluation of multi-scale integrals*, *Comput. Phys. Commun.* **222** (2018) 313–326, arXiv:1703.09692.

[216] G. Somogyi, Z. Trócsányi, and V. Del Duca, *Matching of singly- and doubly-unresolved limits of tree-level QCD squared matrix elements*, *JHEP* **06** (2005) 024, arXiv:hep-ph/0502226.

[217] G. Somogyi and Z. Trócsányi, *A subtraction scheme for computing QCD jet cross sections at NNLO: regularization of real-virtual emission*, *JHEP* **01** (2007) 052, arXiv:hep-ph/0609043.

[218] G. Somogyi, Z. Trócsányi, and V. Del Duca, *A subtraction scheme for computing QCD jet cross sections at NNLO: regularization of doubly-real emissions*, *JHEP* **01** (2007) 070, arXiv:hep-ph/0609042.

[219] G. Somogyi and Z. Trócsányi, *A subtraction scheme for computing QCD jet cross sections at NNLO: integrating the subtraction terms I*, *JHEP* **08** (2008) 042, arXiv:0807.0509.

[220] U. Aglietti *et al.*, *Analytic integration of real-virtual counterterms in NNLO jet cross sections I*, *JHEP* **09** (2008) 107, arXiv:0807.0514.

[221] G. Somogyi, *Subtraction with hadronic initial states at NLO: an NNLO-compatible scheme*, *JHEP* **05** (2009) 016, arXiv:0903.1218.

[222] P. Bolzoni, S.O. Moch, G. Somogyi, and Z. Trócsányi, *Analytic integration of real-virtual counterterms in NNLO jet cross sections II*, *JHEP* **08** (2009) 079, arXiv:0905.4390.

[223] P. Bolzoni, G. Somogyi, and Z. Trócsányi, *A subtraction scheme for computing QCD jet cross sections at NNLO: integrating the iterated singly-unresolved subtraction terms*, *JHEP* **01** (2011) 059, arXiv:1011.1909.

[224] G. Somogyi, *A subtraction scheme for computing QCD jet cross sections at NNLO: integrating the doubly unresolved subtraction terms*, *JHEP* **04** (2013) 010, arXiv:1301.3919.

[225] V. Del Duca, G. Somogyi, and Z. Trócsányi, *Integration of collinear-type doubly unresolved counterterms in NNLO jet cross sections*, *JHEP* **06** (2013) 079, arXiv:1301.3504.

[226] V. Del Duca *et al.*, *Higgs boson decay into b-quarks at NNLO accuracy*, *JHEP* **04** (2015) 036, arXiv:1501.07226.

[227] V. Del Duca *et al.*, *Three-Jet Production in Electron-Positron Collisions at Next-to-Next-to-Leading Order Accuracy*, *Phys. Rev. Lett.* **117** (2016) 152004, arXiv:1603.08927.

[228] V. Del Duca *et al.*, *Jet production in the CoLoRFulNNLO method: Event shapes in electron-positron collisions*, *Phys. Rev. D* **94** (2016) 074019, arXiv:1606.03453.

[229] G. Somogyi, A. Kardos, Z. Szőr, and Z. Trócsányi, *Higher Order Corrections in the CoLoRFulNNLO Framework*, *Acta Phys. Pol. B* **48** (2017) 1195, arXiv:1706.01688.

[230] X. Chen *et al.*, *Fully Differential Higgs Boson Production to Third Order in QCD*, *Phys. Rev. Lett.* **127** (2021) 072002, arXiv:2102.07607.

[231] W.J.T. Bobadilla *et al.*, *May the four be with you: novel IR-subtraction methods to tackle NNLO calculations*, *Eur. Phys. J. C* **81** (2021) 250, arXiv:2012.02567.

[232] M. Czakon, D. Heymes, and A. Mitov, *High-Precision Differential Predictions for Top-Quark Pairs at the LHC*, *Phys. Rev. Lett.* **116** (2016) 082003, arXiv:1511.00549.

[233] M. Czakon, P. Fiedler, D. Heymes, and A. Mitov, *NNLO QCD predictions for fully-differential top-quark pair production at the Tevatron*, *JHEP* **05** (2016) 034, arXiv:1601.05375.

[234] M. Czakon, A. van Hameren, A. Mitov, and R. Poncelet, *Single-jet inclusive rates with exact color at $\mathcal{O}(\alpha_s^4)$*, *JHEP* **10** (2019) 262, arXiv:1907.12911.

[235] H.A. Chawdhry, M. Czakon, A. Mitov, and R. Poncelet, *NNLO QCD corrections to three-photon production at the LHC*, *JHEP* **02** (2020) 057, arXiv:1911.00479.

[236] H.A. Chawdhry, M. Czakon, A. Mitov, and R. Poncelet, *NNLO QCD corrections to diphoton production with an additional jet at the LHC*, *JHEP* **09** (2021) 093, arXiv:2105.06940.

[237] M. Czakon, A. Mitov, and R. Poncelet, *Next-to-Next-to-Leading Order Study of Three-Jet Production at the LHC*, *Phys. Rev. Lett.* **127** (2021) 152001, arXiv:2106.05331.

[238] M. Delto, M. Jaquier, K. Melnikov, and R. Röntsch, *Mixed QCD⊗QED corrections to on-shell Z boson production at the LHC*, *JHEP* **01** (2020) 043, arXiv:1909.08428.

[239] F. Buccioni *et al.*, *Mixed QCD-electroweak corrections to on-shell Z production at the LHC*, *Phys. Lett. B* **811** (2020) 135969, arXiv:2005.10221.

[240] A. Behring *et al.*, *Mixed QCD-electroweak corrections to W-boson production in hadron collisions*, *Phys. Rev. D* **103** (2021) 013008, arXiv:2009.10386.

[241] F. Buccioni *et al.*, *Mixed QCD-electroweak corrections to dilepton production at the LHC in the high invariant mass region*, *JHEP* **06** (2022) 022, arXiv:2203.11237.

[242] W. Bizoń, K. Melnikov, and J. Quarroz, *On the interference of ggH and $c\bar{c}H$ Higgs production mechanisms and the determination of charm Yukawa coupling at the LHC*, *JHEP* **06** (2021) 107, arXiv:2102.04242.

[243] M. Jaquier and R. Röntsch, *Mixed scalar-pseudoscalar Higgs boson production through next-to-next-to-leading order at the LHC*, *JHEP* **06** (2020) 005, arXiv:1911.10631.

[244] K. Asteriadis, F. Caola, K. Melnikov, and R. Röntsch, *Anomalous Higgs boson couplings in weak boson fusion production at NNLO in QCD*, *Phys. Rev. D* **107** (2023) 034034, arXiv:2206.14630.

[245] S. Frixione, Z. Kunszt, and A. Signer, *Three-jet cross sections to next-to-leading order*, *Nucl. Phys. B* **467** (1996) 399–442, arXiv:hep-ph/9512328.

[246] S. Frixione, *A general approach to jet cross sections in QCD*, *Nucl. Phys. B* **507** (1997) 295–314, arXiv:hep-ph/9706545.

[247] S. Catani and M. Seymour, *A general algorithm for calculating jet cross sections in NLO QCD*, *Nucl. Phys. B* **485** (1997) 291–419, arXiv:hep-ph/9605323.

[248] S. Catani, S. Dittmaier, M.H. Seymour, and Z. Trócsányi, *The dipole formalism for next-to-leading order QCD calculations with massive partons*, *Nucl. Phys. B* **627** (2002) 189–265, arXiv:hep-ph/0201036.

[249] G. Altarelli and G. Parisi, *Asymptotic freedom in parton language*, *Nucl. Phys. B* **126** (1977) 298–318.

[250] W.L. van Neerven, *Dimensional Regularization of Mass and Infrared Singularities in Two Loop On-shell Vertex Functions*, *Nucl. Phys. B* **268** (1986) 453–488.

[251] G. Somogyi, *Angular integrals in d dimensions*, *J. Math. Phys.* **52** (2011) 083501, arXiv:1101.3557.

[252] Wolfram Research, Inc, *Mathematica, Version 13.2* (2022) Champaign, IL.

[253] T. Huber and D. Maître, *HypExp, a Mathematica package for expanding hypergeometric functions around integer-valued parameters*, *Comput. Phys. Commun.* **175** (2006) 122–144, arXiv:hep-ph/0507094.

[254] T. Huber and D. Maître, *HypExp 2, Expanding hypergeometric functions about half-integer parameters*, *Comput. Phys. Commun.* **178** (2008) 755–776, arXiv:0708.2443.

[255] C. Anastasiou and K. Melnikov, *Higgs boson production at hadron colliders in NNLO QCD*, *Nucl. Phys. B* **646** (2002) 220–256, arXiv:hep-ph/0207004.

[256] P.A. Baikov, K.G. Chetyrkin, and J.H. Kühn, *Scalar Correlator at $(O)(\alpha_s^4)$, Higgs Boson Decay into Bottom Quarks, and Bounds on the Light-Quark Masses*, *Phys. Rev. Lett.* **96** (2006) 012003, arXiv:hep-ph/0511063.

[257] C. Anastasiou, F. Herzog, and A. Lazopoulos, *The fully differential decay rate of a Higgs boson to bottom-quarks at NNLO in QCD*, *JHEP* **03** (2012) 035, arXiv:1110.2368.

[258] M. Schreck and M. Steinhauser, *Higgs decay to gluons at NNLO*, *Phys. Lett. B* **655** (2007) 148–155, arXiv:0708.0916.

[259] D.I. Kazakov *et al.*, *Complete quartic (α_s^2) correction to the deep-inelastic longitudinal structure function F_L in QCD*, *Phys. Rev. Lett.* **65** (1990) 1535–1538.

[260] E.B. Zijlstra and W.L. van Neerven, *Order-α_s^2 QCD corrections to the deep inelastic proton structure functions F_2 and F_L*, *Nucl. Phys. B* **383** (1992) 525–574.

[261] S. Moch and J. Vermaseren, *Deep-inelastic structure functions at two loops*, *Nucl. Phys. B* **573** (2000) 853–907, arXiv:hep-ph/9912355.

[262] K. Asteriadis, *Application of the nested soft-collinear subtraction scheme to the description of deep inelastic scattering*, Karlsruher Institut für Technologie (2021). doi:10.5445/IR/1000135340.

[263] B.I. Ermolaev and V.S. Fadin, *Doubly logarithmic asymptotic behavior of exclusive cross sections in quantum chromodynamics*, *JETP Lett.* **33** (1981) 269–272.

[264] A. Bassetto, M. Ciafaloni, and G. Marchesini, *Jet Structure and Infrared Sensitive Quantities in Perturbative QCD*, *Phys. Rept.* **100** (1983) 201–272.

[265] Y.L. Dokshitzer, V.A. Khoze, S.I. Troian, and A.H. Mueller, *QCD Coherence in High-Energy Reactions*, *Rev. Mod. Phys.* **60** (1988) 373.

[266] S. Catani and M. Grazzini, *Infrared factorization of tree-level QCD amplitudes at the next-to-next-to-leading order and beyond*, *Nucl. Phys. B* **570** (2000) 287–325, arXiv:hep-ph/9908523.

[267] S. Catani and M. Grazzini, *Collinear factorization and splitting functions for next-to-next-to-leading order QCD calculations*, *Phys. Lett. B* **446** (1999) 143–152, arXiv:hep-ph/9810389.

[268] J. Campbell and E. Glover, *Double unresolved approximations to multiparton scattering amplitudes*, *Nucl. Phys. B* **527** (1998) 264–288, arXiv:hep-ph/9710255.

[269] F. Caola, M. Delto, H. Frellesvig, and K. Melnikov, *The double-soft integral for an arbitrary angle between hard radiators*, *Eur. Phys. J. C* **78** (2018) 687, arXiv:1807.05835.

[270] M. Delto and K. Melnikov, *Integrated triple-collinear counter-terms for the nested soft-collinear subtraction scheme*, *JHEP* **05** (2019) 148, arXiv:1901.05213.

[271] S. Catani and M. Grazzini, *The soft-gluon current at one-loop order*, *Nucl. Phys. B* **591** (2000) 435–454, arXiv:hep-ph/0007142.

[272] I. Bierenbaum, M. Czakon, and A. Mitov, *The singular behavior of one-loop massive QCD amplitudes with one external soft gluon*, *Nucl. Phys. B* **856** (2012) 228–246, arXiv:1107.4384.

[273] Z. Bern, L. Dixon, D.C. Dunbar, and D.A. Kosower, *One-loop n-point gauge theory amplitudes, unitarity and collinear limits*, *Nucl. Phys. B* **425** (1994) 217–260, arXiv:hep-ph/9403226.

[274] Z. Bern, V. Del Duca, and C.R. Schmidt, *The infrared behavior of one-loop gluon amplitudes at next-to-next-to-leading order*, *Phys. Lett. B* **445** (1998) 168–177, arXiv:hep-ph/9810409.

[275] Z. Bern, V. Del Duca, W.B. Kilgore, and C.R. Schmidt, *Infrared behavior of one-loop QCD amplitudes at next-to-next-to-leading order*, *Phys. Rev. D* **60** (1999) 116001, arXiv:hep-ph/9903516.

[276] D.A. Kosower, *All-order collinear behavior in gauge theories*, *Nucl. Phys. B* **552** (1999) 319–336, arXiv:hep-ph/9901201.

[277] D.A. Kosower and P. Uwer, *One-loop splitting amplitudes in gauge theory*, *Nucl. Phys. B* **563** (1999) 477–505, arXiv:hep-ph/9903515.

[278] S. Catani, *The singular behaviour of QCD amplitudes at two-loop order*, *Phys. Lett. B* **427** (1998) 161–171, arXiv:hep-ph/9802439.

[279] T. Becher and M. Neubert, *Infrared Singularities of Scattering Amplitudes in Perturbative QCD*, *Phys. Rev. Lett.* **102** (2009) 162001, arXiv:0901.0722.

[280] T. Becher, G. Bell, C. Lorentzen, and S. Marti, *Transverse-momentum spectra of electroweak bosons near threshold at NNLO*, *JHEP* **02** (2014) 004, arXiv:1309.3245.

[281] G.P. Lepage, *A New Algorithm for Adaptive Multidimensional Integration*, *J. Comput. Phys.* **27** (1978) 192.

[282] G.P. Lepage, *VEGAS – An adaptive multi-dimensional integration program* (1980).

[283] T. Hahn, *Cuba – a library for multidimensional numerical integration*, *Comput. Phys. Commun.* **168** (2005) 78–95, arXiv:hep-ph/0404043.

[284] T. Hahn, *Concurrent Cuba* (2014) arXiv:1408.6373.

[285] H. Kahn, *Random sampling (Monte Carlo) techniques in neutron attenuation problems – I*, *Nucleonics* **6** (1950) 27–37.

[286] H. Kahn, *Random sampling (Monte Carlo) techniques in neutron attenuation problems – II*, *Nucleonics* **6** (1950) 60–65.

[287] E. Byckling and K. Kajantie, *Particle Kinematics: (Chapters I-VI, X)* (1971).

[288] H.H. Patel, *Package-X: A Mathematica package for the analytic calculation of one-loop integrals*, *Comput. Phys. Commun.* **197** (2015) 276–290, arXiv:1503.01469.

[289] H.H. Patel, *Package-X 2.0: A Mathematica package for the analytic calculation of one-loop integrals*, *Comput. Phys. Commun.* **218** (2017) 66–70, arXiv:1612.00009.

[290] F. Buccioni *et al.*, *OpenLoops 2*, *Eur. Phys. J. C* **79** (2019) 866, arXiv:1907.13071.

[291] D. Korneev, *Higgs Strahlung via contact interactions through next-to-next-to-leading order QCD*, PhD thesis, RWTH Aachen University (2023). In preparation.

[292] J. Alwall *et al.*, *The automated computation of tree-level and next-to-leading order differential cross sections, and their matching to parton shower simulations*, *JHEP* **07** (2014) 079, arXiv:1405.0301.

[293] P. de Aquino *et al.*, *ALOHA: Automatic libraries of helicity amplitudes for Feynman diagram computations*, *Comput. Phys. Commun.* **183** (2012) 2254–2263, arXiv:1108.2041.

[294] H. Murayama, I. Watanabe, and K. Hagiwara, *HELAS: HELicity Amplitude Subroutines for Feynman Diagram Evaluations* (1992).

[295] J.R. Andersen *et al.*, *Les Houches 2013: Physics at TeV Colliders: Standard Model Working Group Report* (2014) arXiv:1405.1067.

[296] A. Buckley *et al.*, *LHAPDF6: parton density access in the LHC precision era*, *Eur. Phys. J. C* **75** (2015) 132, arXiv:1412.7420.

[297] T.J. Hou *et al.* [CTEQ Collaboration], *New CTEQ global analysis of quantum chromodynamics with high-precision data from the LHC*, *Phys. Rev. D* **103** (2021) 014013, arXiv:1912.10053.

[298] S. Bailey *et al.*, *Parton distributions from LHC, HERA, Tevatron and fixed target data: MSHT20 PDFs*, *Eur. Phys. J. C* **81** (2021) 341, arXiv:2012.04684.

[299] J. McGowan, T. Cridge, L.A. Harland-Lang, and R.S. Thorne, *Approximate N^3LO parton distribution functions with theoretical uncertainties: MSHT20aN^3LO PDFs*, *Eur. Phys. J. C* **83** (2023) 185, arXiv:2207.04739.

[300] R.D. Ball *et al.* [NNPDF Collaboration], *The path to proton structure at 1% accuracy*, *Eur. Phys. J. C* **82** (2022) 428, arXiv:2109.02653.

[301] A. Voigt, *Polylogarithm, Version 6.13.0* (2022) https://github.com/Expander/polylogarithm.

[302] M. Roughan, *The Polylogarithm Function in Julia* (2020) arXiv:2010.09860.

[303] A. Voigt, *Comparison of methods for the calculation of the real dilogarithm regarding instruction-level parallelism* (2022) arXiv:2201.01678.

[304] W. Porod, *SPheno, a program for calculating supersymmetric spectra, SUSY particle decays and SUSY particle production at e^+e^- colliders*, *Comput. Phys. Commun.* **153** (2003) 275–315, arXiv:hep-ph/0301101.

[305] W. Porod and F. Staub, *SPheno 3.1: extensions including flavour, CP-phases and models beyond the MSSM*, *Comput. Phys. Commun.* **183** (2012) 2458–2469, arXiv:1104.1573.

[306] G. Passarino and M.J.G. Veltman, *One-loop corrections for e^+e^- annihilation into $\mu^+\mu^-$ in the Weinberg model*, *Nucl. Phys. B* **160** (1979) 151–207.

[307] T. Hahn and M. Pérez-Victoria, *Automated one-loop calculations in four and D dimensions*, *Comput. Phys. Commun.* **118** (1999) 153–165, arXiv:hep-ph/9807565.

[308] S. Schael *et al.* [LEP Electroweak Working Group, ALEPH Collaboration, DELPHI Collaboration, L3 Collaboration, and OPAL Collaboration], *Electroweak measurements in electron–positron collisions at W-boson-pair energies at LEP*, *Phys. Rep.* **532** (2013) 119–244, arXiv:1302.3415.

[309] J. Heeck, *Unbroken B–L symmetry*, *Phys. Lett. B* **739** (2014) 256–262, arXiv:1408.6845.

[310] M. Aaboud *et al.* [ATLAS Collaboration], *Search for new high-mass phenomena in the dilepton final state using $36\,fb^{-1}$ of proton-proton collision data at $\sqrt{s} = 13\,TeV$ with the ATLAS detector*, *JHEP* **10** (2017) 182, arXiv:1707.02424.

[311] A.M. Sirunyan *et al.* [CMS Collaboration], *Search for high-mass resonances in dilepton final states in proton-proton collisions at $\sqrt{s} = 13\,TeV$*, *JHEP* **06** (2018) 120, arXiv:1803.06292.

[312] J.C. Romão and J.P. Silva, *A resource for signs and Feynman diagrams of the Standard Model*, *Int. J. Mod. Phys. A* **27** (2012) 1230025, arXiv:1209.6213.

[313] R.K. Ellis, W.J. Stirling, and B.R. Webber, *QCD and Collider Physics*, *Cambridge University Press* (1996) 1–435.

[314] S.D. Drell, D.J. Levy, and T.M. Yan, *Theory of Deep-Inelastic Lepton-Nucleon Scattering and Lepton-Pair Annihilation Processes. I*, *Phys. Rev.* **187** (1969) 2159–2171.

[315] S.D. Drell, D.J. Levy, and T.M. Yan, *Theory of Deep-Inelastic Lepton-Nucleon Scattering and Lepton-Pair Annihilation Processes. III. Deep-Inelastic Electron-Positron Annihilation*, *Phys. Rev. D* **1** (1970) 1617–1639.

[316] J. Blümlein, V. Ravindran, and W. van Neerven, *On the Drell–Levy–Yan relation to $\mathcal{O}(\alpha_s^2)$*, *Nucl. Phys. B* **586** (2000) 349–381, arXiv:hep-ph/0004172.